UNIVERSITY OF STRATHCLYDE

Quantifying the Relationship Between Wind Turbine Component Failure Rates and Wind Speed

Submitted for the Degree of Doctor of Philosophy

Graeme Wilson

Wind Energy CDT

Department of Electronic and Electrical Engineering

Supervisor – Dr David McMillan

April 2015

Contents

Abstract

Onshore wind turbine technology has matured to the point when assets are now expected to produce availabilities greater than 97%. The wind speed a wind turbine operates in has an impact on its reliability. Hitherto this relationship has not been defined, quantified or used to undertake analysis to assess how wind turbine performance would be affected by conditions at a prospective site.

Wind turbine reliability data comes from two modern onshore wind farms, located in Scotland, using multi-megawatt wind turbines. This information is used alongside data from meteorological masts, located on each site, to determine the mean wind speed on the day of each recorded failure that resulted in corrective maintenance. A methodology is proposed in this thesis to define the relationship between wind turbine component failure rates and wind speed using Bayes Theorem. With these relationships known and wind speed dependent failure rates calculated, component reliability is modelled using discrete Markov Chains and Monte Carlo Simulation.

The model is used to extrapolate the failure rate and wind speed relationships found within the onshore dataset to a proposed onshore and offshore site. From the generated data, wind turbine annual component failure rates are calculated for each site and analysis is performed to determine how component failure rates are likely to change throughout a year due to seasonal wind speeds at each site. The calculated seasonal failure rates allow wind turbine performance to be analysed more closely than if using traditional annual failure rates. A spares optimisation model is finally proposed using the wind speed dependent failure rate model. The output of this thesis is of particular relevance to operators of offshore wind farms.

Acknowledgement

Firstly, thanks to my supervisor Dr David McMillan. From the start of my research to the very end, David has been a fantastic supervisor and it has been a pleasure to work with him.

Doing a Ph.D. is supposedly meant to be a solitary process, but I could not have hoped for a better group of people to be surrounded by for the past four years. The frequent trips to the CSR, the odd Friday night at the pub and dominating the Glasgow 5-aside football leagues with the Dolphins has made the whole experience so enjoyable. Special thanks to Drew Smith for creating such a fantastic working environment and to David Infield and Bill Leithead for giving me the opportunity to be a part of the centre.

Finally, thanks to my wife Suzanne, for her encouragement, support and the odd scathing/encouraging remark about not finishing this thesis on time.

This project was funded by EPSRC. Project Reference Number EP/G037728/1.

Index of Figures

Index of Tables

Abbreviations

AC	Alternative Current
ANN	Artificial Neural Networks
°C	Degrees Celsius
CfD	Contracts for Difference
CO_2	Carbon Dioxide
DC	Direct Current
DEWI	German Wind Institute
DFIG	Doubly Fed Induction Generator
DOWEC	Dutch Offshore Wind Energy Convertor
EO	Emergency Order
EPR	European Pressurised Reactor
FMEA	Failure Mode Effects Analysis
GW and GWh	Giga Watts, Giga Watt hour
HC, LC and MC	High Cost, Low Cost and Medium Cost Scenarios
IPCC	Intergovernmental Panel on Climate Change
kW and kWh	Kilo Watt, Kilo Watt hour
LT	Lead time
LWK	Landwirtschaftskammer (Chamber of Agriculture)
MCMCS	Markov Chain Monte Carlo Simulation
MIDAS	Met Office Integrated Data Archive System
MTTF	Mean Time To Failure
MTTR	Mean Time To Repair
MW and MWh	Mega Watt, Mega Watt hour
O&M	Operation and Maintenance
OEM	Original Equipment Manufacturer
OP	Order Period
ORD	Operator's Reliability Dataset
PDF	Probability Density Function
PLP	Power Law Process
rad	Radians
ROC	Renewable Obligation Certificate
SCADA	Supervisory Control and Data Acquisition System
UN	United Nations
USA	Ultra Sound Anemometer

WEI	Wind Energy Index
WMEP	Scientific Measurement and Evaluation Program
WSD	Wind Speed Dependent
WT	Wind Turbine

List of Terms

a	Availability
b	Bandwidth
d, d_{repair} and $d_{extended}$	Downtime, downtime repair, downtime extended
E, E_{lost} and $E_{potential}$	Energy, Energy lost, Energy potential
f(t)	Failure Density Function
h	Height
m	Metre
p, *P(t)*and *P(w)*	Probability, Probability as a function of time and as a function of mean daily wind speed
Q(t)	Failure Distribution
r	Desired Bin Width
R(t)	Survivor Function
S and *s*	Maximum and Reorder levels
t	Time
U	Instantaneous Wind Speed
w	Mean Daily Wind Speed
z_0	Surface Roughness Factor
α	Reliability Database Weighting
β_S and β_s	Maximum and Reorder level factors
γ	Time Factor
θ	Shape Factor
λ and λ(t)	Failure rate and Hazard Rate
τ	Time lag between two signals
ω	Kernel
μ	Repair rate

Chapter 1. Introduction

1. The Drive Towards Clean Electricity Production in the UK

In the UK and across Europe there has been a change in the electricity generation paradigm over the past 10 years or so. This has been led primarily due to the threat of climate change. The Intergovernmental Panel on Climate Change (IPCC) issued their First Assessment Report on climate change in 1990. Their conclusion was that the increased atmospheric concentrations of greenhouse gases was causing a natural greenhouse effect [1-1]. The IPCC recognised that energy production and use was the biggest contributing factors to the greenhouse gas problem and noted that fossil fuel combustion caused 70 – 90% of the total anthropogenic emissions of CO_2 [1-1].

Since the IPCC report was delivered policies gradually were put in place to curb CO_2 and other greenhouse gas emissions. The Kyoto Protocol to the United Nations Framework Convention on Climate Change was signed in 1997 by the member states of the United Nations (UN) [1-2]. This treaty was designed to set national targets to reduce the production of greenhouse gases throughout the world. The UK agreed to reduce their CO_2 levels by 12.5% of the 1990 levels while other nations agreed similar deals. As a result developed nations began to invest in renewable electricity as an alternative to the traditional methods of generation [1-3].

The UK however decided to invest in Closed Cycle Gas Turbine (CCGT) power stations mainly because of falling gas prices, recent technological advances and privatisation of the UK electricity market. From 1990 to 2002 the percentage of electricity in the UK generated by gas rose from 5% to 28 % [1-4]. This period of time was known as the 'Dash for Gas'. In data analysed by the IPCC, it was found that in the 50^{th} percentile, gas produces 469 grams of CO_2/kWh compared to coal that produces 1001 grams of CO_2/kWh [1-5]. Therefore CCGT plants produced significantly lower levels of CO_2 than the coal fired power stations and due to the rapid roll out of gas fired power plants, by 2009 the UK managed to reduce its CO_2 output by 15.2 % of the 1990 levels [1-3].

Part of this reduction in CO_2 was due to renewable electricity technology becoming more attractive to investors as the price of gas increased rapidly in 2004, as shown in Figure 1-1, therefore causing the domestic gas and electricity prices to increase [1-6].

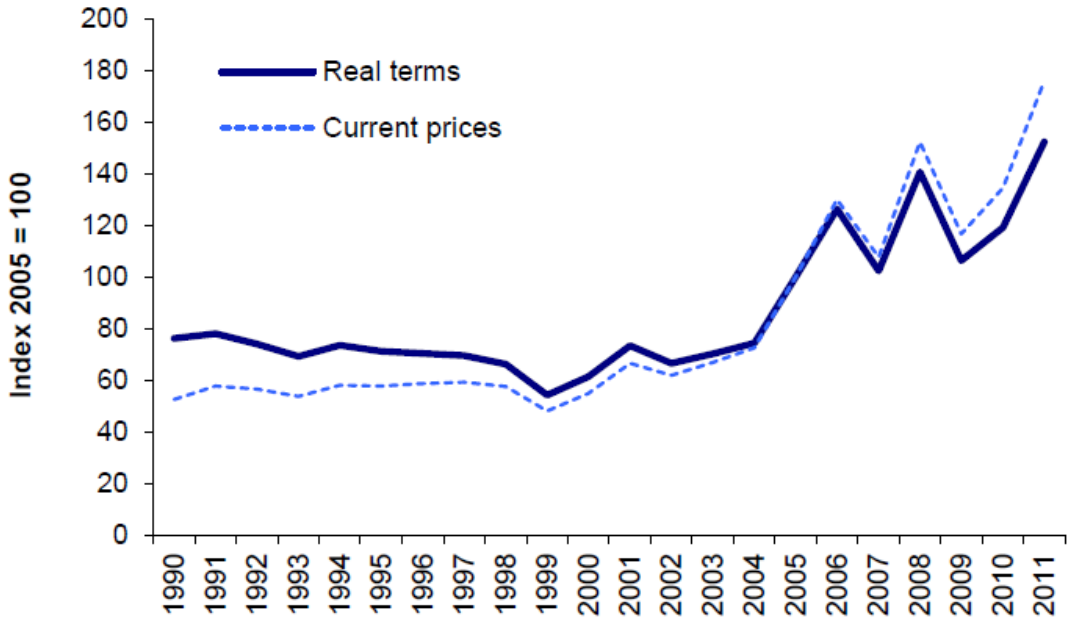

Figure 1-1: Average price of gas at UK delivery points from 1990 to 2011 in real (accounting for inflation) and current terms [1-6]

Advances made in onshore wind energy technology in other areas of Europe meant that Wind Turbines (WTs) became a viable alternative to traditional forms of generation. Additionally, political pressure began to build and further CO_2 reduction targets were set by the UK government with the Energy White Paper in 2003 and the Energy Review in 2006 [1-7], [1-8]. Then in 2007, with the publication of the Energy White Paper - Meeting the Energy Challenge, a target of 10% of electricity generation to come from renewable sources was set for 2010 and additionally an aspirational target of 20% was set for 2020 [1-9]. Finally in 2008 the government passed the Climate Change Act into law which required a reduction in CO_2 emissions by 80%, compared to 1990 levels, by 2050 [1-10]. One of the primary mechanisms for achieving this was through the use of renewable technologies.

Currently the UK still relies heavily on fossil fuels and imports 20% of its primary supply of gas, compared to 2000 when the UK exported 4.2% [1-11]. The UK therefore relies on cheap gas imports from geopolitically sensitive countries. Recently the UK government reacted to these problems by encouraging investment in the next generation of nuclear power stations to be built in England [1]. However nuclear power stations require very high capital costs compared to every other form of generation and also carries operating and decommissioning risks [2]. The new 3rd generation of reactors, called the European Pressurised Reactor (EPR), are relatively untested and recent projects in Flamanville, France and Olkiluoto, Finland are currently over budget and delayed [3]. In an effort to reduce the risk, EDF agreed to a joint venture between themselves and two Chinese companies in 2013 to build EPR reactors in the UK [1-12]. These nuclear power stations will replace the current second generation, advanced gas-cooled reactor, nuclear power stations in the UK that are all due to be decommissioned by 2024.

Despite these developments, the UK government continues to promote investment in wind energy – specifically offshore wind. Onshore wind projects however have had subsidies lowered and as many of the best sites have already been developed, investors are now looking to develop potentially more lucrative offshore sites. From 2001, offshore development rounds have been licenced to operators in UK waters. Currently after two rounds, approximately 3.6 GW of offshore wind energy capacity has been installed. Developers have also competed to develop round 3 sites that are situated further offshore and have the potential to generate 31GW of electricity.

Offshore wind has been targeted by the UK government as a solution to helping the UK meet their 2050 targets. However a lot of uncertainty remains about the technology. The high capital costs of the WTs have not begun to decrease as expected while OEMs compete over new innovative concepts and larger machines. Furthermore large offshore sites have not been

developed as quickly as expected, therefore OEMs have not been able to make savings on economies of scale through the supply chain.

As a result, operational experience is limited, especially for sites located far offshore. One example is Dogger Bank, a Round 3 site located approximately between 125 km - 290 km offshore in the North Sea, with a potential capacity of 13 GW [1-13]. For the UK to meet its targets, sites like Dogger Bank have to be developed. However the logistical challenges posed by this site are more considerable than any site currently in operation in Europe. For the wind farm to transmit a good quality supply of electricity to the mainland it is vital that the WTs are reliable and achieve high levels of availability. Failures at such long distances from shore will be considerably harder to repair and will cost significantly more than those at sites currently operating. And as the sizes of WTs increase, the weight of components is also likely to increase. Therefore expensive heavy lifting vessels may be required more frequently to carry out repairs.

The offshore environment however poses another challenge. Mean annual wind speed offshore is greater than that experienced onshore. This is one of the reasons why offshore wind is so attractive to investors, the potential electricity production is significantly higher, so too therefore are potential profits. The impact this wind speed will have on reliability is not fully understood. Published operational data has been limited to onshore reliability data from European wind farms, using out-dated WT models. Onshore WTs achieve such high levels of performance that the impact of wind speed on reliability has not been a popular focus of research. However this may change as the potential gains and losses offshore are so high.

In order for the UK to continue its drive towards clean electricity production it is vital that offshore wind be an attractive investment to developers. For this to happen and for it to be an effective method of electricity generation, offshore WTs must be as reliable as possible. The

factors that affect WT reliability must therefore be understood clearly. This thesis will attempt to ascertain more about WT reliability by gaining a better understanding into how reliability is affected by wind speed.

2. Publications Resulting From the Work of This Thesis

Wilson, G and McMillan, D (2012) *Modelling the effects of the environment on wind turbine failure modes using neural networks.* In Supergen 2012, 2012-09-08, Hangzhou, China

Wilson, G and McMillan, D (2013) *Modelling the effects of seasonal weather and site conditions on wind turbine failure modes.* In: ESREL 2013, 2013-09-30, Amsterdam.

Wilson, G and McMillan, D (2013) *Modelling the impact of the environment on offshore wind turbine failure rates.* In: EWEA Offshore 2013, 2013-11-19, Frankfurt.

Wilson, G and McMillan, D (2014) *Quantifying the impact of wind speed on wind turbine component failure rates.* In: EWEA 2014 Annual Event, 2014-03-10, Barcelona.

Wilson, G and McMillan, D (2014) *Assessing Wind Farm Reliability Using Weather Dependent Failure Rates.* In: The Science of Making Torque from Wind 2014, 2014-06-26, Copenhagen.

McMillan, D., Dinwoodie, I., Wilson, G., May, A., Hawker, G. (2014) *Asset Modelling Challenges in the Wind Energy Sector*. In Cigre 2014, 2014-08-25, Paris.

3. Key Research on the Impact of Wind Speed on Wind Turbine Reliability

The majority of European research undertaken in the specific area of the impact of wind speed on reliability has been carried out by Peter Tavner and his colleagues at Durham University. Since 2010 they have published four papers in this area, all of which will be discussed in detail in Chapter 2.3.4. Previous to this, the most prominent research was carried out by Berthold Hahn in 1997 [1-14]. Table 1-1 shows a summary of these authors and the papers they have published.

Table 1-1: Matrix of authors and their contribution to notable papers on impact of wind speed on reliability

Author (University/Company)	Influence of Weather on Wind Turbines [1-14]	Reliability of Offshore Turbines - Identifying risks By Onshore Experience [1-15]	Study of Effect of Weather and Location on Wind Turbine Failure Rates [1-16]	Effects of Wind speed on Wind Turbine Availability [1-17]	The Effect of Environmental Parameters on wind Turbine Reliability [1-18]	Study of Weather and Location Effects on Wind Turbine Failure Rates [1-19]
P. J. Tavner (Durham University)		✓	✓	✓		✓
S. Faulstich (Fraunhofer, IWES)		✓	✓	✓		✓
B. Hahn (Fraunhofer IWES)	✓	✓	✓			✓
P. Lyding (Fraunhofer IWES)		✓		✓		
M. Wilkinson (Garrad Hassan, pre. Durham)					✓	
D. M. Greenwood (Durham University)			✓			✓
M. W. G. Whittle (Durham University)			✓			✓
R. Grindele (Durham University)			✓			✓

4. Thesis Contribution to Field of Research

The research carried out in this thesis adds to the field of research in the following areas:

1. The dataset used in this analysis is larger and more advanced than the dataset used by Tavner. It is also more informative than the dataset used by Wilkinson which consisted of SCADA alarm logs which do not accurately describe the location of failure within the WT.
2. The detail of the dataset used in this thesis allows analysis to be undertaken at a component level.
3. The methodology used in this thesis does not assume a linear relationship between wind speed and reliability – as Tavner and Hahn did. Therefore the impact of wind speed on reliability above and below rate wind speed is calculated more accurately.
4. The impact of wind speed on component reliability is quantified in terms of power generation and availability. The economic benefit of using this model as opposed to traditional constant failure rate models is evaluated.
5. Offshore WT reliability is calculated at a component level using the model developed in this thesis.
6. Finally the model developed in this thesis is applied to offshore wind farm spares optimisation to determine if the research undertaken in this thesis is of benefit to industry.

5. Thesis Outline

Chapter 2 introduces some of the basic theories of engineering system reliability covering concepts such as failure rates, repair rates and maintenance that will be referred to throughout the thesis. Then the existing reliability databases that are used frequently in the literature are summarised. Finally WT reliability literature is reviewed, starting from the early research that took place before the arrival of multi-megawatt turbines and concluding with research that has been published on offshore WT reliability. The chapter culminates with a review of the literature, shown in Table 1-1, that specifically focuses on the impact of wind speed on WT reliability.

Chapter 3 outlines the theory behind the proposed model which will be used in the subsequent thesis chapters.

Chapter 4's goal is to summarise the data used in the subsequent chapters. The WT reliability data is introduced and the process in which it is gathered is explained, weather data from onshore and offshore met masts are also analysed. To conclude the chapter a methodology used by Tavner and his colleagues is then replicated using the weather and reliability data. From this the merits of analysing the impact of temperature and humidity, as well as wind speed, are assessed.

Chapter 5 outlines the methodology and describes the motivation for the methods used and how the aims of the thesis will be met. Markov Chains, Monte Carlo Simulation and Bayes Theorem are presented. The approaches used in designing various elements of the model are described and many parameters are defined.

Chapter 6 shows the capabilities of the wind speed dependent failure rate model in calculating component failure rates and site availabilities for when subjected to onshore and offshore wind speed inputs. The impact of wind speed dependent failure rates on electricity

generation is then assessed and the model is compared to a traditional stationary failure rate model.

Chapter 7 demonstrates an offshore wind farm spares optimisation model using the wind speed dependent failure rates. Offshore constraints are added to the model, component costs are estimated and the spares optimisation process is described. A comparison is then made between spare strategies using wind speed dependent failure rates and using stationary failure rates to test the effectiveness of the spares optimisation model.

Finally Chapter 8 presents the main results, conclusions and identifies areas where more research should be undertaken.

6. Chapter 1 References

[1-1] Intergovernmental Panel on Climate Change, “IPCC First Assessment Report,” 1990.

[1-2] United Nations, “Kyoto Protocol to the United Nations Framework Convention on Climate Change,” 1998. [Online]. Available: http://unfccc.int/resource/docs/convkp/kpeng.pdf.

[1-3] International Energy Agency, “IEA Statistics - CO2 Emissions from Fuel Combustion Highlights,” Luxembourg, 2012.

[1-4] Department of Energy and Climate Change, “Digest of UK Energy Statistics,” 2014.

[1-5] W. Moomaw, P. Burgherr, G. Heath, M. Lenzen, J. Nyboer, and A. Verbruggen, “Annex II: Methodology,” in *IPCC Special Report on Renewable Energy Sources and Climate Change Mitigation [O. Edenhofer, R. Pichs-Madruga, Y. Sokona, K. Seyboth, P. Matschoss, S. Kadner, T. Zwickel, P. Eickemeier, G. Hansen, S. Schlomer, C. von Stechow]*, vol. 103, no. 6, Cambridge, UK: Cambridge University Press, 2011.

[1-6] Department of Energy and Climate Change, “Quarterly Energy Prices – September 2013,” 2013.

[1-7] Department for Trade and Industry, “Our energy future – creating a low carbon economy,” London, 2003.

[1-8] Department for Trade and Industry, “The Energy Challenge – Energy Review,” 2006.

[1-9] Department for Trade and Industry, “Meeting the Energy Challenge – A White Paper on Energy,” 2007.

[1-10] Department for Environment Food and Rural Affairs, “Climate Change Act,” 2008.

[1-11] P. Bolton, “Energy imports and exports,” *House of Commons Library*, 2013. [Online]. Available: http://www.parliament.uk/business/publications/res

[1-12] Anon, “UK nuclear power plant gets go-ahead,” *BBC*, 2013. [Online]. Available: http://www.bbc.co.uk/news/business-24604218.

[1-13] T. R. A. of Engineering, *The Cost of Generating*. London: The Royal Academy of Engineering, 2004.

[1-14] World Nuclear News, “Flamanville start-up put back one year,” *2014*. [Online]. Available: http://www.world-nuclear-news.org/NN-Flamanville-start-up-put-back-one-year-1911144.html. [Accessed: 24-Jan-2015].

[1-15] P. Wintour, “Hinkley nuclear power station gets go-ahead as coalition signs off EDF deal,” *The Guardian*, 2013. [Online]. Available: http://www.theguardian.com/environment/2013/oct/20/nuclear-power-station-hinkley-edf. [Accessed: 05-Aug-2014].

[1-16] Forewind, “Dogger Bank,” 2014. [Online]. Available: http://www.forewind.co.uk/dogger-bank/overview.html. [Accessed: 06-Aug-2014].

[1-17] B. Hahn, “Zeitlicher Zusammenhang von Schadenshäufigkeit und Windgeschwindigkeit,” in *FGW-Workshop Einflub der Witterung auf Windenergieanlagen,*, 1997.

[1-18] S. Faulstich, B. Hahn, P. Lyding, and P. Tavner, “Reliability of offshore turbines – identifying risks by onshore experience,” in *EWEA*, 2009.

[1-19] P. J. Tavner, B. Hahn, R. Gindele, M. W. G. Whittle, S. Faulstich, and D. M. Greenwood, “Study of Effects of Weather & Location on Wind Turbine Failure Rates,” in *EWEC 2010*, 2010.

[1-20] S. Faulstich, P. Lyding, and P. J. Tavner, “Effects of Wind Speed on Wind Turbine Availability,” in *EWEA*, 2011.

[1-21] M. Wilkinson, T. Van Delft, and K. Harman, “The Effect of Environmental Parameters on Wind Turbine Reliability,” in *EWEA 2012*, 2012.

[1-22] P. J. Tavner, D. M. Greenwood, M. W. G. Whittle, R. Gindele, S. Faulstich, and B. Hahn, “Study of weather and location effects on wind turbine,” *Wind Energy.*, vol. 16 no.2, pp. 175–187, 2013.

Chapter 2. Wind Turbine Reliability

1. Reliability Analysis of Engineering Systems

The impact of a failure to a WT can range from a minor failure to the control system, to the cataclysmic scenario of a blade fracturing and becoming airborne. In the former's case the power output of the wind farm would decrease by less than 1%, leading to an almost negligible impact on the transmission grid frequency. The WT would be repaired easily and begin operating after a short period of downtime. In the latter's case the damage to the WT would be significant but perhaps less concerning than the danger and risk caused to the general public. Downtime would be long, if indeed the WT could be repaired at all.

As will be demonstrated in this chapter, the probability of the latter occurring is very low – indeed blade fractures are relatively rare events [2-1] . However, it is the job of engineers to ensure that the probability of this happening does not just remain low but decreases as the number of installed WTs increases and the size of machines become larger over time.

A control system failure however is far more likely to occur and does so regularly, as will be discussed [2-2], [2-3]. These types of failures impact the economic viability of the technology and therefore impinge on deployment and limit the growth of the industry.

Reliability is an essential part of engineering and must be considered at all points in the design, deployment and operation of a system. Traditionally reliability was assessed and perfected using engineering judgement [2-4]. However, quantitative methods are used much more frequently now to provide good quality information with which engineers can make better informed decisions. As will be demonstrated throughout this chapter,, systems can now be designed more economically due to an improved knowledge of their operation and behaviour.

1.1. Availability, Failure Rate and Repair Rate

A key reliability metric is availability – this is the percentage of time that a system is operating as it should be. For an operating system this metric is calculated using Equation

2-1 [2-5], [2-6]. The uptime is the period of time that the system is able to operate and the downtime is the time in which the system is not operating due to failure.

$$Availability = \frac{Uptime}{Uptime + Downtime} \quad \textbf{Equation 2-1}$$

This metric gives the probability that a system will operate at a given point in time. It is influenced by two other metrics – failure rate and repair rate. The failure rate λ, is the probability of the system (or a subsystem) failing at a given point in time. It is calculated using Equation 2-2 and Equation 2-3 [2-5]. In general terms, a failure is defined as any fault (or unplanned event) which causes the system downtime [2-5].

$$\lambda = \frac{number\ of\ failures\ to\ a\ component\ in\ a\ given\ period\ of\ time}{total\ period of\ time\ the\ component\ was\ operating} \quad \textbf{Equation 2-2}$$

$$\lambda = \frac{1}{Mean\ Time\ To\ Failure\ (MTTF)} \quad \textbf{Equation 2-3}$$

The repair rate μ, describes the probability of a component being repaired during a given period of time. It is represented by the symbol μ and is calculated using Equation 2-4 and Equation 2-5 [2-5].

$$\mu = \frac{number\ of\ repairs\ to\ a\ component\ in\ a\ given\ period\ of\ time}{total\ period of\ time\ the\ component\ was\ being\ repaired} \quad \textbf{Equation 2-4}$$

$$\mu = \frac{1}{Mean\ Time\ To\ Repair\ (MTTR)} \quad \textbf{Equation 2-5}$$

A failure is defined as being an unplanned event that causes the WT to be unavailable to generate electricity. Low or high wind speed events do not constitute failures as the WTs are available to generate if the resource is within the design limits. Incidents such as the

untwisting of cables and pitch lubrication cycles which cause the WT to stop generating are not defined as failures as these as part of the operational schedule of the WT.

As an illustrative example, Figure 2-1 shows a time series of a single WT's state during a year of operation. The two states the WT can be in are the up state, 1 when the WT is available to generate and the down state, 0 when the WT has failed and is unable to generate electricity. Downtime from annual servicing is omitted from the figure.

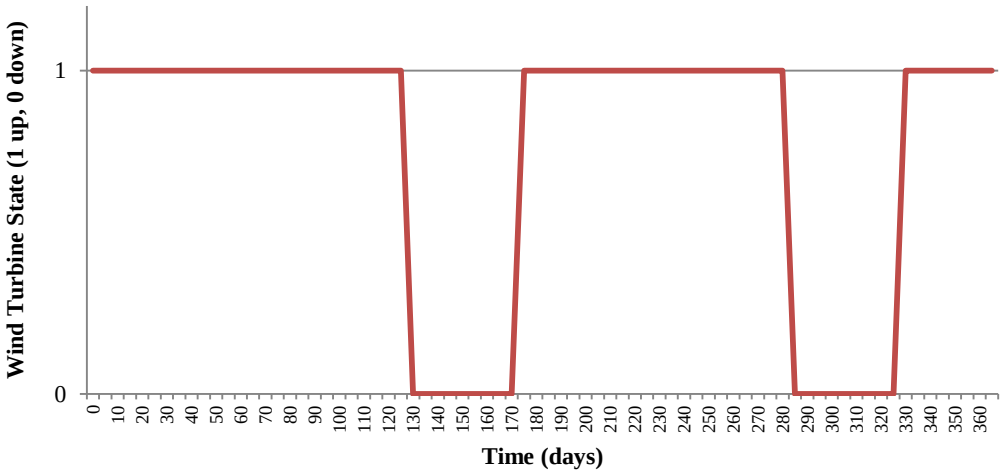

Figure 2-1: Failure rate, repair rate, downtime and availability illustrative example

The first failure occurs on day 130, the WT then remains down until day 175 when it is repaired and resumes operating again. The WT then fails for a second time on day 285 after which it is repaired 40 days later. The WT then remains in the up state until the end of the year.

Table 2-1: Illustrative example reliability metrics

Downtime (days)	85
Uptime (days)	280
Availability (%)	76.7
Failure Rate (failures/WT year)	2.6
Repair Rate (repairs/WT year)	8.6

The uptime of the WT during the year was 280 days, while the downtime was 85 days. The availability, failure rate and repair rate are calculated using Equation 2-1, Equation 2-2 and Equation 2-4 and are shown in Table 2-1.

1.2. Reliability Functions

The hazard rate λ(t) is a function of time that describes the probability of a failure occurring to a component at a time *t*, assuming the component has survived thus far. In WT literature it is often used to mean the same thing as the failure rate; however the difference between the two metrics is that the hazard rate is a function of time.

In mechanical systems the hazard rate is often described as being a bath tub curve. It is by far the most common description of the hazard rate in the reliability text. Its origin is unknown – however it did appear in an actuarial life table analysis in 1693 [2-7] . As shown in Figure 2-2, it divides the hazard rate into three distinct periods of operation:

- Infant mortality or burn in
- Random failures or useful life
- Wear out period

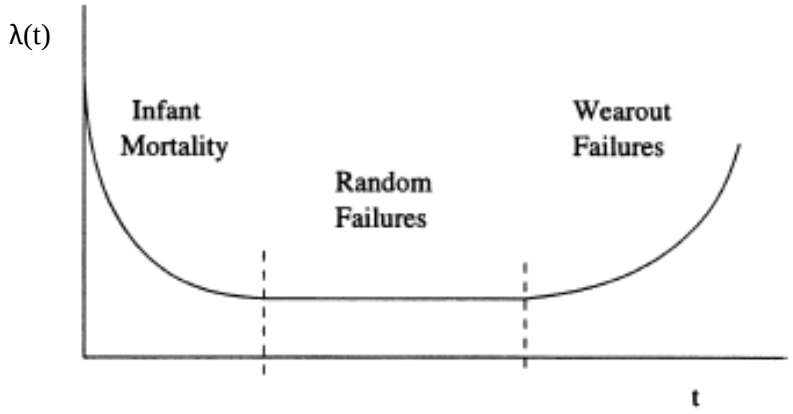

Figure 2-2: The bathtub curve of a mechanical system [2-7]

Theoretically, components should be maintained to keep them within the useful life period of their life before being replaced to prevent them from entering the wear out period and become uneconomical to continue using [2-5]. Equally, new components should be put

through a burn in process before they are installed so that they are within their useful period at the beginning of operation [2-8].

However each component has a different hazard rate and predicting this metric for a WT is a challenge. As components are frequently replaced, in anticipation of the wear out period, this region of the curve is not often well modelled. Many also argue that the bath tub curve is only successful for very few cases in predicting the impacts of aging and equipment failures [2-8], [2-9].

If a hazard rate is calculated using WT reliability data it is often assumed to be constant. Although the bath tub curve is not always appropriate it is also unlikely that components maintain constant hazard rates throughout their lives. However if the population of WTs in the sample have differing or unknown ages, assuming a constant hazard rate is often justified as the data is often not of the quality required to correctly model the underlying distribution [2-5].

A constant hazard rate, or more specifically failure rate, leads to the most commonly used distribution in reliability engineering – the negative exponential distribution [2-10], [2-11]. This is described in Equation 2-6, where the survivor function *R(t)* is defined [2-5].

$$R(t) = e^{-\lambda t} \qquad \textbf{Equation 2-6}$$

The failure density function f(t) and cumulative failure distribution Q(t) is therefore defined as shown in Equation 2-7 and Equation 2-8 [2-5].

$$f(t) = \frac{-dR(t)}{dt} = \lambda e^{-\lambda t} \qquad \textbf{Equation 2-7}$$

$$Q(t) = \int_0^t \lambda e^{-\lambda t}\, dt = 1 - e^{-\lambda t} \qquad \textbf{Equation 2-8}$$

The failure density function *f(t)*, is illustrated in Figure 2-3. The regions Q(t) and R(t) represent the cumulative failure distribution and the survivor function respectively. As time *t* increases, the probability of the component surviving (*R(t)*) decreases and the cumulative failure (*Q(t)*) increases.

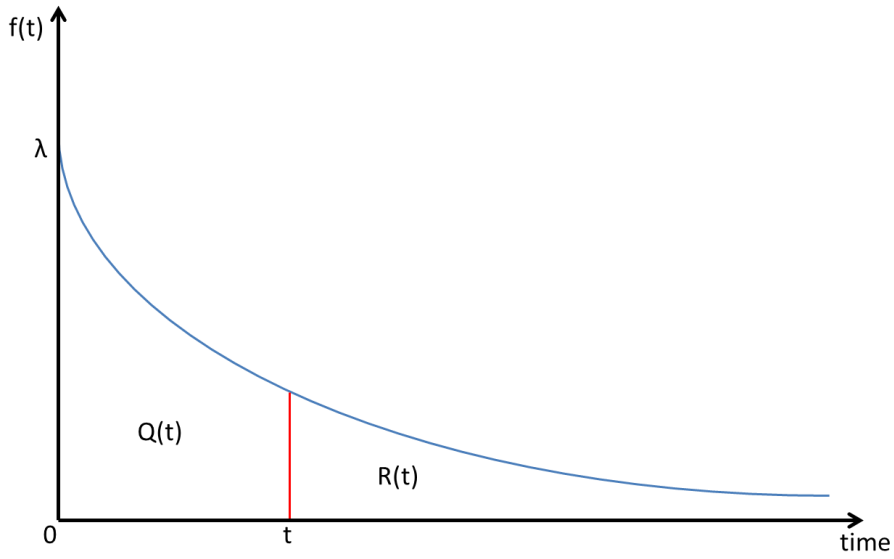

Figure 2-3: Failure density function f(t)

1.3. Maintenance

The purpose of maintenance is to keep the system operating at the required level of performance. Using Figure 2-3 as an example, if the system is operating at *f(t)* and maintenance is carried out, when the system resumes operating at will be at *f(t-x)*.The value of *x* depends on the action performed and how effective it is. If an assumption is made that in the case of a failure a replacement is made and the system resumes operating in an 'as good as new' state where $x = t$. However, if the component is rehabilitated, rather than a completely replaced, the maintenance may be imperfect and the system may resume operating between the 'as good as new' and the 'as bad as old' state, where $x \leq t$ [2-12]. The cost of rehabilitation is generally less than the cost of replacement, therefore to determine the correct course of action, reliability and economics must be considered [2-13].

There are two different classifications of maintenance – preventive and corrective [2-5], [2-6]. Preventive maintenance is undertaken prior to a failure occurring. Tasks such as cleaning, lubricating and replacing components that are believed to be near the wear out period of their life, constitute preventive maintenance. Preventive maintenance is carried out to reduce the risk of failure. In some systems the outcome of a failure is not great enough to merit preventive maintenance; therefore the system is allowed to operate until a failure occurs. However in other systems, a failure during operation could result in huge losses or even death, therefore preventive maintenance is essential to keep the system running at its required performance level.

Preventive maintenance is often performed at regular intervals; corrective maintenance however must be undertaken whenever a component fails. Downtime due to corrective maintenance is also less predictable and manageable than preventive maintenance as often the failure diagnosis requires visual inspection whereas preventive maintenance is planned and scheduled to ensure minimum downtime to reduce any lost revenue.

As a result, it is important to remember that when failure rates are calculated using reliability databases, it is very likely that preventive maintenance has been performed to maintain the system at an acceptable performance level. Therefore when a failure to a component did occur, it happened in spite of efforts to maintain it operating at a suitable *f(t)*. If preventive maintenance was not undertaken on these systems, the failure rates in the reliability databases would very likely be higher.

1.4. Summary

This cost of operating a system is influenced by the losses in output and revenue due to component failure. Failure rates and repair rates of components can be calculated from reliability data to provide a better understanding of the system. Efforts can then be made to increase system availability. This cost is referred to as operation and maintenance (O&M) cost.

Improvements in availability can be achieved through developing an effective maintenance schedule that would ensure that preventive maintenance would minimise system downtime and corrective maintenance events. Preventive maintenance should target the components which cause the most concern, replacing or repairing them before they cause long periods of downtime. It is also important that spares holdings must be maintained to hold enough replacement components in order to account for both preventive and corrective maintenance.

Although these improvements increase revenue they also cost money to implement and sustain. Ultimately reliability evaluation is used to reduce the failure rate of a system and increase the repair rate to an optimum point beyond which it does not become economically viable to spend more money on O&M.

The following section will introduce WT reliability data that has been used frequently in the literature. From this, WT reliability trends will be highlighted and discussed.

2. Accessible Wind Turbine Reliability Data

All of the reliability evaluation analysis discussed in the previous section is conditional on reliability data being available with which to perform analysis. Ideally reliability data should come from homogenous populations that consist of systems of the same age and design, which operate in the same conditions. However WTs operate in different conditions within wind farms that vary in size and in some occasions WT model. WT reliability data is therefore not homogenous at all. However efforts have been made to gather suitable reliability data over many years for many WTs.

. The literature which will be discussed in the following section refers to five wind turbine reliability databases. Other databases such as these exist, however this thesis will focus on these five. They are explained in the following section and Table 2-3 gives a summary of the databases [2-14]–[2-18]. The taxonomy used in each database was different; however the databases used mostly common component descriptions.

2.1. WMEP

Comprising of roughly 64000 maintenance reports from 1500 WTs, the Scientific (Wissenschaftlich) Measurement and Evaluation Program (WMEP) database is compiled by the Fraunhofer IWES [2-14]. The data was collected using logbooks for each WT from 1989 – 2006. All disruptions, repairs, malfunctions and maintenance events were recorded along with monthly production figures.

2.2. LWK

The Landwirtschaftskammer (LWK: English translation Centre for Agriculture) database from Northern Germany whose population was fixed when recording began in 1993 and decreased over time as WTs were decommissioned [2-15], [2-19]. All WTs in LWK consisted of three-bladed, upwind rotors. However there were various models and concepts as shown in Table 2-2.

Table 2-2: Turbine Models in LWK database [2-15]

Turbine Model	Power Control	Concept Name
Tacke TW600	Stall control	Indirect Drive, Base Line Control
Vestas V39 500	Pitch control, hydraulic	Indirect Drive, Advanced Control
Enercon E40	Pitch control, electrical	Direct Drive
Nordex N52/N54	Stall control	Indirect Drive, Base Line Control
Enercon E66	Pitch control, electrical	Direct Drive

2.3. Windstats

Windstats was a quarterly newsletter which published production and operating data from WTs in Germany and Denmark [2-16]. The population was not fixed and the installed capacity of the turbines increased over the ten year period in both Germany and Denmark [2-16].

However the quantity of turbines in the dataset reduced in Denmark over time while the number in Germany increased [2-16] .

This may go some way to explaining the differences in failure rates between the two countries shown in Table 2-3. The German dataset saw a rapid expansion in wind energy over the ten year period where the number of WTs in the dataset increased each year and the average rating of these turbines also increased [2-3]. However in Denmark, WTs were already an established technology and many had been operating across the country for many years. As the older, smaller, machines stopped generating the number of turbines in the database decreased. However larger, more modern turbines were built to the replace the older models [2-3].

Despite the Danish database consisting of older WTs the failure rate of the dataset was lower than that of the German database. This was because the WT models used on the German

wind farms were more complex and less reliable than the older, smaller and less complex turbines used by the Danish in their wind farms [2-3]. See Chapter 2.3.2 for a more detailed discussion about this.

2.4. VTT

The VTT database was maintained by the Technical Research Centre of Finland [2-17]. It comprised of statistical data of performance, downtime and failures for a set of WTs in Finland. The data comes from grid connected WTs in Finland. Production data has been gathered since 1992, while failures statistics from 72 WTs have been analysed since 1996 [2-17]. Annual reports are produced annually and are open for public use [2-17]. Elforsk

Elforsk provided annual reports detailing the performance, downtimes and component failures of most of the WTs in Sweden [2-18]. Statistical data on the wind power systems of Sweden is gatherd by Vattenfall, which then passes this data onto Elforsk who publish an annual report on WT performance in Sweden [2-20]. Most of the WTs in Sweden are included in the analysis and performance data has been collated from as far back as 1989 [2-20].

Table 2-3: Reliability Database Summary

	Country	Time Span	Number of Turbines	WT Years of Experience	Average Failure Rate over whole survey period (failures/ WT year)	Average Annual Downtime over whole survey period (hours/ WT year)	Subassembly with Highest Failure Rate	Subassembly with Longest downtime per failure
WMEP [2-14]	Germany	1989 – 2006	1500	15000	2.4	156	1. Electric 2. Control 3. Sensors	1. Gearbox 2. Drive Train 3. Generator
LWK [2-15]	Germany	1993 – 2006	241	5719	1.9	27	1. Electric 2. Rotor 3. Control	1. Gearbox 2. Rotor 3. Electric
Windstats Germany [2-16]	Germany	1995 – 2004	4285	27700	1.8	93	1. Rotor 2. Electric 3. Sensors	1. Gearbox 2. Rotor 3. Drive Train
Windstats Denmark [2-16]	Denmark	1994 – 2003	904	18700	0.7	-	1. Control 2. Rotor 3. Yaw-System	-
VTT [2-17]	Finland	2000 – 2004	92	356	1.5	237	1. Hydraulic 2. Rotor 3. Gearbox	1. Gearbox 2. Rotor 3. Support & Housing
Elforsk [2-18]	Sweden	1997 – 2004	723	4378	0.8	58	1. Electric 2. Hydraulic 3. Sensors	1. Drive Train 2. Yaw System 3. Gearbox

3. Research into Wind Turbine Reliability

3.1. Early WTs

WT reliability has been an issue since WTs first began to be built commercially in the 1970s. One of the first papers on WT reliability concerned the MOD WT series built in the mid-seventies to eighties in the USA [2-21]. Starting in 1975, NASA designed and built the MOD-0, 100kW WT. It had a blade diameter of 38 m and was used initially as testing apparatus for aerofoil designs, rather than a generating turbine [2-21]. The MOD-0 was then upgraded by Westinghouse to the MOD-0A in 1978; four turbines were built to this design throughout the USA. During routine inspections it was discovered that cracking had begun to appear in the blades [2-21]. The MOD-0A was then superseded by the MOD-1 which was built by General Electric in 1979 [2-21]. This model experienced many engineering problems and as a result had its operation restricted.

The American aerospace company Boeing then undertook the design and installation of the MOD-2 WT [2-21] [2-22]. This was rated at 2.5 MW output – a high output even by today's scale – and had a rotor diameter of 91m. Three were installed in 1980 in Washington State. In 1981 the first turbine suffered a major failure when the hydraulics failed to function and the pitch control system prevented the rotor from accelerating from 17.5 rev/min to 29 rev/min [2-21] [2-22]. The rotor was brought to a halt after which a full safety analysis was carried out where it was discovered that the main shaft was cracking [2-21].

As WTs became bigger, concerns arose over whether the design rules at the time would not be suitable for large WTs and may compromise safety and design. Up until this period, WTs were designed in a deterministic manner [2-4]. The design rules at the time did not address the reliability of the WTs components and did not take into account the severe consequences that may have occurred if a large WT had suffered a major failure [2-4].

Seebregts et al concluded that for large scale, multi-megawatt turbines which would be manufactured in mass production it would not be practical or safe to design the WT using "trial and error" like small WTs had been designed up until that point [2-4]. Therefore systematic and analytical tools would be required to improve WT reliability for the large scale turbines. Seebregts et al proposed using a combination of failure mode and effects analysis (FMEA), fault tree analysis and environmental risk assessment to improve the reliability of WT designs [2-4].

The purpose of the environmental risk assessment was to analyse the impact of a blade failing. This was a common reliability and safety concern in the 1980s and early 1990s and as a result many of the papers at that time, written about WT reliability, focused on addressing this type of failure [2-21] [2-23] [2-24].

Seebregts et al showed that this methodology was beneficial in improving reliability and recommended that it be used along with the existing deterministic analysis used at the time [2-4]. However Seebregts et al did identify that there was "a fundamental lack of knowledge of physical phenomena in WT engineering that may cause hazardous situations, e.g. excessive vibrations" [2-4]. Computers did not have the processing power at the time to accurately model vibrational effects and these could only be analysed by preforming extensive load case situations in the calculation stage [2-4].

Seebregts et al recommended an electronic data collection be installed on every turbine to ensure that O&M data was gathered easily and used to optimise maintenance schedules [2-4]. Modern WTs have a Supervisory Control and Data Acquisition System (SCADA) which preforms this job.

In 1996, when the wind capacity worldwide was 4GW, Sayas and Allan investigated the reliability of WTs and their effect on the transmission and distribution system [2-25]. Markov chains were used to model the stochastic nature of WT failures in order to model the

availability of a WT. Markov chains had been used to model similar processes in previous research [2-26] [2-27] [2-28]. In Figure 2-4 it shows the state diagram for two WTs which operate in binary states, either in an "up" state, which means any power output can be achieved as the machine is fully operational, or the "down" state which means the machine is out of service [2-25].

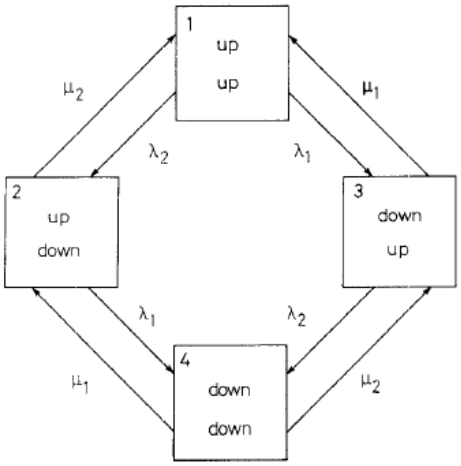

Figure 2-4: State diagram for two binary WTs [2-25]

The operating state the WTs are in depends upon their failure rate λ and repair rate μ, which are determined using [2-5]. A stochastic transitional probability matrix can be calculated from this arrangement. This matrix contains the probability of each state change.

Due to the unpredictable nature of wind, Sayas and Allan wanted to analyse the impact of a wind farm on an electrical grid, so they built their model following the same principles as before [2-25]. Their model is shown in Figure 2-4.

Sayas and Allan developed this model for a wind farm of 14 WTs, with each WT capable of generating 150kW, using real site data which would calibrate the wind model [2-25]. Instead of 4 wind states, as shown in Figure 2-4, there were 15 to increase the accuracy of the results [2-25]. Their results showed that the overall availability of the WTs in their model was very similar to that experienced in reality for onshore wind farms, roughly 98% [2-25].

This research was important as it gave developers an idea of the capacity factor a WT could achieve, taking the reliability of the machine into account. The analysis could also be used by network operators to calculate the amount of energy a wind farm would be likely to produce using a capacity outage probability table. It was also an early attempt to try to model the stochastic nature of WT failures. However, it was quite simplistic and did not consider the differences between major and minor failure modes and the downtimes associated with each. The failure rate used was also for the whole system rather than for specific subassemblies.

3.2. Modern Onshore WT Reliability

In 2005 multi-megawatt WTs were beginning to become more common in Spain, Denmark and Germany [2-3]. But because the technology was relatively new, there were concerns over the operating life of the WTs and how the reliability of the WTs would change over time.

Using WT reliability data from the German and Danish Windstats database Tavner found the average failure rates of WTs based in Germany and Denmark for each year of recorded data, from 1996 - 2003 [2-29] .

Tavner foun that over time the failure rate of both datasets decreased, in both cases by roughly 50% [2-29]. Tavner and his colleagues also concluded that [2-29]:

- German turbines fail approximately twice as often as Danish turbines.
- German failure rates are improving faster than Danish failure rates.
- The failure rates of German mechanical sub-assemblies are about double that of the Danish turbines.
- The German electrical sub-assemblies also fail more often than the Danish electrical sub-assemblies.

Both the German and Danish turbines show similar perturbations, the authors believed this was because of weather which they thought would be similar in both sets of locations.

Tavner compared WT reliability with the failure rates of traditional forms of power generation. He found that although wind generators were less reliable than steam turbine generators, they were better than diesel and gas turbines and their reliability

However there was a significant difference between the reliability of turbines sited in Germany and those sited in Denmark. This difference was because in general the German WTs were younger and had larger installed capacities than the Danish WTs [2-3], [2-16], [2-

30]. They were also variable speed, whereas many of the Danish WTs were constant speed. By maintaining a constant rotational speed, at all times throughout generation, the conversion of energy from wind to electricity is not as efficient. But this more simple design is a lot more reliable as simpler and better established components are used, whereas variable speed WTs at this time were a modern design using more complex and used less tested components [2-3], [2-29].

Tavner et al identified the electrical sub-assembly as an area to focus attention on to improve WT reliability [2-3], [2-29]. This recommendation was however based on their considerably high failure rates which affected the variable speed German WTs. However the authors recognised that the downtime which resulted from a failure to the electrical subassembly tended to be quite short compared to larger mechanical components, such as the gearbox, which failed less often [2-3], [2-30].

To attempt to answer the question of the life span and reliability of WTs through time, Tavner and his colleagues analysed the Windstats data further and in 2007 [2-3]. As discussed previously in 0, the life curve of mechanical components is usually represented by the bathtub curve which describes the hazard rate, or the failure rate of a component of a system over time (λ(t)), as shown in Figure 2-2 [2-3], [2-5]. A life curve can be calculated using equation 3, which is the power law process (PLP) and is used in reliability analysis for complex, repairable equipment [2-3].

$$\lambda(t) = \frac{\gamma}{\theta}\left(\frac{t}{\theta}\right)^{\gamma-1} \qquad \textbf{Equation 2-9}$$

$$\gamma, \theta > 0; t \geq 0$$

The PLP function models a wide range of failure processes by varying the shape (θ) and time (γ) parameters.

- When $\gamma < 1$, the failure rate (λ) decreases with time to model the infant mortality period.
- When $\gamma = 1$ the failure rate remains constant and models the useful life period.
- When $\gamma > 1$, the failure rate increases with time to model the wear out failures.

By estimating the shape and time parameters for the Danish and German WTs, Tavner and his colleagues plotted a life curve for both the Danish and the German WTs using the PLP. The algorithm for this process can be found in [2-3]. The curves correlated well with the actual data.

No attempt was made to produce a deterioration curve because the authors believed that if a WT began to show signs of deterioration it would be taken out of service before serious reliability issues arose [2-3]. There was also no deterioration data available to the authors to validate their results if they were to attempt to model it [2-3].

Tavner and his colleagues observed that there were very significant differences between the two datasets. These differences were due to the differences in WT models prevalent in each dataset. Indeed, the total average yearly failure rate for the German and Danish turbines in Windstats was 1.79 and 0.43 respectively [2-3], [2-16]. Interestingly this showed that the more complex machines, which were designed to be more efficient at extracting energy from the wind, were less reliable [2-3], [2-30]. For these more complex designs to be economically viable the WTs would have had to generate additional power to compensate for the energy they were losing from failing more often. Their maintenance strategies would also have to be better to reduce downtime.

Tavner, van Bussel and Spinato investigated the reliability of different turbine models in 2006 with a conference paper at the IEE 2nd International Conference on Power Electronics, Machine & Drives [2-30]. The authors used the LWK database as opposed to WindStats.

This was because WindStats did not state the concepts of the different WTs in its database – whereas LWK did [2-30].

Failure rates for each turbine concept were calculated using the Homogenous Poisson Process, which produced failure rates which were assumed to be constant over time [2-3] [2-30]. As shown in Figure 2-5, the LWK turbines have similar failure rates to those in the German WindStats database; this is because the two datasets have similar WTs in terms of size and concept [2-30].

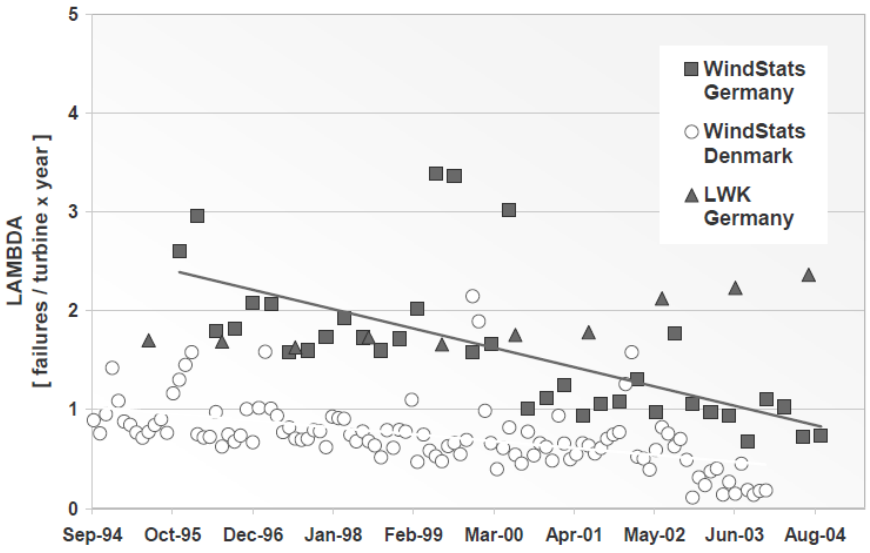

Figure 2-5: Comparison in failure rate between Windstats and LWK databases [2-25]

The LWK database has data for three general WT concepts, several models of which are shown in Table 2-4 [2-15], [2-30]:

- Fixed Speed Indirect Drive
- Variable Speed Indirect Drive
- Variable Speed Direct Drive

Table 2-4: WT Models in LWK Dataset [2-15], [2-30]

Turbine Size Group	Turbine Model	Rating (kW)	Speed
1	Tacke TW600 Vestas V39 500 Enercon E40	600 500 500	Fixed Variable Variable
2	Nordex N52/N54 Enercon E66	800/1000 1500	Fixed Variable

Tavner and his colleagues make several observations about the difference in reliability between the three concepts [2-30]:

- The gain in reliability from using a direct drive is made up from losing the gearbox.
- However, the electronics in the direct drive WT (E40) are more unreliable and actually make the concept less reliable than the indirect drive WT (V39 500).

The fixed speed geared WT (TW600) has the most reliable electronics and benefits from not requiring pitch mechanisms. However the blades of the TW600 are the most unreliable of the The results for the larger turbines, shown in Figure 2-6, led the authors to the conclusion that the indirect drive WTs (N52/N54) were marginally less reliable, on a whole, compared the direct drive turbines (E66) [2-30]. However the failure rate of the generator in the E66 was at least double that of the generator used in the N52/N54.

The authors attribute the greater number of generator failures in the direct drive turbines to the more complex generator which is used in direct drive WTs [2-30]. The direct drive generators from the LWK dataset also suffered from a lack of standardisation because their manufacture was on a smaller scale than the geared induction generators [2-30]. The size of the direct drive generator was also a factor in its reliability as the stator and rotor windings were much longer, it was therefore much harder to seal against external agents [2-30].

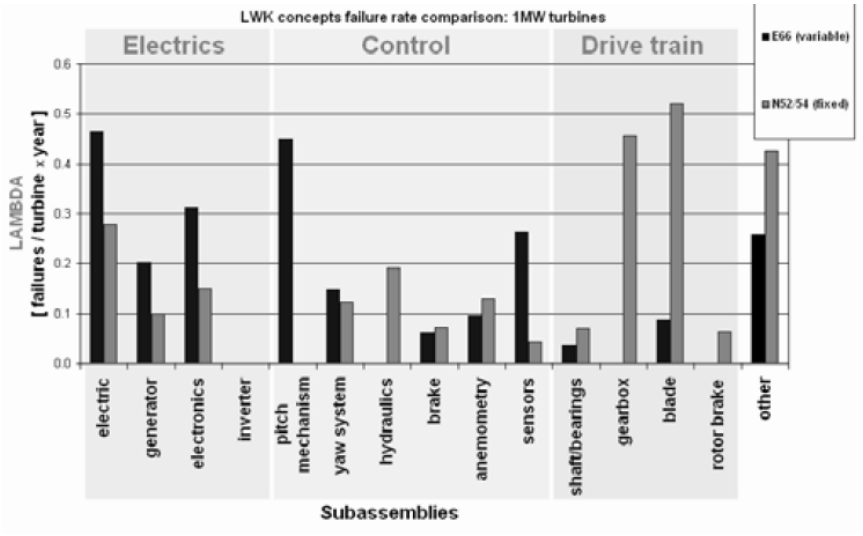

Figure 2-6: LWK concepts failure rate comparison 1MW turbines [2-30]

The conclusion to the research undertaken by Tavner et al into the various concepts was that there were positives and negatives for each configuration. Gains in reliability made in one area inevitably led to sacrifices in another [2-30].

Echavarria and her colleagues like Tavner and his, was also interested in how WT reliability changed over time, and how this changed depending on WT configuration. She instead used the WMEP database which, like the LWK database, recorded the models and concepts of WTs [2-14], [2-31].

By examining individual components Echavarria attempted to understand how the reliability of major components advanced over time and what technologies present in the WMEP database worked most effectively [2-2], [2-31].

The WMEP database comprised of a fixed population turbines of a variety of sizes and ages. Figure 2-7 shows the three size categories of WT with their corresponding failure rates during each recorded year of operation [2-2], [2-31]. The smallest category (less than 500kW) had a relatively constant failure rate throughout this recorded period, while the larger categories (which were made up of many of the newer, more complex turbines)

showed a decrease in failure rate from year one to year six, but then a large amount of failures for years seven and eight. The multi-megawatt turbines were some of the first of their kind to be installed and therefore suffered many early life failures which tend to come from new technologies [2-2], [2-31]. The increase in failure rate in years seven and eight may have been because of a serial defect. The smaller turbines were older and were of a more simplistic design, therefore because of their age and their reliability the failure rate was low and relatively constant throughout the recorded period [2-2], [2-14], [2-31].

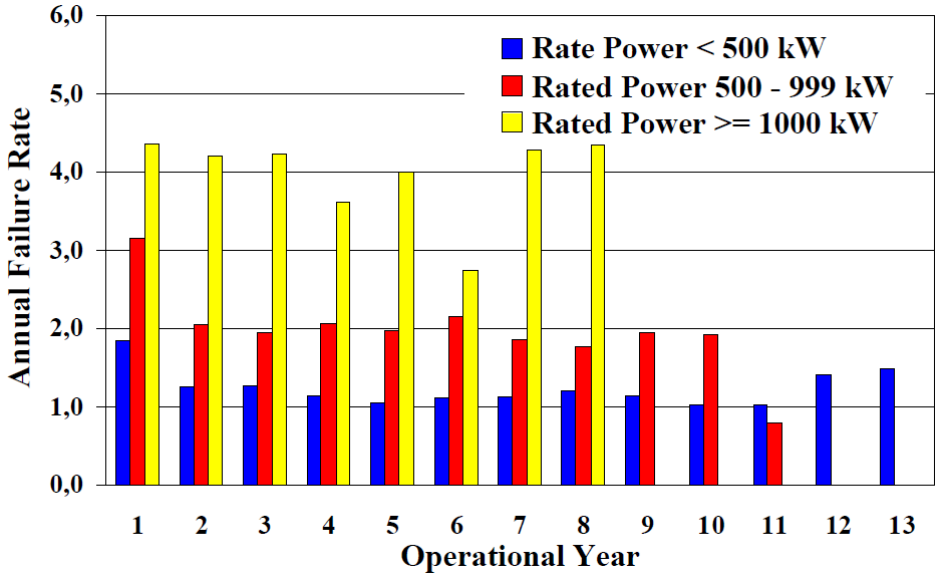

Figure 2-7: Catagorised annual failure rates for WMEP dataset for each operational year [2-2]

Figure 2-8 shows the annual number of exchanges of component in the WMEP database [2-2]. The blades and the generator are the two most exchanged components [2-2]. This is because the WMEP database is made up of many WTs with synchronous generators that fail often and stall regulated turbines which experience many blade failures.

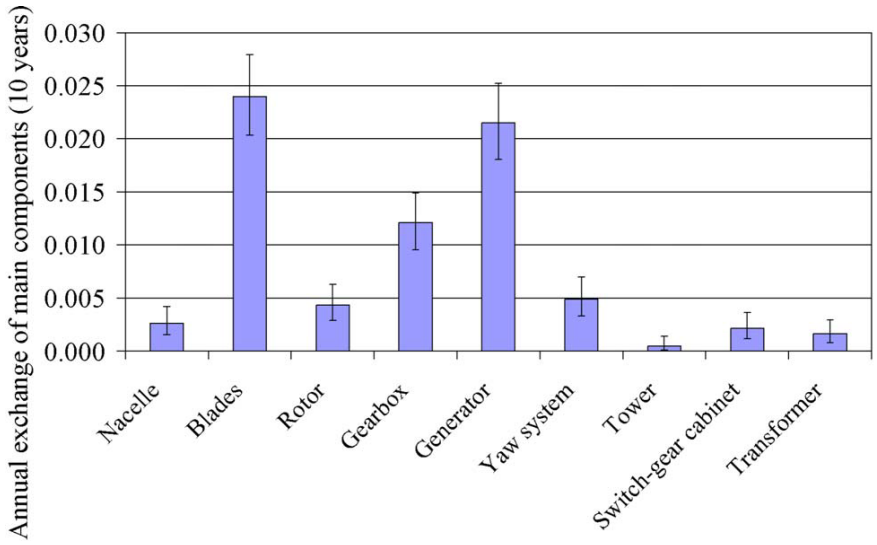

Figure 2-8: Annual exchanges of main components for WMEP database [2-2]

Despite the blades being replaced so frequently in stall regulated turbines the pitch regulated WTs in the database are actually less reliable as shown in Figure 2-9 [2-2]. This is because the pitch system and the rotor (without the blades) fails frequently on the pitch regulated WTs [2-2].

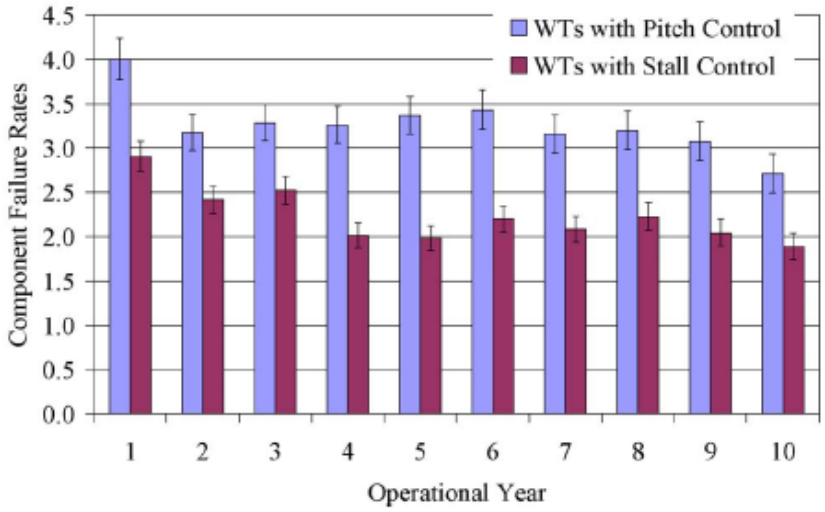

Figure 2-9: Component failure rates throughout operation of WMEP database for pitch and stall regulated WTs [2-2]

Echavarria and her colleagues assessed the reliability of the different types of generators in her dataset. The majority were induction generators, the rest were synchronous generators. Of the synchronous generators, 20% were direct drive WTs [2-2], [2-31]. They found the synchronous generators to have higher annual failures than the induction generators – as shown in Figure 2-10 – but that also their reliability improved over time [2-31].

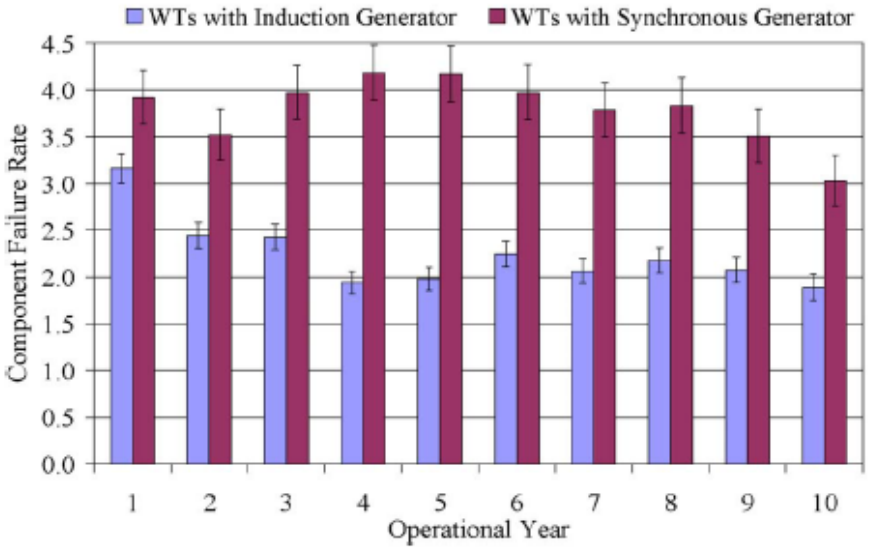

Figure 2-10: Component failure rates throughout operation of WMEP database for induction and synchronous generators [2-2]

This corroborated well with Tavner's conclusions in [2-30], which also found that German turbines – of which many had synchronous generators – failed more often but got more reliable over time.

In general the direct drive WTs were the least reliable in the WMEP dataset, followed by the geared synchronous generator WT and then the geared induction generator WTs which were the most reliable, as illustrated in Figure 2-11 [2-2].

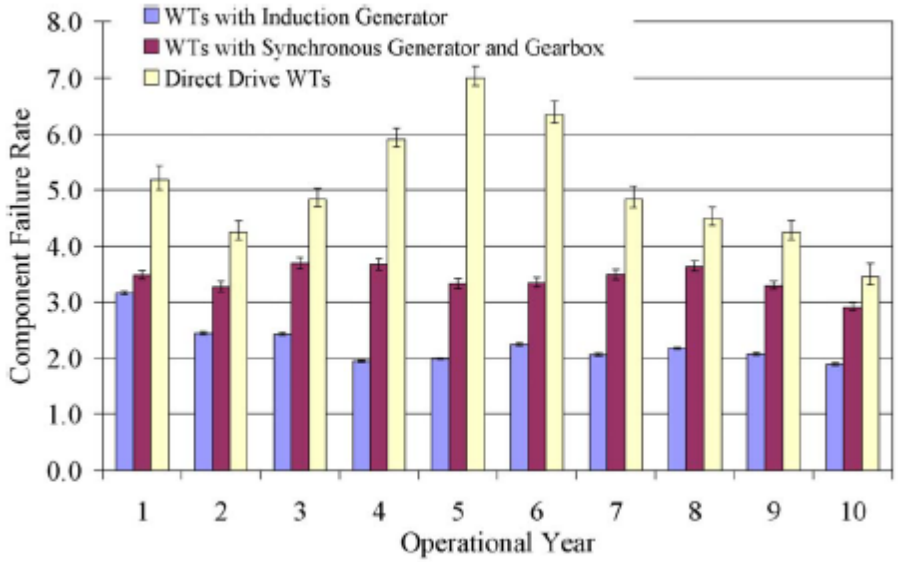

Figure 2-11: Component failure rates throughout operation of WMEP database for induction drive, direct drive and synchronous generators [2-2]

Power electronics were also found to be less reliable in the synchronous generator which again corroborates with Tavner's work with van Bussel and Spinato in [2-30]. Echavarria and her colleagues found that around half of the failures found in their German dataset were due to control systems and electronics [2-31].

With Echavarria's research taking a more in depth look at the individual components and how they performed in different types of WT, Spinato published a paper in 2009 with Tavner, van Bussel and Koutoulakos which looked specifically at the reliability of WT components [2-1].

As with previous research they found that the older, simpler, Danish WTs were the most reliable WTs. But it was clear from Figure 2-12 that this wasn't just for the system as a whole, but also for each component [2-1].

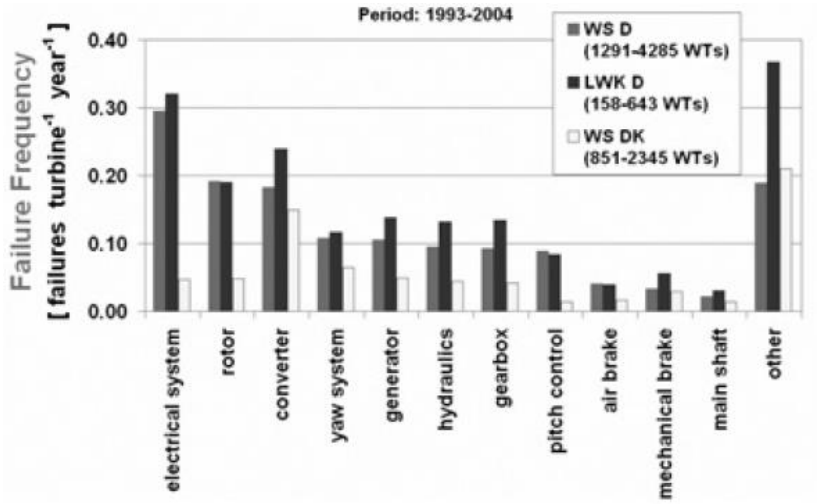

Figure 2-12: Failure rates of components from Windstats database and LWK [2-1]

Spinato and his colleagues found the most unreliable components to be, in descending order of magnitude to be the electrical system, rotor, converter, generator, hydraulics and finally the gearbox [2-1]. However, when taking into account the resultant downtime from each component from the LWK database, shown in Figure 2-13, it was clear that in the LWK case, the gearbox, generator and electrical system were the largest contributors to the mean time to repair MTTR [2-1].

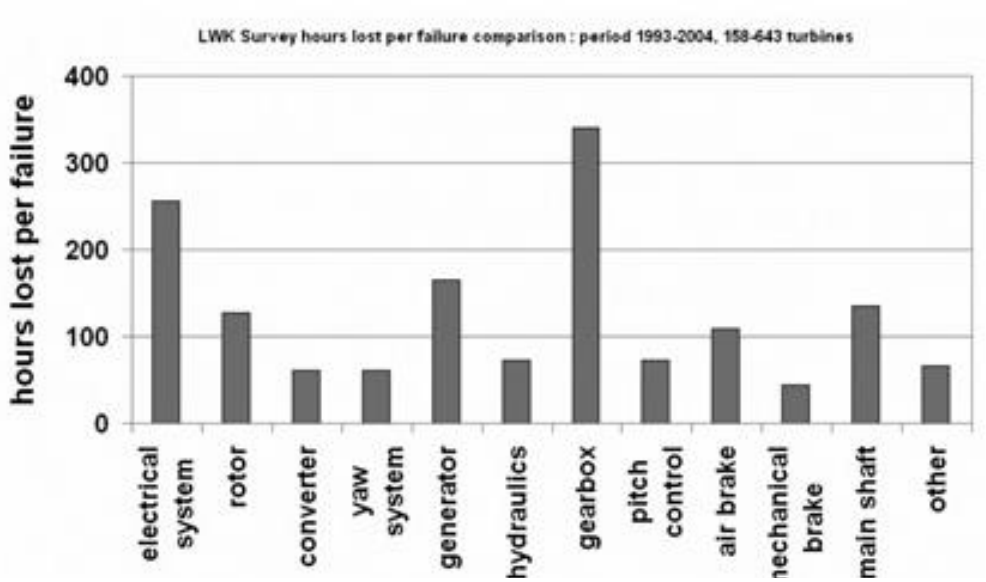

Figure 2-13: LWK survey hours lost per failure comparison for each component [2-1]

This conclusion was also reached by Ribrant and Bertling in their analysis of a Swedish WT dataset which came from two different sources which overlapped each other and comprised of roughly 780 WTs [2-20]. One of the sources was the Elforsk database [2-18].

The most frequently failed subassembly in their dataset was also the electrical system which accounted for 17.5% of the failures from 2000 – 2004 [2-20]. However in terms of downtime, the gearbox was the most troublesome component, taking 19.4% of the downtime and contributing over 11.6 hours of downtime per WT, per year [2-20].

Ribrant and Bertling found that the average gearbox failure took 256 hours to repair [2-20]. Table 2-5 presents details of the gearbox failures in the dataset between 1997 and 2004 [2-20]. Interestingly, the frequency of gearbox failures decreases over time while the average downtime per failure increases. This is most likely because major failures are occurring after the WT has been operating for several years, while the minor failures occur early in the life of the gearbox and then decrease over time.

Table 2-5: Gearbox Failures in Elforsk Dataset between 1997 – 2004 [2-20]

Year	1997	1998	1999	2000	2001	2002	2003	2004	1997-2004
Number of Failures	21	41	52	26	30	42	13	7	232
Total downtime (hours)	4031	2518	5061	6172	5228	12589	3987	2309	41895
Average downtime per failure	192	61	97	237	174	300	307	330	181
Percentage of total downtime (%)	9.4	5.3	7.3	15.5	13.6	33.5	14.8	17.4	14.6

The authors examined the subcomponents within the gearbox; their data is shown in Table 2-6 [2-20]. The last row represents failures where no subcomponent has been specified; Ribrant and Bertling noted that half of these correspond to serious failures which have resulted in the whole gearbox being replaced [2-20]. They also noted that most bearing

failures required a replacement gearbox or all gearbox bearings [2-20]. B1 corresponds to failure caused by wear; this is the most frequent cause of failure in the gearbox.

Table 2-6: Gearbox Subcomponents Failure Data from Elforsk Dataset [2-20]

Component	Number of Failures	Average Downtime (hours)	Number of Failure Cause: B1	Average downtime Cause: B1 (hours)
Bearings	41	562	36	601
Gearwheels	3	272	2	379
Shaft	0	0	0	0
Sealing	8	52	4	30
Oil System	13	26	5	36
Not Specified	44	230	19	299

Table 2-7: Comparison of Swedish, German and Finish WTs Failure Data [2-20]

Country	**Sweden**	**Finland**	**Germany**
Average Number of failures per turbine	0.402	1.38	2.38
Average downtime per year	52	237	149
Average downtime per failure (hours)	170	172	62.6
Most frequent failures	1. Electrical Systems 2. Sensors 3. Blades/Pitch	1. Hydraulics 2. Blades/Pitch 3. Gears	1. Electrical System 2. Control System 3. Hydraulics/ Sensors
Most amount of downtime	1. Gears 2. Control system 3. Electrical system	1. Gears 2. Blades/Pitch 3. Hydraulics	1. Generators 2. Gears 3. Drive Train
Longest downtime per failure	1. Drive Train 2. Yaw system 3. Gears	1. Gears 2. Blades/Pitch 3. Structure	1. Generators 2. Gears 3. Drive Train

The authors compared their Swedish data with statistics from Germany and Finland; this is presented in Table 2-7 [2-20]. Interestingly they found German turbines to be the most unreliable but have the lowest downtime per failure, while Swedish turbines were the most reliable but experienced long periods of downtime per failure [2-20]. The low downtime in

Germany was attributed by Ribrant and Bertling to "…a better and nearer service organisation…" [2-20]. It is interesting to note that the German survey showed a high number of generator failures, this may be due to the high number of direct drive WTs present in the survey.

The comparative differences in reliability between direct drive and indirect drive WTs was researched further by McMillan and Ault [2-32]. They developed a Markov Chain Monte Carlo Simulation model for calculating the merits of direct drive and indirect drive turbines. Models like this had been used previously by [2-5], [2-25], [2-33], [2-34]. Using failure rates and repair rates from [2-2], [2-3]. McMillan and Ault's calculations found that technically, direct drive and indirect drive turbines could achieve very similar availabilities, with direct drive being slightly better, this is shown in Figure 2-14 [2-32].

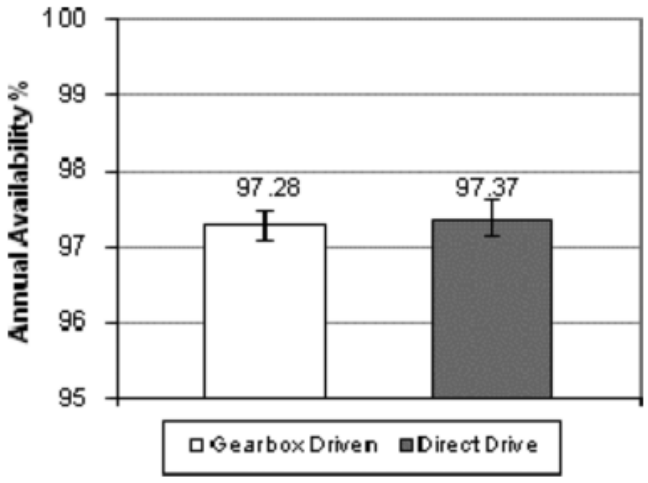

Figure 2-14: Comparison of annual availability of direct drive and gearbox driven WTs [2-32]

However, economically they found that a direct drive turbine did not produce as good a revenue as a geared turbine [2-32]. A direct drive turbine would produce £237k a year, whereas an equivalent geared turbine would produce £291k [2-32]. This difference was attributed to the higher repair and replacement costs for the direct drive concept. The costs for each of the components they were using in their model are found in Table 2-8 [2-32].

Table 2-8: Component Costs Used In Model [2-32]

Component	Indirect Drive (£)	Direct Drive (£)
Gearbox	121,733	N/A
Generator	177,066	313,740
Rotor	210,000	210,000
Electronics	22,133	66,400

However, McMillan and Ault found that if their assumptions of repair rate for the synchronous generator improved sufficiently the direct drive turbine would achieve even greater availability and improve its annual revenue [2-32]. Many generator failures are minor electrical faults that can be easy fixed rather than severe mechanical failures experienced by gearboxes that cause long periods of downtime [2-32].

Despite lots of research currently being undertaken to improve and understand gearbox reliability – for example [2-35]–[2-37] – Spinato makes a very good point that gearbox reliability may not be able to be improved upon as the reliability of gearboxes in other industries is similar to the WT industry [2-1]. Therefore the best solution in improving WT reliability may be improving the reliability of direct drive generators. This may be most advantageous offshore, where the rules of operation and maintenance change significantly.

3.3. Offshore Reliability

In 1999 the Dutch Offshore Wind Energy Converter (DOWEC) project began with the goal to develop technology and concepts which would make large scale offshore wind farms economically viable [2-38]. At this time offshore wind farms were very small (less than 40MW) and were many based in the Baltic Sea, close to shore.

DOWEC recognised that the levels of reliability achieved at that time onshore (approximately 98%) would be very difficult to achieve offshore. Van Bussel and Zaaijer acknowledged that the availability that could be achieved offshore would be determined by the optimal cost expenditure on O&M [2-39]. This problem is illustrated Figure 2-15 which shows the point at which the lifetime cost of O&M is greater than the value of the energy that could be generated with the additional availability. The only way to increase availability economically beyond this point is improve the quality of O&M strategy, without increasing lifetime costs. In Figure 2-15 this would have the effect of reducing the gradient of the direct cost of O&M line.

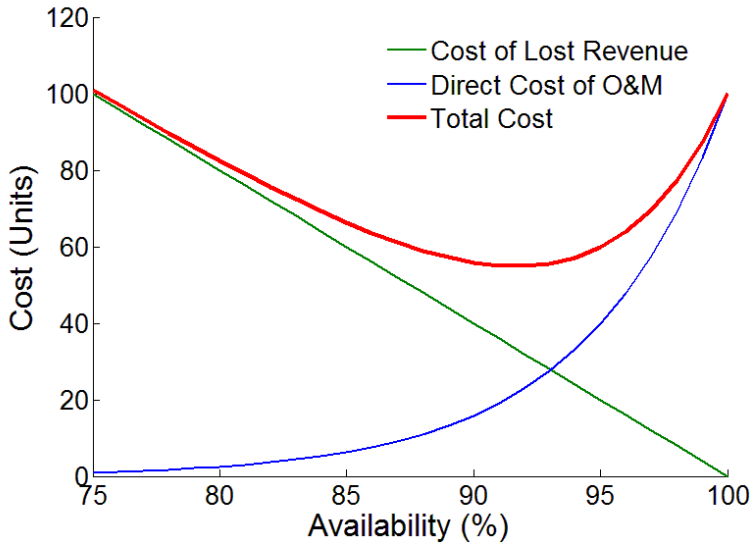

Figure 2-15: The optimum total cost of O&M

One way to reduce the cost of O&M is to decrease the failure rate of the system. Therefore Van Bussel and Zaaijer sought to look at current onshore technology and try to find a concept which was reliable enough that it would be suitable for use offshore.

Using two data sources, Van Bussel and Zaaijer calculated the failure rate for a typical onshore WT. The data, which originates mainly from the northern coast of Germany and contained many small turbines that would never be sited offshore, is shown in the second column of Table 2-9 [2-39].

Table 2-9: Failure Rates for WT Components

Component	Onshore λ (failures/year)	Reduced λ (failures/year)
Shaft & Bearings	0.02	0.02
Brake	0.05	0.05
Generator	0.05	0.05
Parking Brake	0.05	0.05
Electric	0.14	0.10
Blade	0.16	0.11
Yaw System	0.23	0.15
Blade Tips	0.28	0.14
Pitch Mechanism	0.28	0.14
Gearbox	0.30	0.15
Inverter	0.32	0.16
Control	0.34	0.17
Total	**2.20**	**1.28**

The authors recognised that a failure rate of 2.20 would not be suitable offshore [2-39]. Two failures per turbine year and a further two other scheduled downtimes for planned maintenance could mean 800 trips annually to an offshore wind farm of 200 WTs. Research using other data sources has shown that onshore WT were capable in 2001 of improved reliability [2-3], [2-20]. However like the dataset used by Van Bussel and Zaaijer, these WTs were much smaller than WTs which would be sited offshore, their reliability would therefore be better than the larger, more complex offshore machines [2-39].

Van Bussel and Zaaijer used their reliability data to assign failure rates to six alternative WT concepts which they then evaluated [2-39]. The six concepts investigated are dated by comparison to the concepts used today by the major manufacturers. Siemens and Vestas were traditionally users of indirect drive, wound rotor induction generators for their onshore models. But in 2013 Siemens installed their first direct drive permanent magnet WT offshore [2-40]. While also in 2013 Vestas (and their joint venture partners Mitsubishi Heavy Industry) announced that their offshore concept would also use a permanent magnet generator as they believed this would improve reliability [2-41].

Tavner undertook an assessment on WT concepts in 2008. Using the same data they had used in their 2006 and 2007 papers, they assessed the different WT concepts present in their LWK dataset with relevance to offshore use [2-42]. They came to the conclusion that direct drive WTs may produce a higher availability offshore because it removes the long MTTR caused by the gearbox [2-1], [2-42]. Indeed if the direct drive WT concept assessed by Van Bussel and Zaaijer were to improve on its electronics and generator reliability, its failure rate would reduce significantly and their results may have been different [2-39].

Interestingly, the first offshore WTs widely deployed in UK offshore waters added weight to this argument. The Capital Grants Scheme was launched in 2001 by the Department of Trade and Industry. Its aim was to help nurture the growth of an offshore wind industry in the UK and it attempted to do this by supporting medium scale projects in shallow UK waters. Five projects in England were supported; their total installed capacity was 390 MW. Table 2-10 gives a summary of each of the sites [2-43].

Table 2-10: Summary of Round 1 offshore wind farm sites supported by Capital Grants Scheme [2-43]

Location	Capacity (MW)	WT Model	Water Depth (m)	Distance from centre of wind farm to shore (km)	Operator
North Hoyle	**60**	**Vestas V80**	**7-11**	**9.2**	**RWE npower**
Scroby Sands	**60**	**Vestas V80**	**5-10**	**3.6**	**E.on**
Kentish Flats	**90**	**Vestas V90**	**5**	**9.8**	**Vattenfall**
Barrow	**90**	**Vestas V90**	**15-20**	**12.8**	**Centrica/Dong**
Burbo Bank	**90**	**SWT – 3.6 - 107**	**2-8**	**8**	**Dong**

With the exception of Burbo Bank, the other four sites all used Vestas V80/90 WTs. These turbines are variable speed, pitch controlled WTs, which use a gearbox and a doubly fed induction generator (DFIG). As a requirement the operators of North Hoyle, Scroby Sands, Kentish Flats and Barrow had to publish their operational data annually. The reports consist of wind speed, performance and operational data [2-44].

All four sites suffered from severe gearbox reliability. The WTs were originally designed for use onshore, the modifications made to them so they could be deployed offshore was minimal [2-43]. The average availabilities for the four sites was 80.2%, the lowest of which was Barrow with an availability of 67.4% over the single year that its data was published [2-43], [2-44]. The gearboxes on all four sites suffered from bearing failure in the planetary gears, as a result a retrofit program was organised and all the gearboxes were overhauled and replaced [2-43]. Despite this, the average capacity factor for all four sites was 29.5% - the best performing site was North Hoyle which had an average capacity factor over 3 years of 35% [2-43], [2-44]. A significant reason for its high performance - its availability was the highest of the sites at 87.7% - was because the gearboxes were not entirely replaced over a three year period during which the capital grants scheme published its data [2-43].

Another project that published its operational data was the Dutch offshore wind farm Egmond Aan Zee. From 2007 – 2009 it produced annual reports detailing monthly production and availability, component failures and resultant downtimes. It too suffered severe gearbox failures and over the three year period of reporting overhauled each gearbox

in their fleet [2-45]. They too used the Vestas V90 WT and installed 36 of them, in 30 m deep waters, 10 km from shore [2-45], [2-46]. Over the reported period, Egmond Aan Zee achieved an availability of 80% [2-45]. This was mainly because of failures and resultant downtime caused by the gearbox. On average the gearbox contributed to 55% of the total downtime, as shown in Figure 2-16 [2-45].

The downtime data from Egmond Aan Zee is similar to that from the onshore LWK database, analysed by Tavner and his team, shown in Figure 2-13 [2-42]. The gearbox, electrical system/control system and the generator are the components which cause the most downtime for both datasets. For the offshore turbines on Egmond Aan Zee however the gearbox dominated the downtime much more. This difference may be due to the effects of the offshore conditions and the different O&M strategies, but it is also likely to be partially due to the different models of WTs in each dataset. The LWK dataset as mentioned before contained direct drive turbines which have less reliable generators and electronics and no gearboxes.

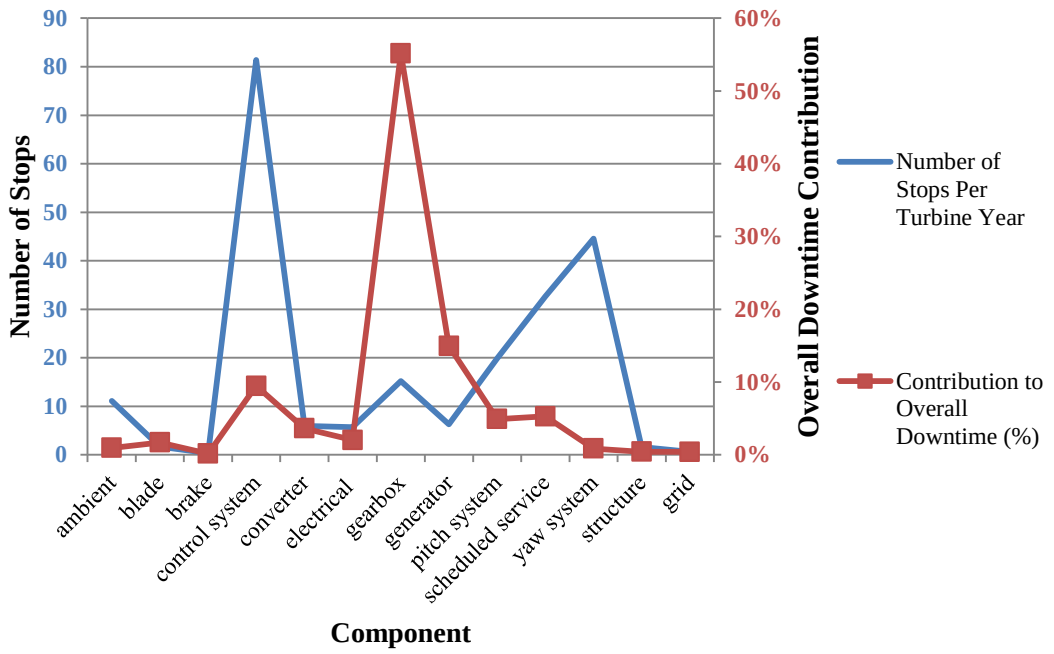

Figure 2-16: Reliability of components at Egmond Aan Zee between 2007 - 2009

The impact of logistics on downtime can be demonstrated in Figure 2-17, which shows the average downtime when a single failure occurred to a component on Egmond Aan Zee. Large components that required a lifting vessel dominated the downtime. Interestingly the average time taken for scheduled maintenance was approximately 3 hours – this equated to 5% of the downtime, as shown in Figure 2-16.

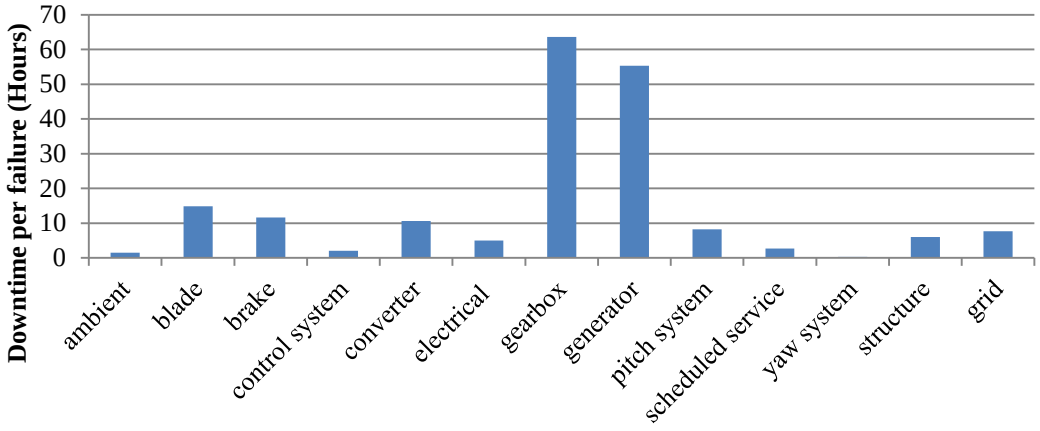

Figure 2-17: Average downtime per component failure at Egmond Aan Zee 2007 - 2009

It is important to note that for all the offshore wind farms discussed, the same WT model was used which suffered from a serial gearbox fault, which required replacement and heavy lift vessels. After reporting for the Capital Grant Scheme stopped at the end of 2007, the capacity factors for the UK offshore sites increased, as shown in Table 2-11, to an average of 33.3% [2-46]. For each site with the exception of North Hoyle this was an improvement, however the capacity factor is influenced by the wind resource and the logistics that year, as well as the reliability. The data for Egmond Aan Zee is not available after 2009.

Table 2-11: Capacity factors for UK offshore wind farms 2008 – 2012 [2-43]

	Capacity Factor (%)					
Wind Farm	2008	2009	2010	2011	2012	Mean
Barrow	39.7	34.2	30.7	40.7	38.2	36.7
Kentish Flats	33.6	29.5	31.0	34.8	32.6	32.3
North Hoyle	36.1	36.2	27.2	32.2	34.7	33.3
Scroby Sands	29.9	32.2	28.2	32.7	32.4	31.1

Despite improvements in reliability it is still interesting to observe the logistical issues that occurred when a major component failed. The consequential downtime which typically resulted from a failed offshore gearbox included the following [2-43]:

1. the time taken to diagnose the failure
2. the time taken to decide how to respond to the failure
3. ordering time for components
4. waiting for a heavy lifting vessel
5. waiting for a safe access window
6. transit time to the wind farm
7. time spent waiting for safe conditions to perform maintenance (see Table 2-12 [2-34])
8. performing maintenance actions

This procedure was not just isolated to gearboxes; it was the same for any major component whose repair or replacement required a heavy lifting vessel. In fact, even for a component which did not require a heavy lifting vessel, the other steps still applied and added significantly to the overall downtime.

Table 2-12: Maintenance Weather Constraints [2-34]

Wind Speed (m/s)	Restrictions
>30	No access to site
>20	No climbing WTs
>18	No opening roof doors fully
>15	No working on roof of nacelle
>12	No going into hub
>10	No lifting roof of nacelle
>7	No blade removal
>5	No climbing met masts

Logistics are vitally important offshore. If a failure occurs in winter when the weather is likely to be hostile, the WT can be down for as long as it takes for a safe weather window to

open, regardless of the failure and whether the equipment required to repair it is available [2-47]. With this issue in mind, Van Bussel and Henderson tried to examine what areas could be improved upon to cope better with the harsh offshore environment and improve downtime and availability [2-48].

The authors observed that the accessibility of a site could determine the economic viability of a project [2-48]. Figure 2-18 was developed from results taken from an earlier project, which evaluated the O&M costs for a 100 unit wind farm site [2-49]. It shows how dramatically the achievable availability falls as the accessibility is reduced.

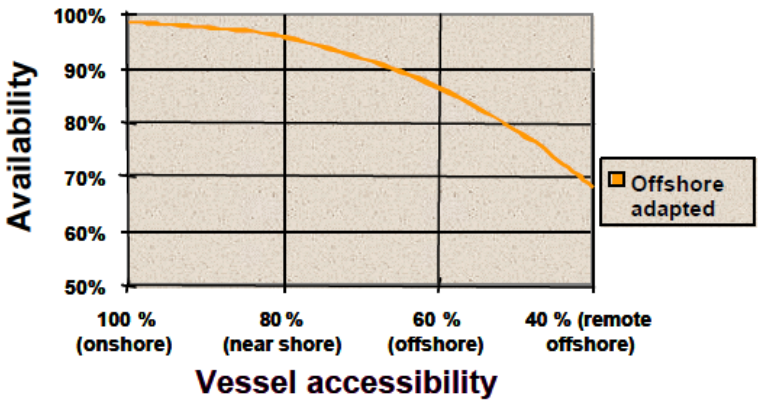

Figure 2-18: Comparison between vassel accessability and WT availability offshore [2-48]

To improve availability Van Bussel and Henderson recommended four areas of focus [2-48]:

- Access methods
- Lifting facilities
- Maintenance strategies
- O&M modelling

Van Bussel and Henderson recognised in 2001 that access had to be less sensitive to the wind and wave conditions [2-48]. Building a walkway from a vessel to a turbine that was able to safely transfer personnel in harsh conditions would be hugely advantageous.

Walkways such as this have been developed by several companies in recent years that allow the safe transfer of personnel during periods which hitherto would have been unsafe to work in [2-50]. Research from Feuchtwang and Infield looked at the impact of access on availability; they found that component repair times actually had a greater impact on downtime than failure rates. They also believed that the gearbox, generator and blades would have the greatest impact on availability as they required lifting vessels which were restricted by the sea state [2-47].

Lifting facilities are easy to come by onshore, however offshore they are very expensive as discussed by Van Bussel and Zaaijer [2-39]. The period over which a vessel can be hired depends on many issues, some of which are: where the vessel is sailing from originally; the time of year; the distance from land to shore; the activity required to be undertaken by the vessel; and the competition in the market for vessels from other wind farms and oil and gas companies [2-51]. Van Bussel and Henderson predicted that once the lifting height exceeded 80 m offshore, costs would become a serious problem. More recently McMillan and Dinwoodie have reached a similar conclusion, that the costs of heavy lifting vessels will become a serious issue as more offshore wind farms begin to be installed, leaving a shortage of available vessels to undertake O&M for operating wind farms, thus increasing the demand and the cost [2-52].

The strategies used to maintain offshore WTs originally were very similar to those employed onshore. However, because of access constraints and the costs involved in vessel hire discussed above, condition monitoring was recommended by Van Bussel and Henderson so that journeys could be planned in advance with the foresight of a particular failure likely to occur [2-48]. By planning journeys in advance, vessels could be booked ahead of time (if required) for a period of time when access was likely, spare components could be sourced and lost energy could be minimised by fixing any problems before they cause a failure [2-34].

The economic argument of installing condition monitoring systems offshore was discussed by McMillan and Ault [2-34]. Using discrete-time Markov Chain Monte Carlo simulation and assuming the offshore maintenance weather constraints, shown in Table 2-12, they concluded that the benefit of installing a condition monitoring system depended on the cost of implementing the system and its accuracy [2-34]. The system would have to be accurate in 60% to 80% of cases for it to be an economical option [2-34]. However the authors doubted whether condition monitoring systems would be able to achieve this level of accuracy offshore [2-34].

However more recent work undertaken by Besnard and Bertling has argued that condition monitoring, of at least the drive train and the blades, is economically beneficial [2-33]. Further research was undertaken by Nilsson and Bertling to assess the life cycle cost of a condition monitoring system installed for an offshore wind farm. They found that improvements to maintenance planning could be made using the condition monitoring system and that the improved performance of the offshore wind farm would justify the cost of the system.

Many issues identified in the research touch upon the impact of the environment on WT reliability. The following section will explore this area of research in more detail by discussing research which is closely aligned with the focus of this thesis.

3.4. Research Focusing on the Effects of Wind Speed on WT Reliability

The effects of wind speed on WT reliability were addressed by Hahn in 1997 [2-53]. Using WMEP data Hahn demonstrated that there was a relationship between the average daily wind speed and the number of failures per day in some of the WT components within his dataset. This is shown in Figure 2-19 [2-53].

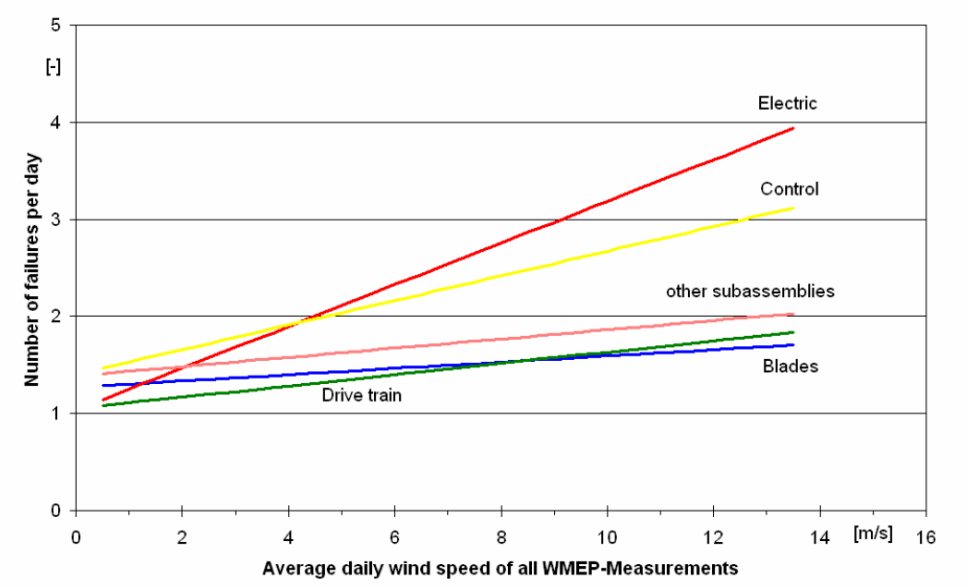

Figure 2-19: Number of failures per day against average daily wind speed using WMEP data [2-53]

Tavner and his colleagues then carried out analysis in 2006 using Windstats data which they hoped would determine if there were was a relationship between failure rate and wind energy index (WEI) [2-54]. The WEI is a measurement that describes the wind speed across the whole of Denmark, by using this index Tavner assumed that the WTs in the Danish Windstats database were distributed uniformly throughout the country [2-54]. Their results compared the average monthly failure rate of the WTs in the dataset between 1994 – 2004 and the WEI for each month in Denmark between the same time period [2-54].

Despite showing a convincing relationship between failure rate and wind speed, the results from Tavner's analysis, by his own admission, were rather simplistic. The Windstats database, as previously discussed, contained lots of different models of WT. As a result a

large degree of underlying detail was lost in the analysis. Assuming that the wind speed across the whole of Denmark was representative of wind speeds experienced on each site was also inaccurate.

In 2010, Tavner and his colleagues built on their earlier work to discover if a relationship existed between wind speed and failure rate [2-55]. To correct the failings of their previous paper the authors this time looked at three individual wind farms in Germany, all with the same WT model, and used weather data from sites sited close to the wind farms. In total their dataset had roughly 202 WT years of data from the WMEPs database [2-14], [2-55].

The three sites were:

- Fehmarn – located on the Baltic Sea coast.
- Krummhorn – Located on the North Sea coast.
- Ormont – located in the highlands in Rhineland Palatinate.

The WTs used on the sites were a mixture of Enercon E30 and E33's. Both concepts were rated at 300kW, had synchronous wound rotors, were variable speed, hydraulic blade pitch controlled and were manufactured from 1988 – 1993. They were the last geared turbines to be produced by Enercon before they switched exclusively to direct drive WTs [2-55].

Similar analysis to Tavner's previous paper on the subject was carried out initially on the German data site by site. However, they showed little evidence of a relationship between WEI and failure rate, unlike the Danish data [2-54], [2-55]. A more detailed analysis was undertaken which considered the cross correlation between particular meteorological parameters and WT failures. The results of this analysis are shown in Table 2-13 [2-55].

Krummhoern had limited cross-correlations because there was no weather station on site [2-55]. The most closely correlated functions were the maximum wind speed and failures [2-55].

Table 2-13: Cross-Correlation Coefficients for German Wind Farm Sites [2-55]

Cross-Correlation	Cross Correlation Coefficients at zero Lag					
	Fehmarn		Krummhoern		Ormont	
	Daily Aggregation	Monthly Aggregation	Daily Aggregation	Monthly Aggregation	Daily Aggregation	Monthly Aggregation
Maximum Wind Speed/Failures	0.23	0.76	0.3	0.76	0.1	0.56
Mean Wind Speed/Failures	0.22	0.74	-	-	0.13	0.55
Standard Deviation of Wind Speed/Failures	0.22	0.73	-	-	0.13	0.57
Temperatures Variation/Failures	0.2	0.68	0.26	0.76	0.13	0.56
Humidity/Failures	0.22	0.73	0.3	0.75	0.13	0.55
Maximum Wind Speed/Standard Deviation of Wind Speed	-	0.99	-	-	-	0.99

Overall there was a significant cross-correlation (55 – 75%) between the weather data and the failure data for each of the sites [2-55]. And the high cross correlations at all three sites with temperature and humidity as well wind speed standard deviation suggested that the true correlation may lie between failure rate and changes in the weather [2-55].

In 2013 the authors published a second paper to update their results, using the same methodology and almost the same dataset [2-56]. This time they looked briefly at the effects of seasonal weather on specific subcomponents. They concluded that humidity had more of an effect on electrical components than on mechanical components [2-56]. They also observed that the WTs in their dataset confirmed engineering experience that electrical subassemblies were more prone to the effects of varying temperatures than mechanical [2-56].

Michael Wilkinson, from the renewable energy consultants GL Garrad Hassan, and his colleagues investigated the effects of the environment on downtime and failure rates [2-57]. Using the GL Garrad Hassan WT database – which contained more than 23,000 WTs – Wilkinson used SCADA Alarm Logs and availability databases to determine the impact of the environment on WT failure rates [2-57].

Their analysis of monthly mean wind speed and temperatures, from their availability data, matched the results that Tavner and his colleagues produced in 2006 that showed there had been more downtime in the winter months when wind speed was higher on average and the temperature was lower [2-54], [2-57]. Wilkinson's analysis is shown in Figure 2-20 and Figure 2-21.

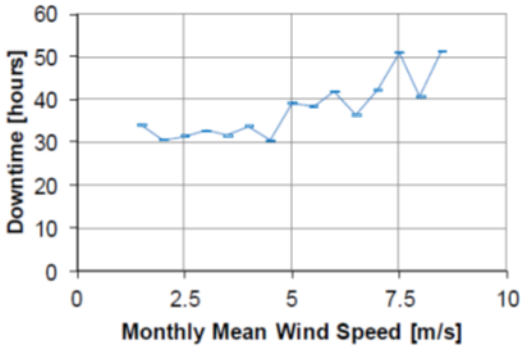

Figure 2-20: Monthly mean wind speed against average downtime [2-57]

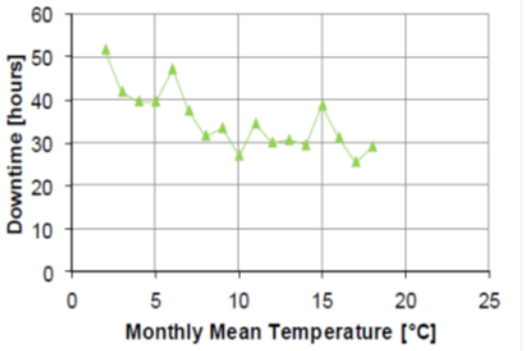

Figure 2-21: Monthly mean temperature against average downtime [2-57]

The SCADA Alarm Log data, shown in Figure 2-22 and Figure 2-23, also showed similar results [2-57]. Although there was a peak around 18°C, both in the alarm log frequency and duration, indicating that lots of failures occurred at 18°C lasting for a long period of time. This may be because the high ambient temperatures caused sensors within the WT to set the alarm off, possibly because the nacelle became very hot inside. It seems unlikely that the high temperatures caused actual failures to occur to components which resulted in downtime – as Figure 2-24 demonstrated; months with high mean temperatures had short downtimes in the availability data of the same wind farms.

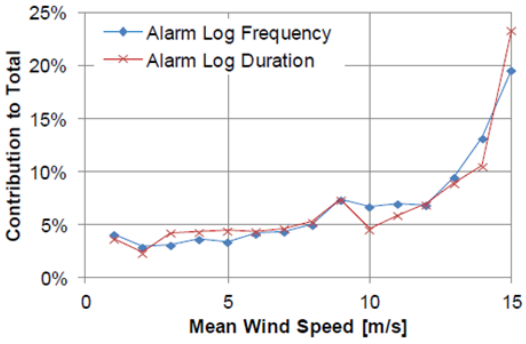

Figure 2-22: Relationship between mean wind speed and SCADA alarm log frequency and duration [2-57]

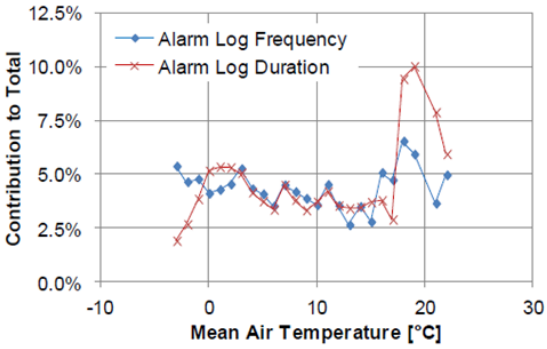

Figure 2-23: Relationship between mean air temperature and SCADA alarm log frequency and duration [2-57]

Figure 2-24 shows the relationship between maximum wind speed and maximum air temperature correlation with failure rate and downtime of the WT [2-57]. It appears from Wilkinson's results that extreme maximum air temperatures, as well as maximum wind speeds of between 28 – 33m/s, cause rises in failure rate and downtime.

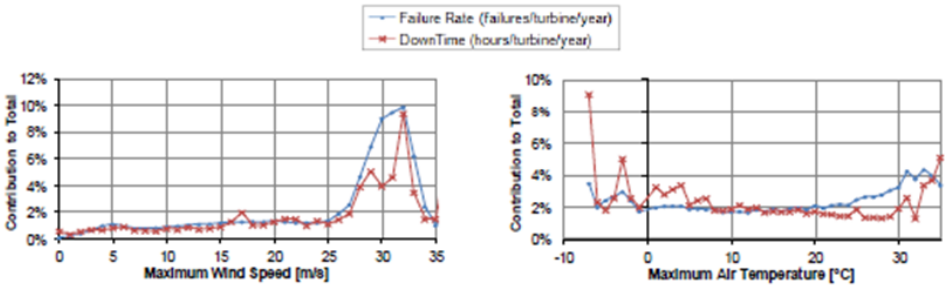

Figure 2-24: Maximum wind speed and air temperature correlation with failure rate and downtime [2-57]

Therefore results from Wilkinson et al would suggest that there is a clear relationship between temperature, wind speed, failure rate and downtime [2-57]. However, there are a number of areas where this could be disputed.

- It is not clear whether inspections, retrofits and scheduled maintenance were included in the availability database. This is important as these operations can only take place when the wind speed is below a certain threshold which means it is safe to climb the turbine.

- Many failures can only be detected by inspection, it is not clear if the failures in this database are recorded to have failed on the date of inspection or the date the SCADA system or condition monitoring detected a failure. If the failure was recorded on the day of inspection this would skew the results to show failures occurring in accessible turbine conditions.
- And Figure 2-24 implies that failures at higher wind speeds and lower temperatures are more severe as they have longer downtimes. However it could be argued that these figures merely show that WTs are more inaccessible in higher wind speeds. High average monthly wind speeds and low average monthly temperatures correlate well as shown in Figure 2-25 [2-57].

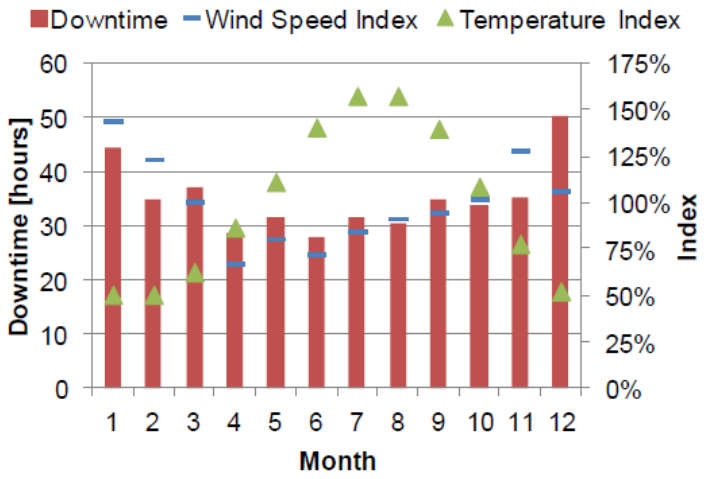

Figure 2-25: Seasonal wind speed and temperature trends against average WT downtime from GL Garrad Hassan database [2-57]

- It is not clear what has to happen for a SCADA alarm to be switched off. If a visual inspection is required this duration will depend on the weather conditions and will affect the results. For instance if the alarm is raised in the winter when the mean wind speed tends to be high, it is reasonable then to assume that downtime will increase due to the accessibility of the turbine.

4. Chapter 2 Summary

Reliability analysis theory was introduced in Chapter 2.1. The failure rate, repair rates and availability are calculated using Equation 2-1, Equation 2-2 and Equation 2-3. These metrics will be used throughout this thesis in describing system reliability.

Reliability databases that have been frequently used in the literature include WindStats Germany and Denmark, LWK, WMEP, VTT and Elforsk. All six databases are comprised of onshore WTs or vary sizes and models. The databases are all classified differently and do not follow a consistent taxonomy. According to these databases the component that fails most frequently is the control system – sometimes classified as the electric system. However the component that causes the longest downtime when it fails is the gearbox.

WT reliability literature was examined in Chapter 2.3. The availability of an onshore WT is typically 97% - 99%; the downtime includes preventive and corrective maintenance [2-48]. System failure rates vary from 2.20 – 0.43 failures per WT year [2-3], [2-39]. It has been found that WT reliability improves after installation, following a bathtub type curve [2-3].

The logistical issues associated with offshore WTs means that availability is likely to be reduced compared to onshore. Components that cause long downtimes and require heavy lift vessels cause the biggest risk to production [2-39].

Offshore reliability data is not well studied in the literature and the type analysis that was undertaken using onshore data has yet to be replicated. Analysis that is available, from the UK round 1 sites and from Egmond Aan Zee, is not typical of offshore WTs that will be used in today's offshore wind farms [2-43], [2-58]. The WTs suffered from serial gearbox issues and as a result availability was extremely low and not representative of typical operation.

Research that has been carried thus far in understanding the impact of wind speed on WT reliability has been carried out by Tavner and colleagues and Wilkinson of GL DNV [2-55]–

[2-57]. They did not focus their attention specifically on wind speed specifically but also did analysis on air temperature and humidity. In the case of both Tavner and Wilkinson the conclusion was reached that wind speed appears to have an impact on WT failure rate.

5. Chapter 2 References

[2-1] F. Spinato, P. J. Tavner, G. J. W. van Bussel, and E. Koutoulakos, "Reliability of wind turbine subassemblies," *IET Renew. Power Gener.*, vol. 3, no. 4, p. 387, 2009.

[2-2] E. Echavarria, B. Hahn, G. J. W. van Bussel, and T. Tomiyama, "Reliability of Wind Turbine Technology Through Time," *J. Sol. Energy Eng.*, vol. 130, no. 3, p. 031005, 2008.

[2-3] P. J. Tavner, J. Xiang, and F. Spinato, "Reliability analysis for wind turbines," *Wind Energy*, vol. 10, no. 1, pp. 1–18, Jan. 2007.

[2-4] A. J. Seebregts, L. W. M. M. Rademakers, and B. A. van den Horn, "Reliability Analysis in Wind Turbine Engineering," *Microelectron Reliab.*, vol. 35, no. 9–10, pp. 1285–1307, 1995.

[2-5] R. Billington and R. N. Allan, *Reliability Evaluation of Engineering Systems: Concepts and Techniques*, 1st ed. New York: Plenum Press, 1983.

[2-6] IEC61400-26-1, *Part 26-1: Time Based Availabiltiy for Wind Turbines*. 2011.

[2-7] G. Klutke, P. C. Kiessler, and M. A. Wortman, "A critical look at the bathtub curve," *IEEE Trans. Reliab.*, vol. 52, no. 1, pp. 125–129, Mar. 2003.

[2-8] H. M. Hashemian and W. C. Bean, "State-of-the-Art Predictive Maintenance Techniques," *IEEE Trans. Instrum. Meas.*, vol. 60, no. 10, pp. 3480–3492, 2011.

[2-9] J. Moubray, *Reliability Centred Maintenance*, 2nd ed. New York: Industrial Press, 1997.

[2-10] R. Billinton and W. Yi, *Reliability Analysis of Electrical Power Systems Using Monte Carlo Methods*. New York: Plenum Press, 1994.

[2-11] R. Billinton and W. Wangdee, "Reliability-Based Transmission Reinforcement Planning Associated With Large-Scale Wind Farms," *IEEE Trans. Power Syst.*, vol. 22, no. 1, pp. 34–41, Feb. 2007.

[2-12] H. Pham and H. Wang, "Optimal (τ , T) Opportunistic Maintenance of a k -out-of-n : G System with Imperfect PM and Partial Failure," *Naval Res. Logisitcs*, vol. 47, pp. 223 – 239, 2000.

[2-13] L. Bertling, R. Allan, and R. Eriksson, "A Reliability-Centered Asset Maintenance Method for Assessing the Impact of Maintenance in Power Distribution Systems," *IEEE Trans. Power Syst.*, vol. 20, no. 1, pp. 75–82, 2005.

[2-14] Institut fur solare Energieversorgungstechnik, "Windenergie Report Deutschland 2000 - 2008," Kassel, 2008.

[2-15] Schleswig-Holstein, "Landwirtschaftskammer,"[Online] Available: http://www.lwk-sh.de/fachinfo/landtechnik/windenergie/inhalt.html Germany.

[2-16] "Windstats." [Online] Available: http://windstats.boschenvanrijn.nl/ [Accessed 22 – Feb – 2015]

[2-17] Tuulivoiman Tuotantotilastot Vuosiraportti, "Wind Power Statistics in Finland," . [Online] Available: http://www.vtt.fi/ [Accessed: 10 – Aug 2014],.

[2-18] Elforsk, "Driftuppföljning av vindkraftverk, årsrapport" (Wind power operations, yearly report)." 2005. [Online] Available: http://www.elforsk.se/ [Accessed: 10 – Aug 2014].

[2-19] P. Tavner, *Offshore Wind Turbines - Reliability , availability and maintenance*. London, UK: IET, 2012.

[2-20] J. Ribrant and L. M. Bertling, "Survey of Failures in Wind Power Systems With Focus on Swedish Wind Power Plants During 1997–2005," *IEEE Trans. Energy Convers.*, vol. 22, no. 1, pp. 167–173, Mar. 2007.

[2-21] J. F. Macqueen, J. F. Ainslie, D. J. Milborrow, D. M. Turner, and D. T. Swift-hook, "Risks associated with wind-turbine blade failures," *IEE Proc. A Phys. Sci. Meas. Instrumentation, Manag. Educ. Rev.*, vol. 130, no. 9, pp. 574–586, 1983.

[2-22] R. Lynette and R. Poore, "MOD-2 Failure Mode and Effects Analysis," 1979.

[2-23] B. Montgomerie, "Horizontal Axis Wind Turbine Blade Failure: Blade Fragment Six Degrees of Freedom Trajectory, Site Risk Level Prediction," in *Proceedings of the Internation Symposium of Wind Energy Systems*, 1982.

[2-24] D. M. Turner, "A Monte Carlo Method for Determining the Risk Presented by Wind Turbine Blade Failures," *Wind Eng.*, vol. 11, no. 1, 1986.

[2-25] F. Castro Sayas and R. N. Allan, "Generation availability assessment of wind farms," *IEE Proc. Gener. Transm. Distrib.*, vol. 143, no. 5, p. 507, 1996.

[2-26] R. Karki and R. Billinton, "Cost-Effective Wind Energy Utilization for Reliable Power Supply," *IEEE Trans. Energy Convers.*, vol. 19, no. 2, pp. 435–440, 2004.

[2-27] R. Billinton and R. Karki, "Application of Monte Carlo Simulation to Generating System Well-being Analysis," *IEEE Trans. Energy Convers.*, vol. 14, no. 3, pp. 1172–1177, 1999.

[2-28] C. Schontag, "Optimisation of Operation and Maintenance of Offshore Wind Farms," Delft, 1996.

[2-29] P. J. Tavner, J. Xiang, and F. Spinato, "Improving the Reliability of Wind Turbine Generation and its Impact on Overall Distribution Network Reliability," in *18th International Conference on Electricity Distribution*, 2005.

[2-30] P. J. Tavner, G. J. W. van Bussel, and F. Spinato, "Machine and Converter Reliabilities in Wind Turbines," in *IEE 2nd International Conference on Power Electronics, Machine & Drives*, 2006.

[2-31] E. Echavarria, T. Tomiyama, G. J. W. van Bussel, and B. Hahn, "How Has Reliability Of Technology Developed Through Time?," in *EWEC*, 2007.

[2-32] D. McMillan and G. W. Ault, "Techno-economic comparison of operational aspects for direct drive and gearbox-driven wind turbines," *IEEE Trans. Energy Convers.*, vol. 25, no. 1, pp. 191–198, 2010.

[2-33] F. Besnard, K. Fischer, and L. Bertling, "Reliability-Centred Asset Maintenance – A step towards enhanced reliability, availability, and profitability of wind power plants," in *EEE PES Conference on Innovative Smart Grid Technologies Europe*, 2010, pp. 1–8.

[2-34] D. McMillan and G. W. Ault, "Quantification of Condition Monitoring Benefit for offshore wind turbines," *Wind Eng.*, vol. 31, no. 4, 2007.

[2-35] K. Smolders, Y. Feng, H. Long, and P. Tavner, "European Wind Energy Conference (EWEC 2010) Reliability Analysis and Prediction of Wind Turbine Gearboxes," in *EWEC*, 2010.

[2-36] Y. Feng, Y. Qiu, C. J. Crabtree, H. Long, and P. J. Tavner, "Monitoring wind turbine gearboxes," *Wind Energy.*, vol 16, no. 5 , pp. 728–740, 2013.

[2-37] K. G. Scott, D. Infield, N. Barltrop, J. Coultate, and A. Shahaj, "Effects of Extreme and Transient Loads on Wind Turbine Drive Trains," in *30th ASME Wind Energy Symposium*, 2012.

[2-38] H. B. Hendriks, C. Lindenburg, H. J. T. Kooijman, H. B. Bulder, J. Bozelie, J. B. Madsen, R. Halfschepel, W. Molenaar, R. van den Berg, and M. Zaaijer, "Application of an Advanced Cost Model in the Different Design Phases of an Offshore Wind Turbine," in *EWEC*, 2001.

[2-39] G. J. W. van Bussel and M. B. Zaaijer, "Reliability , Availability and Maintenance aspects of large-scale offshore wind farms , a concepts study .," in *Proceedings of MAREC*, 2001.

[2-40] J. Shankleman, "DONG Energy hails world's first Siemens 6MW offshore wind turbines," *Business Green*, 2013[Online] Available: http://www.businessgreen.com/bg/news/2294171/dong-energy-hails-worlds-first-siemens-6mw-offshore-wind-turbines [Accessed: 15 - Feb 2015].

[2-41] E. de Vries, "Close up - Vestas V164-8.0 nacelle and hub," *Wind Power Monthly*, 2013. [Online] Available: http://www.windpowermonthly.com/article/1211056/close---vestas-v164-80 [Accessed: 15- Feb 2015].

[2-42] P. J. Tavner, F. Spinato, G. J. W. van Bussel, and E. Koutoulakos, "Reliability of Different Wind Turbine Concepts with Relevance to Offshore Application," in *EWEA*, 2008,.

[2-43] P. J. Tavner, H. Long, and Y. Feng, "Early experiences with UK round 1 offshore wind farms," *Proc. ICE - Energy*, vol. 163, no. 4, pp. 167–181, Nov. 2010.

[2-44] DTI and BERR, “Offshore wind capital grants scheme annual reports.” 2007.

[2-45] Noordzee Wind, “Egmond Aan Zee - operations reports,” 2013. [Online]. Available: http://www.noordzeewind.nl/en/. [Accessed: 03-Sep-2013].

[2-46] LORC Knowledge, “List of Offshore Wind Farms,” 2014. [Online]. Available: http://www.lorc.dk/offshore-wind-farms-map/list. [Accessed: 09-Apr-2014].

[2-47] J. B. Feuchtwang and D. G. Infield, “The offshore access problem and turbine availability - probabilistic modelling of expected delays to repairs,” in *European Offshore Wind Conference*, 2009.

[2-48] G. J. W. van Bussel and A. R. Henderson, “State of the Art and Technology Trends for Offshore Wind Energy : Operation and Maintenance Issues,” *Offshore Conroe TX*, pp. 10–12, 2001.

[2-49] G. J. W. Van Bussel, “The Development of an Expert System for the determination of Availability and O & M costs for Offshore Wind Farms,” in *EWEC*, 1999, pp. 402–405.

[2-50] “Ampelmann.” [Online]. Available: http://www.ampelmann.nl/qhse/. [Accessed: 10-Apr-2014].

[2-51] G. Marsh, “What Price O & M ?,” *Focus (Madison).*, vol. 8, no. June, pp. 22–27, 2007.

[2-52] D. McMillan and I. Dinwoodie, “Forecasting Long Term Jack up Vessel Demand for Offshore Wind,” in *ESREL*, 2013.

[2-53] B. Hahn, “Zeitlicher Zusammenhang von Schadenshäufigkeit und Windgeschwindigkeit”, in *FGW-Workshop Einflub der Witterung auf Windenergieanlagen*, 1997.

[2-54] P. Tavner, C. Edwards, A. Brinkman, and F. Spinato, “Influence of Wind Speed on Wind Turbine Reliability,” *Wind Eng.*, vol. 30, no. 1, pp. 55–72, 2006.

[2-55] P. J. Tavner, B. Hahn, R. Gindele, M. W. G. Whittle, S. Faulstich, and D. M. Greenwood, “Study of Effects of Weather & Location on Wind Turbine Failure Rates,” in *EWEC 2010*, 2010.

[2-56] P. J. Tavner, D. M. Greenwood, M. W. G. Whittle, R. Gindele, S. Faulstich, and B. Hahn, “Study of weather and location effects on wind turbine,” *Wind Energy.*, vol 16, no. 2, pp. 175–187, 2013.

[2-57] M. Wilkinson, T. Van Delft, and K. Harman, “The Effect of Environmental Parameters on Wind Turbine Reliability,” in *EWEA 2012*, 2012, no. April.

[2-58] Noordzee Wind, “Egmond Aan Zee Operations Report 2009,” 2010.

Chapter 3. Models Proposed

1. The Markov Approach

WTs are repairable systems and a common method of modelling a repairable system is through the use of the Markov Approach which can be applied to model systems which exhibit stochastic behaviour which may change discretely or continuously with respect to time and space.

The Markov approach is applicable to a system if it is the case that future states of the system are independent of all past states of the system, except the immediately preceding state. This means that the future random behaviour of the system does not depend on how the system came to be in its current state, but only the state it is in at present. The system must also be stationary, in that probability of making a transition from one state to another must remain the same at all times. This approach therefore applies to systems in which the probability of failure (the failure rate) is the same at all times.

This function is exponential and describes the behaviour of a system that can be modelled by a Markov approach.

When system reliability is modelled using a Markov model, space is discrete and represents the states in which the system and its components can be in, while time can be either discrete or continuous [3-1]. The discrete case is commonly known as a Markov Chain, while the continuous case is known as a Markov Process. These two models will be compared to find what method would be most suitable to model the effect of wind speed on reliability.

1.1. Discrete Markov Chain Theory

The degradation of engineering systems is often described using state based representation [3-1]. Figure 3-1 shows a simple system that can exist in 2 possible states, either *operating* or *failed*. If for example the system was in the *operating* state at time step 1, the probability that at time step 2 the system will be in a *failed* state is the failure rate λ. The probability the system will remain in the *operating* state is 1-λ. If at time step *i*, the system moves into the *failed* state, the probability that at *i+1* the system will be in the *operating* state is the repair rate μ, while the probability it will remain in the *failed* state is 1-μ.

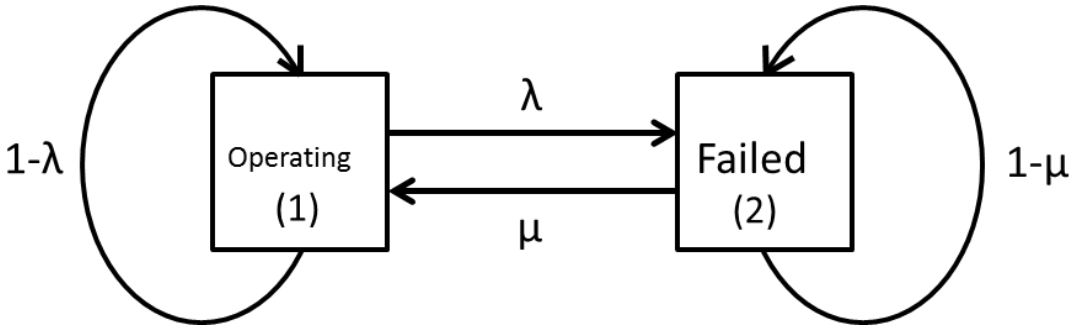

Figure 3-1: Simple Markov system

The stochastic transitional probability matrix for this system is shown in Equation 3-1. The *operating* and *failed* states are denoted by the letters *o* and *f* respectively. P_{ij} represents the probability of making a transition from state *i* to state *j* after a time step.

$$\boldsymbol{P} = \begin{bmatrix} P_{11} & P_{12} \\ P_{21} & P_{22} \end{bmatrix} = \begin{bmatrix} 1-\lambda & \lambda \\ \mu & 1-\mu \end{bmatrix} \quad \textbf{Equation 3-1}$$

If a system were to be modelled where there were intermediate states between operating and failure, this too could be modelled. Markov chains can be used to model systems with *n* states,. In each case the number of row and column denotes the "from state" and the "to state" respectively.

The system shown in Figure 3-1 can change from state 1 to state 2 freely over time, depending on the values of μ and λ. This system can be changed to model a scenario when the probability of failure remains, but the probability of the system being repaired is 0. This means that when the system changes from *operating* to *failed*, the probability it will remain failed is 1. In this case, the *failed* state is referred to as an absorbed state, as it is a state that the system cannot leave once it has entered [3-1].

Absorbed states are often used to evaluate the number of time steps a mission orientated system can be used before it suffers from catastrophic failure. It can also be used to model the reliability of repairable systems if the repair time for a component is always the same and is not probabilistic. If for example a system, which had the same states of the system shown in Figure 3-1, always started in the *operating* state then at some point in its life *failed* but was always repaired after 5 time steps each time, the *failed* state could be modelled as an absorbed state. Therefore the process of the system being repaired is not Markovian, however the failure process is.

1.2. Continuous Markov Process Theory

A Markov Process differs to a Markov Chain in that time is not discretised, but is instead continuous. Like a Markov Chain, the Markov Process is stationary and relies on the assumption that the failure and repair characteristics remain the same during the fixed period of time during which the system is analysed. The failure and repair characteristics are therefore exponential.

Rather than transition probabilities, the Markov Process relies on transition rates. A transition rate is defined by Billingon and Allan as the number of times a transition occurs from a given state, divided by the time spent in that state [3-1]. In the case of a reliability model these can be thought of as failure rates and repair rates.

Stochastic probability matrices can be derived for continuous Markov Processes, much like those developed for discrete Markov Chains. The difference is that in the continuous case, a discrete interval of time Δt can be introduced that is small enough that there is a low probability that more than one transition can take place during the time interval. The probability of a failure taking place during the time interval Δt is equal to the failure rate multiplied by the time interval. For the system shown in Figure 3-1, the stochastic probability matrix is described in Equation 3-2. Like Equation 3-1 the rows of the matrix must sum to 1.

$$\boldsymbol{P} = \begin{bmatrix} 1-\lambda\Delta t & \lambda\Delta t \\ \mu\Delta t & 1-\mu\Delta t \end{bmatrix} \qquad \textbf{Equation 3-2}$$

The stochastic probability matrix can be solved to calculate the survivor function for the time interval $R(\Delta t)$.

1.3. Applications of the Markov Approach in Wind Energy Literature

The Markov approach is used frequently across many different areas of research. This section will however focus on instances when it has been utilised in the field of WT reliability and investigate how the authors solved their models.

1.3.1. Analytical Method

As briefly described in Chapter 2.3.2, Sayas and Allan endeavoured to model the reliability of a WT and the impact of a wind farm on the electricity distribution network [3-2].

Focusing specifically on their attempts to model the failure and repair process, Sayas and Allan stated that the failure rate of a WT increased at higher wind speeds and quoted three references from the American Wind Energy Association conference in 1993 – two of which could not be found [3-2]. The available paper describes the reliability of very small machines by today's standards – the Enertech 44 WT range which consisted of a 13.4m rotor that was capable of generating 25kW, 40kW or 60kW [3-3]. The WTs did seem to fail more often in winter months and due to extreme weather events, but these models had very little in common with their larger, more intelligent and robust successors that operate today.

Sayas and Allan designed their model so that failures that occurred at extreme wind speeds were catastrophic and therefore resulted in expensive and long downtimes [3-2]. They considered the wind speed to be split into two different ranges – wind speeds that were within design limits (wind speed states *I-III*) and wind speeds that were extreme (wind speed state *IV*). Their model would be designed so that when the WT was operating within the former range it would have one set of failure rates and repair rates, while if it were operating in the latter range it would have another set.

The WTs within the model were considered to be binary state components that would either be operating (the *up* state) or failed (the *down* state). A failure within the design limit wind speed would result in *minor damage*, whereas a failure while operating in wind speed state

IV would cause *severe damage*. *Severe damage* led to a longer downtime than *minor damage* and the probability of the WT failing while in state *IV* was higher than in the other lower wind speed states.

Figure 3-2 shows their system, which consists of a total of 12 different states that the WT may be operating within at any time step.

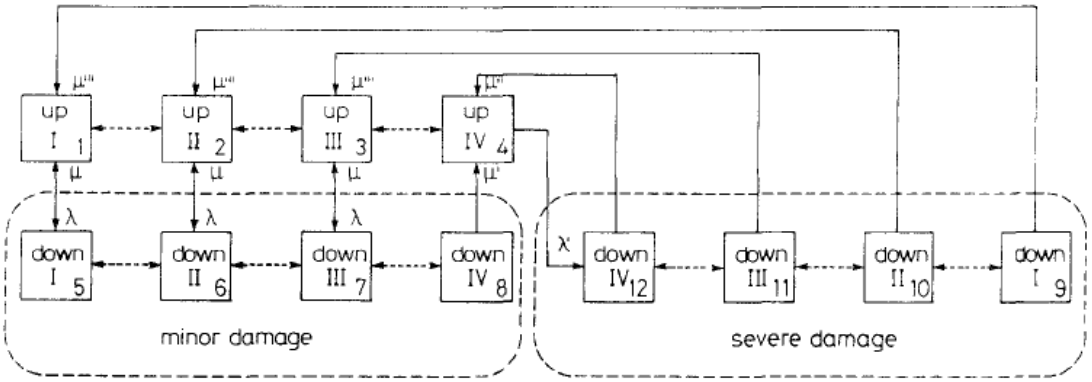

Figure 3-2: Wind Farm model of 1 WT and 12 wind speed states [3-2]

Most relevant to this thesis is that the approach taken by Sayas and Allan in using different failure rates and repair rates for the design wind speed states and the extreme wind speed state actually contravenes one of the properties of a Markov Chain in that the model should be stationary, when in this case the transition probabilities change depending on the wind speeds. Despite this, the model was better at reproducing the sample data as their data showed different failure rates at different wind speeds.

The analytical method used by Sayas and Allan to solve their model was applicable to their model because it was relatively simple. Their WT model had 2 possible states, for a wind farm of *n* WTs the total number of states considered was 2^n for each wind speed state. This means that for a moderately sized wind farm of 30 WTs the total number of states per wind state is 1,073,741,824. For WT model that consisted of 12 main components (each existing either in the up state or the down state), within a wind farm model of 200 WTs, operating in

several potential wind speed states, each with their own failure rate and repair rates for each of the twelve components - the number of potential states that would need to be evaluated for each discrete time interval would be huge. For systems with the level of complexity that would be required to model the impact of wind speed on WT reliability for large scale wind farm projects, there is another method which is more suitable.

1.3.2. Simulation Method

Systems in general can be analysed in two ways, either analytically, or using stochastic simulation. The difference between the two methods is how the stochastic nature of an engineering system is modelled. In the case of an analytical solution, mathematical solutions are calculated for the system which gives the same answers each time to describe the system. Stochastic simulation however simulates the actual random behaviour of systems over and over again, almost like performing continual experiments. Estimates are then made by counting the number of times a different event occurs in the experiments.

In 1996, when Sayas and Allan wrote their paper, analytical solutions could be could be calculated very quickly, while simulation techniques required more computational time. Today however computational power is considerably greater and therefore simulation techniques are a much more practical option of calculating system reliability.

The advantages of using simulation techniques is that they are better at modelling systems and accounting for uncertainty – because analytical techniques return the same answer they may instil false confidence.

There are two types of stochastic simulation, random and sequential [3-4]. The random approach simulates chooses time intervals randomly and while the sequential approach simulates the intervals in chronological order [3-4]. This thesis will consider the sequential approach as the model will attempt to calculate the impact of wind speed.

Monte Carlo Simulation is type of stochastic simulation. It requires an input of uniform random numbers that are used to simulate randomness. If an analytical method was used to evaluate the probability of either getting 'heads' when tossing a coin, it would calculate that the probability was 0.5. If Monte Carlo Simulation was used, a uniform random number – usually between 0 and 1 – would be generated. If the number was between 0 and 0.5 a 'heads' would have occurred, while if a number between 0.5 and 1 was generated, a 'tails' would have occurred. After a simulation of 100 trials it is very likely the result would also be 0.5, the same as the analytical calculation.

1.3.3. Markov Chain Monte Carlo Simulation

Markov Chains and Monte Carlo Simulation are commonly used together in what is called Markov Chain Monte Carlo Simulation (MCMCS). Besnard and Bertling used this method to evaluate how different maintenance strategies would affect the reliability of WT blades [3-5]. The following model, shown in Figure 3-3 was developed to describe the deterioration process of a blade.

The four deterioration states are shown as the states labelled *X*. If no maintenance is performed, the blade starts off at state X_1, before deteriorating through each state until it finally fails at state *F*. Alternatively the blade may leave any of the deterioration states other than *4* and go directly to *F*. Once the blade fails it returns to state $X_1$and was assumed to be as good as new, the simulation then continues until a suitable sample is taken [3-5]. The failure rates λ represent the transition rates – *init* being the probability of a crack forming, *det* denoting the deterioration rate and *l* representing the sudden failure of the blade.

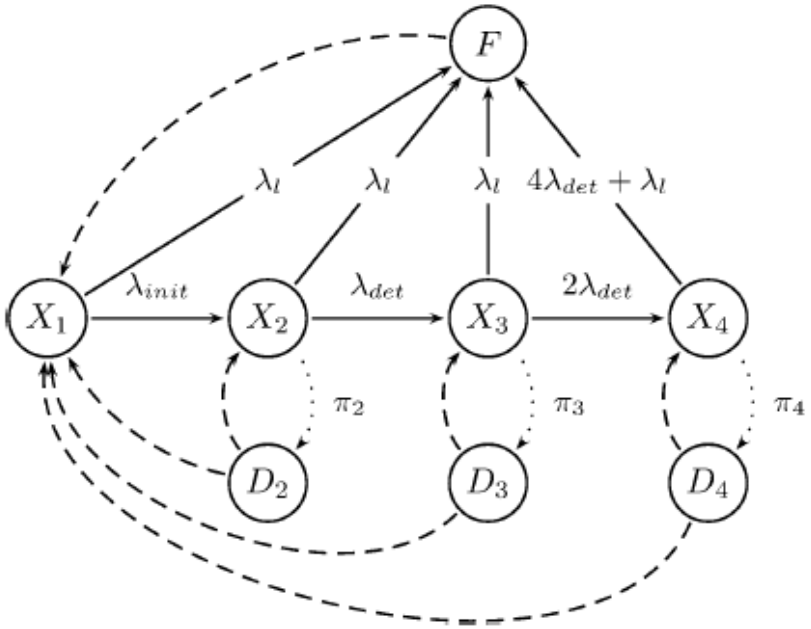

Figure 3-3: Besnard and Bertling's blade deterioration Markov Chain model [3-5]

To prevent the blade from failing different maintenance strategies are trailed which allow the condition of the blade to be known, these are shown as the states *D*. These different strategies are represented by the transition rates π [3-5]. If for instance the maintenance strategy was perfect, all the transition rates π would equal 1 and a fault would be detected as soon as the blade went from deterioration state X_1 to X_2. Maintenance could then be undertaken and the blade would then return to state X_1 at the next time interval. With maintenance strategies it becomes less likely that the blade would be allowed to deteriorate, however it does not change the probability of the blade failing suddenly [3-5].

Besnard and Bertling used Monte Carlo Simulation to solve the Markov Chain for different maintenance strategies [3-5]. So while the failure rates all remained the same, the transition rates π changed for each strategy. Costs were attached to the various aspects of the maintenance strategies as well as production losses, blade replacement, installation, and logistics. Many simulations were then run with differing parameters to determine the most economical strategies in various different scenarios. This flexibility in using MCMCS made

the model highly informative. Other notable examples of models of this type were developed by Negra and his colleagues and McMillan and Ault [3-6], [3-7]. The former developed a model that identified the factors most relevant to offshore wind farm reliability, while the latter used MCMCS to evaluate the benefit that condition monitoring brings to offshore WTs.

1.4. Conclusion

This thesis will use the Markov Chain Monte Carlo Simulation approach in developing a model that describes the effect of the wind speed on WT reliability, much like the models developed by Besnard and Bertling, McMillan and Ault and Negra and his colleagues [3-5]–[3-7]. However this model will also follow the approach taken by Sayas and Allan in using a non-stationary Markov Chain by using different transition rates depending on the wind speed [3-2].

MCMCS was selected for use in this thesis because:

- They are used frequently in the literature for modelling maintenance and deterioration.
- MCMCS models care very flexible and can be used along with other models. Therefore the wind speed dependent failure rates can be incorporated into the MCMCS model.
- Monte Carlo Simulation can be used to solve the Markov Chain accurately and relatively quickly.

The methodology for calculating these transition rates will be explained Chapter 5.1 before being implemented in the wind speed dependent failure rate model in Chapter 5.2

2. Modelling Wind Speed Dependent Failure Rates

In trying to model the relationship between wind speed and the transition rate between the operating state and the failed state, otherwise known as the failure rate, several methods were analysed.

Because of the original work carried out by Tavner and his colleagues in this area, the first method used to quantify the relationship was cross-correlation, as described in the previous Chapter 2.3.2 [3-8], [3-9]. However cross correlation was judged not to be a suitable method for calculating the transition rates, as its main function is to evaluate the similarity between two signals to determine if a relationship exists, rather than describe what the relationship actually looks like.

A high correlation coefficient between a WT component and the wind speed does not tell you anything about the transition rate of that component or how it changes according to wind speed. In modelling using Markov Chains it is vitally important to understand what the relationship looks like so a suitable Markov Chain can be constructed.

Artificial Neural Networks (ANNs) were also identified as a possible method of analysing the relationship. ANN have been applied to WT gearbox condition monitoring systems due to their ability of processing large volumes of data and finding patterns between many variables [3-10].

They were used in this case to take several time series' of wind speed data and wind farm failuresand calculate the difference between operating conditions and conditions that led to component failures. A paper was presented on the subject using data from another operator [3-11].

However like cross-correlation analysis, ANNs were considered to not be a suitable method for determining the failure rate and wind speed relationship. A concern about ANNs is that

they are essentially black boxes and this issue was encountered during analysis. Each time the ANN fitted itself to the input data, the weighting of each of the layers of synapses were different. With a larger dataset this problem may have been overcome as the ORD was split so a proportion of the data could be used for training and another proportion for validation.

Another concern was that there was no limit to the information that could be used to train the ANN, however it was difficult to determine what model inputs added value to the accuracy of the model due to its black box nature.

After a period of time experimenting with ANN it was decided that a more transparent, simpler method should be used to model the impact of wind speed on failure rates.

2.1. Bayes Theorem

Bayes Theorem is used in statistical inference to update the probability of a hypothesis being true as new evidence is discovered. It calculates the posterior probability as a consequence of the prior probability and a likelihood function derived from the observed data.

For example, *A* represents a set of events that have the following properties:

1. *A* is a set of subsets $\{A_1, A_2, \ldots, A_n\}$
2. The subsets A_i do not have any two elements in common.
3. All the subsets together encompass all possible values of set *A* and so are collectively exhaustive.
4. Each one of the subsets A_i has a nonzero probability of occurrence.

B is any event that occurs in the same sample space. To calculate the probability of *B*, the law of total probability is used, shown in Equation 3-3.

$$P(B) = P(B|A_1)P(A_1) + P(B|A_2)P(A_2) + \cdots + P(B|A_n)P(A_n) = \sum_{i=1}^{n} P(B|A_i)P(A_i) \quad \textbf{Equation 3-3}$$

If event *B* has occurred, the probability that event A_k also occurred is calculated using Bayes Theorem, shown in Equation 3-4. $P(A_k|B)$ represents the posterior probability, while $P(B|A_k)$, $P(A_k)$ and $P(B)$ denote the likelihood function, the prior probability and model evidence respectively.

$$P(A_k|B) = \frac{P(B|A_k)P(A_k)}{\sum_{i=1}^{n} P(B|A_i)P(A_i)} = \frac{P(B|A_k)P(A_k)}{P(B)} \quad \textbf{Equation 3-4}$$

2.2. Application

Bayes Theorem is used in this thesis to calculate a component failure rate as a function of wind speed; this is shown in Equation 3-5.

$$P(\lambda_i|w) = \frac{P(w|\lambda_i)P(\lambda_i)}{P(w)} \qquad \textbf{Equation 3-5}$$

If *w* is the average daily wind speed on a given day, λ_i represents a failure to component *i*. The term on the left hand side of Equation 3-5 represents the probability of a failure occurring to a component (λ_i), given the mean daily wind speed *w*. This probability represents the failure rate of component *i*, as a function of average daily wind speed *w*.

On the right hand side of Equation 3-5, the prior probability $P(\lambda_i)$ is calculated very simply using component failure rates and Equation 2-2.

For the model evidence $P(w)$ to be calculated, probabilities are estimated using the met mast data. As the ORD comes from 2 wind farms, which each experience different wind speed conditions, proportional probabilities were calculated from the met mast data from the two sites to create a distribution which is referred to as the calibration wind speed distribution.

The term $P(w|\lambda_i)$, is the probability of wind speed *w* occurring, given a failure has occurred to component *i*. This is calculated by taking probabilities of the daily average wind speeds recorded on days when a failure occurred to component *i*.

In the following sections two methods will be discussed that can be sued to calculate the calibration wind speed distribution $P(w)$ and the probability of a wind speed given a component failure $P(w|\lambda_i)$.

2.3. Kernel Density Estimate

Kernel density estimation allows the probability density function of a random variable to be estimated non-parametrically. It also allows inferences to be made about a population, based on what is known about the data sample – which is very useful in this application because in many components' cases there are very few failures and so plotting $P(w|\lambda_i)$ can be problematic.

$$f(x) = \frac{1}{nb}\sum_{j=1}^{n}\omega\left(\frac{x - x_i}{b}\right) \qquad \textbf{Equation 3-6}$$

If a random sample $X\ (x_1, x_2, \ldots, x_n)$ is taken from some unknown distribution, to calculate the probability density function f a kernel density estimator can be used, shown in Equation 3-6 [3-12]. This involves using a kernel ω, which is a specified symmetrical function and is located at every sample point. The kernel can be a range of functions, but in this case it is a Normal kernel which integrates to 1 and is a function of the bandwidth b, which scales the kernel. The kernels are then summed together to make a kernel density estimate.

The bandwidth of the kernel is very important as it cannot vary across the whole sample. If too large a bandwidth is chosen it would conceal the finer details of the data, if too small a bandwidth is selected the kernel density estimate is spikey and infers less about the population [3-12].

The matlab function 'ksdensity' calculated the bandwidth using the normal distribution approximation, shown in Equation 3-7 [3-13], [3-12].

$$b = \left(\frac{4\hat{\sigma}^5}{3n}\right)^{0.2} \qquad \textbf{Equation 3-7}$$

2.4. Normalised Histograms

A normalised histogram is essentially a discretised PDF. It is calculated very simply by first ordering the samples into bins before determining the proportion of each bin compared to the size of the whole sample.

$$Number\ of\ Bins = \frac{x_{max} - x_{min}}{r}$$ **Equation 3-8**

Bins are generally taken by subtracting the maximum from the minimum reading (x_{max} and x_{min} respectively) and dividing by the desired bin width *r*, as shown in Equation 3-8. The data is then separated into the bins. There is no optimum bin width and bins do not all have to be the same width.

3. Chapter 3 Summary

A non-stationary approach was taken to the failure rates when modelled using the Markov Chains. This means that the component failure rates were able to change at each time step interval, much like in the Markov Chain model developed by Sayas and Allan [5-1].

Bayes Theorem is used to determine the wind speed dependent failure rate using historical wind speed data and component failure data.

Two approaches are used to calculate the three inputs to the Bayes Theorem equation – Kernel Density Estimate and normalised histograms. The chosen method for use in the wind speed dependent failure rate model is discussed in Chapter 5.

4. Chapter 3 References

[3-1] R. Billington and R. N. Allan, *Reliability Evaluation of engineering Systems: Concepts and Techniques*, 1st ed. New York: Plenum Press, 1983.

[3-2] F. Castro Sayas and R. N. Allan, "Generation availability assessment of wind farms," *IEE Proc. Gener. Transm. Distrib.*, vol. 143, no. 5, p. 507, 1996.

[3-3] R. N. Clark and R. G. Davis, "Performance of an Enertech 44 During 11 Years of Operation," in *AWEA Wind Power 93 Conference*, 1993, pp. 204–213.

[3-4] R. Billington and R. N. Allan, *Reliability Evaluation of Engineering Sytems: Concepts and Techniques*, 2nd ed. New York: Plenum Press, 1992.

[3-5] F. Besnard and L. Bertling, "An Approach for Condition-Based Maintenance Optimization Applied to Wind Turbine Blades," *IEEE Trans. Sustain. Energy*, vol. 1, no. 2, pp. 77–83, 2010.

[3-6] N. B. Negra, O. Holmstrøm, B. Bak-jensen, and P. Sorensen, "Aspects of Relevance in Offshore Wind Farm Reliability Assessment," *IEEE Trans. Energy Convers.*, vol. 22, no. 1, pp. 159–166, 2007.

[3-7] D. McMillan and G. W. Ault, "Quantification of Condition Monitoring Benefit for offshore wind turbines," *Wind Eng.*, vol. 31, no. 4, 2007.

[3-8] P. J. Tavner, B. Hahn, R. Gindele, M. W. G. Whittle, S. Faulstich, and D. M. Greenwood, "Study of Effects of Weather & Location on Wind Turbine Failure Rates," in *EWEC 2010*, 2010.

[3-9] P. J. Tavner, D. M. Greenwood, M. W. G. Whittle, R. Gindele, S. Faulstich, and B. Hahn, "Study of weather and location effects on wind turbine," no. May 2012, pp. 175–187, 2013.

[3-10] P. Bangalore and L. B. Tjernberg, "An Artificial Neural Network Approach for Early Fault Detection of Gearbox Bearings," *IEEE Trans. Smart Grid*, no. 99, 2015.

[3-11] G. Wilson, D. Mcmillan, and G. Ault, "Modelling the Effects of the Environment on Wind Turbine Failure Modes using Neural Networks," in *SUPERGEN International Conference of Sustainable Power Generation*, 2012.

[3-12] A. . Bowman and A. Azzalini, *Applied Smoothing Techniques for Data Analysis*. New York: Oxford University Press Inc, 1997.

[3-13] Mathworks, "ksdensity," 2014. [Online]. Available: http://www.mathworks.co.uk/help/stats/ksdensity.html.

Chapter 4. Data Analysis

1. Wind Turbine Reliability Data

Wind turbine reliability data was provided by a utility as a result of a technology and innovation project undertaken at the University of Strathclyde. Due to confidentiality agreements, the utility will be referred to as "the operator" throughout the course of this thesis. The reliability data will be referred to as the operator's reliability dataset (ORD). Throughout this Chapter the ORD will be the dataset analysed and then in Chapters 6 and 7 used in producing the models and results of this thesis.

The WTs were owned and by the operator but were under the warranty of the OEM. Therefore, during the period the data was recorded, the wind farm was maintained by the OEM. However the operator maintained detailed records of all work carried out by the OEM.

1.1. Sites

The reliability data used in analysis, obtained through the operator comprises of reliability records from Site A and Site B wind farms. As shown in Table 4-1, both wind farms use the same model of wind turbine and are roughly the same age, although most WTs at Site B are 19 months older.

Table 4-1: Summary of the ORD

	Site A	Site B
Commission Date	14th December 2007	1st March 2005
Number of WTs	140	54
Installed Capacity (MW)	322	124.2
Capacity Factor (%)*	26.7	22.6
Wind Turbine Model	SWT-2.3-101	SWT-2.3-101
Duration of recorded data (First failure – last failure)	07/01/2010 – 31/01/2012	03/01/2010 – 20/12/2011
Dataset Size (WT Years)	278.5	105.9

* From June 2013 – May 2014 [4-1], [4-2]

The sites are both located in central Scotland, within roughly 25 miles of each other, as shown in Figure 4-1 and Figure 4-2. In total the dataset amounts to 384.4 wind turbine years of data.

At the end of 2012, Scotland had an installed onshore wind capacity of 3,739 MW [4-3]. The ORD accounts for 11.9% of Scotland's installed capacity during the time the data was recorded.

Figure 4-1: Location of wind farms

Figure 4-2: Location of wind farms

1.2. Wind Turbine Model

The SWT-2.3-101 is a Siemens WT, with an installed capacity of 2.3MW and a rotor diameter of 101m [4-4]. The WT is variable speed, pitch controlled which means that:

1) Cut-in to rated wind speed – the rotational speed of the blades increases, as does the torque.
2) Rated to cut-out wind speed – the rotational speed of the blades and the torque remains constant, controlled by the pitching of the blades
3) Above cut-out wind speed – the blades are pitched fully and the rotation speed reduces to zero. The mechanical brake is then applied.

Figure 4-3 shows an example of a rotor speed, torque curve for a variable speed, pitch regulated wind turbine. The control system keeps the WT operating in the most efficient part

of the power coefficient curve for as long as possible. The efficiency then decreases as the wind turbine reaches rated speed – shown in Figure 4-3 between 8 – 11.5 m/s. Then at 11.5 m/s the wind turbine maintains a constant power output by pitching the blades to adjust the lift and therefore the torque.

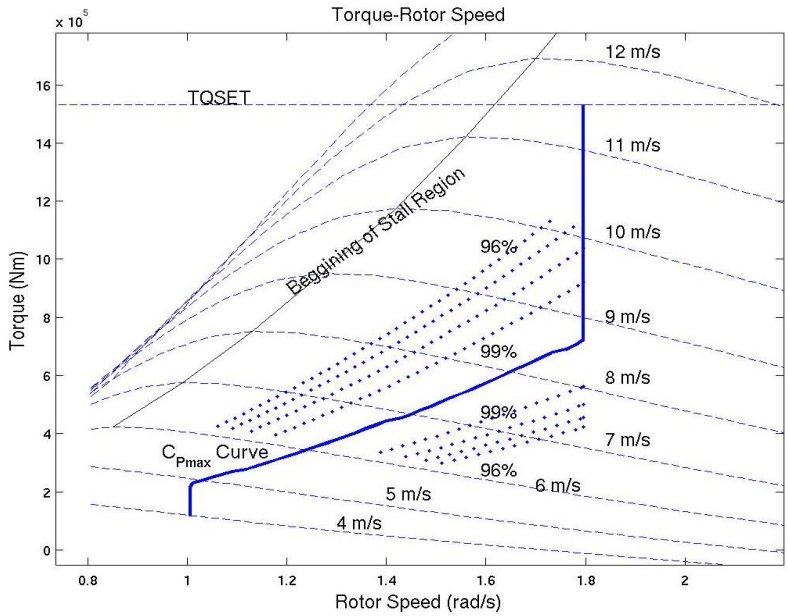

Figure 4-3: Torque - Rotor Speed curve for variable speed, pitch regulated WT [4-5]

The SWT-2.3-101 is a doubly fed induction generator (DFIG), which consists of a wound rotor induction generator with slip rings, which takes current into or out of the rotor, and a gearbox [4-6].

As the blades rotate a torque is produced in the low speed shaft, linking the rotor to the gearbox. The gearbox then steps up the rotational speed and passes this on, through the high speed shaft to the generator where electricity is produced. The electricity is then converted from AC to DC and then back to AC via the power converters before passing into the network [4-6]

The variable speed operation is achieved by a controllable voltage which is injected into the rotor at slip frequency [4-7]. Figure 4-4 shows how the power converters decouple the WT

from the grid and the position of the crowbar which protects the power converters and the generator from high voltages and currents [4-7].

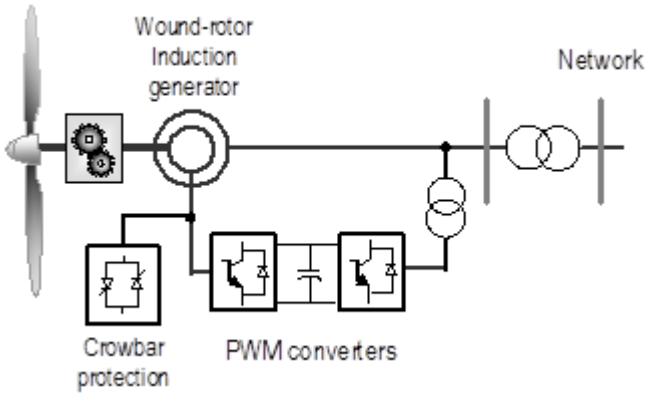

Figure 4-4: Schematic of a DFIG WT [4-7]

The WT system consists of twelve main components, shown in Figure 4-5 in the medium sized boxes. They are the:

- Emergency System
- Meteorological Instruments
- Rotor
- Blade Pitch System
- Drive Train
- Yaw System
- Hydraulic System
- Control System
- Main Generator
- Lifting System
- Nacelle
- Tower

The taxonomy of the WT system follows the Reference Designation System for Power Plants (RDS-PP) which has been adapted specifically for WTs [4-8]. This system is used by many operators in classifying failures. The taxonomy used by the operator comes from RDS-PP and is shown in Figure 4-5.

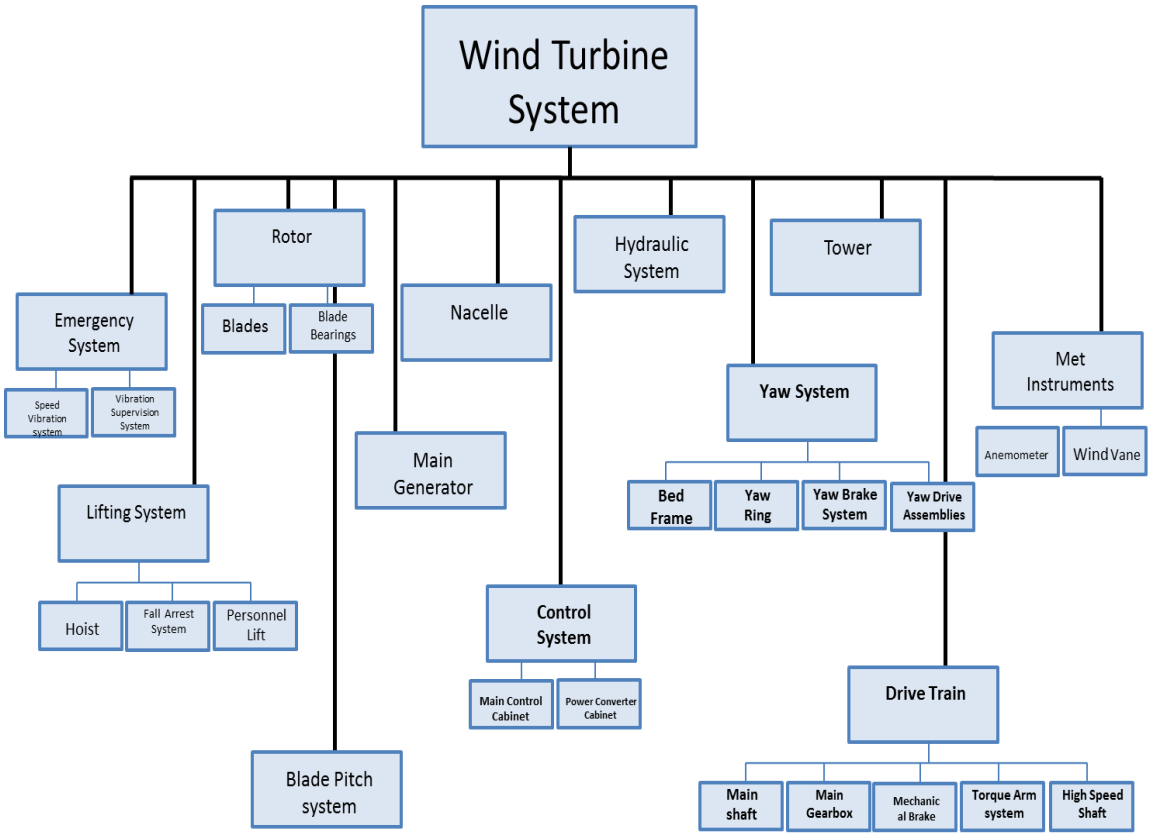

Figure 4-5: Taxonomy of WT system using RDS-PP system [4-8]

1.3. Reporting Mechanism

When a WT was shut down at either Site A or Site B, a record was taken at the operators control centre. The record included information of the time, reason for the stoppage, the component responsible for the failure (if a component was responsible), the WT that the fault occurred in and the downtimes attributed to that fault. Reasons for a WT being shut down included:

- Maintenance – preventative and corrective
- An external causes the stoppage – this could be national grid curtailing the wind farm
- High wind speeds (above rated wind speed)
- Low wind speeds (below cut-in wind speed)

A component did not have to be replaced for it to necessarily be considered a failure – repairs were quite often made to components rather than installing new components and on many occasions the WT shut down because of low oil pressures or component overheating. Therefore a failure to the main gearbox did not require the entire gearbox to be replaced each time.

The identity of the failed component was determined by technicians on site. Importantly however, the time the failure occurred was not the time at which the fault was diagnosed; it was the time at which it was decided to stop the WT and to make it unavailable. For the analysis which will be described in the following chapters, it was necessary that the initial time recorded in the reliability data be as close as possible to the time when the component actually failed.

The component to which the failure occurred was identified in the ORD according to their functional location. The functional location was a code of letters and numbers which signified the wind farm, wind turbine and location within the wind turbine system in which the failure took place.

An example of this code is "SIA1A040MDY". The first 2 characters indicate the first 2 letters of the wind farm's name, in this case Site A. The following 3 characters distinguish Site A from any other wind farms owned by the operator that also have the first 2 letters of their name to be "SI". The 6th, 7th and 8th characters, which are always numbers, represent the asset to which the failure occurred – in this case WT number 40. The last characters indicate the component that failed which in the example's case was the control system. Codes which indicate the location of the failure within the system are shown in Table 4-2. There are 33 in total.

Table 4-2: Description of functional locations

Functional Location	Description
CHI	**Emergency System**
CHI01	Speed Vibration system
CHI02	Vibration Supervision System
CVK	**Meteorological Instruments**
CVK01	Anemometer
CVK02	Wind Vane
MDA	**Rotor**
MDA01	Blades
MDA02	Blades Bearings
MDB	**Blade Pitch System**
MDK	**Drive Train**
MDK01	Main Shaft Assembly
MDK02	Main Gearbox
MDK03	Mechanical Brake System
MDK04	Torque Arm System
MDK05	High Speed Shaft Transmission
MDL	**Yaw System**
MDL01	Bed Frame
MDL02	Yaw Ring
MDL03	Yaw Brake System
MDL04	Yaw Drive Assemblies
MDX	**Hydraulic System**
MDY	**Control System**
MDY01	Main Control Cabinet
MDY02	Power Converter Cabinet
MKA	**Main Generator**
SMA	**Lifting System**
SMA01	Hoist
SMA02	Fall Arrest System
SMA03	Personnel Lift
UMC	**Nacelle**
UMD	**Tower**

The functional locations in bold are classified and referred to in this thesis as components, the others are sub-components. For example, the yaw system as a whole will be considered a component but the bed frame will be considered a sub-component of the yaw system.

The downtime attributed to each failure is the total time lost from when the WT stops operating, to when it becomes available to operate if the wind conditions allow it to do so. The length of the downtime is influenced by a number of variables, shown in Figure 4-6.

The WT is shut down when the SCADA system detects a fault during data analysis. Once this happens the time of the stoppage is recorded and engineers try to make a partial diagnosis of the fault. Very often the same failures occur and require only a remote reset. If the WT cannot be reset remotely engineers must access the WT to repair the fault, this can only be done below certain wind speeds and so the engineers must wait until it is safe to access the WT before they make a full diagnosis of the fault [4-9]. Once the engineers know the reason for the fault they must decide whether a replacement component is required. If it is not the engineer will repair the component, after which the WT will be available to resume operation. If a replacement component is required and is available immediately to the engineers, they will make their repair. But if it is not available a spare must be ordered. Once the component arrives the WT can then be repaired and allowed back into normal operation.

Some components however require a crane if they are to be replaced or repaired. If for example a blade is damaged and needs replaced, a crane must lift the blade from the hub and then reattach a replacement. In this case there will be further waiting time for the crane to arrive on site and for it to be prepared for lifting. Furthermore, cranes cannot operate at high wind speeds for safety reasons; therefore there may be more waiting time once the crane is prepared to lift.

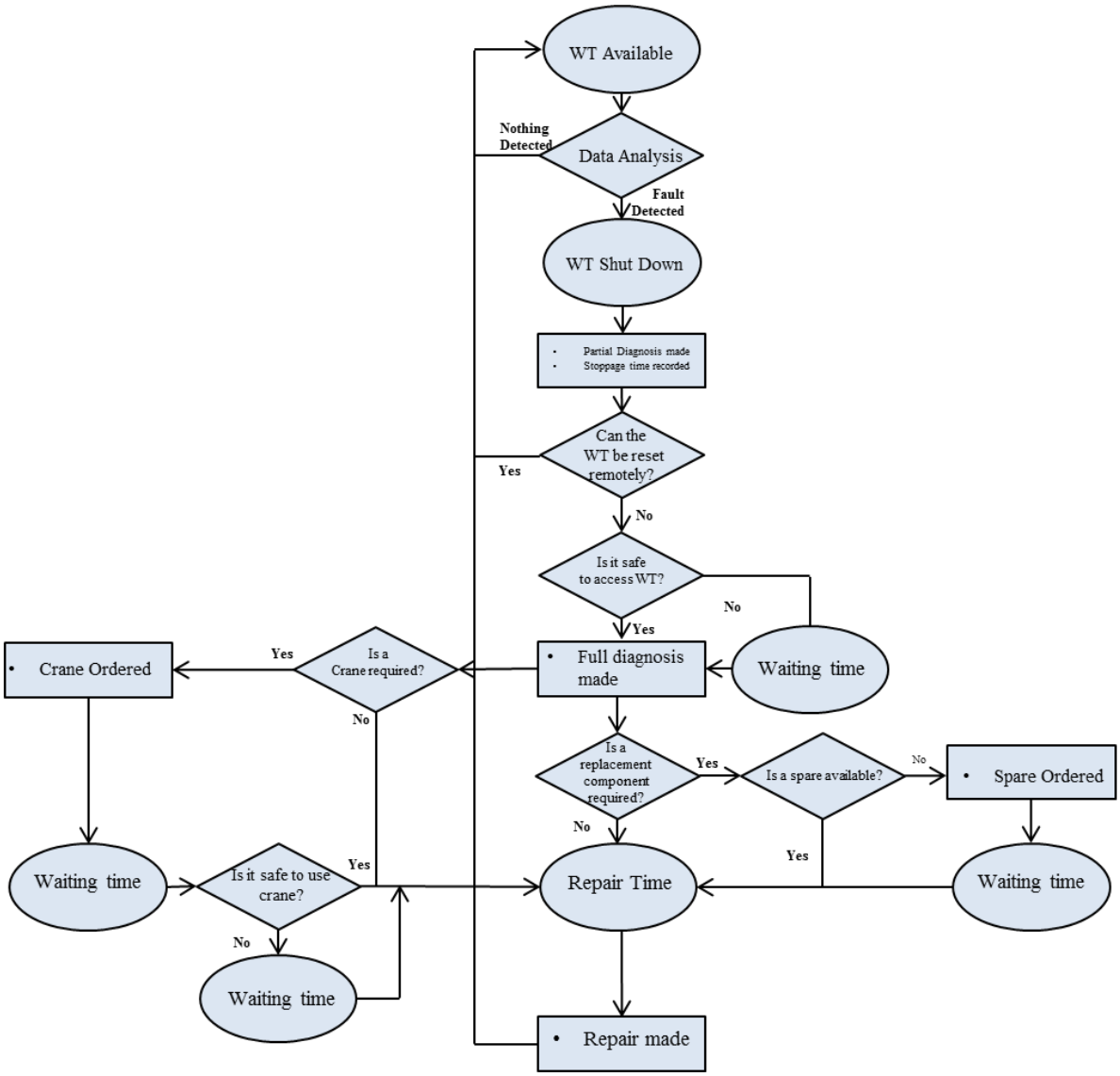

Figure 4-6: Flowchart downtime process

The downtime recorded in the reliability records is therefore a function of waiting time caused by accessibility, logistics, and repair time.

Interestingly, in some instances the OEM would use components which had failed previously but had subsequently been refurbished. In some cases, components which had been in one WT and had then failed and been refurbished, were then fitted to a second WT when it

required a replacement. It is possible therefore that one component may have failed multiple times and been used in multiple WTs.

This means that this dataset cannot be used to estimate the number of loading cycles each component is subjected to before it fails. A bathtub curve for each component also cannot be calculated because the age of each component is unknown.

Because of this uncertainty over the age and state of replacement components the assumption was made that when a component failed it was replaced by a new component.

1.4. Reliability Analysis

The following sections show failure data from the ORD. These failures only account for corrective maintenance as the aim is to determine the impact of wind speed on component failure rates. Preventative maintenance is not included as by definition this refers to maintenance that is carried out to prevent a failure and not as a result of an actual failure.

Using the reliability analysis theory described in Chapter 2.1, the reliability data from the ORD will be evaluated to determine the component failure rates. The seasonality of these failures will then be analysed to establish whether the WT fails more frequently in the winter, when wind speeds are higher.

1.4.1. Component Failures

The following section describes analysis of the ORD data. Figure 4-7 shows the failure rate and average downtime per failure for each component within the ORD. The component that caused the highest average downtime per failure was the rotor. The rotor had a low failure rate of 0.047 failures per WT year – amounting to 18 failures during the recorded period. One of these failures caused a downtime of 110 days. The average downtime of the remaining rotor failures was 11.4 hours.

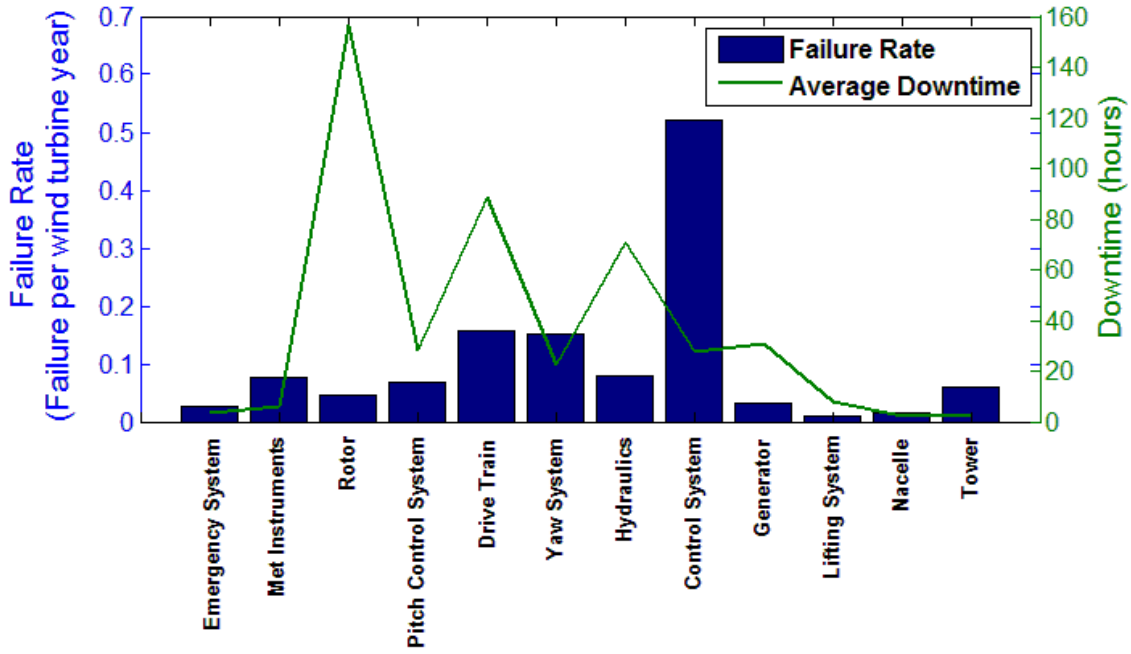

Figure 4-7: Average component downtime per failure and component failure rate of ORD

The control system failed the most frequently of all the components, the resultant downtime however was not as problematic as the rotor, drive train or hydraulics. The drive train was the second most unreliable component and caused the second longest downtime per failure.

Figure 4-8 shows major failures, which are failures that caused downtimes greater than 24 hours. These more severe failures occurred again most frequently to the control system, which is not unexpected as the control system experienced the most failures of all the

components. The emergency system, lifting system, nacelle and tower did not experience any failures that caused a downtime of greater than 24 hours.

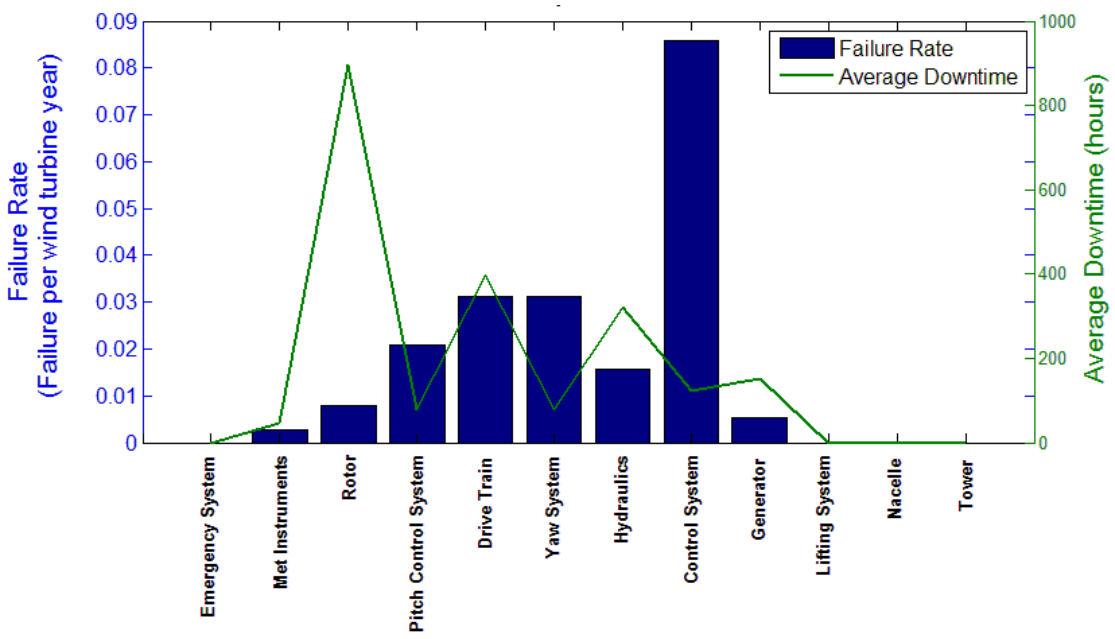

Figure 4-8: ORD average component downtime per failure and component failure rate only considering failures that resulted in downtimes greater than 24 hours.

Figure 4-9 shows the percentage of the total failures that experienced downtimes greater than 24 hours, 48 hours and 168 hours (a week). The pitch control system had the highest percentage of its failures that had caused downtimes greater than 24 hours.

The control system, despite causing the most failures lasting over 24 hours, had a relatively low percentage of its failures contribute to downtimes of 24 hours or over. The rotor that as shown in Figure 4-7, caused the longest downtimes per failure had a relatively low percentage of its failures cause excessive downtime. If the single failure to the blade (that caused a downtime of 110 days) is not considered, the rotor was actually a relatively reliable component that generally did not cause long downtimes.

Interestingly, the drive train was almost as probable to fail for 48 hours as it was 24 hours. It had the highest percentage of failures that caused downtimes greater than 48 hours and a

week. In terms of downtime distribution the drive train was most comparable to the generator, as many of its failures also caused downtimes greater than a week. However the drive train fails 5 times more frequently than the generator, as shown in Table 4-3. Because of its relatively high failure rate and likelihood of causing long downtimes, the drive train was a component that caused significant reliability problems.

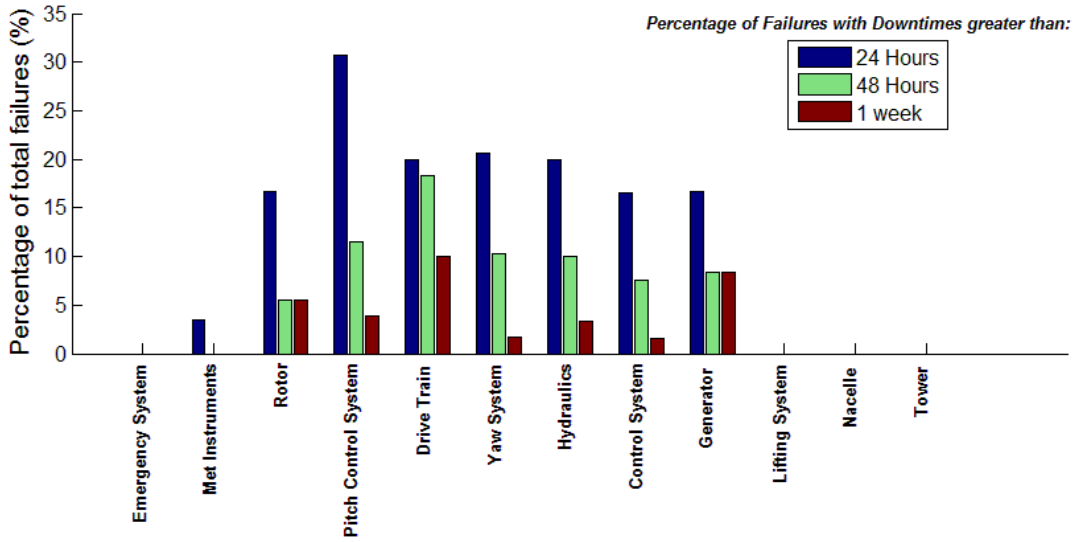

Figure 4-9: Percentage of component failures that cause downtimes greater than 24 hours, 48 hours and 1 week in ORD.

Of the drive train components, the main gearbox failed by far the most frequently, as shown in Figure 4-10. There were no failures categorised by the operator to be general drive train failures (MDK) or torque arm system failures (MDK04) during the time in which the data was recorded.

Failures to the main shaft assembly, which rarely happened, always resulted in downtimes of greater than 48 hours. The most severe failure that occurred caused a downtime of 2203 hours (92 days roughly) and was a result of a failed main bearing. Another failure to the main bearing caused a downtime of roughly 160 hours.

The main gearbox – which had a failure rate of 0.1275 as shown in Table 4-3 – had only 8% of its failures lead to a downtime of greater than 24 hours and half of those failures lasted longer than a week. These long term failures comprised of a failed gearbox motor that required 74 hours to repair and a failed gearbox that had to be completely replaced – this resulted in 10 days (241 hours) of downtime.

The high speed shaft transmission behaved similarly to the main shaft assembly in that it failed infrequently, but caused long periods of downtime. The most severe failures were due to the damage to the high speed shaft that ultimately required the high speed shaft to be replaced.

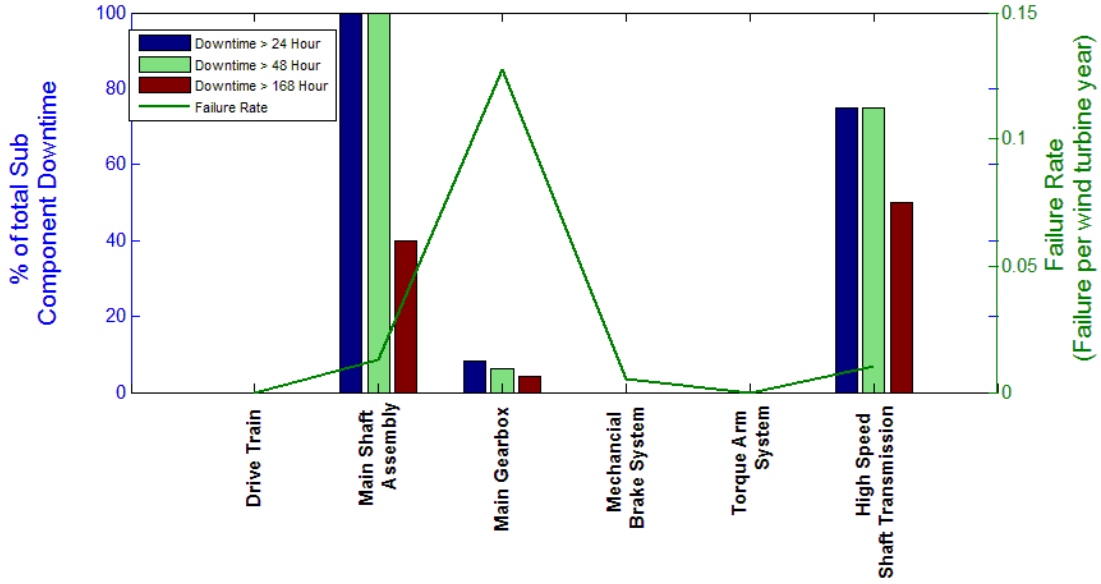

Figure 4-10: Sub-component failure rate and percentage of sub-component failures that cause downtimes greater than 24 hours, 48 hours and 1 week in ORD.

The drive train components are generally very large and heavy and so would have required heavy lifting equipment whenever they needed to be replaced. They are also very expensive and rarely require replacement. Therefore is possible that when the drive train components failed there were not spare components in storage. Therefore when a component in the drive

train needed replaced it could lead to long periods of downtime spent waiting for components to arrive and for a heavy lifting crane to become available.

Failures that only caused downtimes of less than 24 hours, classed as minor failures, are shown in Figure 4-11. The components with the highest failure rates for failures of this type were the control system, followed by the drive train and then the yaw system. This is to be expected as the majority of failures were minor and these three components experienced the highest number of failures. As shown in Figure 4-12, between 79.3 % to 83.5 % of failures that occurred to the control system, drive train and yaw system were minor.

In terms of total downtime experienced in the whole dataset throughout the recorded period, the control system is the highest contributor as shown in Figure 4-13. This is followed by the drive train, rotor and hydraulics. There was an incident where a failure to the hydraulics of a Site A WT led to a gearbox failure which required the gearbox and the hydraulic component replacement. This caused a downtime of 1600 hours for that WT. The likely reason for this long period of downtime was probably due to the gearbox and logistics involved in its replacement, however according to the reliability records the failure appeared to initially be caused by a fault to the hydraulics, which then led to the gearbox failing. The incident was therefore classified by the operator as a hydraulics failure.

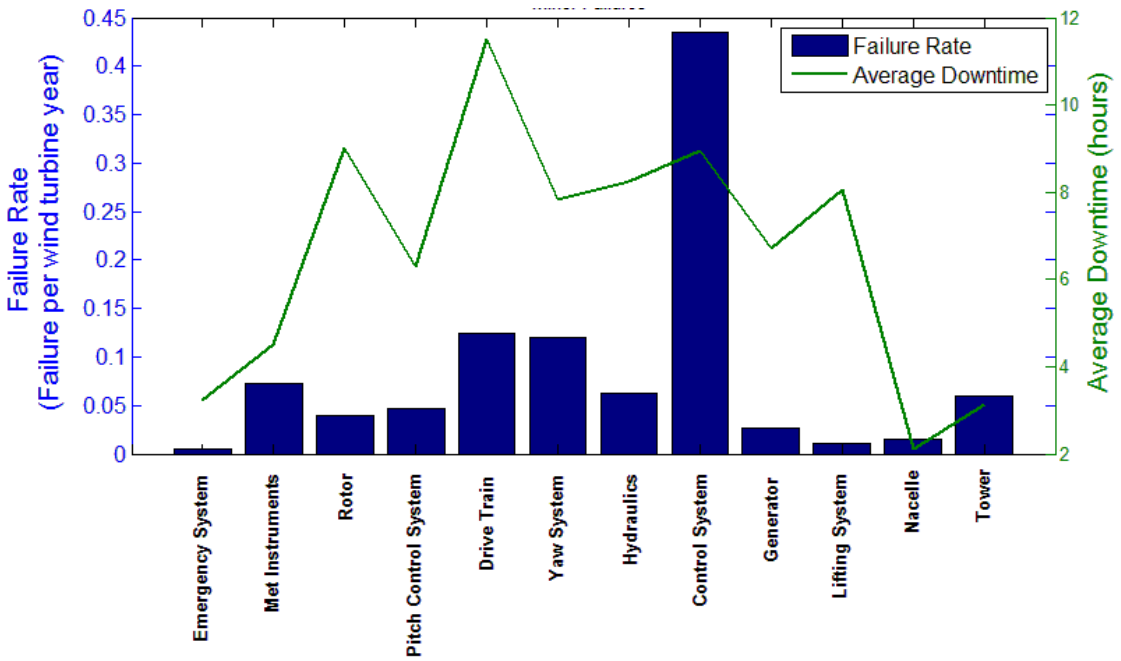

Figure 4-11: ORD average component downtime per failure and component failure rate only considering failures that resulted in downtimes less than 24 hours.

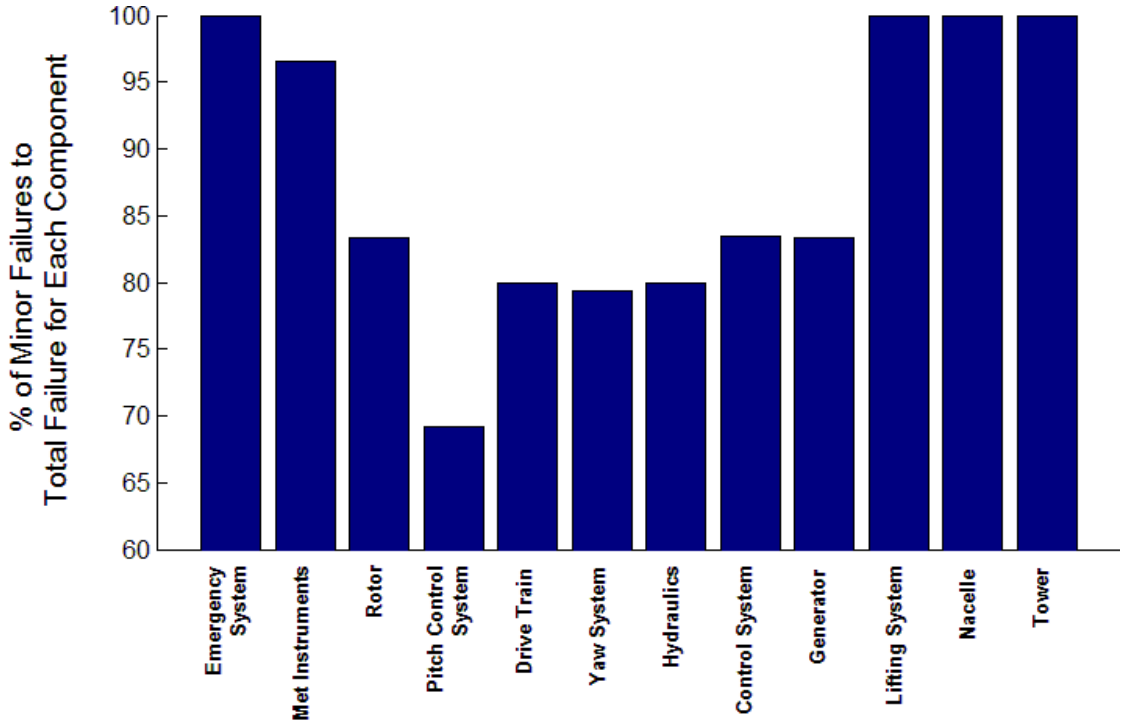

Figure 4-12: Percentage of component failures that result in downtimes of less than 24 hours in ORD

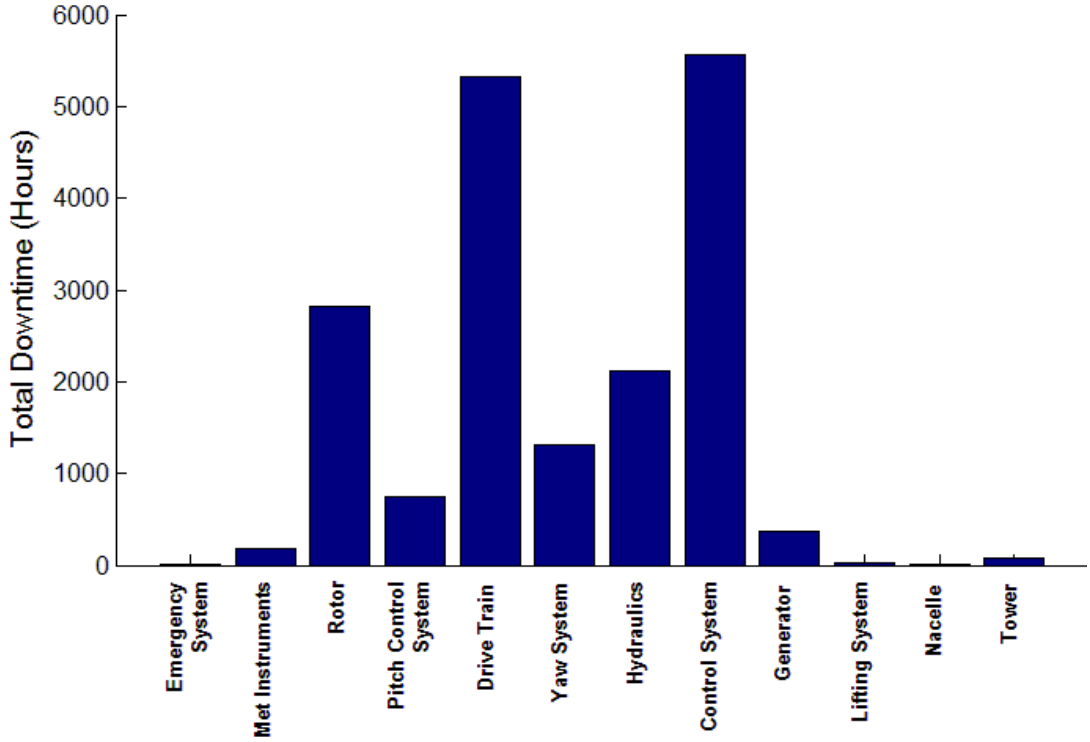

Figure 4-13: Total downtime contributed by each component in ORD

The control system failed the most frequently and it is this reason it contributes the most to downtime. As shown in Figure 4-7, the average downtime of a control system failure is actually a relatively short period of time. This is mainly because most control system failures can be repaired quite quickly using spares that are inexpensive and easy store. The control system in a Siemens 2.3 MW WT is located at ground level and so repairs can be made with little regard to the environmental conditions.

1.4.2. Seasonal Failures

The ORD began to be reocrded from the beginning of January 2010 to the very start of January 2012 (or in Site B's case right to the end of December 2011), as shown in Table 4-1. The whole dataset therefore encompasses each day during 2010 – 2011.

The failures that occurred in each month, of the two years for both sites, are shown in Figure 4-14. The combined 2010 and 2011 failures show a rough seasonal trend where the WTs failed more often in the winter months than in the summer months.

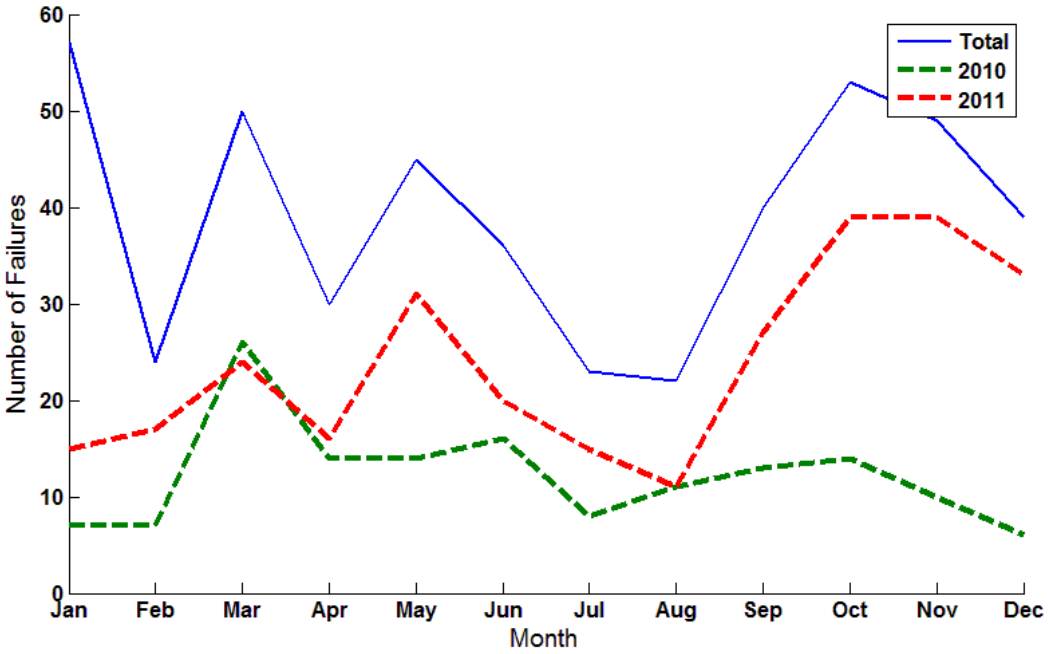

Figure 4-14: Number of failures that occur in each month in 2010, 2011 and both years combined for both wind farms in ORD

These results agree with research performed by Tavner *et al* and Wilkinson *et al* that found that failures in their dataset also showed a seasonal trend, shown in Figure 2-22 and Figure 2-23 [4-10], [4-11].

The trend is not so obvious when only looking seperately at the data from both years, shown in Figure 4-14. However it is likely that with more data, from over a greater period of time, the seasonal trend would become more obvious, as found by Tavner and Wilkinson [4-10], [4-11].

Site A and Site B have very different seasonal trends. As shown in Figure 4-15, Site A failed less often in the summer months, while Site B appears to have suffered more failures in the summer months and fewer from November to February. As there are only 2 years of data available, this difference may be due to a lack of data at Site B, as its dataset is a third of the size of the Site A dataset.

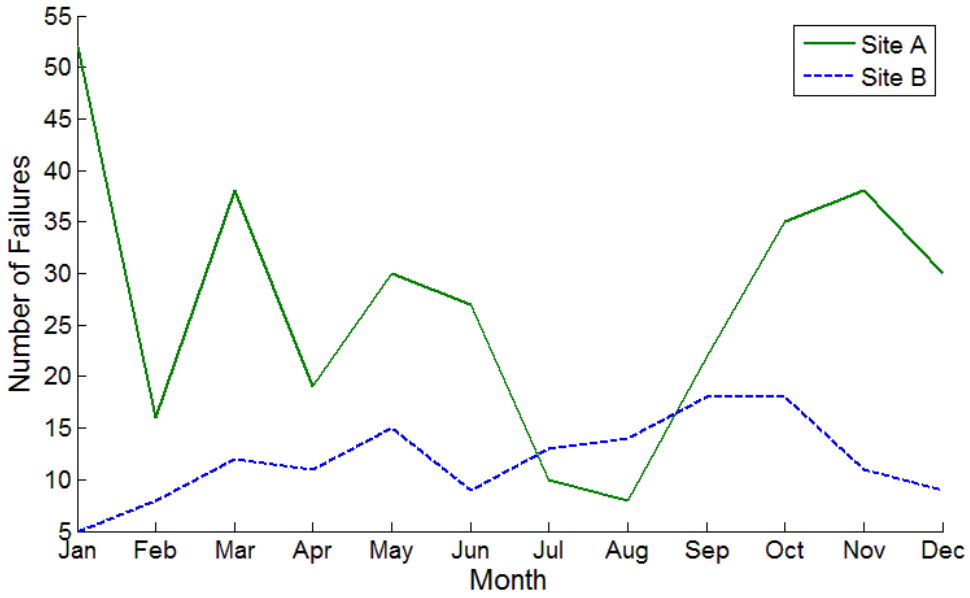

Figure 4-15: Number of failures that occur in each month for Site A and Site B

The three most frequently failed components, the control system, drive train and yaw system, appear to follow seasonal trends, as shown in Figure 4-16. The yaw system perhaps shows the strongest seasonal trend, clearly failing less often in the summer months compared to the winter months. The control system and drive train have very similar trends, failing often in May, before declining over the summer and increasingly again in October.

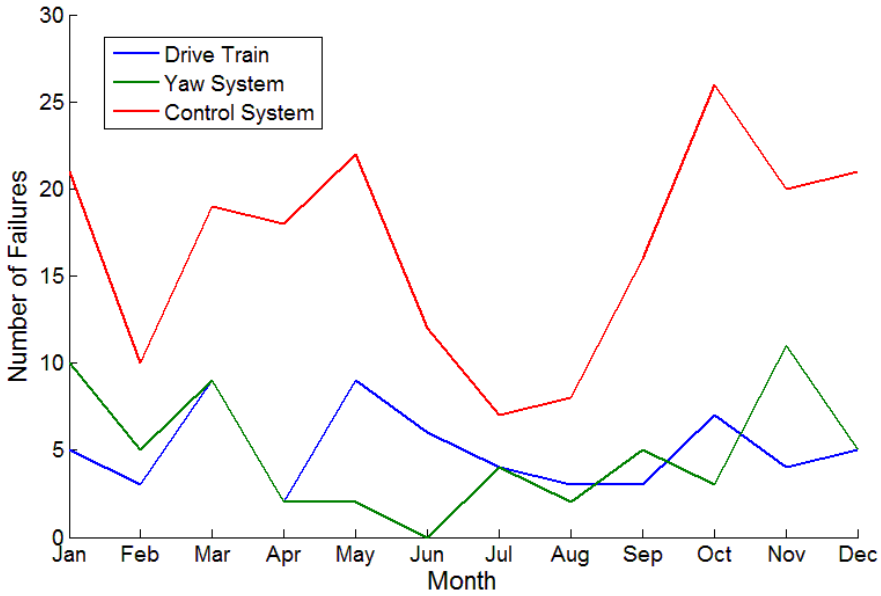

Figure 4-16: Seasonal reliability trends for the control system, drive train and yaw system in ORD

There is less evidence of anything that could resemble a seasonal trend in any of the other components. This could be because there are too few failures that occur to these components for a seasonal trend to be identified from the data. The generator for example only failed 12 times over the duration of the recorded period.

Interestingly the tower failed most frequently in May, specifically in 2011. The sub-component that failed in every one of these cases was the tower fan, this required the WT to shut down for no more than 3 hours for it to be replaced. It could be that the tower fan failed most often in May because the temperature increased sharply inside the tower in May 2011 due to the ambient temperature rise at the beginning of summer. This may have caused the fans to work harder than usual and thus caused a failure. It is unclear whether the WT was stopped specifically for the fan to be repaired or whether it was discovered broken when preventative maintenace was carried out and the WT was shut down while the technicians were inside the tower.

1.4.3. Failure Rate Summary

Table 4-3 shows a summary of failure rate data for the components and their subcomponents on both wind farms. There were 202 failures in 2010 at Site A compared to 88 in 2011. The 35 failures that occurred in 2012 all took place in January.

In contrast, 2011 was the year that Site B experienced the most failures. Its control system and hydraulic system suffered the highest level of failures. The hydraulic system of the WTs at Site B failed 4 times more often than those at Site A. Overall Site B was a less reliable site than Site A, the failure rates of the two being 1.35 and 1.17 failures per WT year respectively.

This difference may have been due to Site B being slightly older than Site A and so it may have began to suffer failures that were not observed at Site A over the recorded period, but may have occurred subsequently. However, as discussed in Chapter 4.1.3 the age of the components is not known as it was policy to often repair, refurbish and then fit the component to another WT. The effects of aging are therefore not considered.

This thesis will investigate another potential cause for this difference. If Hahn and Peter Tavner and his colleagues are correct, the differences in reliability between these two sites could be due, at least in part, to the weather conditions each site is subjected to.

Table 4-3: Component failure rate summary

Component Code	Site A			Failure Rate (Failures per WT year)	Site B			Failure Rate (Failures per WT year)	Total Failure Rate (Failures per WT year)	Grouped Component Failure Rate (Failures per WT year)
	2010	2011	2012		2010	2011	2012			
CHI	0	0	0	0.0000	0	0	0	0.0000	0.0000	0.0052
CHI01	1	0	0	0.0036	0	0	0	0.0000	0.0026	
CHI02	1	0	0	0.0036	0	0	0	0.0000	0.0026	
CVK	1	1	0	0.0072	0	5	0	0.0472	0.0182	0.0754
CVK01	2	0	0	0.0072	0	0	0	0.0000	0.0052	
CVK02	20	0	0	0.0718	0	0	0	0.0000	0.0520	
MDA	0	2	0	0.0072	0	3	0	0.0283	0.0130	0.0468
MDA01	1	2	2	0.0179	4	4	0	0.0756	0.0338	
MDA02	0	0	0	0.0000	0	0	0	0.0000	0.0000	
MDB	7	8	2	0.0610	4	5	0	0.0850	0.0676	0.0676
MDK	0	0	0	0.0000	0	0	0	0.0000	0.0000	0.1561
MDK01	0	1	0	0.0036	1	3	0	0.0378	0.0130	
MDK02	29	17	1	0.1687	2	0	0	0.0189	0.1275	
MDK03	0	0	0	0.0000	0	2	0	0.0189	0.0052	
MDK04	0	0	0	0.0000	0	0	0	0.0000	0.0000	
MDK05	2	2	0	0.0144	0	0	0	0.0000	0.0104	
MDL	18	4	5	0.0969	4	5	0	0.0850	0.0936	0.1509
MDL01	0	0	0	0.0000	0	0	0	0.0000	0.0000	
MDL02	0	0	0	0.0000	0	0	0	0.0000	0.0000	
MDL03	2	1	2	0.0179	0	0	0	0.0000	0.0130	
MDL04	5	2	0	0.0251	4	6	0	0.0945	0.0442	
MDX	3	6	3	0.0431	5	13	0	0.1701	0.0780	0.0780
MDY	35	29	2	0.2369	9	13	0	0.2079	0.2289	0.5202
MDY01	5	2	3	0.0359	6	8	0	0.1323	0.0624	
MDY02	44	10	11	0.2333	14	9	0	0.2173	0.2289	
MKA	3	0	1	0.0144	5	3	0	0.0756	0.0312	0.0312
SMA	0	0	0	0.0000	0	0	0	0.0000	0.0000	0.0104
SMA01	3	0	1	0.0144	0	0	0	0.0000	0.0104	
SMA02	0	0	0	0.0000	0	0	0	0.0000	0.0000	
SMA03	0	0	0	0.0000	0	0	0	0.0000	0.0000	
UMC	2	0	0	0.0072	0	4	0	0.0378	0.0156	0.0156
UMD	18	1	2	0.0754	0	2	0	0.0189	0.0598	0.0598
Total	**202**	**88**	**35**	**1.1665**	**58**	**85**	**0**	**1.3511**	**1.2174**	**1.2174**

2. Weather Data

The weather data used in the analysis is shown in Figure 4-17. The red arrows indicate the locations of weather stations while the yellow triangles show the wind farms and their respective met masts.

Figure 4-17: Weather station and met mast locations. Yellow triangle represents a met mast while red arrows indicate the location of a weather station.

The weather variable focused upon in this thesis is wind speed. However analysis will be undertaken in Chapter 4.3 using temperature and humidity data as well for each site. Therefore the aim of this section is to provide wind speed, temperature and humidity time series data for both Site A and Site B over the period in which the ORD was recorded. It will therefore be possible to know the weather conditions when a failure occurred to a component.

2.1. Meteorological Masts

Both Site A and Site B are served by 2 meteorological masts (met masts) that log data every 10 mins. Data from each mast was provided by the operator. The Site A data includes:

- Wind direction
- Minimum wind speed
- Maximum wind speed
- Mean wind speed

These measurements are taken at 17m, 27m, 61m and 66m from ground level. The Site B wind speed data provided by the operator is not as extensive as the Site A data and only contains the mean wind speed every 10 mins at 66m.

The wind speed measurements from 66m are used to calculate the wind speed at WT hub height of 80 m. This is done by using the logarithmic wind profile, shown in Equation 4-1, where U is the instantaneous wind speed, h is the height that the wind measurement has been taken (*1*) and is required to be calculated (*2*) [4-6].

$$U_2 = U_1 \left(\frac{\log\left(\frac{h_2}{z_0}\right)}{\log\left(\frac{h_1}{z_0}\right)} \right) \qquad \text{Equation 4-1}$$

The surface roughness, z_0 is assumed to be 0.04 as Site A and Site B are not areas within cities or forests, there are not many trees or hedges, but neither would be considered a flat grassy plain. Surface roughness lengths for different terrains are shown in Table 4-4 [4-6].

Table 4-4: Typical Surface Roughness Lengths [4-6]

Type of terrain	Roughness Length, z_o (m)
Cities, forests	0.7
Suburbs, wooded countryside	0.3
Villages, countryside with trees and hedges	0.1
Open farmland, few trees and buildings	0.03
Flat grassy plains	0.01
Flat desert, rough sea	0.001

2.1.1. Site A Meteorological Mast

All wind speed data shown in this section and all successive sections are calculated speeds, for an 80m hub height, using Equation 4-1. In onshore and offshore cases z_o equals 0.04m and 0.001m respectively.

Site A wind farm possesses two met masts; data was made available from 1st January 2009 to the 30th April 2013. During that period of time the second met mast was not operating, therefore measurements could only be taken from one location on the site.

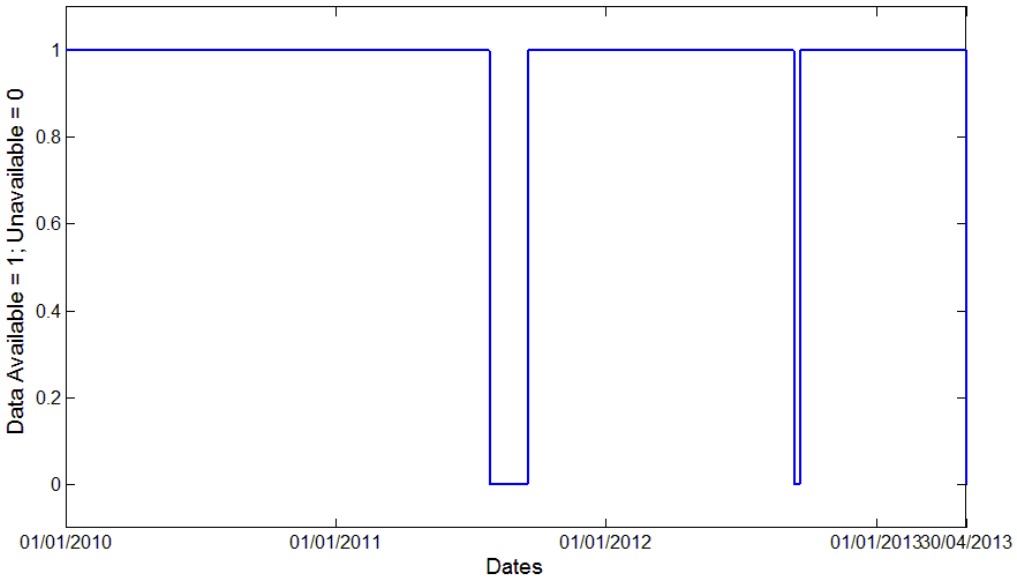

Figure 4-18: Met mast 1 availability

There were also occasions when the operational mast was not functioning either and there was therefore no obtainable met mast data. Figure 4-18 shows the available period and the unavailable periods – first from 01/07/2011 to 30/09/2011 and second from 01/09/2012 to 30/09/2012. The met mast availability was 95.1% during this period. For these periods where there was no Site A met mast data available, Met Office weather station data from Prestwick was used to fill the remaining gaps. Data from this weather station will be presented in Chapter 4.2.2.1.

The average wind speed of Site A between 01/01/2010 and 30/04/2013 was 5.98 m/s; this however is calculated while there is data missing in several summer months and only including the first 4 months of 2013.

2.1.2. Site B Meteorological Mast

Only 10 minute mean wind speeds were made available from both Site B met masts 1 and 2. The readings were taken from 01/01/09 to 31//12/11 and were measured at WT hub height. Met mast 2 was available 97.6% of the time between 01/01/09 and 31/12/11, while met mast 1 was unavailable for much longer periods of time and had an availability of only 83%.

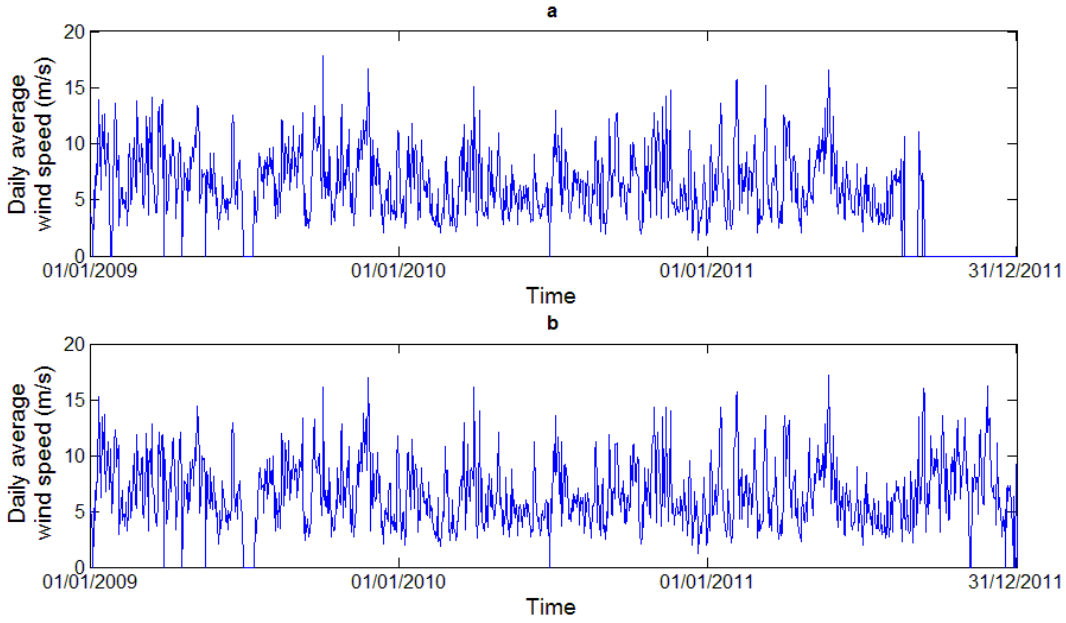

Figure 4-19: Time series of Site B met masts at hub height: a) Met Mast 1 b) Met Mast 2

A wind speed time series of Site B was constructed using the data from both met masts. Met mast 2 is available for the longest period of time, importantly during which time the ORD was recorded by the operator, it was therefore used as the primary source of data.

The periods of time when data was missing from met mast 2 are shown in Figure 4-19b) as days when the mean wind speed is 0 m/s. These gaps in data for met mast 2 were filled in using readings made by met mast 1 for the same period of time. If data was missing from

both datasets, Met Office weather station data from Salsburgh was used to fill the remaining gaps . Data from this weather station will be discussed in Chapter 4.2.2.1. The Site B average daily wind speed time series, using data from both met masts and Salsburgh data, is shown in Figure 4-20.

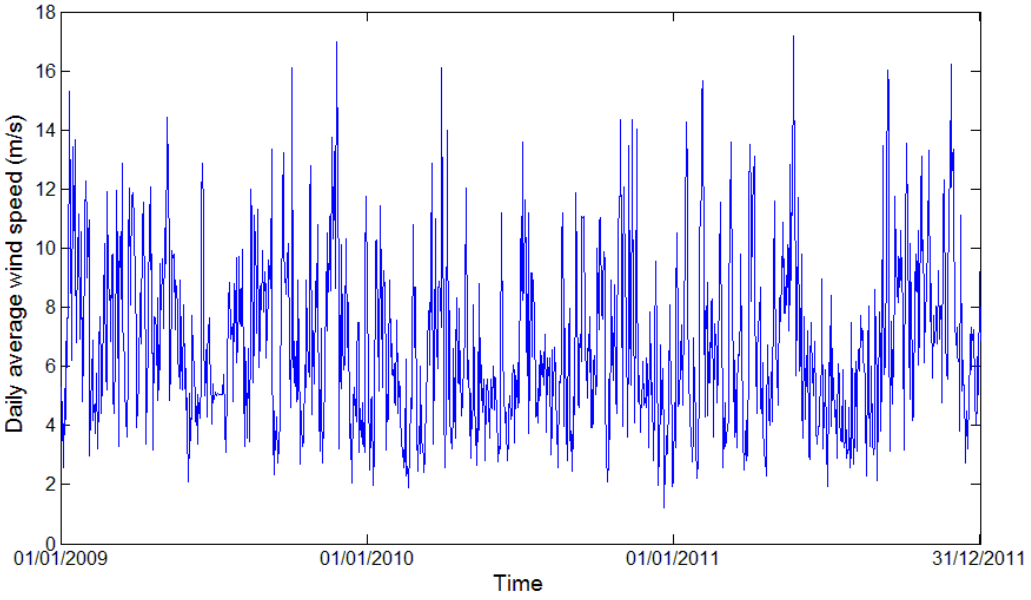

Figure 4-20: Site B daily average wind speed time series at hub height

From the completed Site B wind speed time series, the average wind speed of the site from 01/01/2010 – 31/12/2012 was 6.72 m/s at WT hub height. The average daily maximum and minimum wind speed, taken from the 10 minute mean wind speeds, was 11.96 m/s and 2.64 m/s respectively. Daily wind speed histograms of the Site B time series are shown in Figure 4-21.

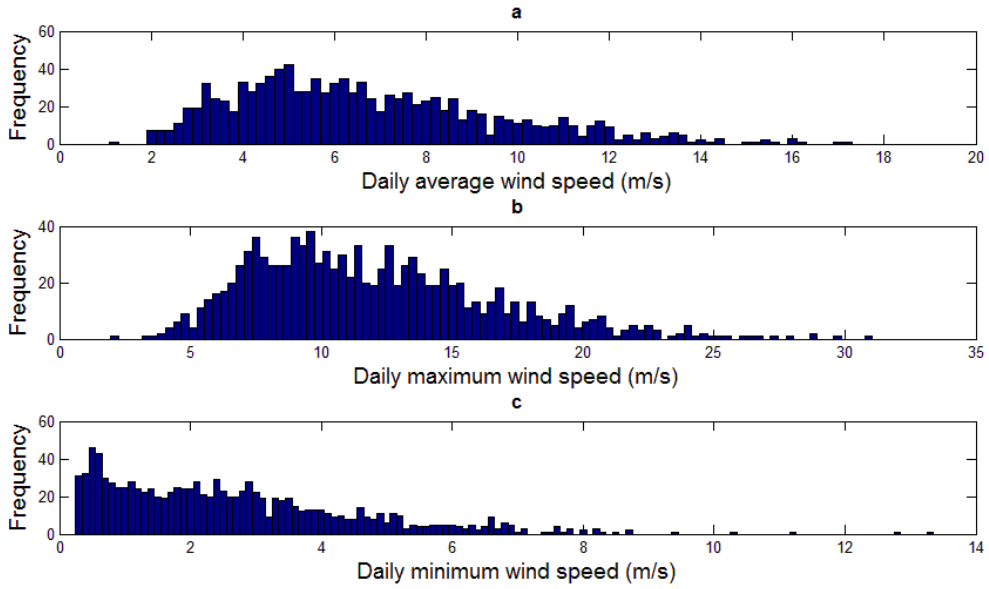

Figure 4-21: Site B histograms a) Daily average wind speed b) Daily maximum wind speed and c) Daily minimum wind speed at hub height

2.2. Met Office Weather Stations

Two Met office weather stations were required to fill gaps in wind speed data from Site A and Site B. They are described in Chapter 4.2.2.1. An additional station was used to gather data for analysis later in this thesis, in Chapter 4.2.2.2.

2.2.1. Prestwick and Salsburgh

UK land and marine surface weather station data can be attained through the Met Office Integrated Data Archive System (MIDAS) [4-12]. Daily weather tables were obtained for Prestwick and Salsburgh weather stations, containing hourly mean temperature, wind speed and humidity measurements. The Prestwick data was from the period of the 1st of January 2010 until the 31st of December 2011, while the Salsburgh data was from the 1st of January 2010 to the 31st of December 2012.

Site A and Site B are located 13km and 27 km away from Salsburgh and Prestwick weather stations respectively, as shown in Figure 4-17.

Prestwick and Salsburgh are sited relatively close to Site A and Site B respectively and so their measurements will be used to provide measurements for days when the met masts were down. However as Salsburgh weather station is sited at a higher elevation than Site B and Prestwick will be affected more by coastal winds than Site A the wind speeds recorded at the weather stations will not be very accurate reflections of the wind speeds on the wind farms. The topographies of the sites are also very different. However these measurements will not contribute significantly to the overall dataset and nearby weather stations have been used before in the literature to give approximate weather conditions by Tavner [4-13].

Temperature and humidity readings were taken from each of the stations and used to compile Site A and Site B weather datasets to be used in analysis for Chapter 4.3. The temperature and humidity was measured at 1.25 meters using a louvered white screen [4-14]. Therefore two assumptions were made in compiling the weather datasets. Firstly that the conditions

recorded at the weather stations were the same as those recorded at their respective wind farms and secondly that the humidifies and temperatures recorded at 1.25m were the same as those conditions experienced by all the WT components and sub-components.

Wind speeds were measured using standard Met Office met masts that were 10 m tall. Equation 4-1 was used to estimate the wind speed a hub height of 80 m [4-6].

The daily averages were calculated by taking the mean of the hourly mean measurements. The time series of daily average wind speed, temperature and humidity are shown in Figure 4-22 and Figure 4-23 for Prestwick and Salsburgh respectively.

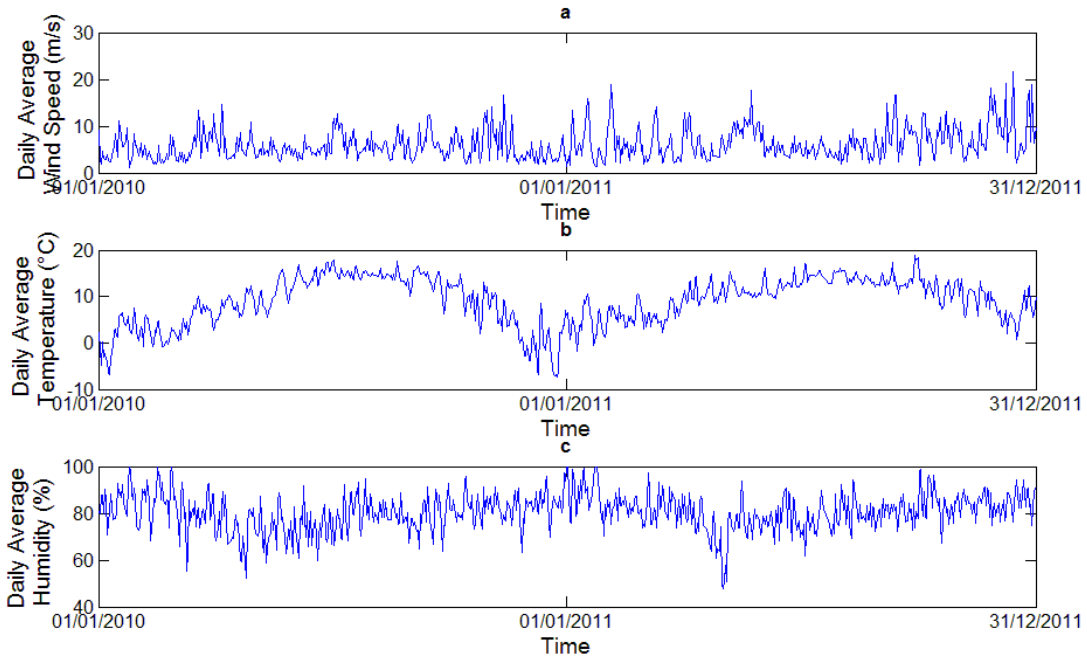

Figure 4-22: Prestwick time series of a) Daily average wind speed b) Daily average temperature and c) Daily average humidity hub height

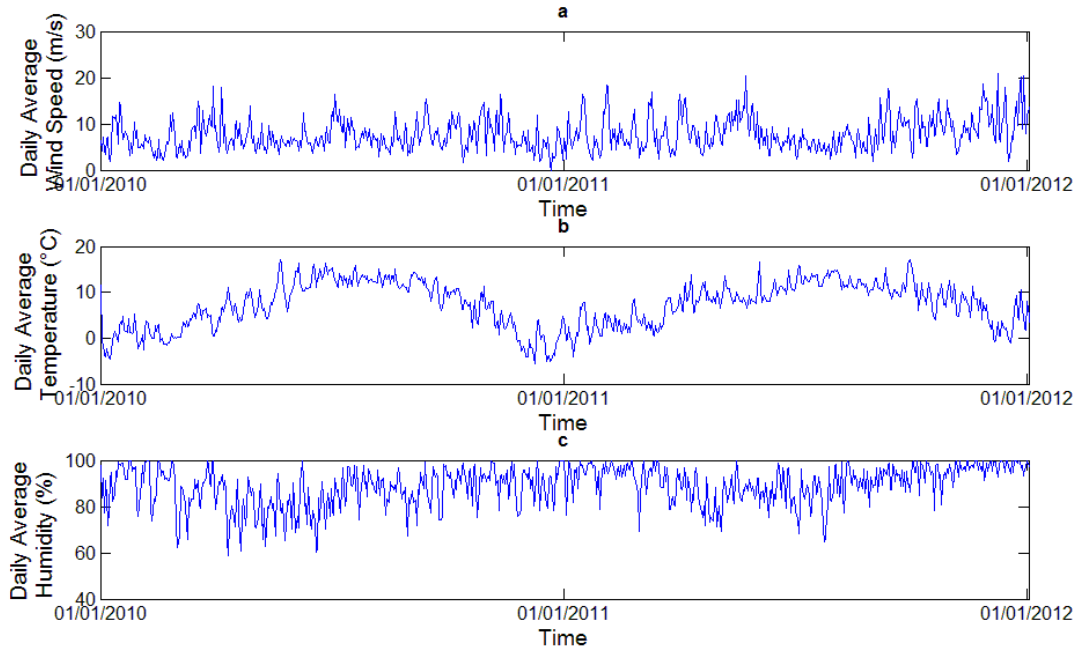

Figure 4-23: Salsburgh time series of a) Daily average wind speed b) Daily average temperature and c) Daily average humidity hub height

The average wind speed, temperature and humidity of Prestwick and Salsburgh are shown in Table 4-5.

Table 4-5: Average site conditions

Site	Average Hub Height Wind Speed (m/s)	Average Humidity (%)	Average Temperature (°C)
Prestwick	6.46	81.03	9.64
Salsburgh	7.92	89.86	7.38

2.2.2. Leuchars

Data from Leuchars met office weather station will be used in analysis undertaken throughout this thesis [4-12]. As shown in Figure 4-17, the site is located on the East coast of Scotland. The measurements taken at Leuchars are the same as those taken at Prestwick and Salsburgh. However, as will be discussed in Chapter 4.3.3, only the wind speed data will be used for Leuchars in the analysis. Equation 4-1 is used to calculate the wind speed at a hub height of 80 m.

Figure 4-24 shows a histogram of mean daily wind speed for the Leuchars weather station. The mean daily wind speed of the site is 6.59 m/s.

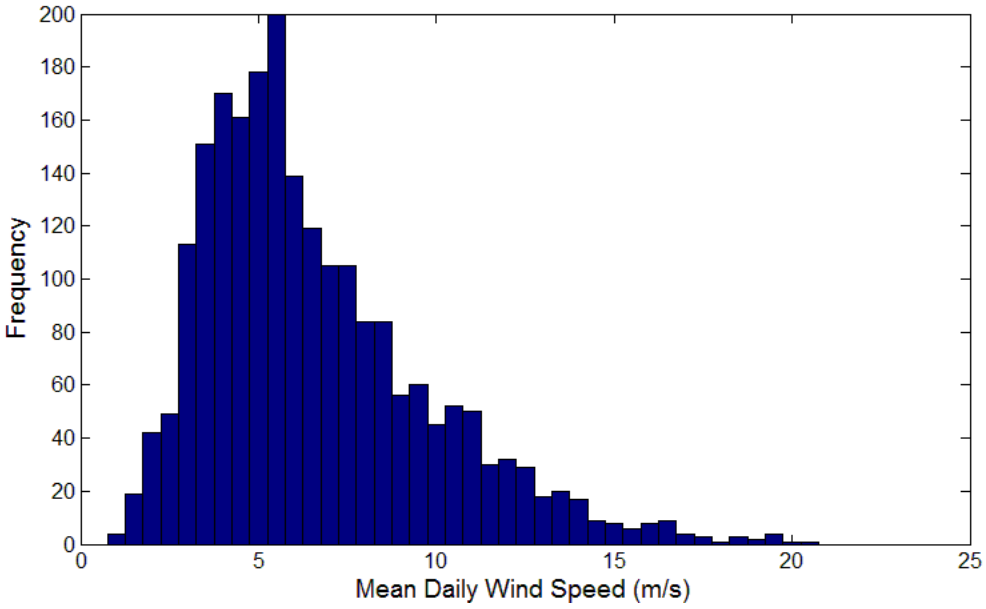

Figure 4-24: Leuchars mean daily wind speed at hub height histogram

2.3. Offshore Data

The FINO 1 platform was erected in mid-2003 in the North Sea, roughly 45 km from the island of Borkum, as shown in Figure 4-25 [4-15]. The goal of the platform was to gain more data for that region of the sea for the development of future offshore wind farms. The data would then serve to reduce the risks in the design, erection and operation of the offshore WTs. In 2009 the offshore wind farm Alpha Ventus was commissioned to the East of FINO 1, as shown in Figure 4-25.

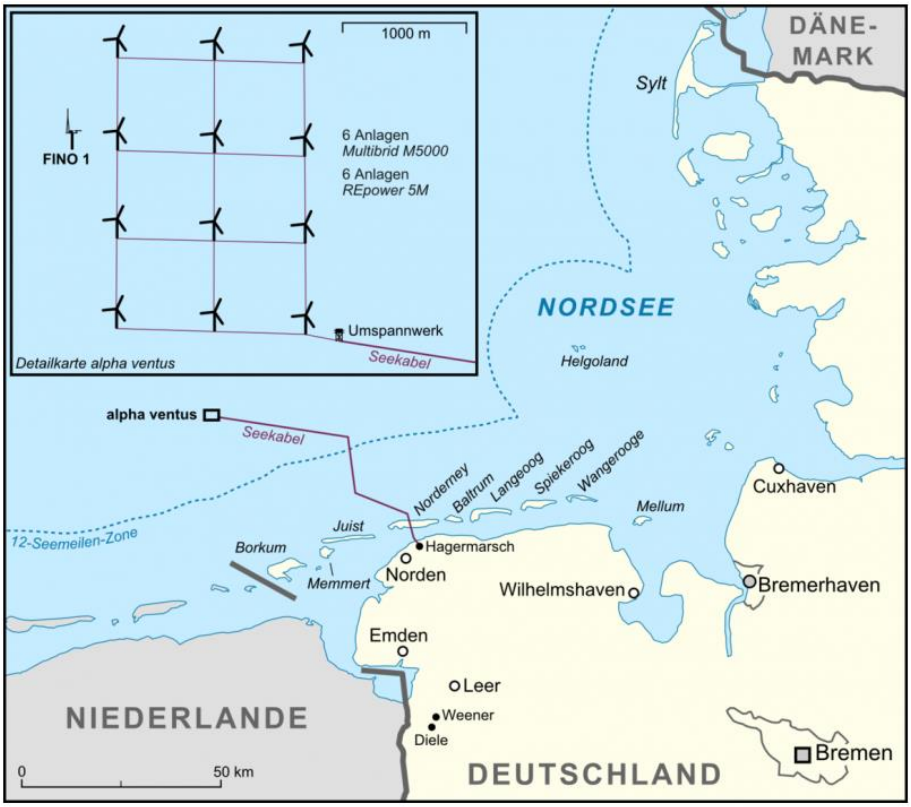

Figure 4-25: Location of FINO 1 platform [4-15]

The German Wind Institute (DEWI) is responsible for the measurements taken at the platform [4-15]. The platform is the site for a 100 m meteorological mast that is equipped with cup anemometers, wind vanes and ultrasonic anemometers (USA) – their positions are shown in Figure 4-26 [4-15].

Figure 4-26: Positions of measurement equipment on FINO 1 platform

DEWI provides 10 – minute mean measurements of wind direction data from the wind vanes and cup anemometers and 10 Hz data from the USA's. Data was obtained between 01/01/2006 and 31/12/2011 from the 70 m cup anemometer. Using Equation 4-1, and a surface roughness length of 0.001 m, the wind speed was calculated for a hub height of 80 m [4-6]. This is a relatively low hub height for an offshore wind turbine – the Siemens 6MW offshore WT has blades that are 75m long – but it keeps the offshore data comparable to the onshore data and with such a low surface roughness length the wind speed profile does not differ significantly above 80 m. With the wind speed adjusted, the mean daily wind speed at FINO 1 is calculated to be 9.48 m/s. The FINO 1 wind speed PDF and time series between 01/01/2006 and 31/12/2011 are shown Figure 4-27.

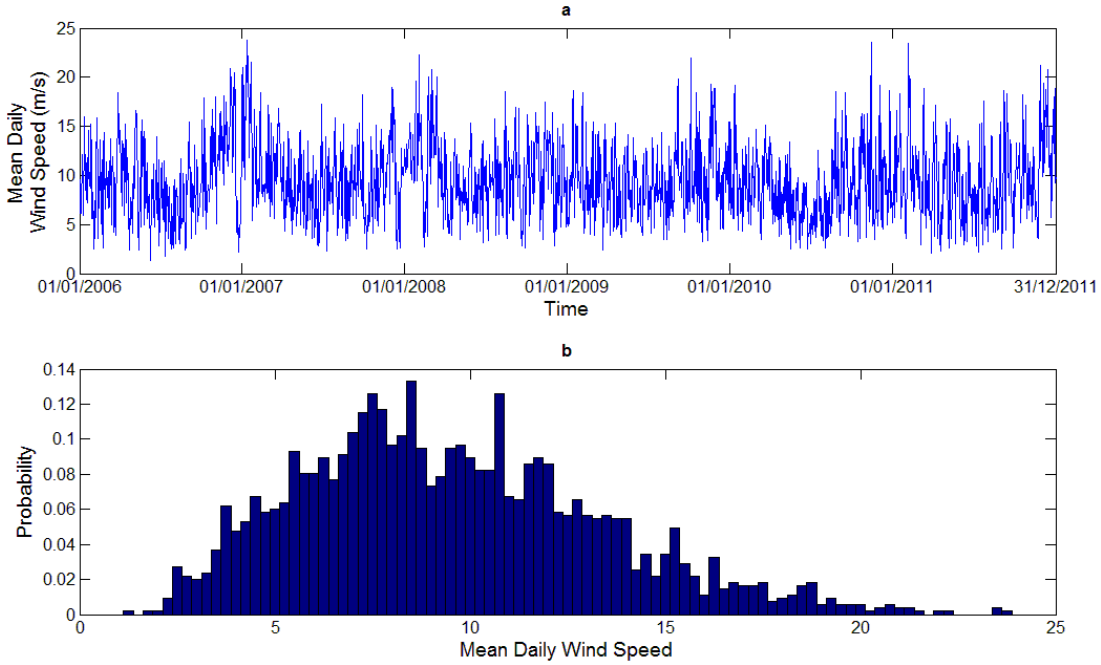

Figure 4-27: FINO 1 hub height met mast data a) Mean daily wind speed time series b) Mean daily wind speed normalised histogram

3. The Impact of Temperature and Humidity on Reliability

Analysis was undertaken to investigate the impact of wind speed, temperature and humidity on WT reliability by Tavner and his colleagues in 2013, building on work carried out in 2006 and 2010 [4-10], [4-13], [4-16].

They compared several wind farm availability time series with time series of the local weather conditions. The weather data that represented two of the sites came from onsite met masts while a weather station, located 17 km away, was used to provide data for the third.

Cross correlations were taken between the wind farm availability time series and the corresponding weather time series over the same period. The aim of the analysis was to show that the weather has a direct effect on the reliability of a wind turbine. This work has been discussed in more detail in Chapter 2.3.4.

Tavner and his colleagues concluded that temperature and humidity had an impact on WT reliability as well as wind speed. The purpose of this section is to undertake similar analysis using the available reliability and weather data and determine if the same conclusion can be drawn using this dataset. If it is the case that temperature and humidity have a direct impact on reliability, they will be included in the analysis undertaken in Chapter 6 and Chapter 7.

3.1. Cross Correlation Analysis

Cross-correlation is a measure of similarity between two signals, shown in Equation 4-2 [4-13], [4-17]. In this case, f(t) and g(t) are the two signals, τ the time lag between the signals and R_{fg} representing the cross-correlation [4-17].

$$R_{fg}(\tau) = \int_{-\infty}^{\infty} f(t)g(t + \tau)dt \quad \text{Equation 4-2}$$

This can be written as shown in Equation 4-3, where T is the period of observation [4-13].

$$R_{fg}(\tau) = \lim_{T \to \infty} \frac{1}{2T} \int_{-T}^{T} f(t)g(t + \tau)dt \quad \text{Equation 4-3}$$

In the case of sampled signals, the expression is rewritten as shown in Equation 4-4, where N is the number of data points and m is the lag [4-13]. Each time series must be sampled uniformly.

$$R_{fg}[3 - m] = \lim_{N \to \infty} \frac{1}{2N + 1} \int_{-N}^{N} f[n]g[3 - n + m] \quad \text{Equation 4-4}$$

Cross-correlation can now be calculated where signals f(t) and g(t) are a finite length. The biased cross-correlation is calculated as shown in Equation 4-5 [4-13].

$$R_{fg}[3 - m] = \frac{1}{N} \sum_{n=1}^{N-m+1} f[n]g[3 - n + m] \quad \text{Equation 4-5}$$

As the lag, *m* increases in Equation 4-5, the cross-correlation decreases as the overlap of the signals reduces [4-13]. This problem is fixed by wrapping the signals around themselves in

time. This is done by taking the reliability and weather data for an equal number of years and wrapping the signals so the final December is then proceeded by the first January.

$$R_{fg}[3-m] = \frac{1}{N-[3-m]} \sum_{n=1}^{N-m+1} f[n]g[3-n+m] \qquad \text{Equation 4-6}$$

As it is not possible that future weather conditions can have an impact on present WT reliability, only positive lags are considered. Therefore m = 1,…,M + 1 [4-13].

The cross-correlation coefficient *C*, is the normalised version of the cross-correlation divided by the signal power, shown in Equation 4-7 [4-13]. A cross-correlation coefficient can be calculated for any lag, *m*.

$$C[3-m] = \frac{R_{fg}[3-m]}{[3-R_{ff}[0]\cdot R_{gg}[0]]^{0.5}} \qquad \text{Equation 4-7}$$

The cross-correlation coefficient is then between -1 and 1. If C = 0 there is no cross-correlation between the two signals; if C = 1 then the signals are perfectly positively correlated and if C = -1, the signals are perfectly negatively correlated [4-13].

3.2. Results

Using the same methodology as Tavner and his colleagues, the cross correlation of the time series of the number of WT failures at both Site A and Site B were calculated with the site daily average weather conditions. Only downtimes that were due to corrective maintenance were considered. Downtimes due to preventative maintenance, low wind and high winds were not included.

Only failures and weather conditions that took place between 01/01/2010 and 31/12/2011 were analysed. Failures that occurred to Site A WTs in 2012 were omitted as including them would mean that the time series would be 761 days long and this would distort the analysis due to the seasonality of the weather measurements and the wrapping of the weather time series.

Table 4-6: Correlation coefficients of Site A and Site B

Site		Minimum Temperature	Maximum Temperature	Average Temperature	Average Wind Speed	Maximum Wind Speed	Average Humidity
Site A	Correlation at zero lag	0.36	0.43	0.41	0.52	0.52	0.46
	Maximum correlation	0.41	0.47	0.46	0.52	0.52	0.47
Site B	Correlation at zero lag	0.39	0.36	0.39	0.40	0.40	0.40
	Maximum correlation	0.41	0.36	0.39	0.40	0.40	0.40

The weather condition that is most closely correlated with the wind farm availability time series at Site A and Site B is the average wind speed and maximum wind speed time series. As shown in Table 4-6 their correlation at zero lag was 0.52 and 0.40 at Site A and Site B respectively; in both cases the maximum was at zero lag indicating that the wind speed had an immediate impact on wind turbine availability. The high correlation suggests that an increase in wind speed coincides with an increase in the number of failed WTs.

Average humidity at Site B was also as equally highly correlated as average wind speed and maximum wind speed. The highest maximum correlation at Site B was minimum temperature with a correlation coefficient of 0.41. However this maximum occurred after a lag of several months. After this period of time it is unlikely that the minimum temperature has impacted WT reliability.

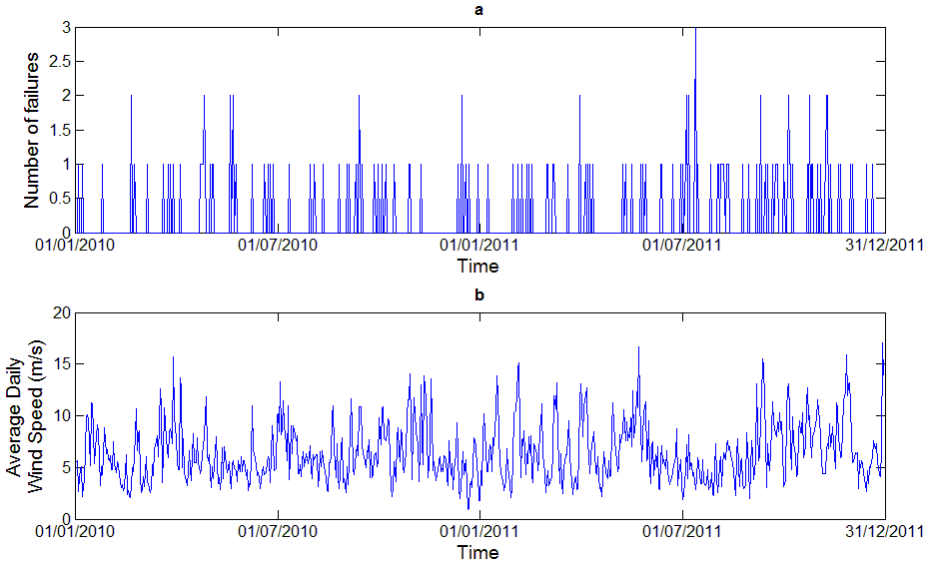

Figure 4-28: Site B time series of a) number of failures and b) mean daily wind speed

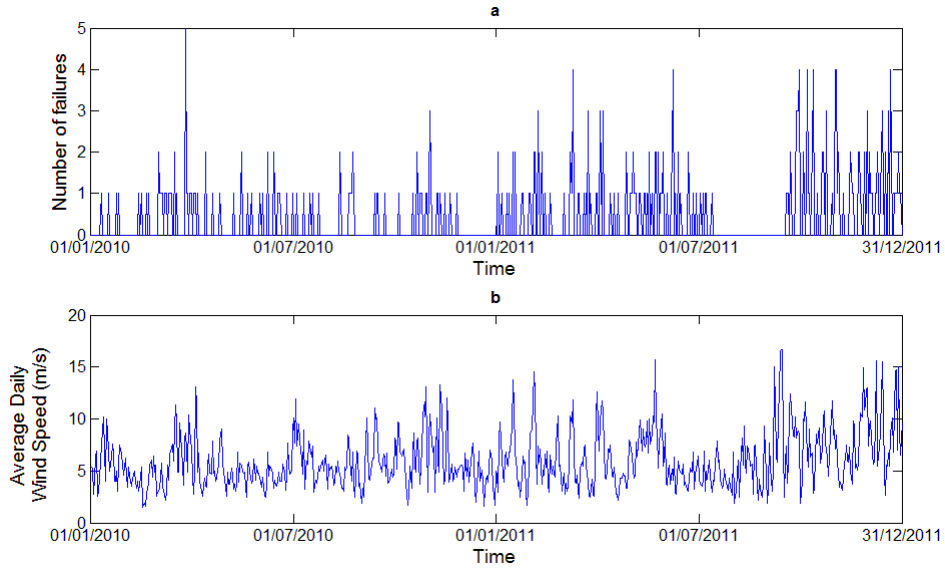

Figure 4-29: Site A time series of a) number of failures and b) mean daily wind speed

The time series for both the mean daily wind speed and the number of failures for Site A and Site B are shown in Figure 4-28 and Figure 4-29 respectively.

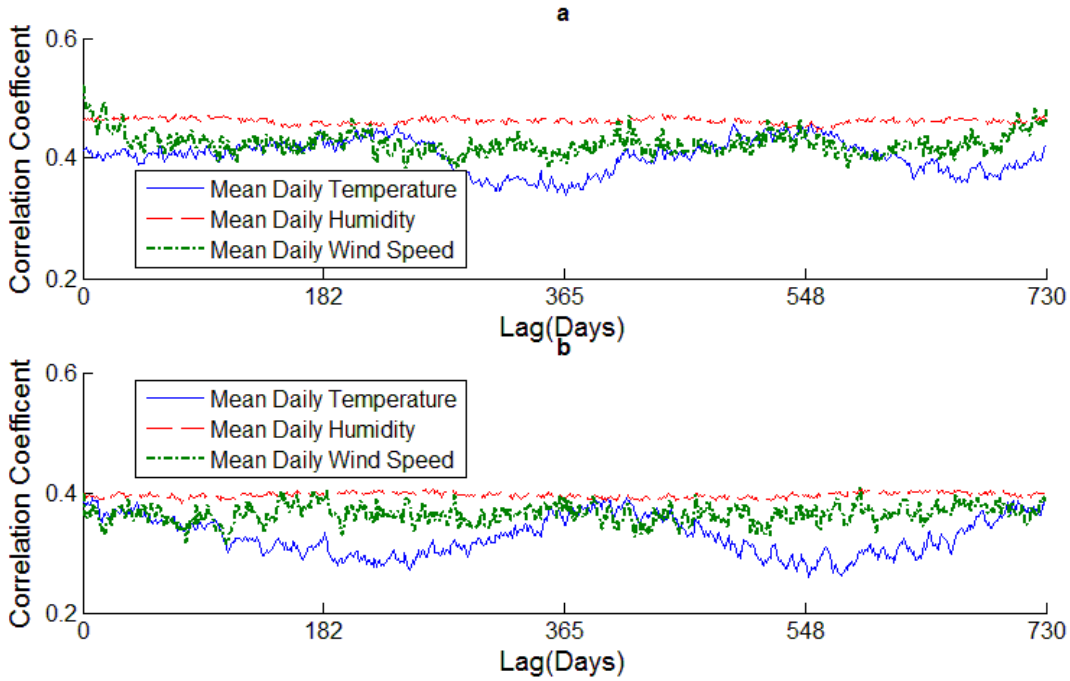

Figure 4-30: Correlelograms of wind farm availability and mean daily temperature, humidity and wind speed for a) Site A and b) Site B

Figure 4-30 shows the correlelograms of mean daily temperature, humidity and wind speed signals for both Site A and Site B, with a lag of 0 days to 730 days. The seasonality of the mean daily temperature can be seen in Figure 4-30a) and Figure 4-30b), with peaks and troughs occurring at intervals of roughly 365 days. The maximum correlation coefficient for the mean daily temperature and failure frequency at Site A is 238 days. This suggests that it is the temperature 238 days before a failure that has the greatest impact on the reliability of the component. Similarly the maximum correlation coefficient of mean daily temperature at Site B occurs at a lag of 414 days. It seems very unlikely that failures could be caused by conditions 414 days beforehand. The correlation coefficient remains relatively constant as the lag increases however.

.

3.3. Discussion

The results from the Tavner study and from this analysis are very similar, as shown in Table 4-7 [4-13]. They clearly show that there was a correlation between the WT reliability and wind speed, temperature and humidity. The Tavner study achieved their results to a 99.9% level of significance, however just how that metric was calculated was not explained. This metric is therefore not calculated using this dataset.

The ORD has far more WTs than the dataset used by Tavner and his colleagues, however the period over which the data was recorded was less. Overall Tavner and his colleagues used 202 WTYs of data, whereas the ORD dataset contains 372.5 WT years (minus the 2012 Site A data which was omitted because of the wrapping process).

Table 4-7: Cross correlation analysis from Tavner *et al* [4-13]

Weather Condition	Fehmarn		Krummhorn		Ormont	
	Correlation at zero lag	Maximum Correlation	Correlation at zero lag	Maximum Correlation	Correlation at zero lag	Maximum Correlation
Max Wind Speed	0.23	0.25	0.29	0.31	0.13	0.14
Standard Deviation of Wind Speed	0.22	0.24	-	-	0.14	0.16
Maximum Temperature	0.19	0.22	0.27	0.28	0.11	0.13
Minimum Temperature	0.18	0.21	0.24	0.26	0.09	0.11
Temperature Variation	0.19	0.23	0.26	0.28	0.12	0.14
Average Humidity	0.23	0.24	0.30	0.31	0.13	0.14

It is understandable how the wind speed could have a direct impact on how the WT operates; this is described in Chapter 2.3.4 and shown in Figure 4-3. It is much harder to explain how the temperature and humidity have a direct impact on reliability. However, why does there appear to be a relationship between the temperature (and humidity) and the number of WT failures?

Another issue when attempting to understand the impact of temperature and humidity on component failures is that the measurements taken in both this analysis and Tavner's case were of the surroundings, rather than those experienced inside the nacelle (or the tower) by the failed components. In the case of the SWT-2.3-101 model, the temperature and the humidity inside the WTs were monitored and controlled by an internal climate control unit [4-4]. This is the case now with all modern multi-megawatt machines. It is not clear whether a unit like this was fitted to the WTs in Tavner's dataset; no mention is made within the product brochure of the 330kW model [4-18]. If a system was not fitted it would be reasonable to assume the ambient temperature to be related to the nacelle temperature. However in the case of the SWT-2.3-101 that same assumption cannot be made due to the interference of the climate control system. Why then was there a clear correlation between temperature and humidity and wind turbine reliability shown in Table 4-6 and Table 4-7?

Table 4-8: Cross-correlation coefficients of daily mean temperature, humidity and wind speed for Site A and Site B

Site		Daily mean cross-correlation Coefficient		
		Temperature and Humidity	Temperature and Wind speed	Humidity and Wind Speed
Site A	Zero lag correlation	0.88	0.82	0.91
	Max correlation	0.88	0.82	0.91
Site B	Zero lag correlation	0.82	0.77	0.92
	Max correlation	0.82	0.77	0.92

Wind is the movement of air which is caused by differences in atmospheric pressure due to temperature differences. Therefore the wind speed is related to temperature which in turn also influences humidity. Because these factors are all closely related and are not independent from one another it is difficult to determine whether the correlation they each show with WT reliability is due to causation, or if they are indirectly linked. The cross-

correlation coefficients of temperature and wind speed for Site A and Site B is 0.82 and 0.77 respectively, as shown in Table 4-8.

Seasonally, the wind speed, temperature and humidity follow clear trends. The temperature in the Site A and Site B datasets increase in the summer and decrease in the winter, as shown in Figure 4-31b. The humidity also follows a predictable pattern in Figure 4-31c, rising in the winter and falling in the summer. The wind speed generally decreases in the summer and increases in the winter, as shown in Figure 4-31a. It is likely that the high correlation between all of the weather characteristics and WT reliability, shown in Table 4-6 and Table 4-7, is due to the predictable and regular relationships between the weather characteristics, rather than their direct influence on the reliability of the WTs. Therefore the high cross-correlation coefficients relating the temperature and humidity to WT reliability may be due to their close relationship with the wind speed, rather than because the temperature and humidity are influencing the WT directly.

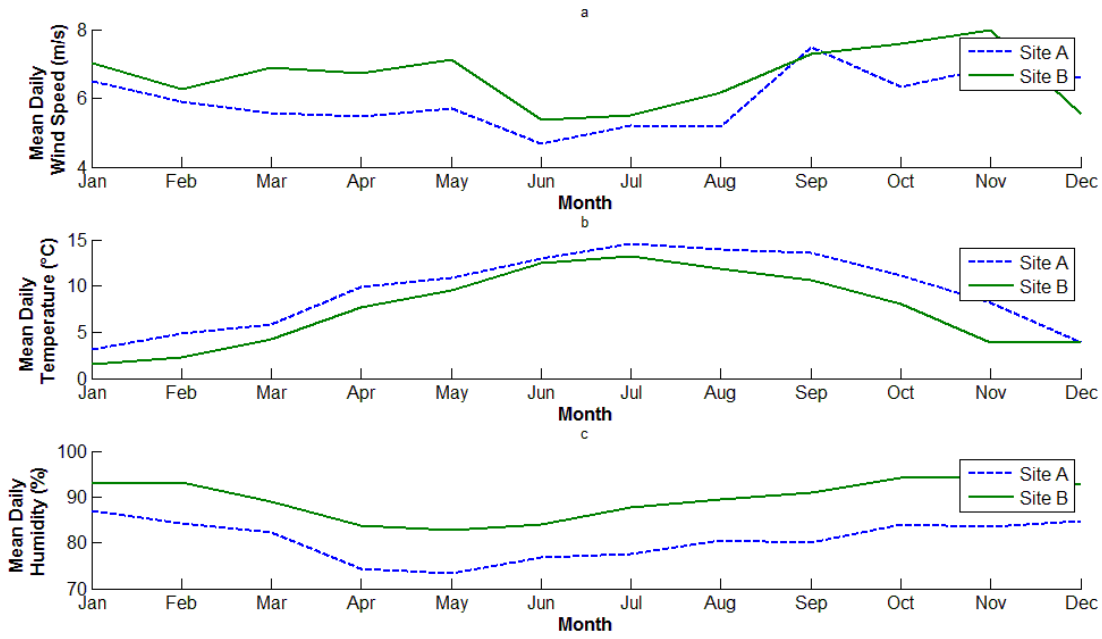

Figure 4-31: Monthly weather trends for Site A and Site B a) mean daily wind speed b) mean daily temperature and c) mean daily humidity

Because a climate control system is employed within the SWT-2.3-101 and because of the ambiguity over the direct impact of ambient temperature and humidity on WT reliability, it is difficult to determine if ambient temperature or humidity have any direct effect on WT reliability. Therefore this thesis will subsequently focus solely on the impact of wind speed on WT reliability. The following chapter will describe the methodology that will be used to model the relationship between the two variables.

4. Chapter 4 Summary

The purpose of this Chapter was to introduce and perform initial analysis on the ORD and to find weather data for the wind farm sites over the recorded period.

The WT reliability data used in this thesis comes from two sites in Scotland that have a combined total of 194 WTs. The size of the dataset is 384.4 WT years and is called the ORD. The WTs used at both wind farms are the same model and have an output capacity of 2.3 MW. Each WT comprises twelve components, shown in An example of this code is "SIA1A040MDY". The first 2 characters indicate the first 2 letters of the wind farm's name, in this case Site A. The following 3 characters distinguish Site A from any other wind farms owned by the operator that also have the first 2 letters of their name to be "SI". The 6th, 7th and 8th characters, which are always numbers, represent the asset to which the failure occurred – in this case WT number 40. The last characters indicate the component that failed which in the example's case was the control system. Codes which indicate the location of the failure within the system are shown in Table 4-2. There are 33 in total.

Table 4-2. The downtimes are also recorded by the ORD, Figure 4-6 shows what happens during the downtime period of each failure.

Reliability analysis is undertaken in Chapter 4.1.4 using the ORD dataset. The analysis compares well to previously published reliability data shown previously in Chapter 2.3.4. The least reliable components are the control system, yaw system and drive train. On average the rotor, drive train and hydraulics cause the longest periods of downtime. A summary of component failure rate data from the ORD is shown in Table 4-3.

The weather data used in this thesis comes from three sources – the met office MIDAS database, onsite met masts from the operator and the offshore FINO1 met mast located in the North Sea. Weather time series are constructed for Site A and Site B using the onsite met mast data and MIDAS data from nearby weather stations, shown in Figure 4-17.

Research undertaken by Tavner suggested that temperature and humidity may also impact WT reliability [4-13]. Using the WT reliability and weather data Tavner's methodology was followed to determine if temperature and humidity should be included in the analysis undertaken in this thesis. It was found in Chapter 4.3 that although the methodology used by Tavner suggested that temperature and humidity were related to WT reliability, there was not enough evidence to suggest that they had a direct effect. Therefore it was decided that the thesis would maintenance its focus exclusively on the impact of wind speed on WT component failure rate (see Chapter 4.3.3).

Using the data presented in this Chapter, Chapter 5 will utilise the methodologies discussed in Chapter 3 to calculate the relationship between wind speed and reliability. A model will then be developed in Chapter 6 and Chapter 7 that will be able to extrapolate this relationship to sites where component failure rates are unknown.

5. Chapter 4 References

[4-1] Variable Pitch, "Site B," 2014. [Online]. Available: http://www.variablepitch.co.uk/stations/65/. [Accessed: 04-Jul-2014].

[4-2] Variable Pitch, "Site A," 2014. [Online]. Available: http://www.variablepitch.co.uk/stations/718/. [Accessed: 01-Jul-2014].

[4-3] Scottish Renewables, "Scotland's Renewable Energy Sector in Numbers," 2014. [Online]. Available: http://www.scottishrenewables.com/scottish-renewable-energy-statistics-glance/#chart1. [Accessed: 17-Sep-2014].

[4-4] Siemens, "Siemens Wind Turbine SWT-2.3-101 - The new standard for moderate wind conditions," Erlangen, Germany, 2012.

[4-5] W. Leithead, *Wind Turbine Technology Lectures*. University of Strathclyde, 2010.

[4-6] T. Burton, D. Sharpe, N. Jenkins, and E. Bossanyi, *Wind Energy Handbook*, 1st ed. Chichester: John Wiley and Sons Inc, 2008, p. 19.

[4-7] O. Anaya-Lara, *Leucture notes - Doubly-fed induction generator-based wind turbines*. University of Strathclyde, 2010.

[4-8] Reference Designation System for Power Plants (RDS-PP) Best Practice Group, "RDS-PP Renewables (Best Practices)," 2014. [Online] Available: http://www.rds-pp.com/ [Accessed 20-Jan-2015].

[4-9] D. McMillan and G. W. Ault, "Condition monitoring benefit for onshore wind turbines : sensitivity to operational parameters," *IET Renew. Power Gener.*, vol. 2, no. 1, pp. 60 – 72, 2008.

[4-10] P. Tavner, C. Edwards, A. Brinkman, and F. Spinato, "Influence of Wind Speed on Wind Turbine Reliability," *Wind Eng.*, vol. 30, no. 1, pp. 55–72, 2006.

[4-11] M. Wilkinson, T. Van Delft, and K. Harman, "The Effect of Environmental Parameters on Wind Turbine Reliability," in *EWEA 2012*, 2012,.

[4-12] Met Office, "Met Office Integrated Data Archive System Land and Marine Surface Stations Data," 14-Oct-2013. [Online]. Available: http://badc.nerc.ac.uk/view/badc.nerc.ac.uk__ATOM__dataent_ukmo-midas.

[4-13] P. J. Tavner, D. M. Greenwood, M. W. G. Whittle, R. Gindele, S. Faulstich, and B. Hahn, "Study of weather and location effects on wind turbine," *Wind Energy.*, vol 16, no. 2, pp. 175–187, 2013.

[4-14] Met Office, "Met Office Surface Data Users Guide." [Online]. Available: http://badc.nerc.ac.uk/data/ukmo-midas/ukmo_guide.html#2.2. [Accessed: 02-May-2014].

[4-15] DEWI, "FINO 1 – Off-shore research platform," 2012. [Online]. Available: http://www.dewi.de/dewi/index.php?id=152. [Accessed: 02-May-2014].

[4-16] P. J. Tavner, B. Hahn, R. Gindele, M. W. G. Whittle, S. Faulstich, and D. M. Greenwood, "Study of Effects of Weather & Location on Wind Turbine Failure Rates," in *EWEC 2010*, 2010.

[4-17] G. E. P. Box and G. M. Jenkins, *Time Series Analysis: Forecasting and Control*. San Francisco: Holden-Day, 1970.

[4-18] Enercon, "ENERCON Wind energy converters Product overview," Aurich, Germany, 2010.

Chapter 5. Wind Speed Dependent Failure Rates Methodology

1. Calculating Wind Speed Dependent Failure Rates

Following on from the models discussed in Chapter 3, Chapter 5.1 uses these proposed models to calculate wind speed dependent failure rates. Failure rates are calculated first using Kernel density functions, (discussed previously in Chapter 3.2.3) and then normalised histograms (discussed in Chapter 3.2.4).

Both methods use Bayes Theorem (as discussed in Chapter 3.2.1), shown in Equation 5-1.

$$P(\lambda_i|w) = \frac{P(w|\lambda_i)P(\lambda_i)}{P(w)} \qquad \textbf{Equation 5-1}$$

The chosen method to be used in the wind speed dependent failure rate model is decided upon in Chapter 5.1.3.

1.1. Kernel Density Functions

The calibration wind speed distribution *P(w)* was calculated first by taking kernel density estimates of both Site A and Site B and binning the data from both wind farms at the same intervals. This was done using the Matlab function 'ksdensity' [5-2].

Table 5-1: Site A and Site B minimum and maximum mean daily wind speeds

Mean Daily Wind Speed	Site A	Site B
Maximum (m/s)	15.72	17.07
Minimum (m/s)	1.24	0.96

The bins were calculated by taking the minimum and maximum mean daily wind speed of both sites and dividing the range between into 100 equal intervals. The minimums and maximums are shown in Table 5-1. The first and last bins are at 0.96 m/s and 17.07 m/s respectively. The intervals are each 0.16 m/s.

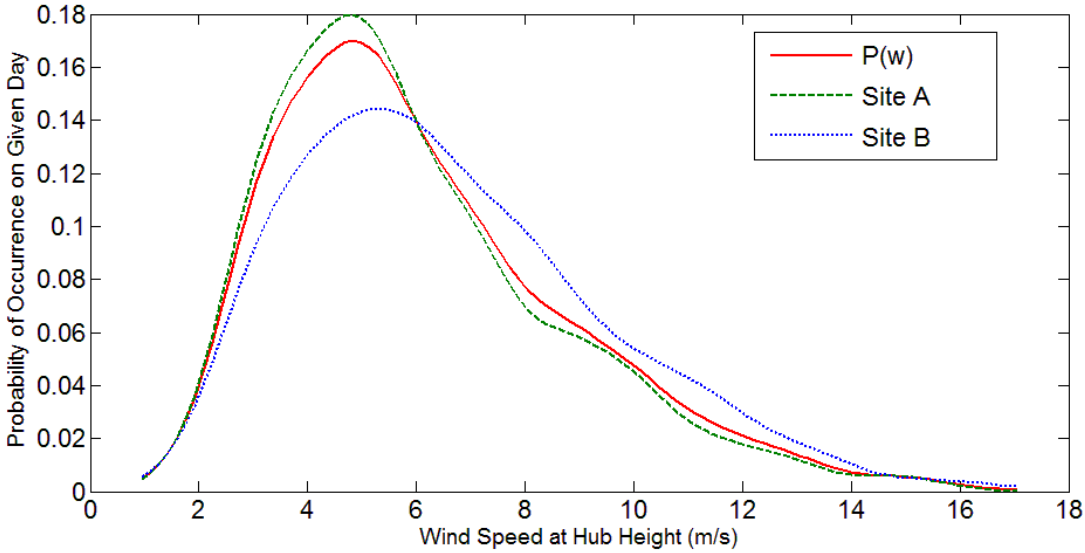

Figure 5-1: Site A, Site B and calibration (P(w)) datasets mean daily wind speed PDF calculated using kernel density estimates

Figure 5-1 shows the PDFs of Site A and Site B. Site A consists of 278.5 WT years of data, while Site B consists of only 105.9 WT years of data - therefore 72.5% of the data comes from Site A. *P(w)* must reflect that difference in size and be a weighted combination of the two datasets. Equation 5-3 is used to calculate the calibration wind speed PDF, j and α represent the bin number and the weighting respectively. The weighting was calculated using Equation 5-2. The calibration wind speed dataset *P(w)* is shown in Figure 5-1.

$$\alpha = \frac{Size\ of\ Site\ A\ dataset}{Total\ size\ of\ dataset} \qquad \textbf{Equation 5-2}$$

$$P(w_j) = P(Site\ A_j)\alpha + P(Site\ B_j)(1-\alpha) \qquad \textbf{Equation 5-3}$$

The term $P(w|\lambda_i)$, is the probability of wind speed w occurring, given a failure has occurred to component i. This is calculated by taking a PDF of the daily average wind speeds recorded on days when a failure occurred to component i. The data is binned at the same intervals as *P(w)*.

An advantage of using kernel density estimation is that this method allows probabilities to be calculated for wind speeds where no data was available from Site A or Site B . This means however that a probability is given that the mean daily wind speed will be less than 0 m/s, which is not possible.

However the disadvantage of using kernel density estimates is that there may not be enough data to accurately represent. The circles in Figure 5-2 and Figure 5-3 represent the raw data which are the probabilities of each daily wind speed occurring calculated from the ORD data of the control system and drive train, while the line is the estimated PDF. A non-parametric distribution is used because although mean daily wind speed follows a Weibull distribution, it is not known what distribution mean daily wind speed will follow when only considering days when an individual component fails [5-3].

In the control system's case, the PDF fits the data well – the sum of squares *S*, calculated using Equation 5-4 where *y* is the raw data and *m* is the estimated PDF, equals 0.003. But in the case of the drive train it fits less well, as shown in Figure 5-3.

$$S = \sum_{i=1}^{n} (y_i - m_i)^2$$ **Equation 5-4**

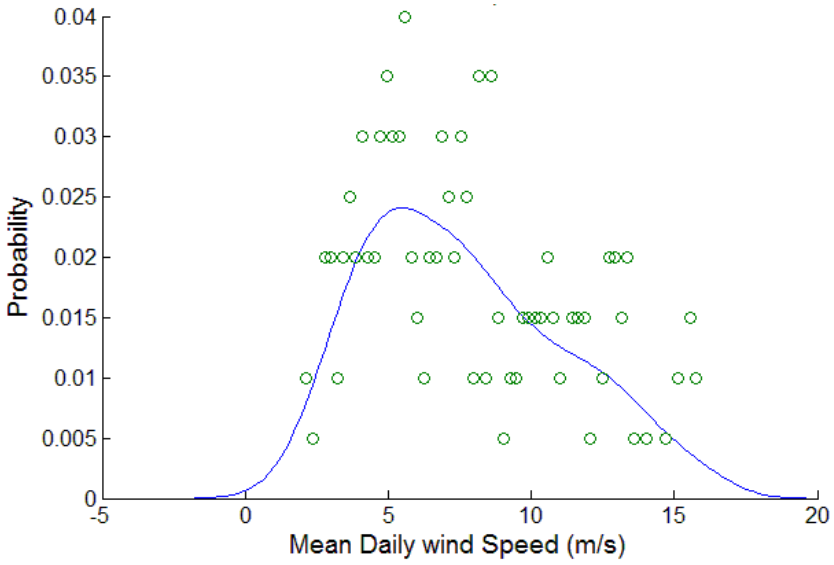

Figure 5-2: PDF of wind speed conditions on days when the control system failed. S = 0.003.

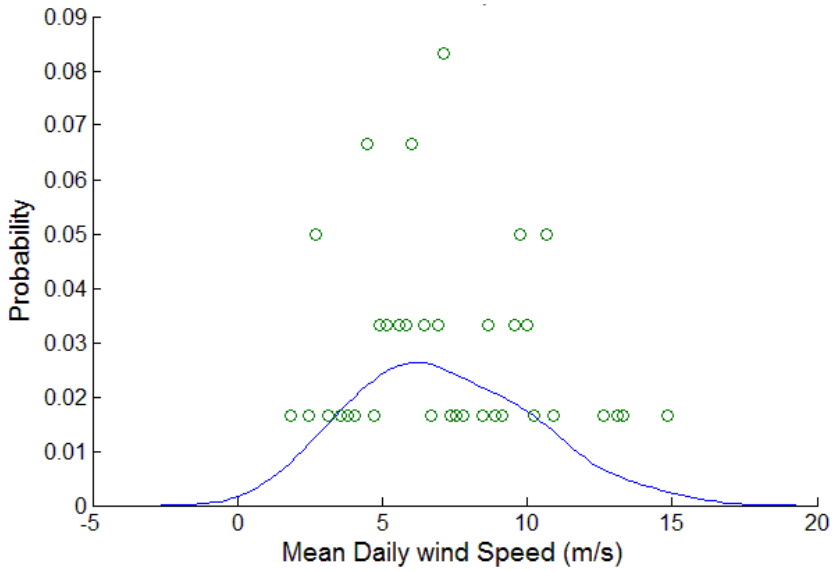

Figure 5-3: PDF of wind speed conditions on days when the drive train failed. S = 0.013.

For components that fail less often there are fewer data points for the PDF to be fitted to and the goodness of fit reduces as the kernel estimator function struggles to accurately fit a suitable curve to so few data points. As shown in Figure 5-4, in the case of the emergency system which fails only twice, S equals 0.460. This is clearly very inaccurate and improvements would have to be made before using this estimated PDF in the model but because these components fail so infrequently and have such low failure rates ($P(\lambda_i)$), when

$P(\lambda_i|w)$ is calculated it is so small compared to other less reliable components that the inaccuracy of the fitting has very little impact on the overall model. Therefore the less reliable components that are more interesting for the purposes of this analysis are modelled more accurately than the more reliable components that contribute less to the overall downtime.

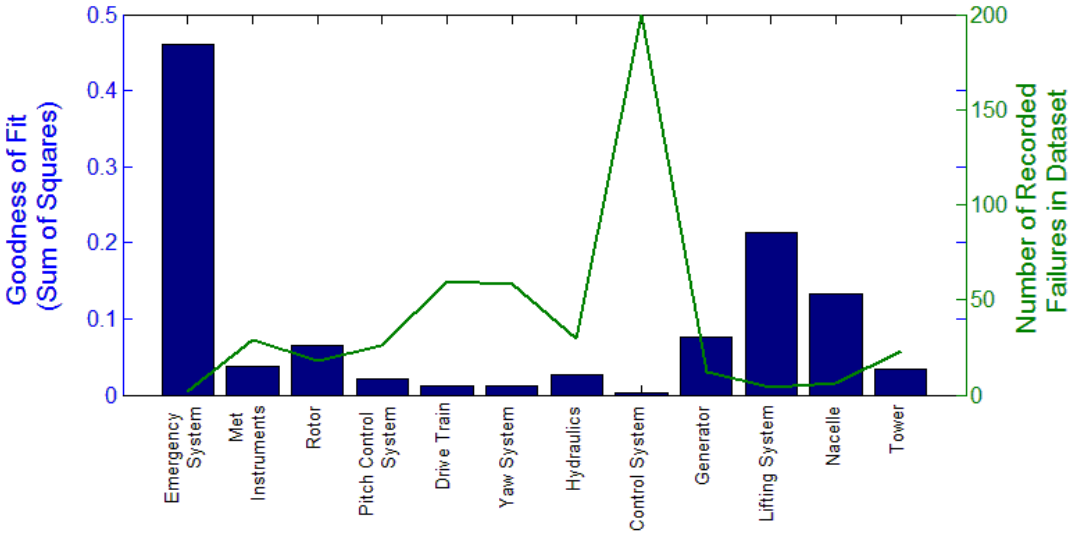

Figure 5-4: Goodness of fit of kernel estimates of *P(w|λ_i)* and number of failures of each component in dataset

1.1.1. Component Wind Speed Dependent Failure Rates Using Kernel Density Function

Using the probability density estimates of *P(w|λ_i)* and *P(w)* calculated in the previous section by using kernel density estimates, the probability of failure given a mean daily wind speed $P(\lambda_i|w)$ can be calculated.

$$P(\lambda_t|w) = \sum_{i=1}^{t} P(\lambda_i|w) \qquad \textbf{Equation 5-5}$$

When the WSD failure rates of all 12 components were summed and multiplied by the system failure rate, as shown in Equation 5-5 to calculate the probability of a failure to the WT system given the wind speed ($P(\lambda_t|w)$) for each wind speed bin, the plot in Figure 5-5 was produced. It showed that as the mean daily wind speed increased the probability of failure increased. This was especially the case at mean daily wind speeds greater than 15 m/s. When downtime filters were applied to remove failures which did not result in downtimes of less than 12 hours, 24 hours and 48 hours, the trend continued as illustrated in Figure 5-5.

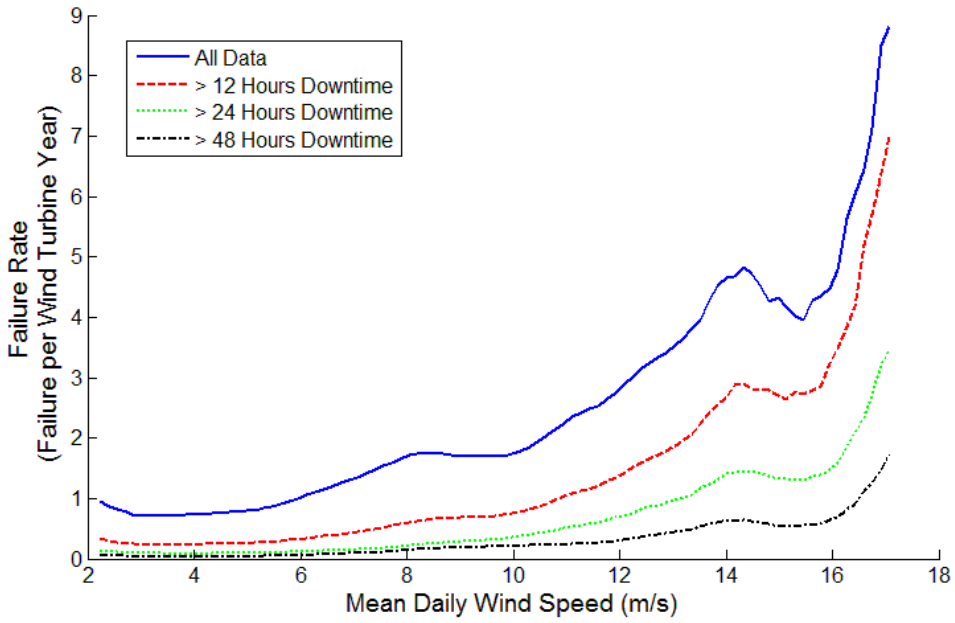

Figure 5-5: *P(λ_t|w)*, with downtime filters of 0 hours, 12 hours, 24 hours and 48 hours.

Only mean daily wind speeds upwards of 2 m/s were considered because firstly, as discussed in the previous section, one of the problems with estimating the PDF of $P(w|\lambda_i)$ was that it calculated that there was a probability of the average wind speed being less than 0 m/s – this skews the probability estimation for wind speeds less than 2 m/s. Secondly, as shown in Equation 5-1, calculating $P(\lambda_i|w)$ requires $P(w|\lambda_i)$ to be divided by $P(w)$ – therefore if the

model evidence shows that the probability of the wind speed being less than 1 m/s is zero, $P(\lambda_i|w)$ will equal infinity.

As the mean daily wind speed increased, the proportion of all the failures which caused downtimes greater than 12 hours, 24 hours and 48 hours also increased as shown in Figure 5-6. This showed that as the mean daily wind speed increased, the failures which occur at these higher wind speeds caused longer downtimes. This could be partially because failures that happened on days with high wind speeds statistically were more likely to be followed by periods of time with high wind speeds, as would be expected in winter. This then would result in maintenance crews being unable to access the WT to make their repairs, thus increasing downtime. But it was unlikely that wind speeds would remain so high for over 48 hours without giving the crews the opportunity to access the WT, it is therefore also reasonable to suggest that failure severity appears to increase as the mean daily wind speed increases.

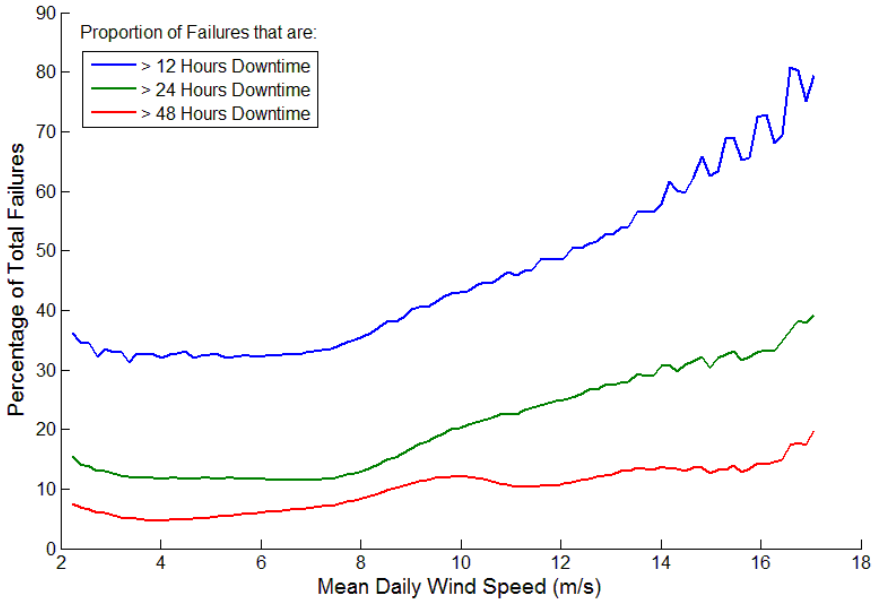

Figure 5-6: Percentage of total failures to the whole system against mean daily wind speed and failures which result in downtimes of greater than 12 hours, 24 hours and 48 hours.

The control system suffered the greatest amount of failures of all WT components in the dataset. As a result the shape of the plot shown in Figure 5-5 was influenced significantly by the relationship between the control system and mean daily wind speed. As shown in Figure 5-7 the failure rate of the component increased as the mean daily wind speed increased, especially above 15 m/s. The plot displays the same false peak at roughly 14 m/s as that shown in Figure 5-5. The peak was the result of the fitting of $P(\lambda_i|w)P(\lambda_i)$ shown in Figure 5-2.

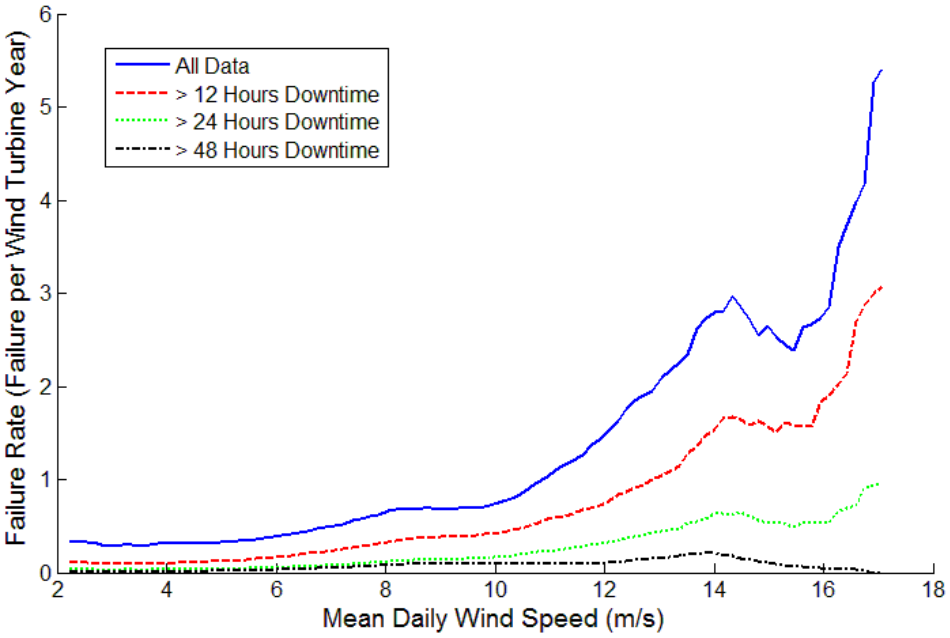

Figure 5-7: *P(λ$_i$\|w)* of the control system, with downtime filters of 0 hours, 12 hours, 24 hours and 48 hours.

The proportion of failures which cause downtimes greater than 24 hours and 48 hours decreases as the mean daily wind speed increases. This backs up the preliminary data analysis undertaken in Chapter 4.1.4.1 that showed that although the control system frequently failed; when it did it was for a relatively shorter period of time.

Figure 5-8 shows that counter to many other WT components, increasingly high wind speeds do not cause the control system to suffer long periods of downtime. Above 10 m/s, the percentage of failures that caused downtimes greater than 24 hours and 48 hours against all

control system failures, declined. Although like other components the proportion of failures causing downtimes greater than 12 hours did increase.

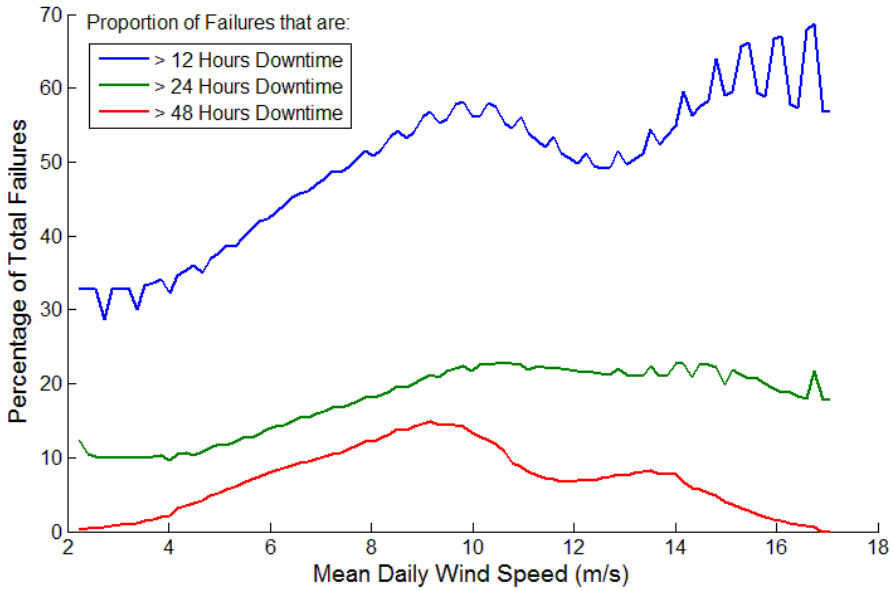

Figure 5-8: Percentage of total failures to the control system against mean daily wind speed and failures which result in downtimes of greater than 12 hours, 24 hours and 48 hours.

Interestingly the drive train shows a slightly different plot of WSD failure rates as shown in Figure 5-9.

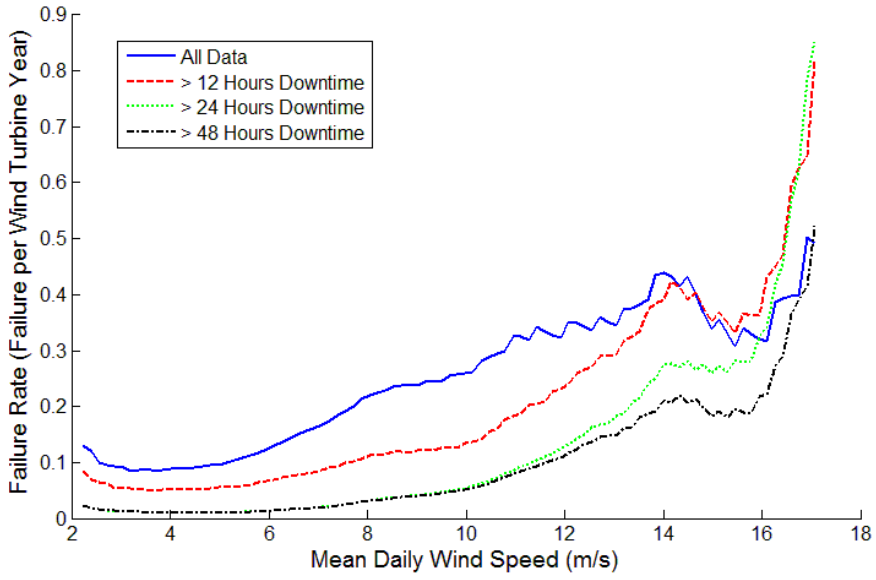

Figure 5-9: $P(\lambda_t|w)$ of the drive train, with downtime filters of 0 hours, 12 hours, 24 hours and 48 hours.

Firstly the drive train WSD failure rate reached its second highest point at 14 m/s when no downtime filter was applied; it then peaked at 17 m/s. The failure rate did not increase beyond these two points. In the case of the control system (and the yaw system) the failure rate accelerated in this region. However this flattening, which was also seen when the downtime filters were applied, makes sense when the operation of the drive train is considered at wind speeds in this region.

At wind speeds above rated the gearbox maintains a constant torque while the control system operates the pitching of blades which keep the rotor turning at as near to a constant wind speed as possible. The drive train therefore does not work as hard beyond rated wind speed and may suffer fewer failures as a result. However from Figure 5-5it is clear that the WT does fail more often above rated wind speed as the two highest peaks are situated at 14 m/s and 17 m/s.

The reason for the peak at 14 m/s could have been a result of the drive train changing its operating strategy frequently while the wind speed varied between below and above rated. Rated wind speed for the SWT-2.3-101 is between 8 m/s – 11.5 m/s, but because it is not instantaneous wind speed being measured but mean daily wind speed, a day which has an average wind speed of 14 m/s would spend a good proportion of time below rated and above rated wind speed causing the WT to operate between the two strategies.

The final peak at 17 m/s is likely to be a result of the fitting of $P(w|\lambda_i)$ and $P(w)$ at the tails, a problem that is evident in the tails of the filtered 12 hour and 24 hour curves in Figure 5-5. The failure rate should always be higher for the series with the highest number of failures – when a filter is applied data points are removed, therefore the failure rate should be the same or lower at all points of the 12 hour and 24 hour filtered data, compared to the series with no filter. The data points for each component, after a downtime filter is applied, are presented in Table 5-2. Similarly the 24 hour filter series should not have a higher failure rate than the 12

hour filter series. This is again due to curve fitting and will be discussed in more detail in the subsequent section.

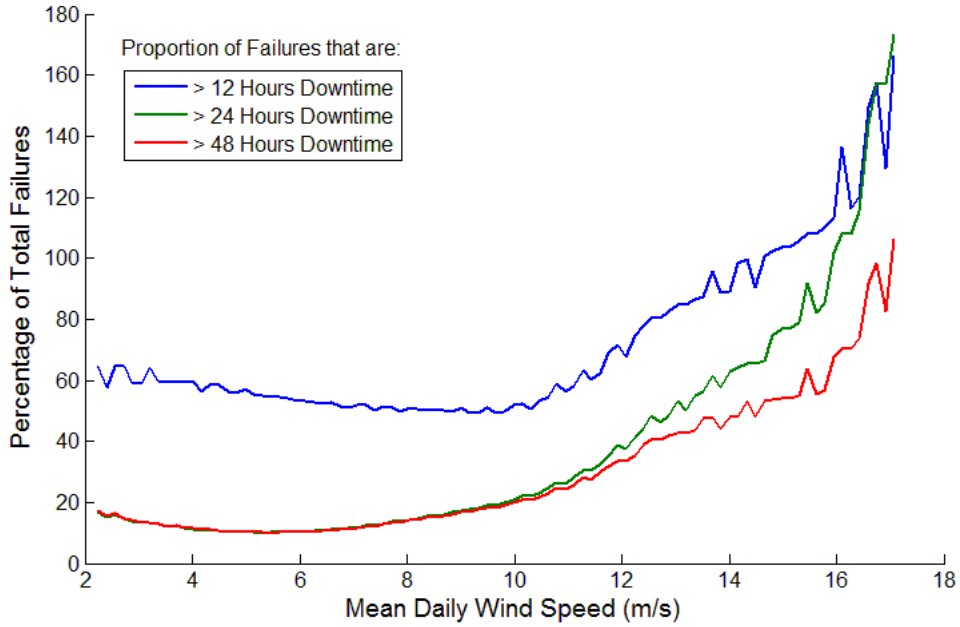

Figure 5-10: Percentage of total failures to the drive train against mean daily wind speed and failures which result in downtimes of greater than 12 hours, 24 hours and 48 hours.

The severity of failures appeared to increase at high wind speeds for the drive train, as shown in Figure 5-10. Unlike the control system, failures which caused downtimes greater than 48 hours increased at high wind speeds. To highlight the issue of curve fitting at wind speeds, Figure 5-10 shows that beyond 15 m/s the percentage of failures that caused a downtime greater than 12 hours was over 100%, which is obviously incorrect as there 25 fewer failures as shown in Table 5-2. This occurs because of *P(w)* being so close to 0 for these mean daily wind speeds.

Table 5-2: Data points for each component when downtime filters are applied

Component	Number of Failures when Downtime Filter Applied				
	0 Hours	6 Hours	12 Hours	24 Hours	48 Hours
Emergency System	2	1	0	0	0
Met Instruments	29	5	4	1	0
Rotor	18	13	5	3	1
Blade Pitch System	26	16	11	8	3
Drive Train	60	49	35	12	11
Yaw System	58	37	20	12	6
Hydraulics	30	18	13	6	3
Control System	200	122	92	33	15
Generator	12	6	4	2	1
Lifting System	4	2	1	0	0
Nacelle	6	1	0	0	0
Tower	23	3	0	0	0

The yaw system, which has the third highest failure rate of all the components, has a WSD failure rate similar to the control system in that it increases as the wind speed increases as shown in Figure 5-11. Again there is a problem with the failure rate of the 12 hour downtime filtered data as it is greater than the non-filtered data above 16 m/s.

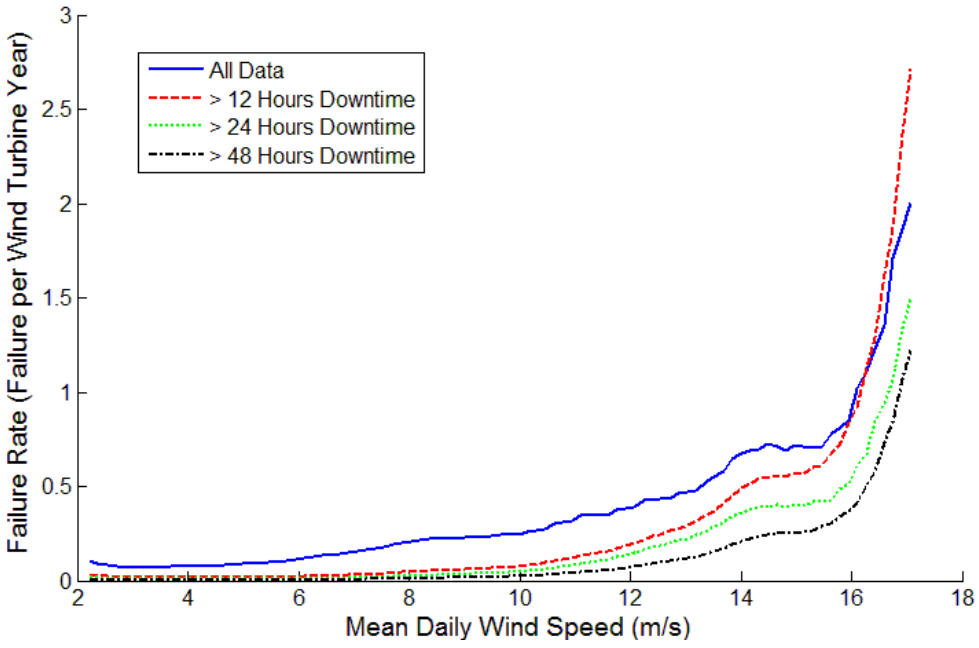

Figure 5-11: $P(\lambda_t|w)$ of the yaw system, with downtime filters of 0 hours, 12 hours, 24 hours and 48 hours.

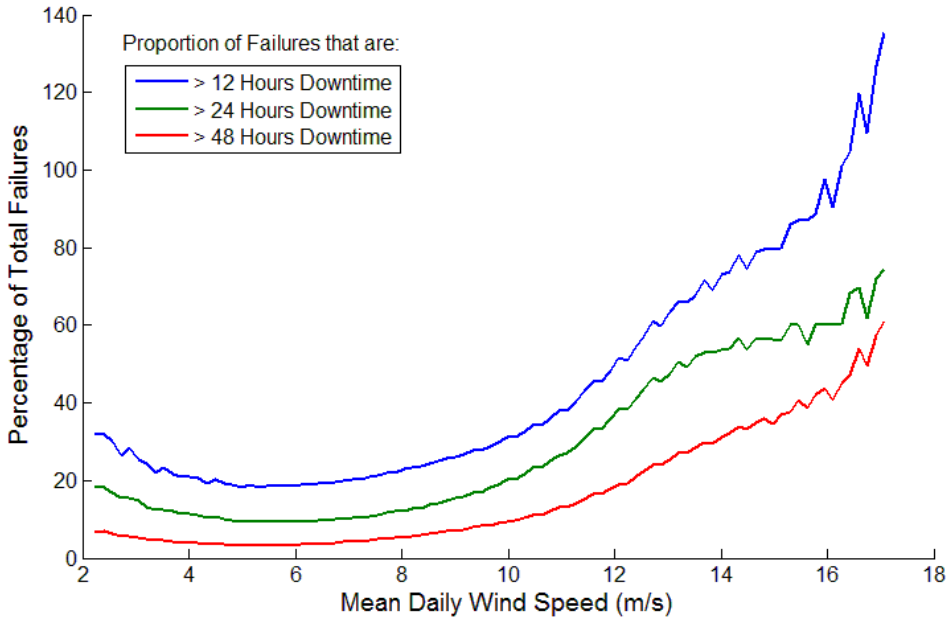

Figure 5-12: Percentage of total failures to the yaw system against mean daily wind speed and failures which result in downtimes of greater than 12 hours, 24 hours and 48 hours.

The yaw system also appeared to fail for longer periods of time as the wind speed increased, as shown in Figure 5-12.

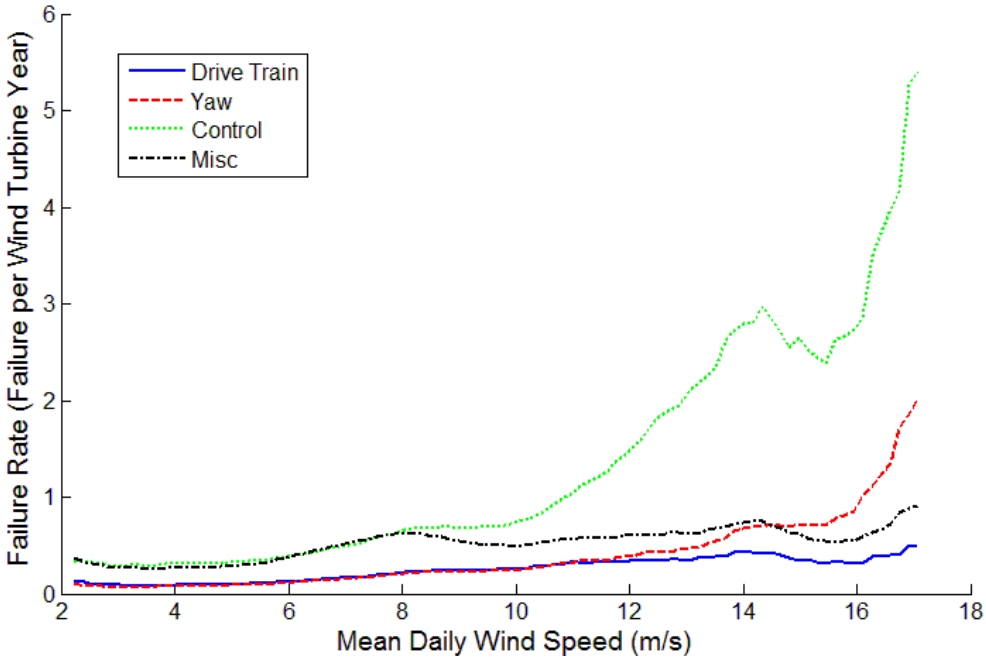

Figure 5-13: Plot of $P(\lambda_i|w)$ for the control system, drive train, yaw system and the remaining nine components, labelled as Misc.

Comparing the $P(\lambda_i|w)$ of the three least reliable components it is clear that in general there was an increase in the probability of failure as the wind speed increased, as shown in Figure 5-13. When the $P(\lambda_i|w)$ of the remaining nine components were summed together, labelled as Miscellaneous in Figure 5-13, they too showed an increase in failure rate as the wind speed increased.

The failure rates of all four sets similarly increased rapidly beyond 16 m/s and also increased between 4 m/s and 2 m/s. In both cases it was caused by the kernel estimates taken of $P(w|\lambda_i)$ and $P(w)$. The following section will discuss why this happens and consider a possible solution in using normalised histograms instead.

1.2. Normalised Histograms

The bins used in for the normalised histograms in this chapter are selected in Chapter 5.2.5.2, where the model is validated.

Normalised histograms were taken of the mean daily wind speed met mast data from Site A and Site B and then were combined wind speed in the same manner described in Chapter 5.1.1, Equations 5-2 and 5-3, to produce a calibrated wind speed (*P(w)*) dataset that describes the data from both sites, shown in Figure 5-15. Similarly a normalised histogram was also taken of the mean wind speeds when failures occurred to the individual components. This returned probabilities of the wind speed being within each bin when a failure occurred to a component $P(w|\lambda_i)$, an example of which is shown in Figure 5-14.

The WSD failure rate of the WT system is shown in Figure 5-16. It differs slightly to the WSD failure rate calculated using the kernel density estimate in Figure 5-5. One of the obvious differences is that the failure rate beyond 13 m/s in Figure 5-16 is less than that modelled in Figure 5-5. This is the case for the 0 hour, 12 hour, 24 hour and 48 hour filtered datasets.

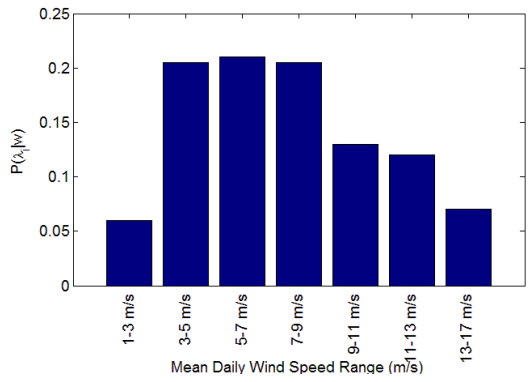

Figure 5-14: The probability of a mean wind speed w occurring on a given day, when a failure has occurred to i.

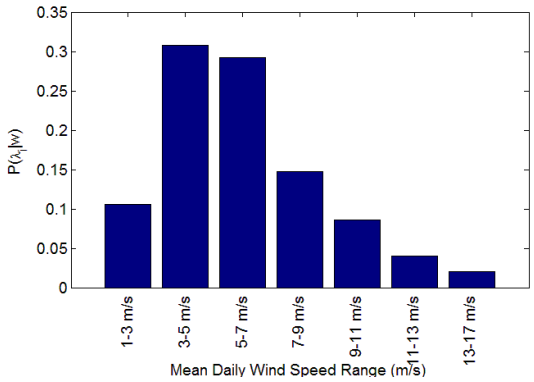

Figure 5-15: The probability of a mean wind speed w occurring on a given day.

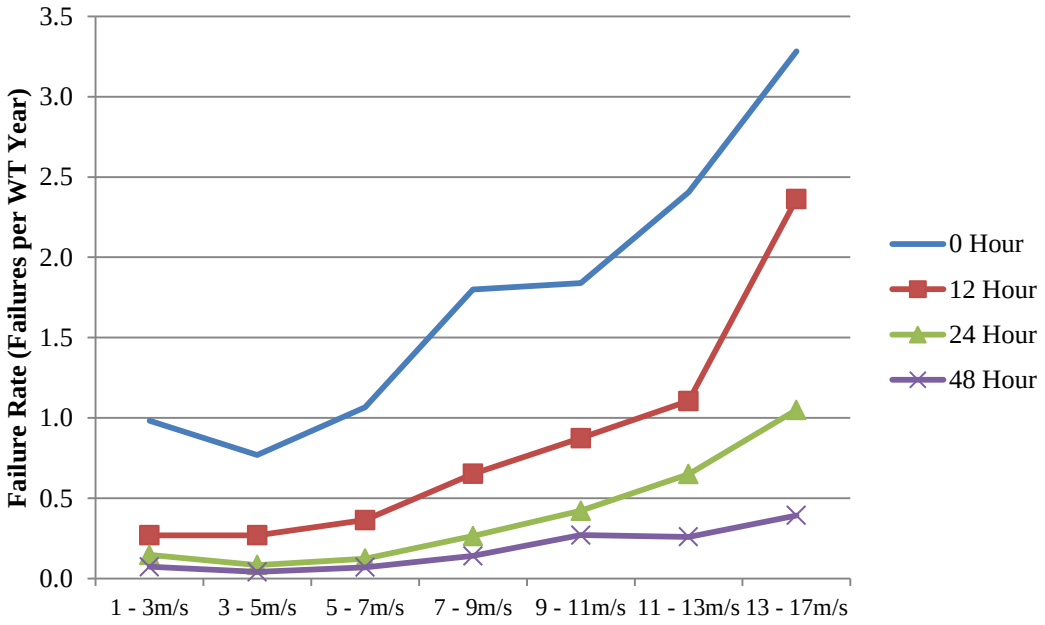

Figure 5-16: $P(\lambda_i|w)$ for the control system, calculated using normalised histograms, with 0 hour, 12 hour, 24 hour and 48 hour downtime filter

The reason for this difference is shown in Figure 5-17 where the numerator of Equation 5-1 is shown against the denominator for the control system when no downtime filter is applied. For the failure rate to increase in the final bin as dramatically as it does in with the kernel density estimate method, either $P(w)$ would need to decrease or, as the failure rate $P(\lambda_i)$ remains constant for each of the bins, $P(w|\lambda_i)$ would need to increase.

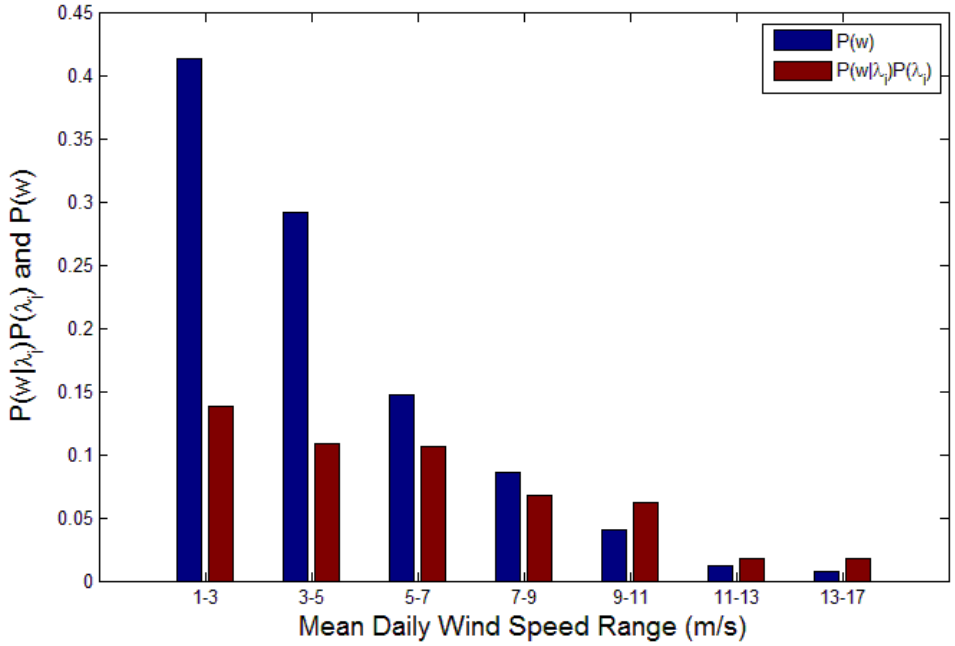

Figure 5-17: *P(w)* and $P(w|\lambda_i)P(\lambda_i)$ for the control system with 0 hour downtime filter when the histogram method is used

The drive train and yaw system WSD failure rates are shown Figure 5-18. Both the drive train and the yaw system show very similar trends to those shown in Figure 5-9 and Figure 5-11. The yaw system finishes with its highest failure rate at the highest wind speed range, whereas the drive train reliability shows a similar trend as illustrated in Figure 5-9.

The WSD failure rates for the remaining components are shown in Appendix II. Unlike Figure 5-13, if all the failure rates were summed together for each of the nine most reliable components the highest failure rate would not occur at the highest wind speed range but between 7 – 9m/s.

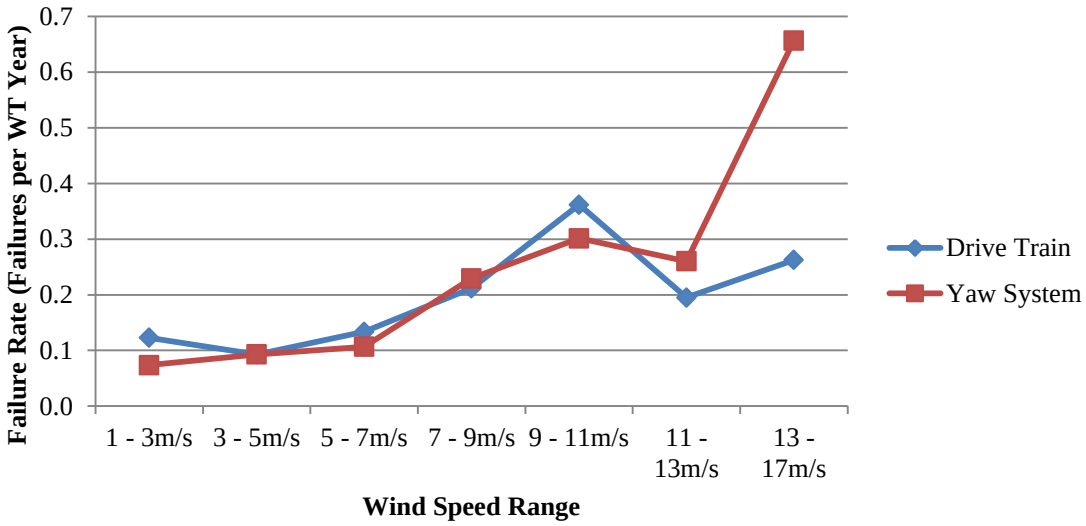

Figure 5-18: $P(\lambda_i|w)$ for the yaw system and the drive train with no downtime filter applied

1.3. Conclusion

In the case of the drive train and the yaw system, both methods modelled the WSD failure rates similarly. These components failed more frequently than any of the other components, with the exception of the control system, so it is important that there is good agreement between the two methods in how the WSD failure rates were modelled.

The modelling of the nine most reliable components will not affect the accuracy of the overall model as much as the fitting of the least reliable components. However as shown in Figure 5-16 the modelling of $P(\lambda_i|w)$ was very similar apart from at the highest wind speed ranges.

This was also the case with the control system which was modelled very similarly in the wind speed ranges between 1 m/s to 13 m/s, but beyond 13 m/s the two methods interpreted the failure rates differently. The histogram method was optimistic and believed that the failure rate would not increase as sharply beyond 14 m/s. The kernel density estimate plotted that the failure rate would increase rapidly as the wind speed increased. The reason for this difference is due to the way the kernel density estimate works. Because normal distributions were used to model the PDF assumptions were made beyond the sample due to the tails of the distributions.

This is demonstrated in Figure 5-19 which shows a normalised histogram and kernel density estimate of a synthetic sample which shows the probability of mean daily wind speed given the failure to a component $P(\lambda_i|w)$, created using distributions of the met mast data and ORD. The histogram only plots up until the wind speed bin 16 m/s -18 m/s, beyond that point there are no data points that fall into the higher bins – therefore failure rates would be equal to 0 above this range.

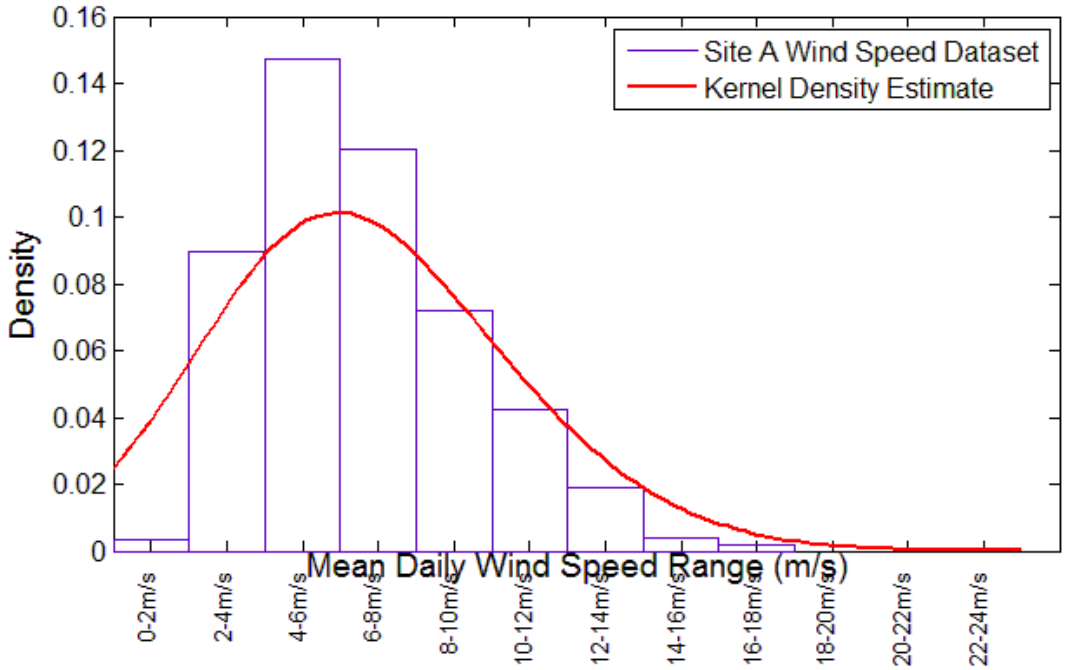

Figure 5-19: Comparison between kernel density estimate method and normalised histogram using Site A wind speed dataset

The kernel density estimate however plots beyond the range of the sample and makes a prediction about the whole population, rather than just the three year sample of wind speed data. Failure rates are calculated beyond 16 m/s – 18 m/s using this method, even although such events did not occur in the data. However because the probability of the wind speed being at this range are so improbable, $P(\lambda_i|w)$ becomes very large. This is the reason why the failure rate increased almost exponentially for all the components in Figure 5-13. This is also the case in the above example for wind speeds less than 0 m/s, which in reality would have a probability of 0. This problem can be solved by using tighter bandwidths – this makes the model more accurate but the benefits of estimating beyond the limits of the sample are lost.

The reason it would be beneficial to estimate failure rates for wind speeds beyond the limits of the sample data is because many sites operate at higher wind speeds than those experienced on the ORD sites. For the model to become more valid in these cases it would be valuable to extrapolate the relationships to higher wind speed ranges. If reliability does

decrease with wind speed as the results in this section suggest, it is these existing sites and potential sites like these that would benefit most from this model. This would be especially applicable to assessing the impact of the offshore environment.

Of course the impacts of offshore could not be properly appreciated without an O&M model that accounts for logistics and accessibility, which is somewhat beyond the bounds of this thesis. But to model the impact of wind speed on component reliability offshore it would be advantageous to use ORD from an offshore wind farm using WTs which have been designed specifically for that environment. Currently however this data is not easily accessible because of industrial confidentiality. In many cases were it available it may only be of limited use due to the age of the WTs, with many of them likely to be operating in the early failure region of the bathtub curve. Experience from Egmond Aan Zee and the Round 1 sites demonstrated that the early years of operation for an offshore wind farm can be very difficult and may not represent their long term reliability [5-4]–[5-6].

So to summarise, the key difference in the two methods was the way in which the tails of the $P(w)$ and $P(w|\lambda_i)$ distributions were modelled. Although the kernel estimation method may be more applicable for windy sites, the modelling of failure rates at high wind speeds is not particularly accurate and may lead to inaccurate results. It is also inaccurate at low wind speeds. In both cases these events do not happen often, although this may be a problem if the model is extrapolated to another much more or less windy site. The histogram method is more accurate as it only considers the data present in the sample – which consists of 3 years of wind speed data and 2 years of ORD – and does not make assumptions about the long term site conditions or component reliability. There are also no issues with goodness of fit. However at wind speeds above 17 m/s the histogram method calculated the failure rates of all components to be 0, which is clearly not the case.

The method decided upon for the model was the histogram method and the problem with it predicting a failure rate of 0 beyond 17 m/s was solved by making the assumption that the failure rate $P(\lambda_i|w)$ beyond 17 m/s was the same as that calculated in the last wind speed bin, 13 m/s – 17 m/s in this case. This was the chosen option as although it might be optimistic in assuming the failure rate of a component at 13 m/s to be the same the failure rate at 20 m/s, the assumption is based on reliable figures and the model can therefore give a logical prediction that is neither the worst case nor the best case scenario. In any case the probability of the mean daily wind speed being above 17 m/s is relatively low, even offshore as shown in Chapter 4.2.3. The majority of the failures will still occur on days when the mean daily wind speed is within the accurately modelled range of between 2 m/s – 13 m/s

2. Wind Speed Dependent Failure Rate Model Description

The basic purpose of the WSD failure rate model used in this thesis is to simulate the impact of wind speed on WT reliability. A schematic of this model is shown in Figure 5-20. This section will describe the model step by step and will then present some of the outputs after validation.

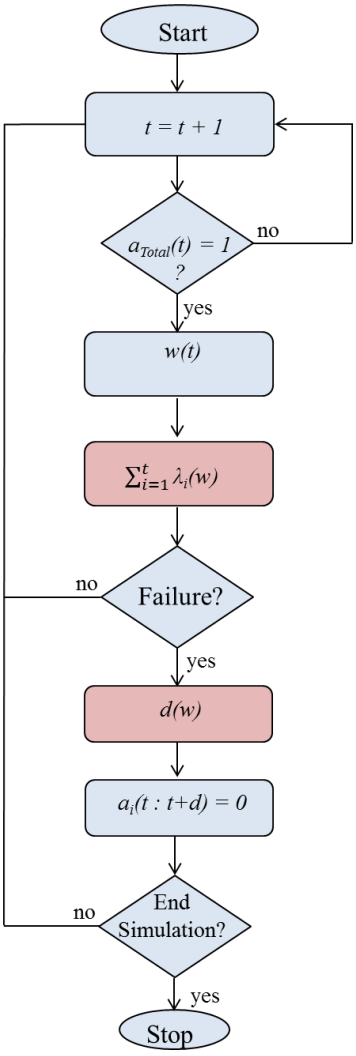

Figure 5-20: Flow chart showing model process for one WT

The model has a daily resolution and begins simulation at day $t = 1$. It continues to run until it has simulated the lifetime of a WT, which for the purposes of this thesis is defined as being

twenty years or 7300 days – this is a common period of life which is used by other authors [5-7]–[5-9].

Figure 5-20 shows the layout of a model consisting of 1 WT. To model a wind farm this model is layered and the steps are repeated in parallel for however many WTs there are designated to be in the farm. A schematic of this is shown in Figure 5-21 for a wind farm of *n* WTs.

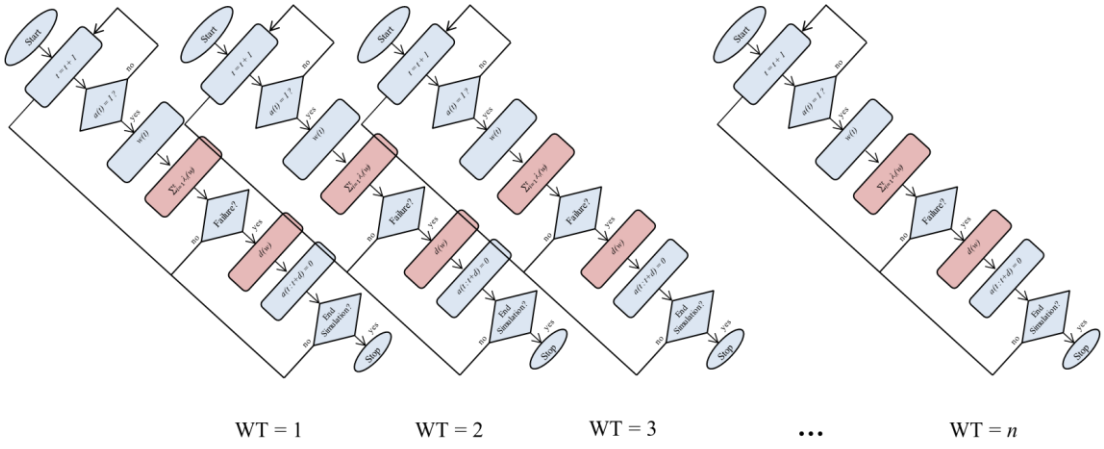

Figure 5-21: Multi WT model

The simulations are carried out until the results converge. This is described in more detail in Appendix I.

2.1. Wind Speed

It will be explained later in Chapter 6.2 and Chapter 7.2 how further inputs can be added to model income and O&M expenditure but while the model is in its basic form, shown in Figure 5-20, the wind speed is the only model input.

The wind speed input is a time series of mean daily wind speed which will be wrapped to create a 20 year time series, therefore it is important that at a minimum the input time series should be 1 year long and for anything larger it must be whole years to avoid any discontinuity in the seasonal variations. An example is shown in Figure 5-22 where a wind speed time series that is 3 years long has been wrapped to produce a 20 year dataset.

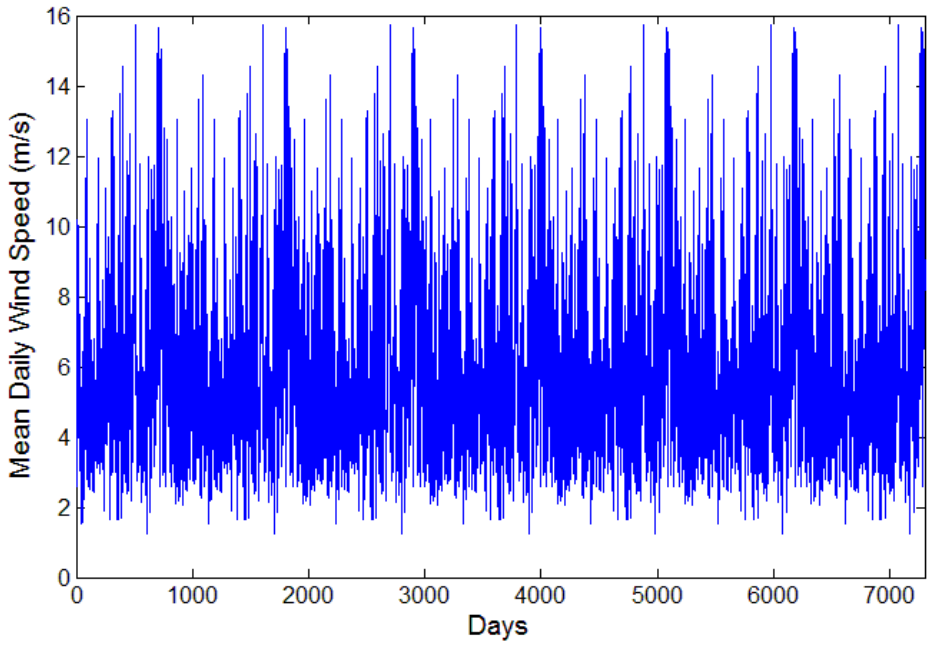

Figure 5-22: Wrapped time series of mean daily wind speed over 20 year period

Each daily mean wind speed is fed into the model in order. In the examples used in this thesis the wind speed time series always begins on the 1st of January – therefore when t = 1 the wind speed is that of the 1st of January, at t = 2 it is the 2nd of January and so on.

2.2. Failure Simulation

Failures are stochastically simulated using MCMCS, as discussed in Chapter 3.1.3.3. The model must construct a Markov Chain each time step, representing all 12 components. Figure 5-23 describes this Markov Chain. The model creates a vector ***λ(w)***, shown in Equation 5-6, which contains the failure rate (or transition rate) λ from the 'operating' state to the 'failed' state of each of the 12 components *i*.

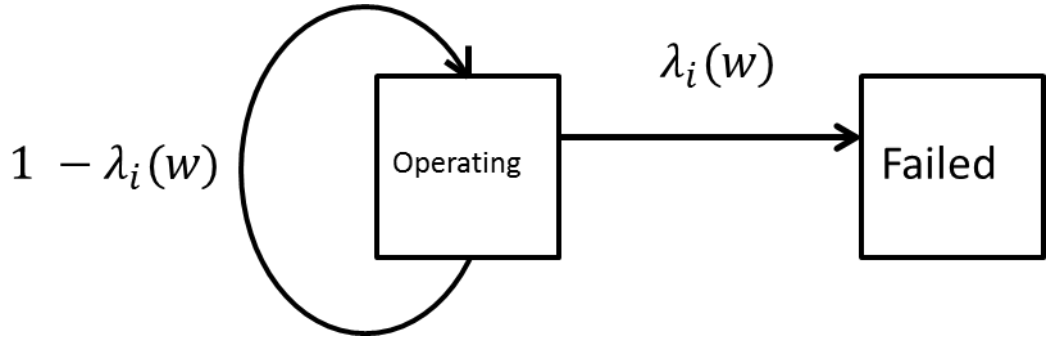

Figure 5-23: Markov chain used for failure simulation

$$\boldsymbol{\lambda}(\mathbf{w}) = (\lambda_1(w), \lambda_2(w), \lambda_3(w), \dots, \lambda_{12}(w)) \qquad \textbf{Equation 5-6}$$

For example, to calculate $\boldsymbol{\lambda}$ at time step *j* the mean daily wind speed is found to be *w(j)* = 5.3 m/s. As *w* falls in the range 4 m/s – 6 m/s, the WSD failure rates for that wind speed range are used to populate the vector. These failure rates are shown previously in Figure 5-16, Figure 5-18 and Appendix II as annual failure rates; these are divided by 365 to calculate daily failure rates. This process constitutes step 1, which is shown in Table 5-3.

Step 2 requires that the vector is cumulatively summed. If λ_{12} is greater than 1 the vector is normalised in Step 3. In the example shown in Table 5-3 this final term is less than 1 and so the vector is does not change from step 2 to step 3. The purpose of these 2 steps is to create a vector that represents the cumulative probability of a transition from the operating state to

the failed state. Monte Carlo Simulation can be used subsequently to simulate stochastic failures.

Table 5-3: Process of calculating λ(w)

Component Code	i	Step 1	Step 2	Step 3
		$\boldsymbol{\lambda_i}$	$\boldsymbol{\lambda_i}$ = cumsum($\boldsymbol{\lambda_i}$)	$\boldsymbol{\lambda_i}$ = normalise($\boldsymbol{\lambda_i}$)
CHI	1	0.00E+00	0.00E+00	0.00E+00
CVK	2	6.57E-05	6.57E-05	6.57E-05
MDA	3	8.77E-05	1.53E-04	1.53E-04
MDB	4	1.75E-04	3.29E-04	3.29E-04
MDK	5	3.29E-04	6.57E-04	6.57E-04
MDL	6	3.07E-04	9.64E-04	9.64E-04
MDX	7	1.53E-04	1.12E-03	1.12E-03
MDY	8	9.86E-04	2.10E-03	2.10E-03
MKA	9	6.57E-05	2.17E-03	2.17E-03
SMA	10	2.19E-05	2.19E-03	2.19E-03
UMC	11	0.00E+00	2.19E-03	2.19E-03
UMD	12	1.10E-04	2.30E-03	2.30E-03

For a wind farm of *n* WTs it is assumed that the mean daily wind speed is the same across the entire site and therefore at time step *j* is equal to 5.3 m/s. Hence the component failure rates at each WT are the same. The model generates a uniform random number $0 \geq x \leq 1$ for time step *j*. If *x* is less than any of the variables $\boldsymbol{\lambda_i}$ then a failure occurs. If for instance in this example *x* = 1.90E-03, this is less than $\boldsymbol{\lambda_{12}}$ so a failure has occurred. The component to which the failure occurred is identified by the cumulative probability density shown in Figure 5-24.

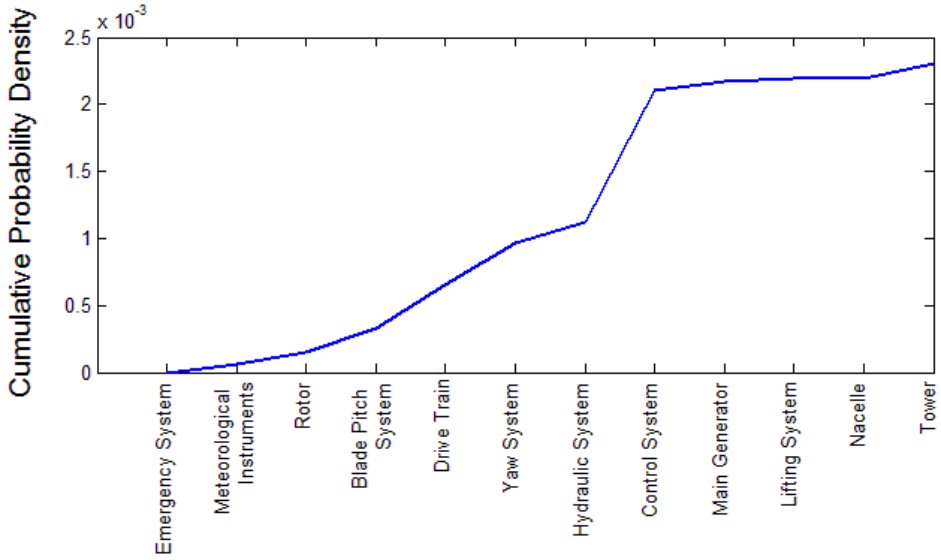

Figure 5-24: Cumulative probability density of λ(w)

As x is less than λ_8, but more than λ_7, the failure is due to a controller failure, which is λ_8. Had x been greater than λ_{12} then no failure would have occurred.

With the probabilities used in this example it would be much more likely that no failure would occur. But as the size of the wind farm increases the probability that x will be less than λ_{12} during time step j increases.

If a failure does occur to a WT during the simulation, it is recorded by the model and a downtime is calculated. However if a failure does not occur the model continues to simulate through the remaining WTs until all n have been analysed. Once the model reaches n and finishes analysing the final WT it returns to the beginning of the model, as shown in the flow chart in Figure 5-20, and then moves onto the next time step and begins the process again.

2.3. Downtime Calculation

If a failure occurs in a component, the model then simulates downtime *d* through Monte Carlo Simulation. Continuing the example used in the previous section of a failure to the control system at time step *j*, when the mean daily wind speed was 5.3 m/s, the model follows the following steps shown in Figure 5-25.

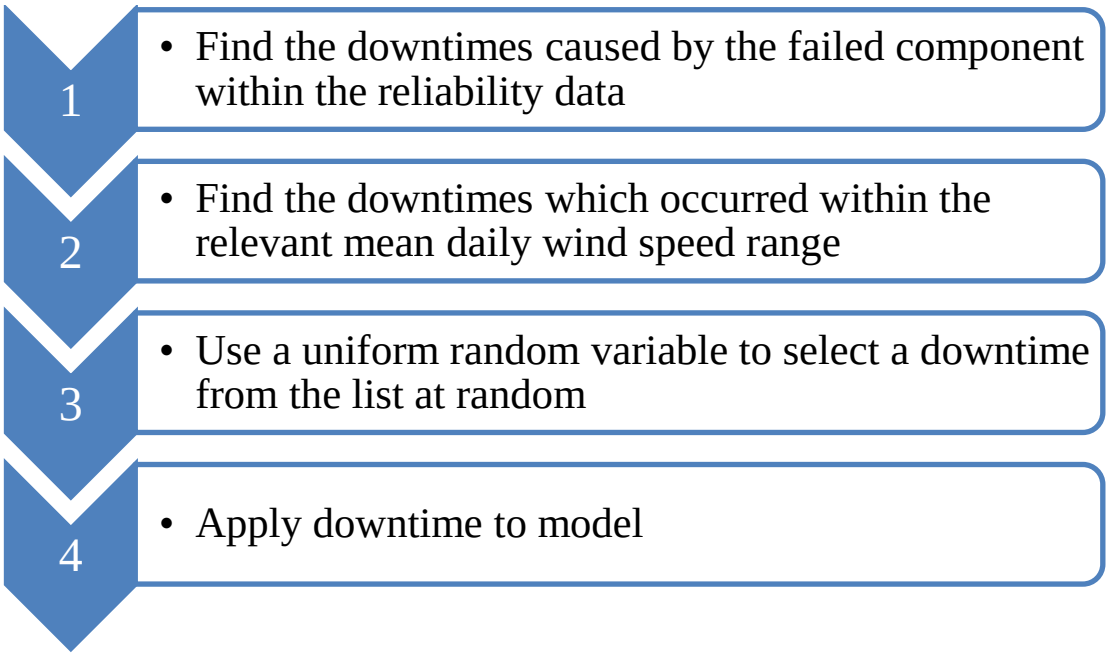

Figure 5-25: Downtime calculation flow chart

Firstly the model finds the downtimes caused by failure to the control system. It then isolates the failures which occurred at wind speeds between 4 m/s – 6 m/s. In doing this the model starts with 200 failures and then reduces it to 48. Figure 5-26 shows a normalised distribution of the downtimes within this dataset - it resembles a negative exponential distribution.

The uniform random number is then generated which selects an integer between 1 and 48. The integer in turn selects a downtime from the list of 48 which is then applied to the model.

This downtime *d* is then transformed from hours into days and used to populate the component availability matrix.

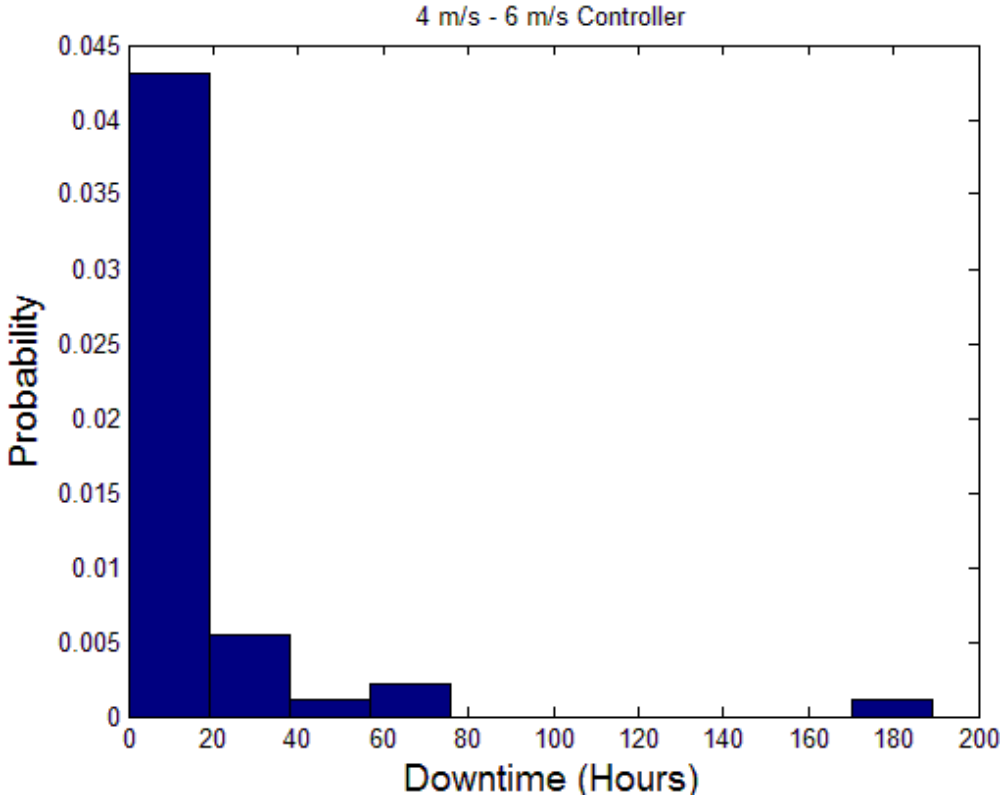

Figure 5-26: Normalised histogram showing distribution of downtimes caused by control system failures at mean daily wind speed between 4 m/s and 6 m/s

2.4. Availability

The component availability matrix is 12 columns by 7300 rows. Each WT in the wind farm has an availability matrix. The columns represent the components while the rows correspond to the time steps, of which there are 7300. Before the simulation commences the availability matrix is populated with 1's. If the row mean is 1 the WT is in an operating condition.

In the previous example a downtime *d* was calculated for the control system failure. If *d* is less than 1 day, 18 hours for example, then this equals 0.75 days. So when the control system fails at time step *j*, the row *j* is changed from a row of 1's to a row of eleven 1's and a single 0.25 at column 8 because it was only available for 0.25 of the day.

If *d* was 180 hours this equates to 7.5 days. The model would change column 8 in rows *j* to *j+d-2* to 0's and *j*+d-1 to 0.5 meaning that there would be 7.5 days of downtime, including the day in which the failure occurred as it is assumed that all failures occur at the very start of the day.

Using the availability matrix WT availability can be calculated as well as component availability.

This simulation was required to meet the convergence criterion (discussed in Appendix I). A single simulation scenario of a 200 WT wind farm over 20 years took several hours before the results had converged.

2.5. Validation

To check the validity of the WSD failure rate model a wind speed dataset was generated using the calibration wind speed wind speed distribution shown in Figure 5-1. The dataset was produced using random numbers so there was therefore no seasonality, as shown in the moving average time series of the calibration wind speed dataset shown in Figure 5-27.

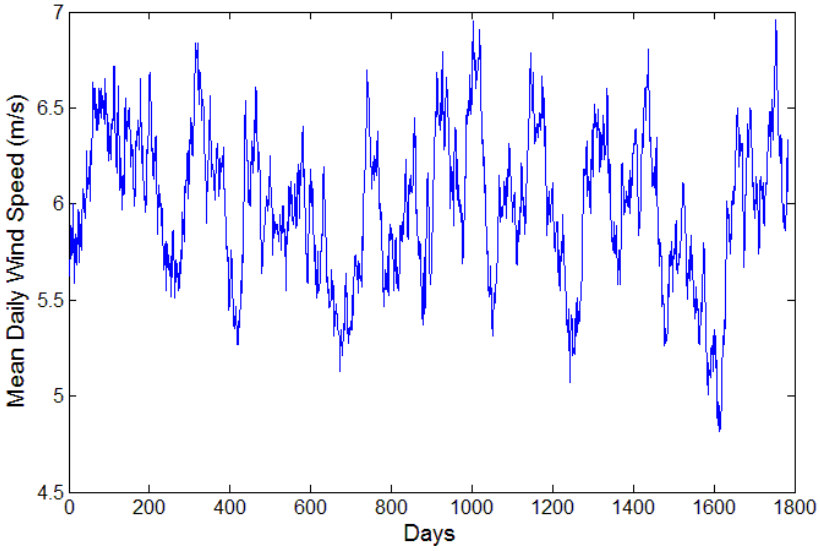

Figure 5-27: Moving average plot of calibration wind speed wind speed dataset

However the model did calculate failure rates for each component using the generated simulation data from the model and wind farm availability. There were 100 simulations of a 200 WT wind farm with a life cycle of 20 years, this equalled 400,000 WT years of simulated data.

2.5.1. Component Failure Rates

In total there was 0.32% difference between the model's estimation of the failure rate of the whole system and the failure rate measured according to the ORD, as shown in Table 5-4. In general the components were modelled well and those with the highest failure rates were modelled the most closely. This difference in failure rate calculation is most likely due to the calculation of the failure rate which assumes that the wind turbine is in operation 100 % of

the year, when in reality there are periods of downtime when it has already failed and so is not available to fail again. This is why the failure rate is underestimated by the model, because it does account for downtime and therefore operates for a shorter period of time and fails less often as a result.

The mean availability of a wind farm subjected to the wind speeds of the calibration wind speed dataset time series was calculated by the model to be 99.46 %. The availabilities of Site A and Site B were 99.46 % and 99.40 % respectively, the weighted availability of the whole dataset was 99.44 %. This slight difference between the model and the dataset is again due to the underestimation in failure rate.

Table 5-4: Component failure rates – modelled and recorded values from ORD

Component	Failure Rate (Failures per WT year)	
	WSD failure rate model	ORD
Blade Pitch System	0.069	0.068
Control System	0.517	0.520
Drive Train	0.159	0.156
Emergency System	0.025	0.026
Hydraulic System	0.079	0.078
Lifting System	0.010	0.010
Main Generator	0.031	0.031
Meteorological Instruments	0.076	0.075
Nacelle	0.015	0.016
Rotor	0.046	0.047
Tower	0.057	0.060
Yaw System	0.150	0.151
Total	1.234	1.238

When Site A and Site B were used as inputs, the WSD model returned availabilities of 99.49 % and 99.39 % respectively – a 0.03 % and 0.01 % difference from their actual values. This corresponded to a difference of 2.6 hours and 0.9 hours downtime difference respectively per WT per year.

There were two main reasons for these differences. Firstly the WSD model was calibrated using a mixture of values from the Site A and Site B time series. Therefore when the model

was inputted with the time series of only one of the sites it produced an estimate that was slightly skewed by the relationship found between the component failure rates and the wind speed conditions of the other site.

Secondly both the Site A and Site B wind speed time series also covered periods of time in which the reliability data was not recorded by the operator. In Site A's case the wind speed data was gathered between 1/1/2010 to 31/12/2012, while the ORD was only gathered between 1/1/2010 to 31/1/2012, there was therefore 11 months of wind speed data in the time series which was not used to calibrate the model. The Site B wind speed time series has 12 months of met mast data that preceeded the period during which its reliability data was gathered.

When the input data was altered to only consist of the wind speed time series covering the period over which the ORD was measured (and therefore the same data used to calibrate the WSD model) the availability for Site A and Site B was calculated to be 99.45% and 99.40% respectively. This gave the actual value of Site B but gave a slightly pessimistic result for Site A, 0.01% less available than was actually the case. This difference is likely to be due to the wind speed data from January 2012 which was omitted from the Site A wind speed time series because of the requirement of the model to have time series inputs that consist of whole years to maintain the effect of seasonality.

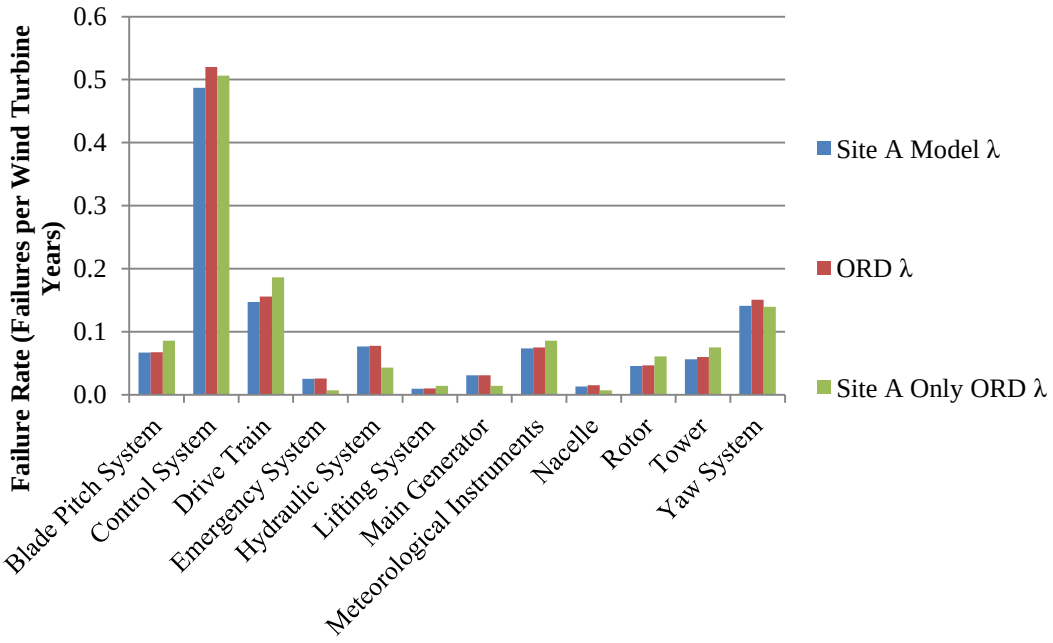

Figure 5-28: Comparison in component failure rates calculated by the model with Site A time series input and failure rates calculated using the whole ORD and only the data from the ORD corresponding to Site A

The component failure rates calculated by the WSD model using the Site A input (Site A Model) compared well to the failure rates calculated using the whole dataset (Site B and Site A) and ORD data from only Site A wind farm as presented in Figure 5-28.

Mean monthly failure rates were calculated from the simulated data of each component generated by the model. These monthly failure rates of the three least reliable components at Site A, the control system, yaw system and drive train are shown in Figure 5-29. All three components showed seasonal trends – failing less often in the summer and failing more often in the winter months when the wind speed was greater. The control system was approximately 46 % more likely to fail in December than in June according to the model.

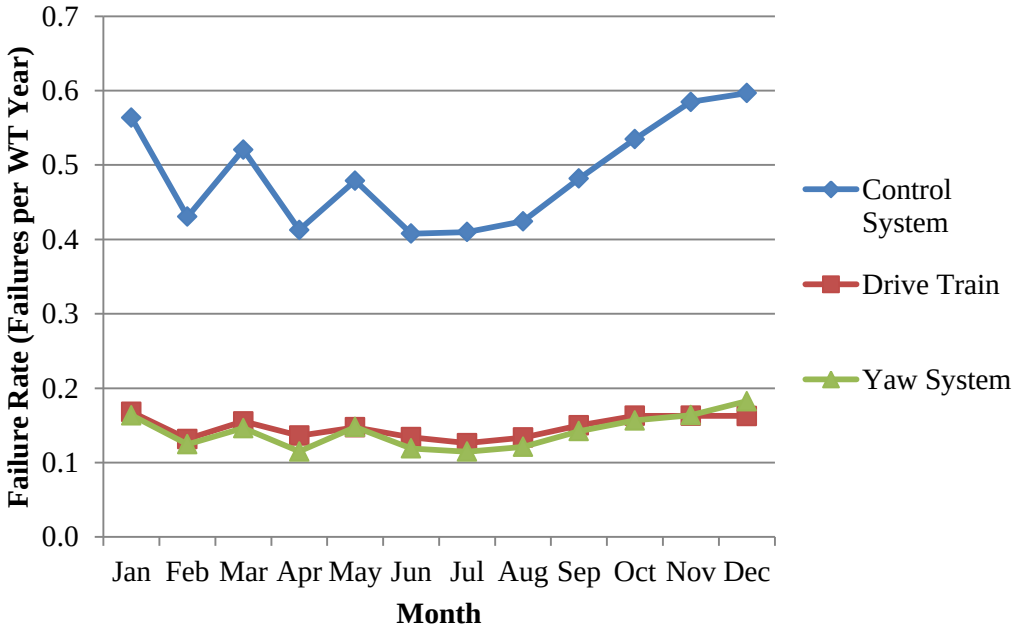

Figure 5-29: Monthly failure rates for the three least reliable components calculated by the model with Site A wind speed data input

The results when Site B was used as an input (Site B model) also compared well to the output of the model. The model produced a whole system failure rate only 0.05 % greater than the failure rate calculated from ORD and 4.5 % less when comparing it to the failure rates calculated only considering the Site B contribution to the ORD. However the failure rates modelled for the drive train and hydraulics were not as accurately modelled as other components, as shown in Figure 5-30. The model was biased by the relationship between the wind speed at Site A and the failure rates of the drive train and the hydraulic system.

That is one of the problems with the use of the two datasets; Site A is represented much more by the model than Site B because it has a larger dataset. Ideally both datasets would be of a similar size, use similar WT models but preferably experience different climates to give a good comparison and range of scenarios – but because Site A is a bigger dataset and both wind farms operate in similar conditions, the relationship that the WTs have at Site A to their

surroundings is stronger in the model than those from Site B. This means that any interesting features at Site B are lost in the model quite easily.

However because Site B is a smaller dataset it is difficult to know whether the WTs there do display any interesting behaviour that is different statically to the Site A sample. For instance, if 54 WTs were selected randomly from the Site A dataset, their relationship between wind speed and component failure rates may differ to the rest of the population similarly to the way that the Site B dataset does.

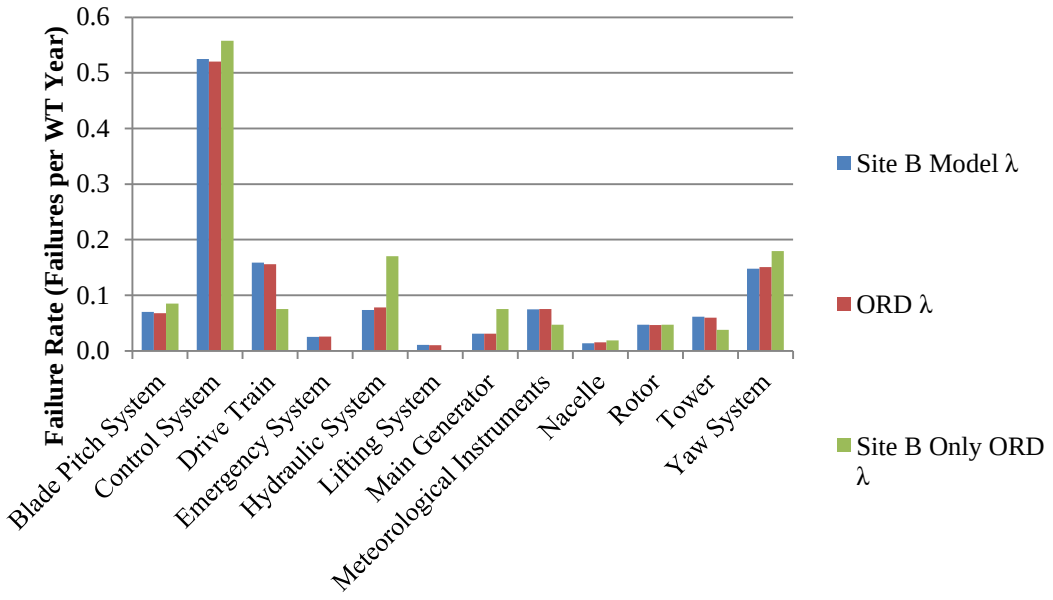

Figure 5-30: Comparison in component failure rates calculated by the model with Site B time series input and failure rates calculated using the whole ORD and only the data from the ORD corresponding to Site B

Overall the model was well calibrated to the data, but the model could be improved if a larger dataset was available. In the following chapter this model will be developed further to include income from the sale of electricity and expenditure due to operation and maintenance. Finally the model will be developed for use in planning spares strategies for different wind farms.

2.5.2. Bin Width Selection

The bins used in the model validation and in Chapter 5.1.2 were selected after various bins were tested using the model. The number of bins and their widths that could have been tested is limitless. Therefore after some initial analysis it was decided that three options would be evaluated, they are shown in Table 5-5.

Table 5-5: Bin options tested

Bin	Bin Options (m/s)		
	a	b	c
1	1-3	1-5	1-4
2	3-5	5-7	4-6
3	5-7	7-9	6-8
4	7-9	9-11	8-10
5	9-11	11-13	10-12
6	11-13	13-15	12-14
7	13-17	15-17	14-17
Availability	**99.46**	**99.47**	**99.48**

Using the three bin options, the model calculated that option a) was the most accurate according to the availability the model produced. As discussed in the previous section, the availability of Site A and Site B during the period in which the ORD was gathered was 99.44%.

When the component failure rates, calculated by the WSD model, were analysed for each bin option, a) was again the most accurate, as shown in Table 5-6. The failure rate of the whole system was only 0.32% less than the failure rate of the whole system calculated using the ORD. Options b) and c) produced failure rates that were 0.48% and 2.4% lower than the ORD. Using the bin widths of option a) also produced the most accurately modelled failure rates of the three least reliable components, the drive train, control system and yaw system.

Table 5-6: Accuracy of bin options

Component	λ (Failures Per WT year)			
	Bin Options			ORD
	A	b	c	
Emergency System	0.025	0.025	0.024	0.026
Meteorological Instruments	0.076	0.077	0.072	0.075
Rotor	0.046	0.044	0.047	0.047
Blade Pitch System	0.069	0.069	0.069	0.068
Drive Train	0.159	0.158	0.152	0.156
Yaw System	0.150	0.150	0.149	0.151
Hydraulic System	0.079	0.079	0.075	0.078
Control System	0.517	0.514	0.508	0.520
Main Generator	0.031	0.033	0.031	0.031
Lifting System	0.010	0.010	0.011	0.010
Nacelle	0.015	0.016	0.015	0.016
Tower	0.057	0.058	0.057	0.060
Total	**1.234**	**1.232**	**1.208**	**1.238**

3. Chapter 5 Summary

The MCMCS approach was adopted in Chapter 5 to develop a model that would describe the effect of wind speed on the WT component failure rate. The model would be similar those developed previously by other authors in the area of WT reliability, discussed in Chapter 3.

The WSD failure rates used in the MCMCS model are calculated using Bayes' Theorem. The wind speed and ORD is put into mean daily wind speed range bins, shown in before the probability of a failure occurring to a component, given a mean daily wind speed $P(\lambda_i|w)$, is calculated.

The WSD model was then validated in Chapter 5.2.5 by using the calibration wind speed time series as a model input. The WSD model calculated a whole system failure rate 0.32% less than the actual failure rate of the average WT in the ORD. The availability calculated by the WSD model was 99.46%, slightly higher than the actual availability of 99.44% for both Site A and Site B combined.

The following section will use the model developed in this Chapter and apply other onshore and offshore wind speed time series inputs from Leuchars weather station and the FINO offshore met mast. Annual and monthly component failure rates will be calculated for each WT component before analysis is undertaken to determine the difference in estimated annual production using a WSD model and a stationary failure rate model.

4. Chapter 5 References

[5-1] F. Castro Sayas and R. N. Allan, "Generation availability assessment of wind farms," *IEE Proc. Gener. Transm. Distrib.*, vol. 143, no. 5, p. 507, 1996.

[5-2] Mathworks, "ksdensity," 2014. [Online]. Available: http://www.mathworks.co.uk/help/stats/ksdensity.html.

[5-3] T. Burton, D. Sharpe, N. Jenkins, and E. Bossanyi, *Wind Energy Handbook*, 1st ed. Chichester: John Wiley and Sons Inc, 2008, p. 19.

[5-4] P. J. Tavner, H. Long, and Y. Feng, "Early experiences with UK round 1 offshore wind farms," *Proc. ICE - Energy*, vol. 163, no. 4, pp. 167–181, Nov. 2010.

[5-5] Noordzee Wind, "Egmond Aan Zee - operations reports," 2013. [Online]. Available: http://www.noordzeewind.nl/en/. [Accessed: 03-Sep-2013].

[5-6] LORC Knowledge, "List of Offshore Wind Farms," 2014. [Online]. Available: http://www.lorc.dk/offshore-wind-farms-map/list. [Accessed: 09-Apr-2014].

[5-7] K. Smolders, Y. Feng, H. Long, and P. Tavner, "European Wind Energy Conference (EWEC 2010) Reliability Analysis and Prediction of Wind Turbine Gearboxes," in *EWEC*, 2010.

[5-8] E. Martínez, F. Sanz, S. Pellegrini, E. Jiménez, and J. Blanco, "Life-cycle assessment of a 2-MW rated power wind turbine: CML method," *Int. J. Life Cycle Assess.*, vol. 14, no. 1, pp. 52–63, Oct. 2008.

[5-9] E. Martínez, F. Sanz, S. Pellegrini, E. Jiménez, and J. Blanco, "Life cycle assessment of a multi-megawatt wind turbine," *Renew. Energy*, vol. 34, no. 3, pp. 667–673, Mar. 2009.

Chapter 6. Applications of Wind Speed Dependent Failure Rates

1. Basic Reliability Analysis

The model described in Chapter 5.2 is used in this chapter to analyse the impact of wind speed on WT failure rates. From the previous chapter a methodology was selected using MCMCS, this model used WSD failure rates calculated using wind speed data and reliability data from two onshore wind farms.

The model will be used in this section to analyse two wind speed datasets. The first dataset is from an onshore met office weather station located in Leuchars, Scotland – described previously in more detail in Chapter 4.2.2.2. This station was selected because its mean daily wind speed time series is typical of the sort of conditions experienced by an onshore wind farm. It will therefore be used to analyse how WSD failure rates can be applied to a wind farm subjected to wind speeds typical onshore.

The second dataset is the FINO offshore met mast, described in detail in Chapter 4.2.3. This mean wind speed time series is representative of the wind speeds faced by an offshore wind farm. The model will use the WSD failure rates to calculate component failure rates when subjected to offshore conditions.

In the literature, WT reliability is described by failure rates and downtimes experienced by onshore wind turbines. The problem with comparing onshore and offshore reliability is that although the definition of a failed WT is the same, what happens before and after the failure is different. Preventative maintenance is carried out differently offshore and downtime is likely to increase due to logistical issues and accessibility problems. The longer downtime periods offshore mean that if two WTs were to be compared, one offshore and the other onshore, were they to fail twice in a year the failure rate would be very likely be greater for the offshore WT. If the onshore WT had an annual downtime of 4 days and the offshore WT had a downtime of 12 days, the availability of the two WTs was 98.63% and 96.71% respectively, as shown in Table 6-1. Although both WTs failed as frequently throughout the

year, because the offshore WT had a longer period of downtime (due to logistics and access) it operated for a shorter period of the year. Therefore the period of time it was available to fail was less, increasing the failure rate by 2.27%.

Table 6-1: An example of the differences in failure rate calculated onshore and offshore

	Annual Downtime	Annual Availability	Annual Number of Failures	λ
Onshore	4 days	98.63%	2	2.022
Offshore	12 days	96.71%	2	2.068

Therefore it is important to remember that the results in the following sections are calculated using a model that was calibrated with onshore wind turbine reliability data. Any discussions relating the results to how a WT may perform offshore should consider that they may be optimistic because of these differences in calculating onshore and offshore failure rates.

In the following sections the model and its outputs will be referred to as the FINO model or the Leuchars model, depending on which wind speed time series was used as an input. As discussed previously, the ORD refers to the reliability data recorded at Site A and Site B.

1.1. Availability and Component Failure Rates

Using the FINO and Leuchars models, failures are generated via MCMCS using input wind speed times series datasets and WSD failure rates for each component much like in the previous section. The model consists of a 200 WT wind farm, with a life span of twenty years. Simulations are run until the results converge (as described in Appendix I).

From the simulated data, the average annual availability of WTs in the FINO and Leuchars model respectively are calculated to be 98.90% and 99.39%. It is to be expected that the FINO model would have a lower availability as the wind speed time series has a high average wind speed and therefore would induce higher component failure rates when used as an input.

The downtime therefore for each model is 4.1 days per annum for the FINO model and 2.2 days per annum for the Leuchars model. However these values do not include periods that the WT is shut down for preventative maintenance or for any other reason throughout its lifetime. This is the case because as discussed previously the ORD does not include stoppages for preventative maintenance. According to Nilsson and Bertling, onshore WTs have preventative maintenance undertaken every 6 months, each time lasting between 4 – 7 hours for two people [6-1]. For the offshore site Kentish Flats, preventative maintenance occurs more frequently at three to six month intervals and annually contributes to two days of downtime per WT year [6-1].

1.1.1. FINO Model

The FINO and Leuchars models record the number of failures which occur to each component throughout the simulations so that the average failure rate of each component can be calculated. The FINO model returns the component failure rates shown in Figure 6-1.

The largest difference between the component failure rates of the ORD and the failure rates calculated using the FINO model were the control system, the yaw system and the Nacelle, as shown in Table 6-2.

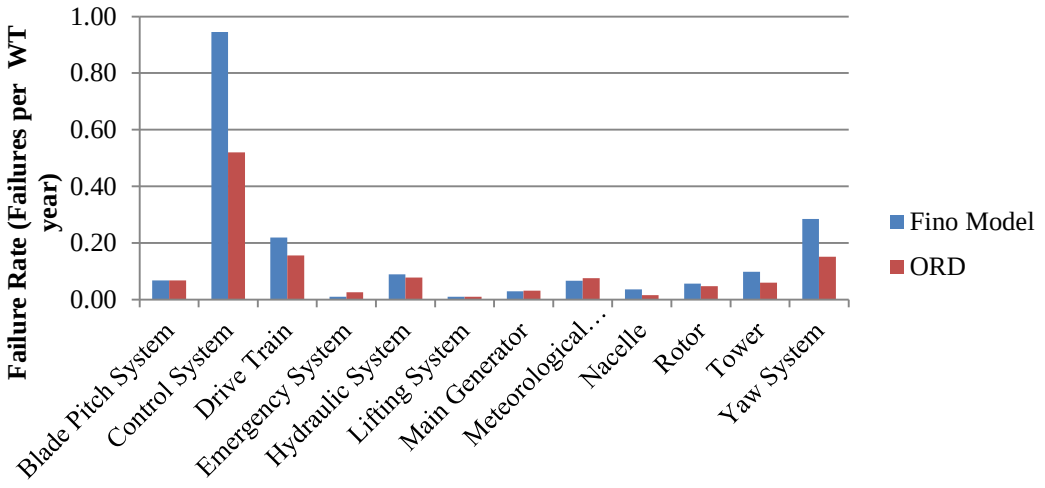

Figure 6-1: Comparison between the component failure rates calculated by the model using the FINO wind speed time series as an input and the failure rates calculated with the ORD

The failure rate of the drive train is calculated to increase by roughly 40% and the whole system by 54%. This meant that with a WT subjected to FINO wind speeds it would be expected to experience 2 failures every year, double that expected by the WTs at Site A and Site B. The control system would also be expected to fail almost twice as often during its lifetime. For a 200 WT wind farm there would be approximately 189 control system failures expected per year.

In the case of Egmond Aan Zee, roughly 85 stoppages occurred per year between 2007 and 2009 that were due to control system failures and this was for a wind farm of only 36 WTs [6-2]. The gearbox failure rate also increased to roughly 0.47 failures per year, compared to data from WMEP which shows onshore gearboxes failing only 0.12 times a year [6-2]. However the WTs in WMEP are much less advanced than the 36 Vestas V90s used at Egmond Aan Zee, they also did not suffer from a serial gearbox fault that the V90s did.

Table 6-2: Comparison of component failure rates generated by FINO model and calculated using the ORD

Component	FINO Model (Failures per WT year)	ORD (Failures per WT year)	Difference
Blade Pitch System	0.068	0.068	0%
Control System	0.946	0.520	82%
Drive Train	0.219	0.156	40%
Emergency System	0.009	0.026	-64%
Hydraulic System	0.089	0.078	14%
Lifting System	0.010	0.010	-6%
Main Generator	0.029	0.031	-8%
Meteorological Instruments	0.066	0.075	-12%
Nacelle	0.036	0.016	130%
Rotor	0.056	0.047	20%
Tower	0.098	0.060	63%
Yaw System	0.285	0.151	89%
Total	1.910	1.238	54%

1.1.2. FINO Model 12 Hour Filter

From the information recorded in the ORD it was clear that not all control system failures required an engineer to visit the WT to fix the failure as many caused downtimes less than 15 mins long. Therefore it would be inaccurate to say that were the WTs in this simulation sited offshore there would be 189 trips offshore per year, purely to repair the control system. Firstly it is likely that more than one WT could be repaired per trip and secondly many failures could be repaired remotely as is the case onshore.

However assuming that any control system failure fixed remotely required less than 12 hours of downtime, it is possible to use the model to analyse only the failures that caused downtimes greater than 12 hours. It can be assumed that these are the failures that required an engineer to fix the WT on site, which could also be assumed to be the case offshore.

If this 12 hour assumption were the case for the other components as well, it leads to the conclusion that within the ORD, there were 137 failures per year on average during the recorded period that required an engineer to visit the failed WT in order to make the repair.

When the 12 hour downtime filter was applied to the output of the FINO model, it calculated that there would be 241 failures per year to a 200 WT wind farm that would require an

engineer to visit the failed WT to make the repair. For the control system alone there would be 38 failures, an increase of 97 % compared to the ORD, as illustrated in Table 6-3.

Table 6-3: Comparison of component failure rates generated by FINO model and calculated using the ORD when a 12 hour filter has been applied

Component	FINO Model (Failures per WT Year)	ORD (Failures per WT Year)	Difference
Blade Pitch System	0.058	0.042	39%
Control System	0.626	0.317	97%
Drive Train	0.191	0.127	50%
Emergency System	0.000	0.013	-100%
Hydraulic System	0.051	0.047	8%
Lifting System	0.005	0.005	-12%
Main Generator	0.005	0.016	-71%
Meteorological Instruments	0.011	0.013	-19%
Rotor	0.046	0.034	36%
Yaw System	0.213	0.096	122%
Total	1.205	0.710	70%

1.1.3. FINO Model 48 Hour Filter

To analyse very serious failures, a 48 hour downtime filter can be applied. This results in a 123% increase in the whole system failure rate from the ORD to the FINO model output. This means that in terms of failures that cause downtimes greater than 48 hours, the impact of the FINO wind speed time series causes the failure rate to more than double to 0.44 failures per WT year. The individual component failure rates are shown in Figure 6-2 – the failure rates of the control system, yaw system and drive train were calculated to increase by 117 %, 264 % and 129 % respectively in the FINO model compared to the ORD.

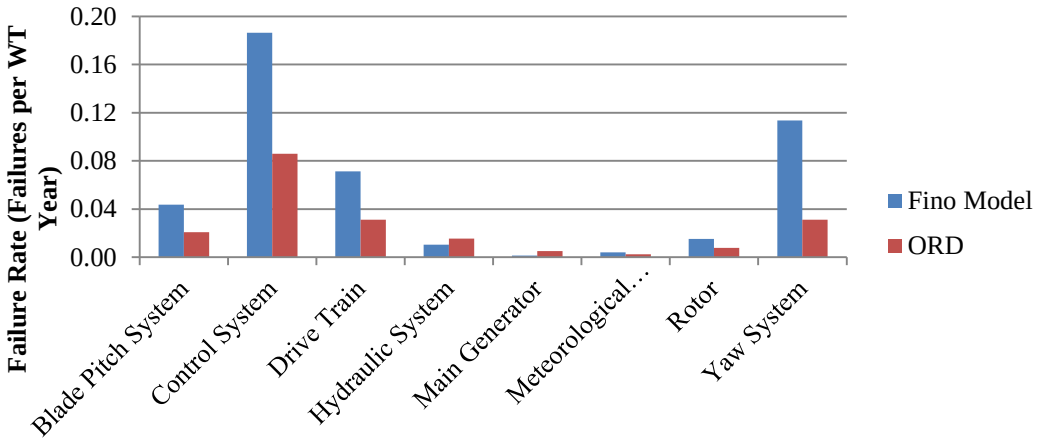

Figure 6-2: 48 hour downtime filtered comparison between the component failure rates calculated by the model using the FINO wind speed time series as an input and the failure rates calculated with the ORD

Table 6-3 and Figure 6-2 demonstrate that the FINO model calculates that the impact of higher wind speeds will not just be increased component failure rates, but also failures that are more severe and cause longer downtimes. This has particular significance for offshore WTs as logistical issues and accessibility reduces availability significantly even if failure rates and downtimes remain the same as those recorded onshore. However, offshore availability could be improved by gaining a better understanding of the impact of wind speed on component failure rates and enhancing the quality of maintenance.

1.1.4. Leuchars Model

In contrast to the results produced by the FINO model, the outputs of the Leuchars model were more similar to the component failure rates calculated in the ORD, as illustrated in Figure 6-3. Although there is an increase in failure rate for the three most troublesome components, it is not as dramatic a change compared to those calculated by the FINO model.

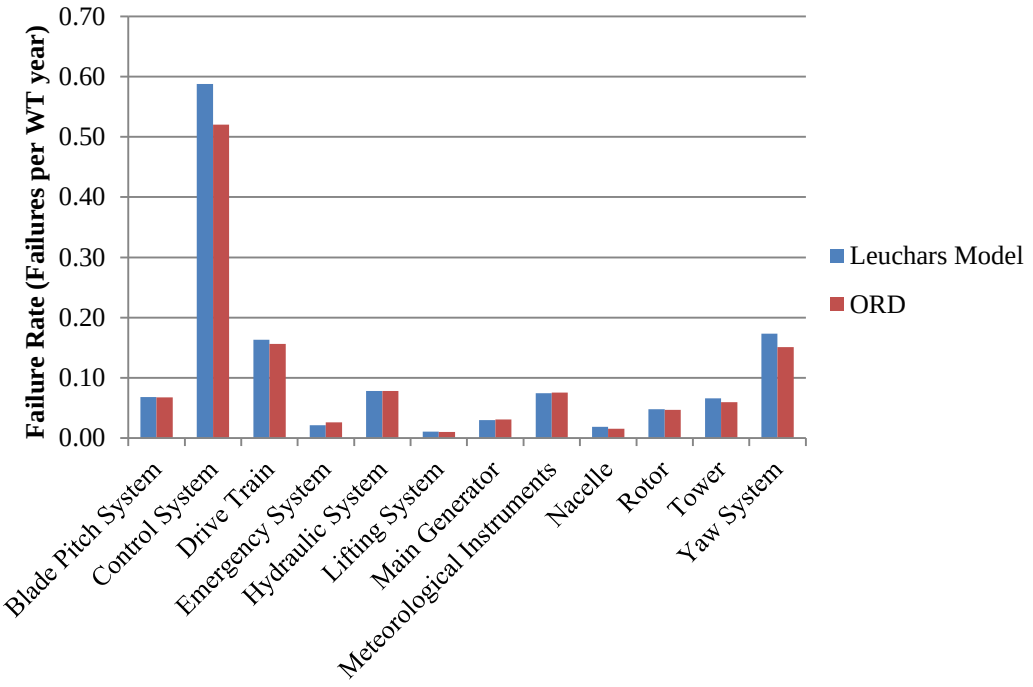

Figure 6-3: Comparison between the component failure rates calculated by the model using the Leuchars wind speed time series as an input and the failure rates calculated with the ORD

The differences in the output from the two models are due to the different input wind speed time series, with the exception of this there is no difference between the two models. In the case of the control system the model recognises that the failure rate increases as the wind speed increases as shown in Figure 6-4. This WSD failure rate of the control system is the same as that presented in Figure 5-16. However the wind speed time series input from Leuchars is differently distributed to FINO. More often the mean daily wind speed at Leuchars is between 3 – 7 m/s where the failure rate is relatively low. The FINO wind speed time series has wind speeds that are more frequently at the high wind speed ranges where the failure rate is greater. Therefore when Leuchars is used as an input wind speed the control system failure rate is less than that calculated by the FINO model.

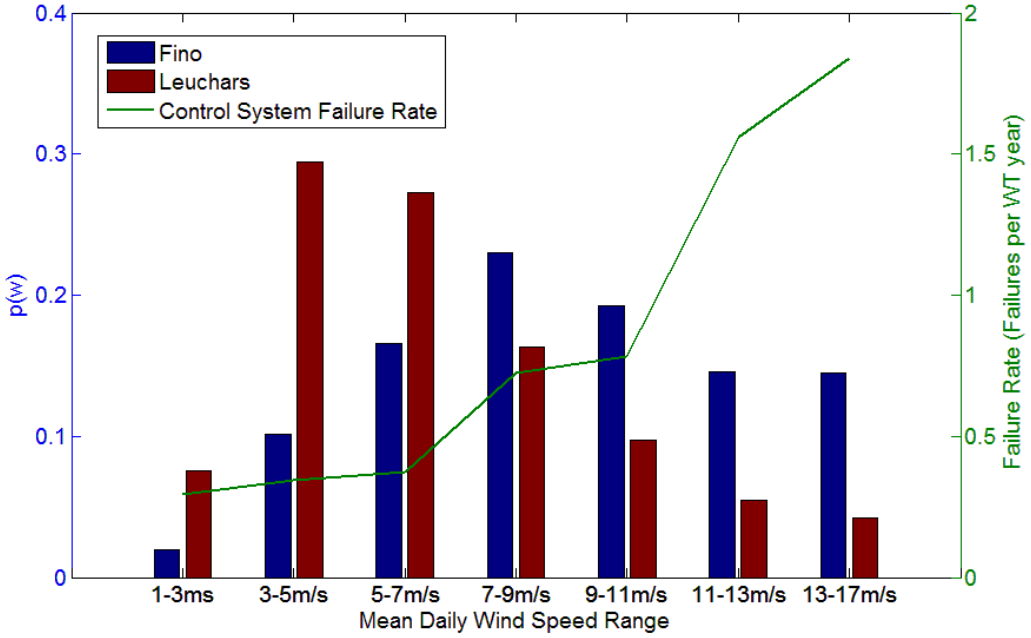

Figure 6-4: *P(w)* for FINO and Leuchars wind speed datasets and the control system WSD failure rate over the daily wind speed range

The mean daily wind speed at Leuchars is 6.59 m/s compared to the calibration wind speed dataset which was 5.98 m/s. As shown in Table 6-4, the model calculates that this slight increase in wind speed at Leuchars will lead to an 8 % increase in whole system failure rate and significantly a 13 % and 15 % increase in control system and yaw system failure rate.

Table 6-4: Comparison of component failure rates generated by Leuchars model and calculated using the ORD

Component	Leuchars Model (Failures per WT Year)	ORD (Failures per WT Year)	Difference
Blade Pitch System	0.068	0.068	0%
Control System	0.588	0.520	13%
Drive Train	0.163	0.156	4%
Emergency System	0.021	0.026	-19%
Hydraulic System	0.078	0.078	0%
Lifting System	0.011	0.010	10%
Main Generator	0.030	0.031	-3%
Meteorological Instruments	0.075	0.075	0%
Nacelle	0.019	0.016	19%
Rotor	0.048	0.047	2%
Tower	0.066	0.060	10%
Yaw System	0.173	0.151	15%
Total	1.340	1.238	8%

As Figure 6-5 shows, the higher wind speeds were more frequent at Leuchars than in the calibration wind speed dataset. Therefore the control system failure rate was higher more often in the Leuchars model as $P(w)$ was higher from 9 m/s to 17 m/s.

The model is more complex than simply calculating the mean daily wind speed of a site and using that value to calculate the WT failure rate. It is the distribution of the wind speed at a site that has the largest influence on the calculated failure rates. This was demonstrated when the calibration wind speed dataset was modified by increasing every mean daily wind speed reading by 0.6 m/s. The average wind speed of this modified dataset was 6.59 m/s, the same as the Leuchars dataset. However when this new time series was used as an input in the model the availability and failure rate were 99.44% and 1.312 failures per WT year respectively. These calculations predicted Leuchars to still be a less reliable site despite both time series having the same mean.

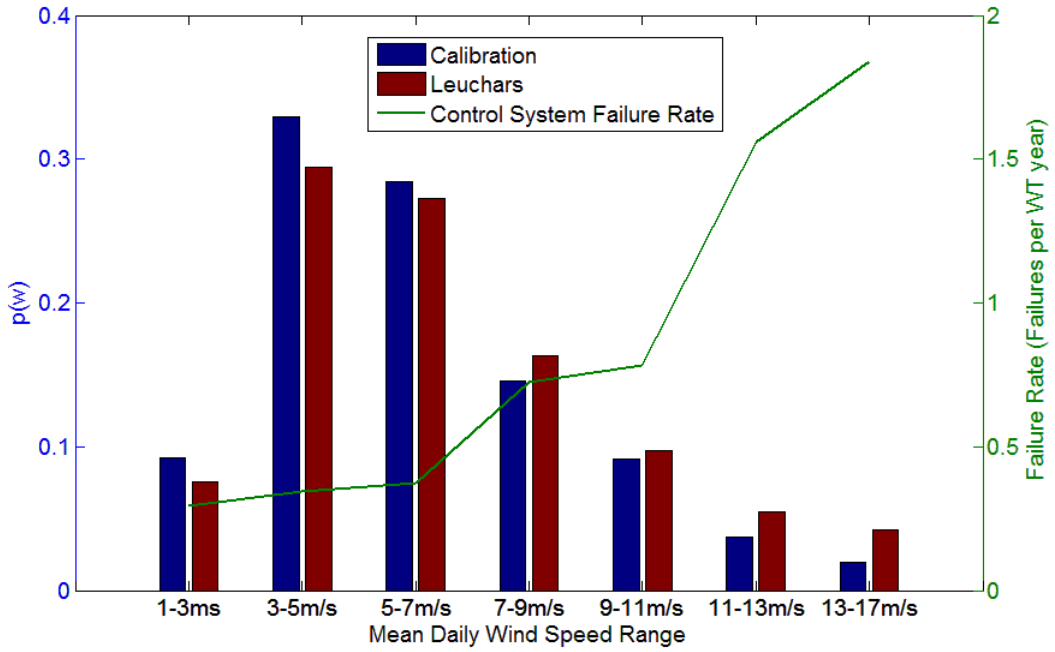

Figure 6-5: *P(w)* for the Calibration and Leuchars wind speed datasets and the control system WSD failure rate over the daily wind speed range

The reason for the difference in results between these two datasets is demonstrated clearly in Figure 6-6, which shows the failure rate of the yaw system on the secondary axis and *P(w)* on the primary axis. The Leuchars model calculated that the yaw system failure rate was 5 % greater than when the modified calibration wind speed dataset was used. The main reason for this difference is in the 13 – 17 m/s wind speed bin, shown in Figure 6-6, where *P(w)* is higher at Leuchars meaning that the yaw system failure rate will be at its highest more frequently at Leuchars. So despite both wind speed datasets having the same average wind speed, the wind speed distribution shape is the most significant factor in calculating reliability with the model.

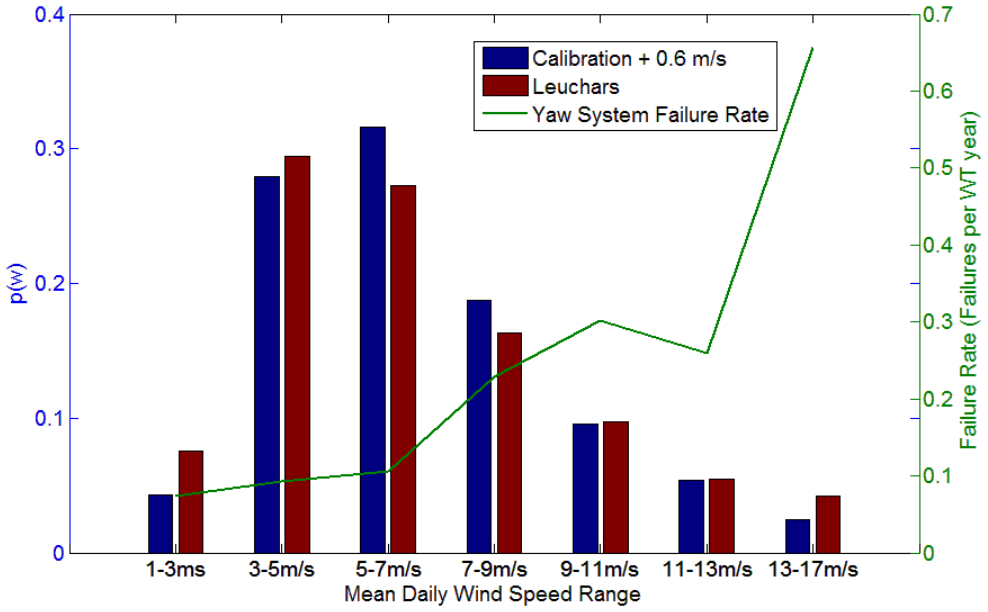

Figure 6-6: *P(w)* for the Calibration wind speed dataset plus 0.6 m/s, Leuchars wind speed dataset and yaw system failure rate over the daily wind speed range

1.1.5. Leuchars Model 12 Hour Filter

When the downtime filter of 12 hours was applied to the Leuchars model and the ORD, the whole system failure rate of the Leuchars model increased by 9% compared to the ORD. Similarly the control system and yaw system failure rates also increased in the Leuchars model compared to the ORD, by 20 % and 21 % respectively as shown in Table 6-5

Table 6-5: Comparison of component failure rates generated by Leuchars model when 12 hour downtime filter is applied and ORD failure rates

Component	Leuchars Model (Failures per WT Year)	ORD (Failures per WT Year)	Difference
Blade Pitch System	0.032	0.029	13%
Control System	0.287	0.239	20%
Drive Train	0.099	0.091	9%
Emergency System	0.000	0.008	-100%
Hydraulic System	0.034	0.034	1%
Lifting System	0.009	0.010	-16%
Main Generator	0.010	0.010	-1%
Meteorological Instruments	0.013	0.013	3%
Rotor	0.074	0.052	41%
Yaw System	0.117	0.096	21%
Total	0.777	0.710	9%

1.1.6. Leuchars Model 48 Hour Filter

When a 48 hour filter was applied to only analyse the very serious failures that led to long periods of downtime, the total failure rate was calculated to increase by 20 % compared to the ORD, as shown in Table 6-6. The impact of the Leuchars wind speed time series was therefore not as severe as the FINO offshore wind speed data.

Table 6-6: Comparison of component failure rates generated by Leuchars model when 48 hour downtime filter is applied and ORD failure rates

Component	Leuchars Model (Failures per WT Year)	ORD (Failures per WT Year)	Difference
Blade Pitch System	0.025	0.021	21%
Control System	0.101	0.086	18%
Drive Train	0.038	0.031	21%
Hydraulic System	0.014	0.016	-8%
Main Generator	0.005	0.005	-13%
Meteorological Instruments	0.003	0.003	6%
Rotor	0.008	0.008	8%
Yaw System	0.046	0.031	46%
Total	0.240	0.200	20%

This section has shown how, using WSD failure rates, the model can be used to calculate the availability and component failure rate of a potential site, using only a wind speed time series. However a more detailed analysis can be undertaken that describes how the failure

rate of each component changes seasonally. By gaining an understanding of how the probability of component failure changes from month to month, maintenance strategies could potentially be planned based on this knowledge. The following section describes how failure rate of various components change seasonally in the FINO and Leuchars model.

1.2. Seasonal Component Failure Rate

The wind speed changes seasonally – increasing in the winter and decreasing in the summer. With this in mind and according to the results shown in the previous section and from the WSD failure rates introduced in Chapter 5.2.5.1, it must be the case that component failure rate must change seasonally due to the wind speed conditions.

In the previous section, annual failure rates and availabilities were presented. In the onshore literature these metrics are very useful in describing the reliability of onshore WTs. However in the offshore environment, seasonal failure rates would be a much more valuable metric due to the seasonality of WT accessibility. This point is illustrated by Figure 6-7 which shows the exceedence probability of significant wave height for each season from wave buoys sited in the North Sea [6-3]. Offshore WT access is limited by wind speed and significant wave height [6-4], [6-5]. Chapter 4.2.3 shows the high wind speeds experienced by FINO, while Figure 6-7 shows that in Winter and Autumn the probability of the significant wave height exceeding 1.5 m was higher than in Summer and Spring [6-6]. This difference may increase at distances further from shore.

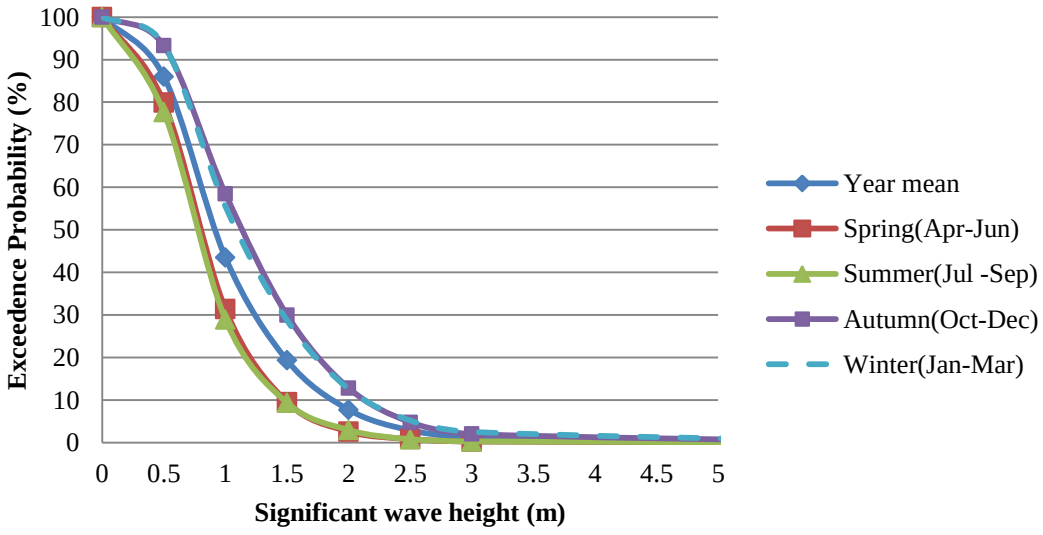

Figure 6-7: Seasonal exceedence probability of significant wave height for site in North Sea

If an offshore WT were expected to require a visit from a technician due to failure twice a year, the time of year these failures occur has a big impact on its productivity. Were they to occur in the summer, the WT could be repaired relatively easily due to the higher probability of access. Or if the failures occurred in the winter, the productivity would be reduced significantly because of poor access due to higher significant wave heights. Were the failures to occur randomly, the impact of the failures that occurred in winter would have a far greater impact than those that occurred in the summer.

In the case of onshore WTs, although it is unclear whether the failure rate varies significantly seasonally, the accessibility does not create problems to the same degree as those experienced offshore because they operate at lower wind speeds and are obviously not affected by sea state. Were failures to occur more often in the winter they could be repaired relatively easily compared to offshore WTs.

However if offshore WTs do fail more frequently in the winter, knowing the failure rates at this time of year becomes very valuable to the owners and operators of offshore WTs due to the poor accessibility and therefore likely long periods of downtime they will experience in the winter. An annual failure rate does not adequately describe the reliability of the asset as what happens in periods of poor access has the greatest impact on the productivity of the wind farm.

This section therefore aims to establish whether WT component failure rates vary seasonally onshore and offshore. The FINO model will be used to evaluate the impact offshore while the Leuchars model will be used to assess the affects onshore.

Seasonal failure rates will be generated in each model by inputting their respective daily mean wind speed time series in the correct chronological order. Therefore the overall impact of each month on the failure rate of every WT component can be evaluated.

1.2.1. FINO Model

The figures shown in this section and the following section show the average failure rates that are calculated after taking enough samples so that the results converge. The failure rates presented in each of the graphs are annual failure rates, not monthly failure rates even although each data point is in reference to a calendar month. They are presented in this convention so that these results can be easily discussed and compared alongside failure rates presented in previous sections throughout this thesis, all of which represented annual failure rates.

Figure 6-8 is produced using outputs from the FINO model. It clearly shows an increase in the failure rate of the control system and yaw system in winter and a reduction in failure rate in summer. In November the failure rate of the control system was modelled to increase by 82 % compared to June. While for those same months the yaw system failure rate increased by 44 %.

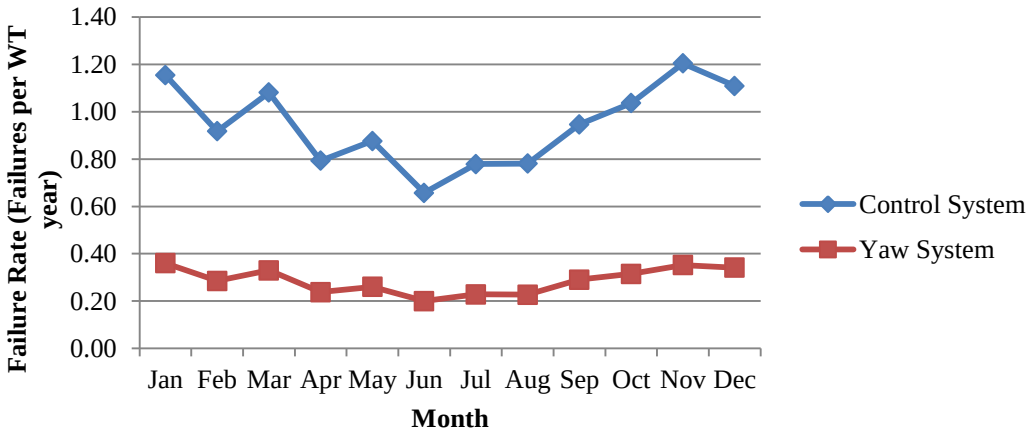

Figure 6-8: FINO model seasonal output for the control system and the yaw system

The blade pitch system, drive train, hydraulic system, nacelle and tower all show signs of seasonality in the FINO model too, as illustrated in Figure 6-9, although not as variable as the yaw system or control system. Despite the failure rate of the yaw system and drive train

were calculated to be so similar, the two components were modelled to fail differently throughout the year. The drive train reliability is more consistent, only failing 14 % more often in November than in June. This is due to the differences between the WSD failure rates of the two components. Interestingly the nacelle was modelled to fail very seasonally. It is however a very reliable component that only failed 6 times in the ORD – as such it is difficult to draw any definitive conclusion from results concerning it. This is also the case with the emergency system, generator and lifting system that failed 0, 12 and 4 times in the FINO model respectively.

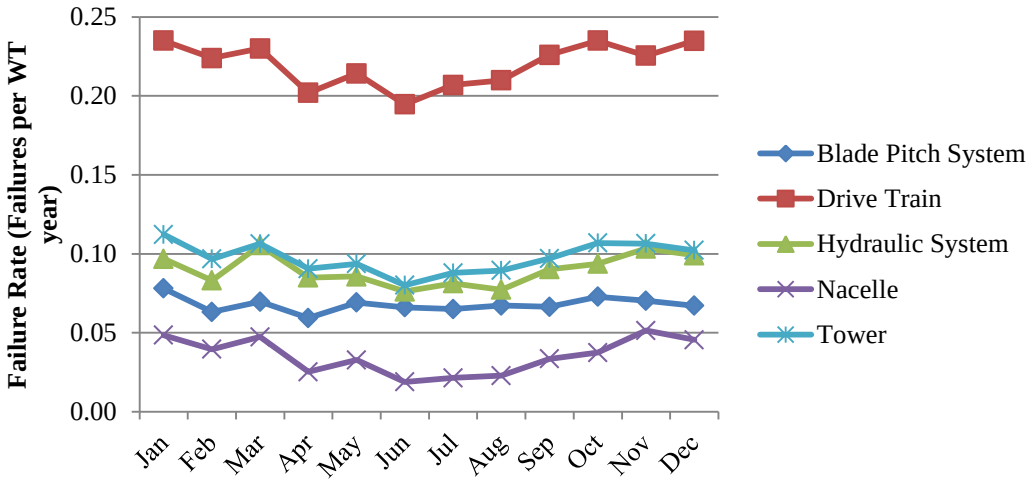

Figure 6-9: FINO model seasonal output for the blade pitch system, drive train, hydraulic system, nacelle and tower

Several of the components showed seasonality but in the opposite way expected, with the meteorological instruments, rotor, emergency system, generator and lifting system modelled to failed more often in the summer and less often in the winter. The reason for this – especially in the case of the emergency system, generator and lifting system – is likely to be due to a lack of data. Another possibility could be that preventative maintenance has been labelled incorrectly as corrective maintenance, although this is unlikely given there are relatively few failures attributed to each component.

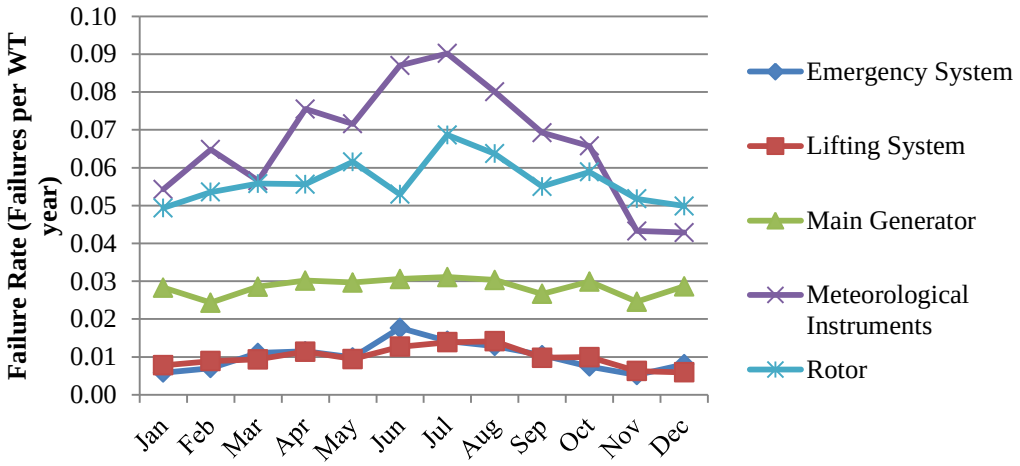

Figure 6-10: FINO model seasonal output for the emergency system, lifting system, main generator, meteorological instruments and rotor

A factor that certainly does have an impact on the seasonal failure rate of these components that appear more reliable in the winter is shown in Figure 6-11. The failure rate of the generator, meteorological instruments and rotor at the 13 – 17m/s bin is 0 failures per WT year.

The reason the failure rate is 0 for this bin is due to lack of data, rather than these components resisting failure at these wind speeds. The wind speeds did not reach these levels very often at Site A and Site B; therefore reliable components such as these were unlikely to fail during the relatively short period of time over which the data was recorded. However this shortcoming in the data becomes very apparent when the FINO model is used. Because the wind speed distribution at FINO is so different to the distributions at Site A and Site B, illustrated in Chapter 4.2.1 and Chapter 4.2.3, these rare high wind speed events become more apparent in the FINO model. For components like the control system, that fails so frequently, there is enough data to plot the relationship between failure rate and wind speed at this bin. And as the model works by assuming that any wind speed higher than 17 m/s has a failure rate equal to that calculated in the 13 – 17 m/s bin, the control system can be properly modelled. Thus in the case of the three components shown in Figure 6-11, any time

the wind speed is greater than 13 m/s (or 11 m/s in the case of the meteorological instruments) the failure rate is 0 and a failure cannot therefore occur. These wind speeds occur more frequently in the winter and this explains why the components appear to be more reliable in the winter months when the FINO model is used.

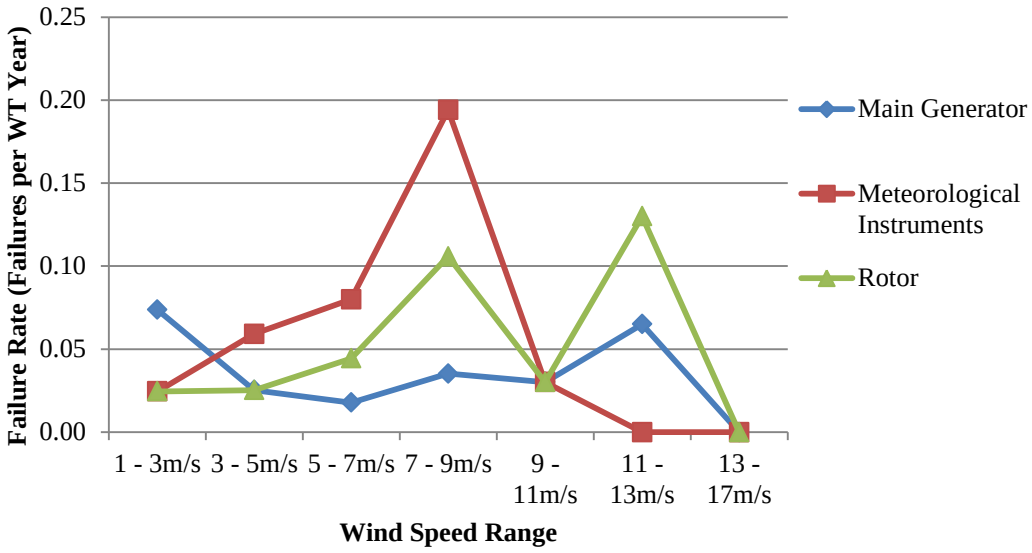

Figure 6-11: WSD failure rates for the main generator, meteorological instruments and rotor

1.2.2. FINO Model with Downtime Filters

A downtime filter can be applied to the FINO model to assess how the seasonal failure rates change as the severity of the failure increases. When no filter was applied, the control system appears very seasonal as shown in Figure 6-8. However if a 12 hour, 24 hour and 48 hour filter are applied to the model it becomes more seasonal as the failures considered become more severe, as shown in Figure 6-12. This means that very severe failures that cause the WT to suffer long downtimes are more likely to occur in the winter months than the summer months. The difference between the failure rates in November compared to June when the 48 hour downtime filter was applied is 91.94 %, whereas as mentioned previously when no filter is applied the difference was 81.89 %.

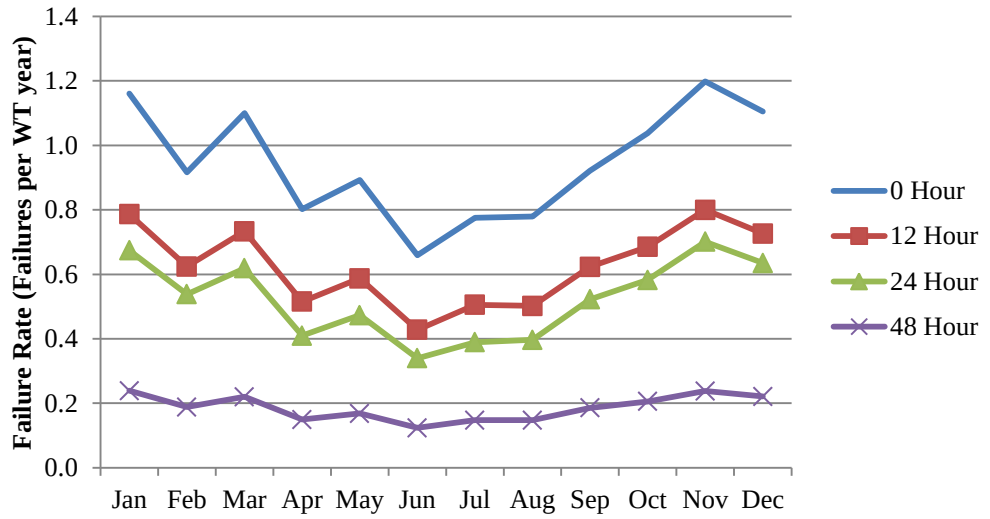

Figure 6-12: Seasonal failure rate of control system from FINO model when downtime filters were applied

This change in seasonality as the failure severity increases is even more apparent in the yaw system. As demonstrated in Figure 6-13, the difference in failure rate in November compared to June is 283.09 % when a 48 hour downtime filter is applied. As discussed previously, when no filter is applied it was 44.02 %. Therefore the yaw system is almost 3 times more likely to suffer a severe failure in November compared to June and if a failure does occur in November there is a 49.64 % chance it will cause more than 48 hours of downtime, whereas in June it is only 23.15 %.

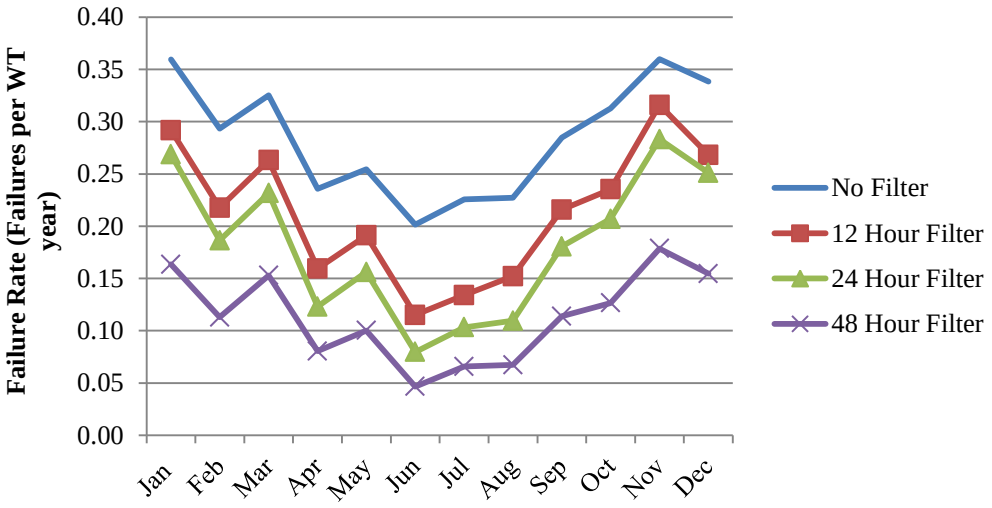

Figure 6-13: Seasonal failure rate of the yaw system in FINO model when downtime filters were applied

In the case of the drive train, the seasonality also becomes greater as downtime filters are applied, as shown in Figure 6-14. There were 105.77 % more 48 hour failures in November compared to June in the model; therefore a failure in November is twice as likely to suffer a failure greater than 48 hours.

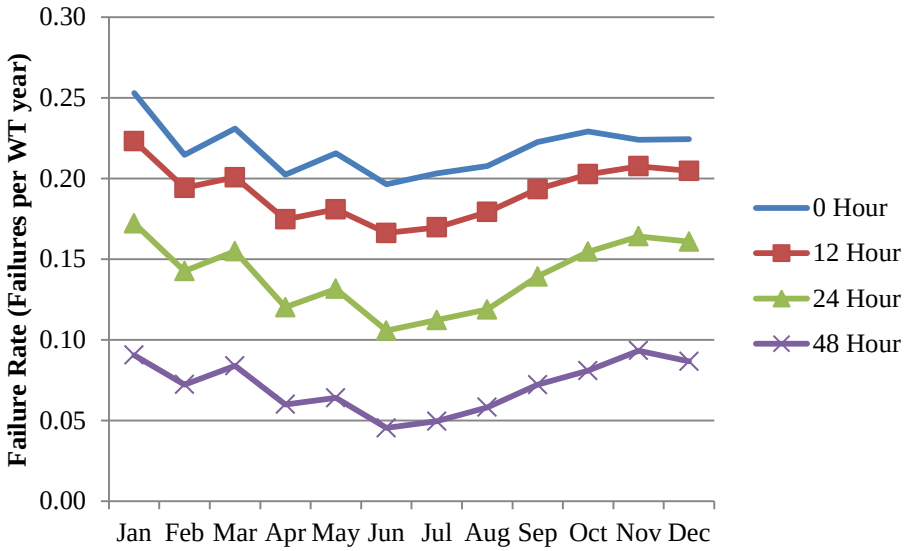

Figure 6-14: Seasonal failure rate of the drive train from FINO model when downtime filters were applied

1.2.3. Leuchars Model

The seasonal changes in wind speed are not as great at Leuchars compared to FINO, as shown in Chapter 4.2.2.2 and Chapter 4.2.3. This is to be expected however as Leuchars is a typical onshore site – the Leuchars model therefore used to investigate the seasonality of onshore WTs in following section.

The seasonal failure rates of the control system, yaw system and drive train in the Leuchars model were therefore less variable than the FINO model as shown in Figure 6-15. Although the control system still varied seasonally (the failure rate in November being 57.10 % higher than in June), it did not vary as much as it did in the FINO model. This was also the case for the drive train and the yaw system which for the same months varied 28.23 % and 53.78 % respectively.

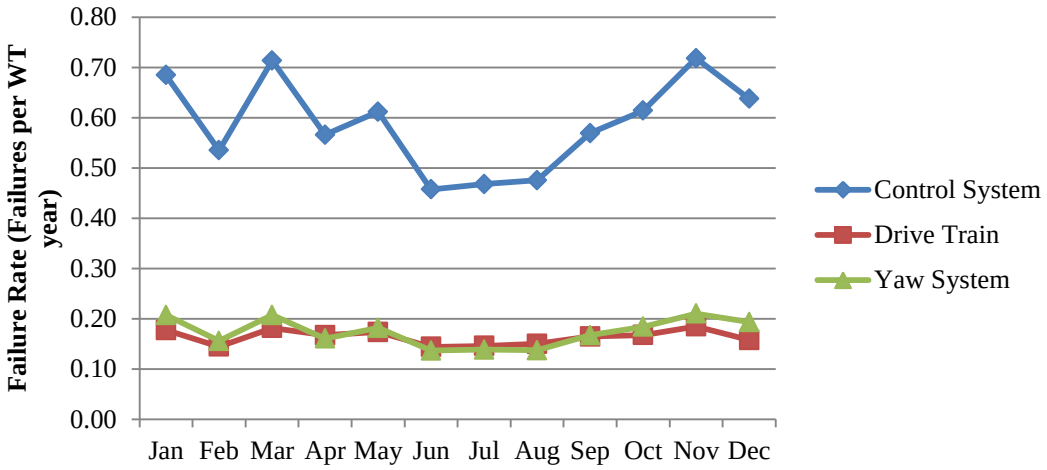

Figure 6-15: Leuchars model seasonal output for the control system and the yaw system

Like the FINO model the hydraulic system, nacelle and tower all failed seasonally too - albeit like the more unreliable components the failure rates did not vary as much as those calculated by the FINO model. However, unlike the FINO model the blade pitch system in the Leuchars model did not fail seasonally. In Figure 6-9 the blade pitch system in the FINO model does not vary much but there is an increase in failure rate of 18.46 % from June to

January. However in Figure 6-16 over the same two months there is only a variation of 2.18 % and the most reliable month was November.

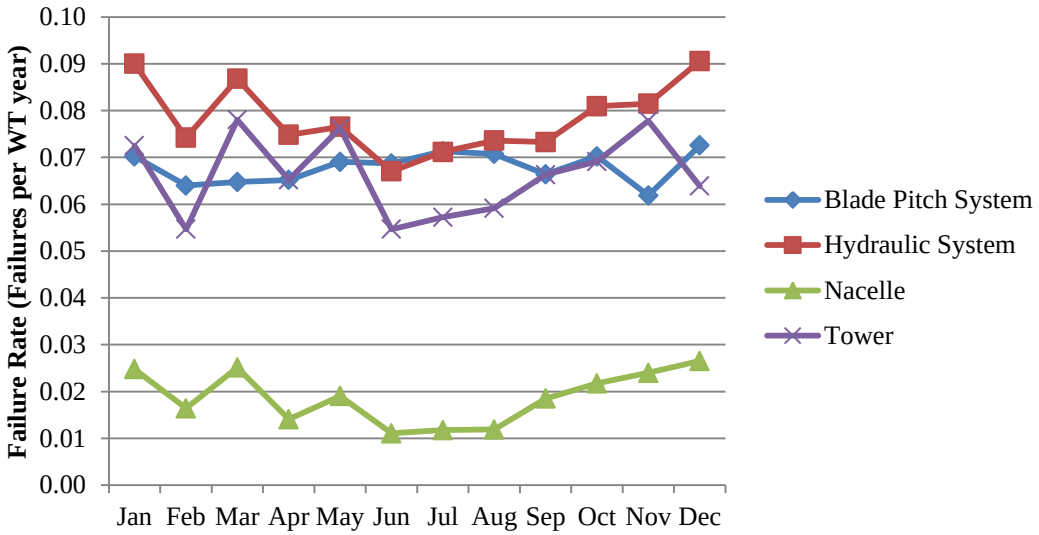

Figure 6-16: Leuchars model seasonal output for the blade pitch system, hydraulic system, nacelle and tower

This difference is most likely due to the WSD failure rate, which is shown in Figure 6-17. Although in general the failure rate increased with the wind speed, there was a dip between 9 m/s and 13 m/s. This – very similarly to the issues discussed in Chapter 6.1.2.1 with the meteorological instruments, generator and lifting system – is likely to be due to a lack of data rather than because the blade pitch system was more reliable between these wind speeds.

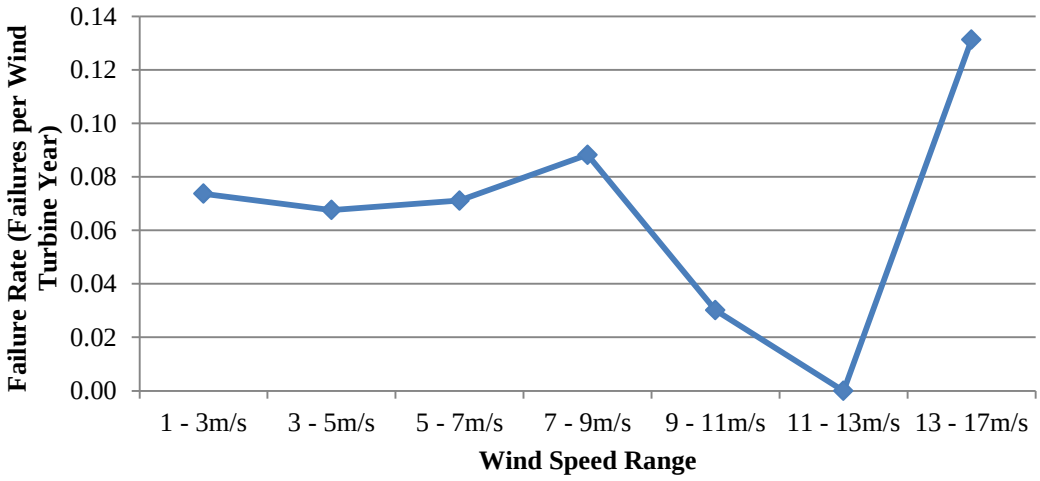

Figure 6-17: Blade pitch system mean WSD failure rate for each wind speed bin

In a variable speed WT, the blade pitch system is used to control the rotational speed of the blades above rated wind speed. It should be expected therefore that the blade pitch system would fail where it operates most frequently on days when the mean daily wind speed is above rate wind speed.

In the case of this WT model rated wind speed was roughly 11.5 m/s. The failure rate for each wind speed bin is shown in Figure 6-17. Although the 9 – 11 m/s bin is below this threshold it is important to remember that the model uses mean daily wind speeds as an input, not instantaneous wind speed. On a day with a mean wind speed of 9 m/s it is very likely that the wind speed will be above rated for a good proportion of the day. The mean daily wind speed gives an indication how often the blade pitch system may be operating, in the case of a day with a 9 m/s average wind speed it is very likely that the blade pitch system will operate often. This is also the case for the bin 11 – 13 m/s. In total this component only failed 26 times during the recorded period; more data is clearly required to accurately describe its relationship with the wind speed.

The remaining components in the Leuchars model do vary considerably from month to month as shown in Figure 6-18. Similar problems occur with the meteorological instruments

in the summer months that occurred in the FINO model. These issues are again due to how the component's WSD failure rate is modelled and because as shown previously in Figure 6-5, high wind speeds occur more frequently at Leuchars in comparison to the calibration wind speed data.

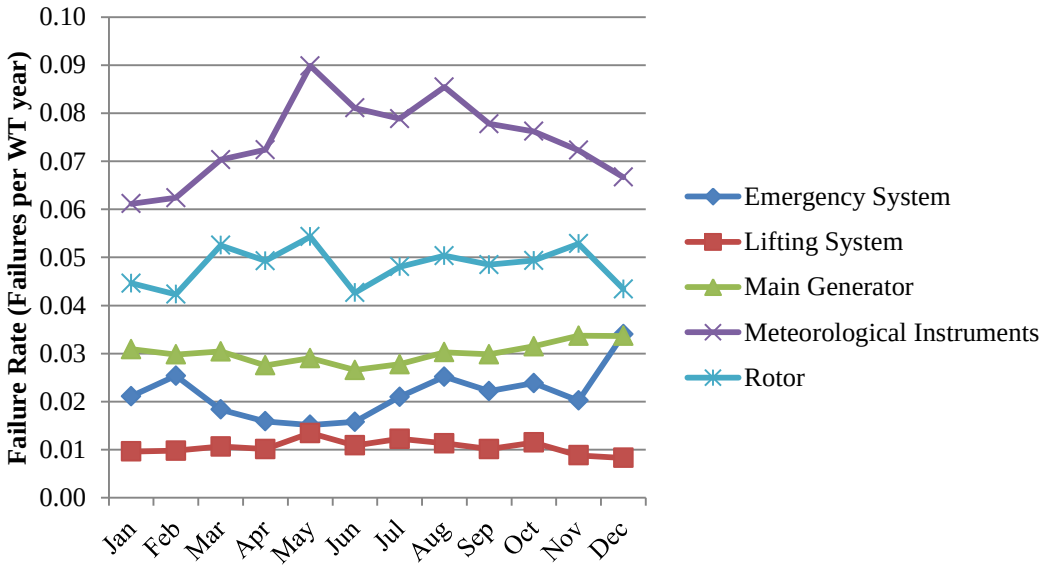

Figure 6-18: Leuchars model seasonal output for the emergency system, lifting system, generator, rotor and meteorological instruments

1.2.4. Leuchars Model with Downtime Filters

The seasonality of the control system, like the FINO model, also becomes more seasonal as longer downtime filters are applied and only the most severe failures are examined. In the case of the control system, as shown in Figure 6-19, the difference between June and November increased from 57.10 % when no filter was applied to 105.38 % when a 48 hour downtime filter was applied. The difference also increased when a 12 hour and a 24 hour filter were applied.

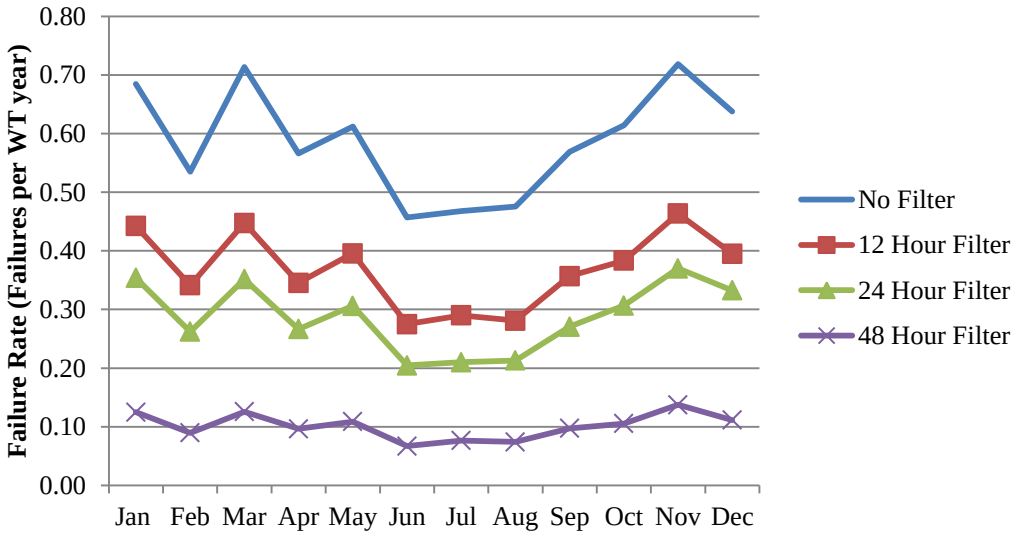

Figure 6-19: Seasonal failure rate of the control system from Leuchars model when downtime filters were applied

Like the FINO model, this pattern continued with the yaw system and the drive train as shown in Figure 6-20 and Figure 6-21 respectively. Although the seasonal failure rates of the drive train and the yaw system are very similar when a 48 hour downtime filter is applied, the downtime of a typical drive train failure is greater than the yaw system. So although failures to the drive train that cause downtimes greater than 48 hours are approximately as frequent seasonally in both models, those drive train failures that last more than 48 hours have far longer downtimes than those caused by the yaw system. This is illustrated in Figure 4-8.

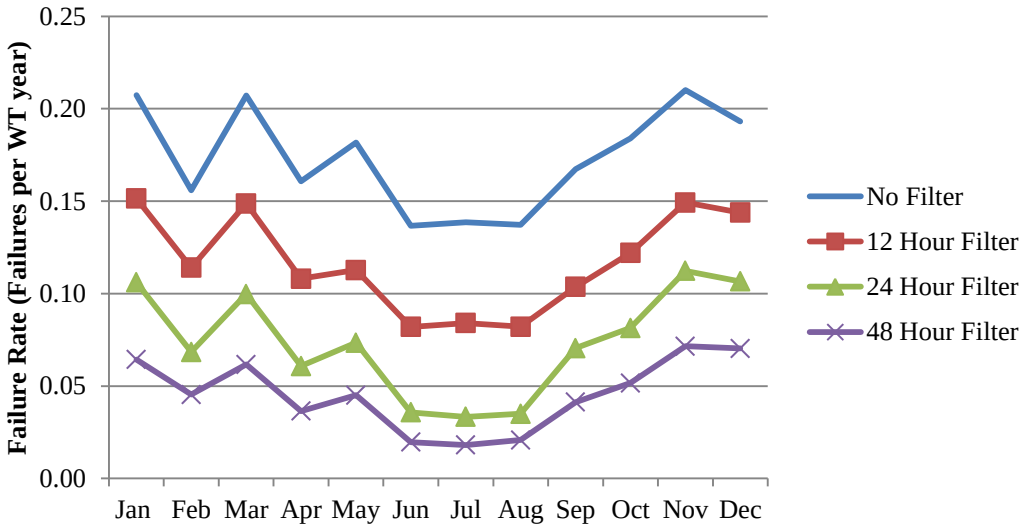

Figure 6-20: Seasonal failure rate of the yaw system from Leuchars model when downtime filters were applied

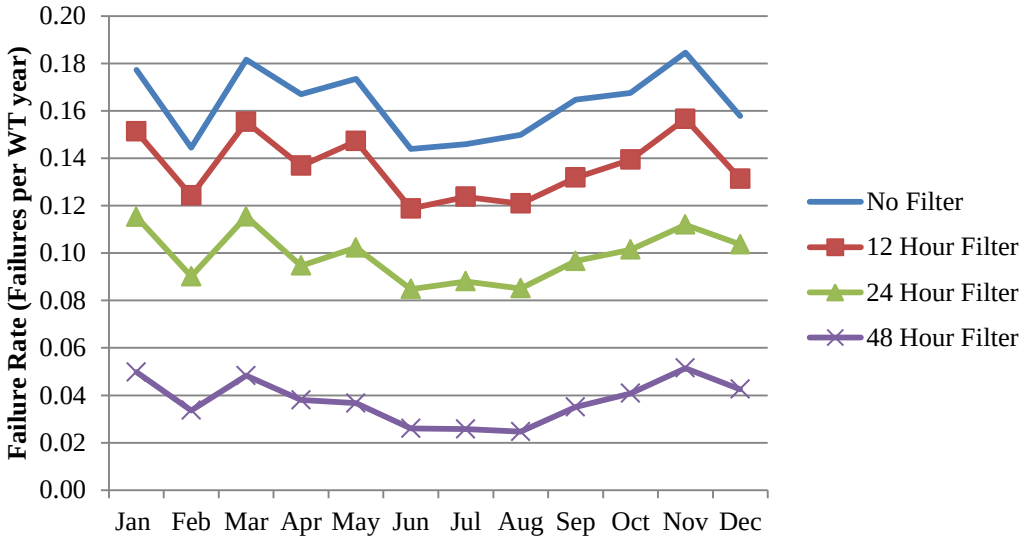

Figure 6-21: Seasonal failure rate of the drive train from Leuchars model when downtime filters were applied

1.3. Discussion

It is important to consider that the ORD recorded very few details beyond the functional location, the date and time and the downtime. The logistics involved with repairing the WT were not included within the data. There was not enough detail to distinguish between failures that caused *x* hours of downtime because of the severity and the damage caused and failures that also had *x* hours of downtime, but were due to waiting on ordered parts or because the high wind speeds meant that the nacelle was inaccessible for a long period of time.

With knowledge that these logistical and accessibility issues exist it would be sensible to assume that there will be more failures with long downtimes in winter compared to summer, regardless of failure severity. But it also makes sense intuitively that the harsher winter months would put more stress on the WT and cause more component failures. The results clearly show that in most cases, component downtime increases with wind speed, however the failure data is not detailed enough to be able to say with certainty what the actual reason for this relationship was.

It is probable that that rather than it being for a single reason it is due to a combination of both the failures being more severe in winter and the logistics and accessibility issues. Unfortunately, an accurate model would be required to understand this relationship better. However this model, like the majority of others, used reliability data that cannot help describe this relationship. It therefore must be assumed that any potential site will experience the same logistical and accessibility issues that Site A and Site B did and therefore all results using other wind speed time series will be biased by the maintenance procedures used at Site A and Site B.

Site A, which contributes the most data to the reliability records, had a relatively low mean wind speed of 5.86 m/s during the recorded period as previously discussed. Although the

maintenance procedures for the site are not known it is reasonable to assume that the nacelles are accessible for a larger proportion of the year than most UK onshore wind farms, which tend to have higher mean wind speeds. Therefore it is likely that the downtimes are dictated more by the severity of the failures and logistical issues such as spares holdings and waiting times for components.

These seasonal failure rates are used throughout the remainder of this thesis and it is therefore essential that these shortcomings with the model are considered. Ideally data of greater quality and quantity would have been available for analysis, but because large scale, multi-megawatt, onshore wind farms have only been operating for a relatively short period of time, data of adequate quality and quantity is scarce. However the data used in this analysis is as good as, if not better quality than the data used by Tavner and colleagues in their recent publication on this area [6-7]. It is both a larger dataset and one that consists of modern WTs of the same age and model that is not too dissimilar to WTs that will be deployed offshore. For these reasons the quality of the ORD is superior to the data from Wind Stats, WMEP and LWK used by so many other authors.

Using these results from the FINO and Leuchars models, the following section will examine the impact of seasonal failure rates on electricity production and determine whether they have an impact on the performance of onshore and offshore WTs.

2. Electricity Generation

From the previous section it is clear that both models calculate that more failures occur to a WT in the winter months and that the downtime per failure would also increase in winter. The opposite was found in summer, where the number of component failures and the downtime per failure deceased.

Standard models that use annual failure rates and repair rates do not account for these changes throughout the year. As a result it is possible that the production could be overestimated in the winter months and underestimated in the summer months.

The FINO and Leuchars models will be developed from the previous section to account for electricity generation. This will be done by incorporating a power curve into the models that will calculate the electricity generated at each time step from the input mean daily wind speed time series.

In both the case of the Leuchars and the FINO model more failures will occur in the winter and these failures will cause longer downtimes. Therefore a relatively high volume of potential electricity will be lost at this time of year, when the wind speed is highest. However, if the WT fails less frequently in the summer and for shorter periods of time, will the WSD failure rates, have any impact on net production?

The following section will attempt to answer this question by analysing how onshore electricity generation is affected when WSD failure rates are used in analysis, rather than constant failure rates.

2.1. The Power Curve

The simple model used in Chapter 6.1 was developed by calculating the potential electricity and actual electricity generated by each WT. This is shown in Figure 6-22 as $E_{Potential}$ and E_{Actual} respectively.

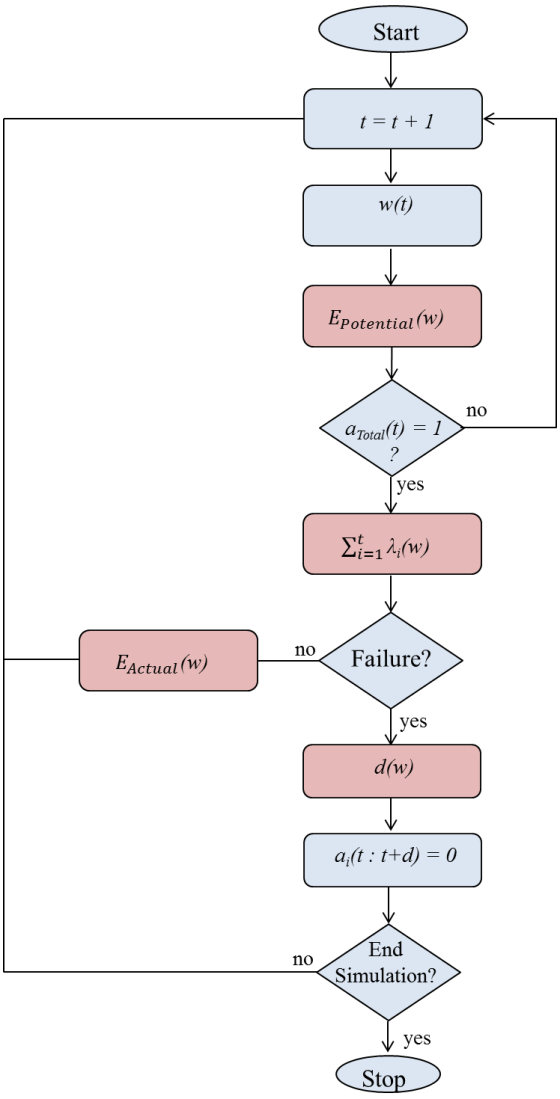

Figure 6-22: Model flow chart with electrical generation calculation included

The potential electricity is calculated at every time step, regardless of the availability of the WT. However the actual electricity is only calculated if the WT is operating. These two variables are then used to calculate the lost generation E_{Lost}, shown in Equation 6-1.

$$E_{Lost} = E_{Potential} - E_{Actual}$$ **Equation 6-1**

To calculate the electricity output a power curve must be developed. In both the FINO model and the Leuchars model the parameters used in calculating the power curve are identical and they are shown in Table 6-7.

Table 6-7: Estimated power curve properties

Rating	2.3 MW
Power Coefficient (C_p)	0.275
Swept Area (A)	9.17 x 10^3 m^2
Air Density (ρ)	1.2 kg/m^3
Cut-in Wind Speed	3 m/s
Rated Wind Speed	11.5 m/s
Cut-out Wind Speed	25 m/s
Hub Height	80 m

The rating of the WTs used in each model are 2.3MW – the same as the output of the WTs used at Site A and Site B. The power curve is generated using Equation 6-2 between cut in and rated wind speed and then assuming zero output below cut in and rated output above rated wind speed.electricity

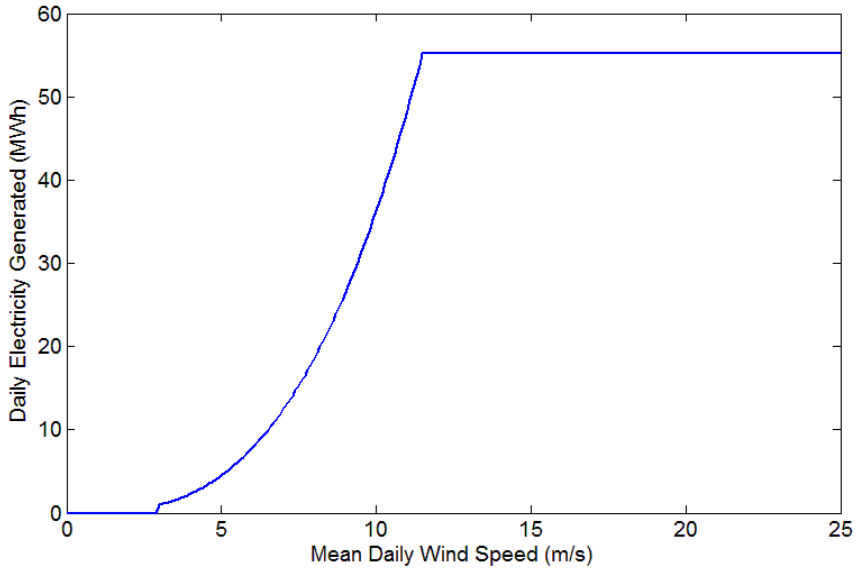

Figure 6-23: Power curve used to calculate WT output

$$P = \frac{1}{2} C_p \rho A V^3 \times 24$$ **Equation 6-2**

The output calculated by the model using the power curve is an approximation of the energy actually generated in a day. Mean daily wind speed is a metric that does not fully describe the conditions experienced by a site throughout a day and as the power curve in non-linear there can be big differences in generation between two days that have the same mean daily wind speed. Also the control systems used in variable speed WTs are not perfect – therefore power curves in reality provide a guide as to what the expected output of a WT should be in standard operating conditions [6-8]. As wind speed changes at very high frequencies, the actual output can vary significantly from expected output [6-8].

Another issue to consider is that the optimum WTs for sites with the wind speed conditions of Leuchars and FINO would be different. Leuchars, a typical onshore site, would be served well by a 2.3MW WT. FINO however has such a good wind resource that a larger machine with a higher output would be more appropriate. However, because the ORD corresponds to a 2.3MW WT and so a comparison can be made between both models, for the initial analysis the power curve is identical.

2.2. Price of Electricity

As this thesis has used data from UK onshore wind farms, the price of electricity that will be used in the analysis undertaken in this Chapter and Chapter 6 will be taken from the UK. The unit price of electricity in the UK is currently dictated by the market price of a unit of electricity and the market price of the subsidy. Market electricity prices vary seasonally, however for the analysis undertaken in this thesis a constant price is assumed.

Currently each form of renewable generation is given a specified quantity of Renewable Obligation Certificates (ROCs) for each generated unit. In the case of onshore and offshore wind, 0.9 ROCs and 2 ROCs are currently received per unit generated [6-9]. These rates however depend on the date that the generation was commissioned. For offshore sites commissioned in 2015/2016 and 2016/2017 this rate will drop to 1.9 ROCs and 1.8 ROCs per unit. Beyond 2017 the ROC scheme expires, however commissioned sites that agreed to be part of the ROC scheme will continue to receive their subsidy for 20 years beyond their commission date [6-10].

Table 6-8: Strike price for onshore and offshore wind depending on commission date

	Strike Price (£/MWh)				
	2014/15	2015/16	2016/17	2017/18	2018/19
Onshore Wind	95	95	95	90	90
Offshore Wind	155	155	150	140	140

This system will change in March 2017 when the new scheme Contracts for Difference (CfD) begins [6-11]. Under this arrangement generators are protected from market fluctuations and are instead guaranteed a strike price. In the case of onshore and offshore wind this will be £95/MWh and £155/MWh if they are commissioned in 2014/2015. This reduces the later a project is commissioned as shown in Table 6-8.

These reductions serve two purposes, firstly they encourage developers to invest quickly in generation capacity and secondly the prices account for the reduction in the cost of energy which will hopefully occur with an increase in deployment and improved designs.

The strike price is given to the generator for each generated unit. If a generator is producing onshore wind electricity at a price less than the strike price they will make a profit from whatever the difference is between their costs and their subsidy. However, if it costs the generator more than the strike price to generate electricity, they make a loss as the strike price does not cover their costs [6-11].

Until March 2017 generators can apply for either scheme. The analysis undertaken in this Chapter will use the CfD price of electricity in its analysis as it is the system that will be implemented for at least 5 years. Therefore the sale price for a unit of onshore electricity used in the model is £95/MWh for onshore generation. This price does not account for electricity sold through the spot market and this will not be considered in the analysis.

2.3. Site Production

As discussed previously, the impact of wind speed on failure rate is not accounted for in models that use constant failure rates. The following sections examine the impact of WSD failure rates and downtimes on electricity production.

To demonstrate the advantage of using WSD failure rates failure rates, comparisons will be made between results generated using the WSD FINO and Leuchars models – demonstrated in the previous section – and calculations produced by constant FINO and Leuchars models. These constant models comprise of failure rates that remain constant throughout the year regardless of wind speed, such that are used traditionally.

These constant failure rates used in this analysis are taken simply from the annual component failure rates calculated by the FINO and Leuchars models in Table 6-2 and Table 6-4, using the WSD failure rates. Therefore if for instance the FINO model is run twice, first using the constant failure rates and secondly the WSD failure rates, the system failure rates after both simulations will be the same. But the distribution of failures throughout a typical year will be different and therefore so will the energy generated. The WSD failure rate model will simulate failures that occur at times of high wind speed, whereas in the constant failure rate model failures will occur uniformly throughout a year.

The purpose of this comparison is to identify the difference in calculated yield between a model that uses constant failures rates, as most models do, and a model whose failure rates change according to the daily mean wind speed (the WSD failure rates). A comparison will also be made using constant failure rates calculated from the ORDbase. This is to compare the difference in yield if the WTs subjected to the FINO and Leuchars wind speeds are assumed to have the same failure rate as those at Site A and Site B.

The model will calculate production using the power curve developed in Chapter 6.2.1 to convert the wind speed time series to electricity and then determine the income generated by

taking the electricity prices established in 0. Chapter 6.2.3.3 will use a power curve for a 5 MW WT, calculated in the same way as the 2.3 MW power curve. The difference between the constant and WSD failure rate models will then be compared and discussed.

The WSD failure rate models have component failure rates that change each at each time step of the simulation with the mean daily wind speed of the wind speed time series. The constant failure rate model consists of component failure rates at each time step that are calculated simply by dividing the annual component failure rates of Table 6-2 and Table 6-4 respectively by 365. This is also the case with the ORD data model, using annual component failure rates calculated in Table 4-3.

2.3.1. FINO Model

The WSD FINO model produces the monthly failure rates and generated power shown in Figure 6-24. The failure rates shown are annual failure rates, calculated in the same way as the seasonal failure rates in Chapter 6.1.2. The power generated shown in Figure 6-24 is calculated by averaging the total output each month throughout the simulations. It therefore shows the annual average output of each month.

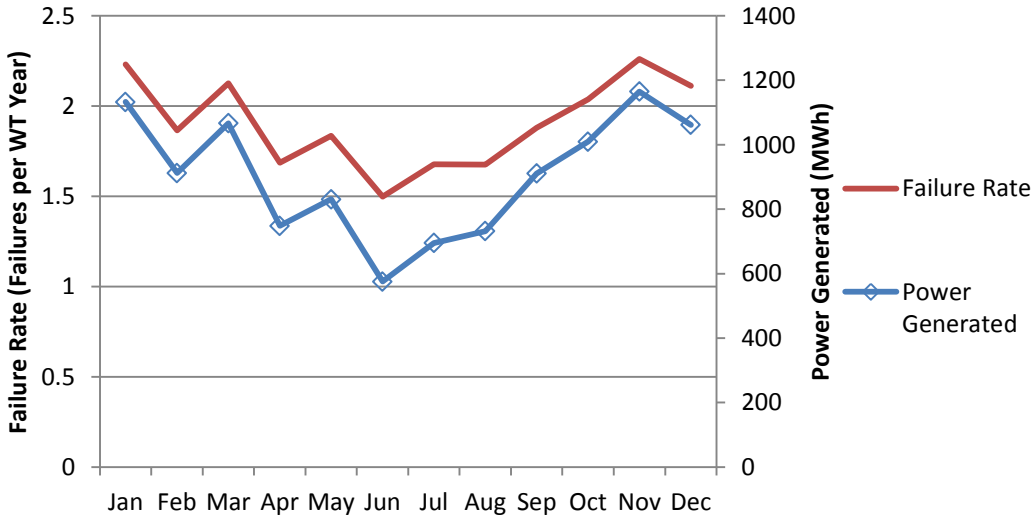

Figure 6-24: Mean monthly failure rate and mean monthly power generated for WSD failure rate FINO model

Figure 6-24 shows the an expected output given that in the WSD failure rate FINO model, a WT is more likely to fail in the winter months but will also generate more power at this time of year because of high wind speeds; despite spending more time unavailable. The monthly power generated does not appear to be affected by the higher failure rates in the winter – this is because onshore WTs have high availabilities, even when faced with strong wind speeds such as those experienced at FINO.

The results from the constant failure rate FINO model differ greatly. The MCMCS in this case uses constant failure rates, therefore failures are as likely to occur in summer as in

winter – as shown in Figure 6-25. The power generated does not change significantly compared to the output generated in Figure 6-24 in the WSD failure rate model.

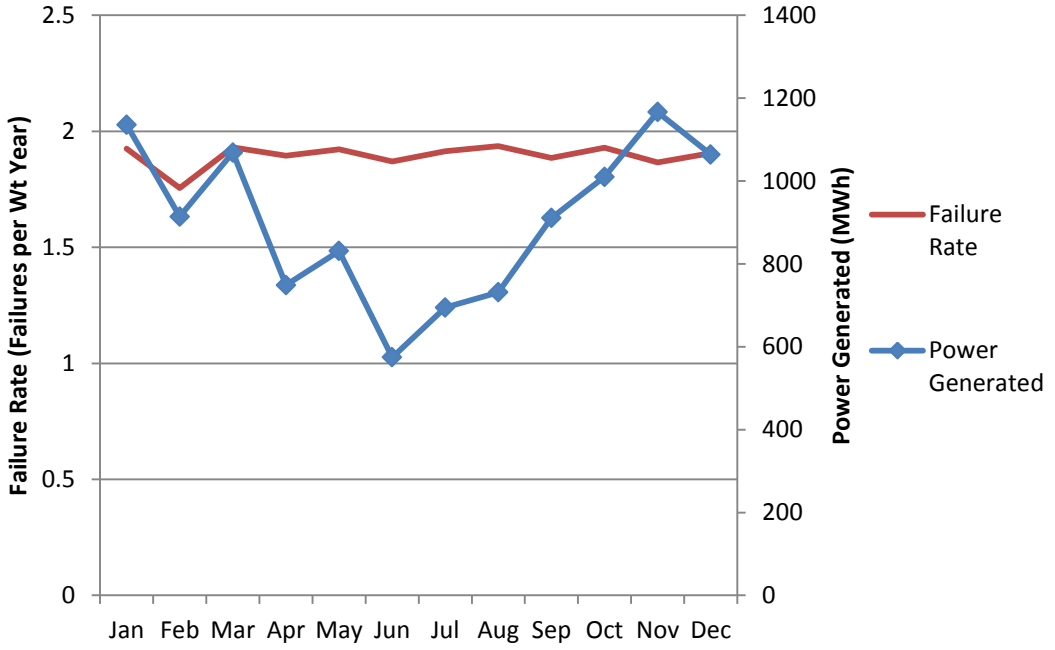

Figure 6-25: Mean monthly failure rate and mean monthly power generated for constant failure rate FINO model

When analysing the power lost E_{Lost}, of the WSD failure rate FINO model it is higher in winter than in summer as illustrated in Figure 6-26. This is to be expected given the higher monthly failure rates in winter shown in Figure 6-24. The impact of failing at a time when wind speeds are high is that the WT is likely to lose more potential electricity than in summer. The downtimes in winter are also more likely to be longer.

Due to the WSD failure rates and downtimes, the model calculates that the percentage of lost power to power generated will increase in the winter and decrease in the summer, as shown in Figure 6-26. Therefore according to the WSD failure rate FINO model, the WTs underperform in winter compared to the summer because they are modelled to fail more often for longer periods of time. Therefore due to reliability issues WTs in the WSD failure rate model are less productive in the winter than they would be calculated to be if using

constant failure rates. Equally however the WTs are more productive in the summer when the failure rate and downtime per failure decreases. However, does this increase in productivity compensate for the reduction experienced in winter?

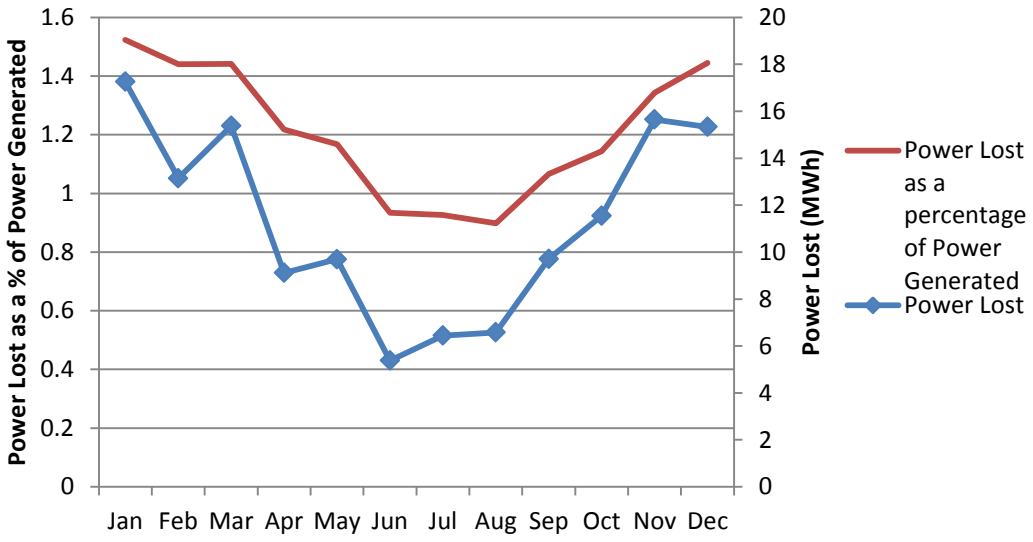

Figure 6-26: Power lost as a percentage of power generated and lost power for WSD failure rate FINO model

The FINO constant model calculates that average power lost as a percentage of generated power would be roughly 1.1 % throughout the year. However the FINO model calculated that approximately 1.5 % is lost in winter compared to approximately 0.9 % in the summer – the average throughout the year is 1.2 %.

A comparison in annual outputs of the WSD failure rate FINO model and the constant failure rate model is shown in Table 6-9. The annual failure rates of the two models are the same; however the WSD failure rate model does not generate as much power as the constant failure rate model. Therefore in the case of the WSD failure rate model, the greater production in summer does not make up for the bad production in the winter. The difference between the two calculations is 9.206 MWh per WT year. For a 200 WT wind farm this equals £174,914 in difference between the incomes expected had constant failure rates been used in analysis.

Table 6-9: Summary of FINO model power generated, power generated and failure rate for WSD, constant and ORD data failure rates

Model	Per WT Year			
	Total Power Generated (MWh)	Total Power Lost (MWh)	Total Power Lost as a percentage of Total Power Generated (%)	Mean Failure Rate
FINO WSD Failure Rates	10841.125	135.218	1.247	1.910
FINO Constant Failure Rate	10850.331	126.012	1.161	1.910
ORD Constant Failure Rates	10914.875	61.468	0.563	1.238

The difference in using WSD failure rates as opposed to standard constant failure rates, in terms of calculating annual generation, is worth roughly £875 per WT year for an onshore wind farm with FINO wind speed conditions, using a 2.3 MW WT.

The constant failure rates are initially calculated using the FINO model. If an operator were to assume that the failure rates experienced at Site A and Site B in the ORD were the same for every site, the yield would be calculated to be 0.60% higher than if the constant failure rates were used in the simulation. Therefore the difference between using the ORD failure rates and those calculated using the constant annual failure rates is £6131.68 per WT year. If the WSD failure rates are used to calculate the yield, this difference increases to £7006.25 per WT year.

2.3.2. Leuchars Model

Similarly to the FINO model comparison in the previous section, the WSD failure rate Leuchars model is contrasted against a stationary annual failure rate Leuchars model. The purpose of this analysis is to determine if the difference in the models is as great for an onshore wind speed time series model, as a model that uses an offshore wind speed time series.

Figure 6-27 shows the monthly mean whole system annual failure rate and the mean power generated on average each month simulated by the WSD failure rate Leuchars model. Like the results of the WSD failure rate FINO model, there is a clear correlation between the two measurements, both increasing in the winter and then declining in the summer.

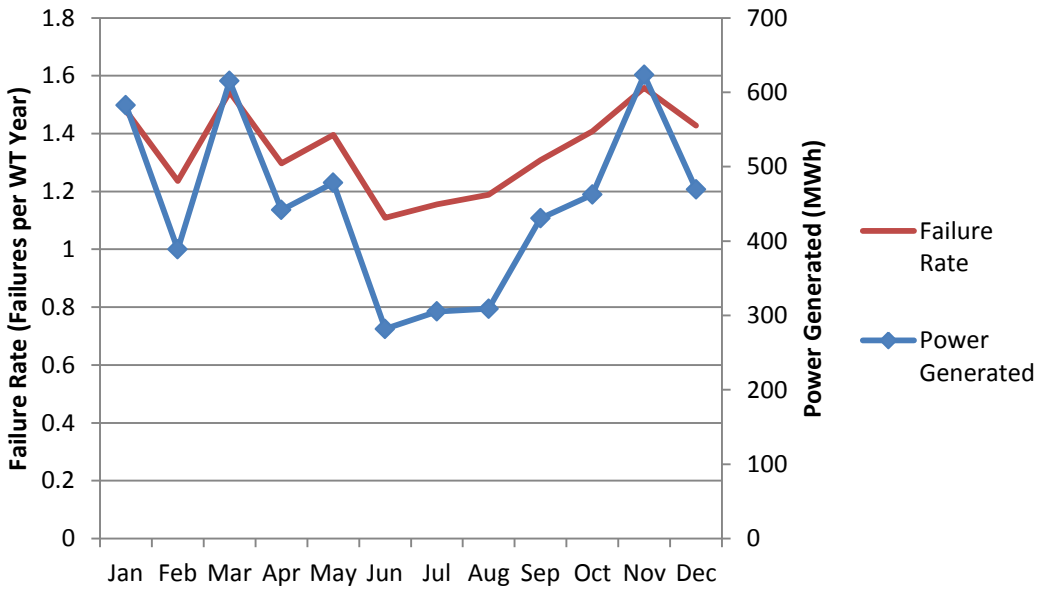

Figure 6-27: Mean monthly failure rate and mean monthly power generated for WSD failure rate Leuchars model

The variation in power generated however is greater in the Leuchars model. The power generation increases by 121.3 % from June to November in the Leuchars model compared to 102.4 % in the FINO model, the results of which are shown in Figure 6-24. This difference in variation is not due to the seasonality of the wind speeds in both time series, as FINO

varies considerably more throughout the year than Leuchars, but because the high wind speeds at FINO mean that the 2.3 MW WT used in the model operates more often above rated where the power production is constant. The seasonal variation in generated power may increase when a larger WT is tested in the FINO model in Chapter 6.2.3.3.

The impact of the higher winter failure rates and downtimes is not so severe in the Leuchars model compared to the FINO model as shown in Figure 6-28. The power lost as a percentage of power generated is less than calculated with the FINO model in Figure 6-26. The power lost is also considerably less than in the FINO model due to the lower potential energy in the Leuchars wind speed time series.

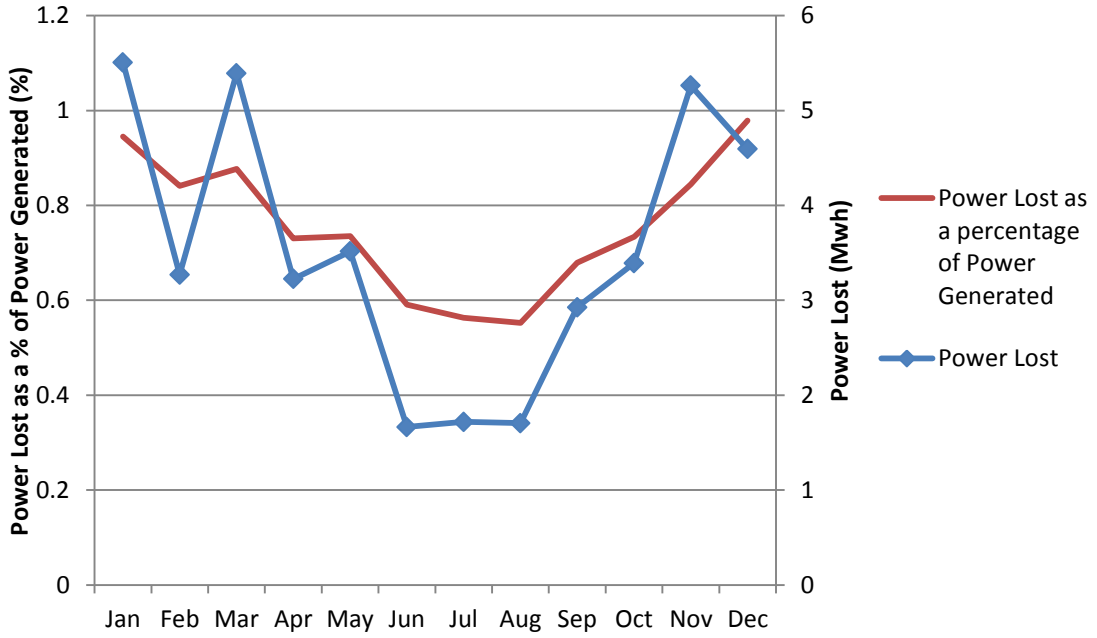

Figure 6-28: Power lost as a percentage of power generated and lost power for the WSD failure rate Leuchars model

Similarly to the FINO constant failure rate model, the Leuchars constant model has a monthly failure rate that remains relatively constant as expected. The Power generation is very similar to that modelled in the WSD failure rate FINO model shown in Figure 6-27.

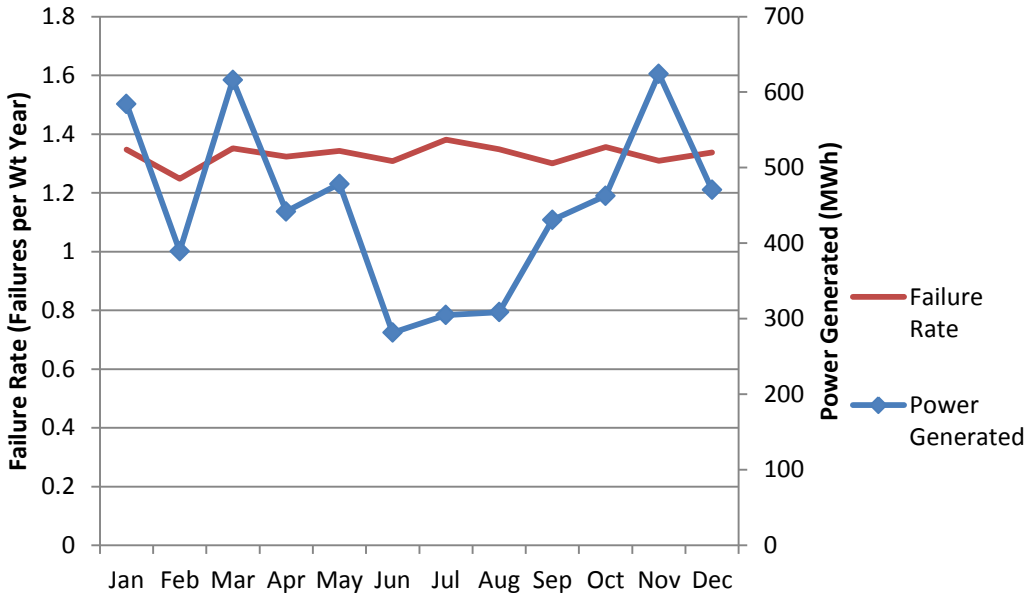

Figure 6-29: Mean monthly failure rate and mean monthly power generated for the constant failure rate Leuchars model

As expected the power lost as a percentage of power generated remains constant throughout the year due to the relatively constant monthly system failure rates. This constant model therefore underestimates the losses in winter and over estimates the losses in summer compared to the WSD Leuchars model.

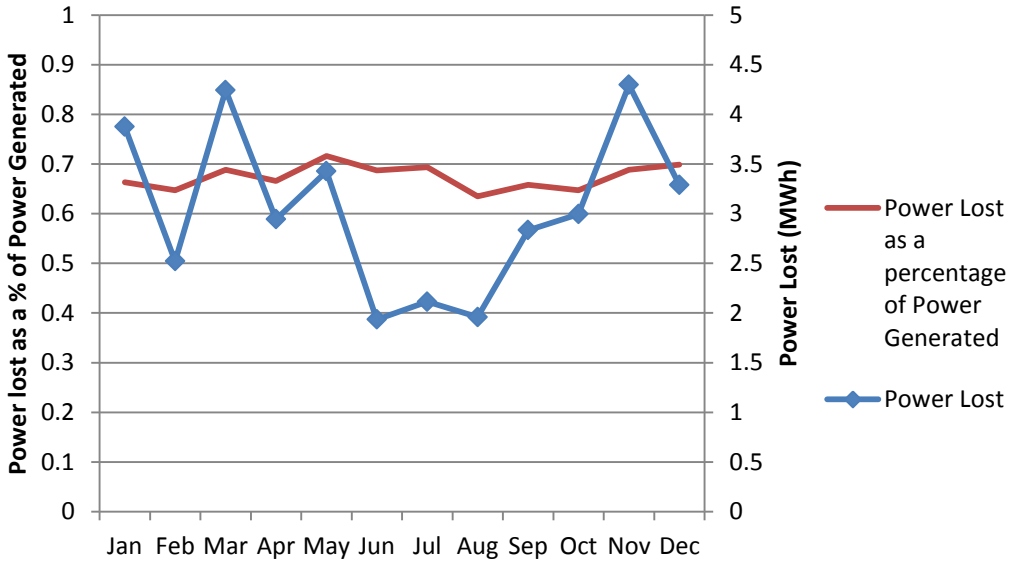

Figure 6-30: Power lost as a percentage of power generated and lost power for the constant failure rate Leuchars model

The impact of these differences in the calculation of the annual production is fairly minimal, as shown in Table 6-10. Per WT year the WSD failure rate model calculates a difference of 5.746 MWh in the calculated site outputs. This equates to £545.87 per WT year, which for a site of 200 WTs would represent a reduction of £109,174 in income per year, compared to the income expected had constant failure rates been used.

Table 6-10: Summary of Leuchars model power generated, power generated and failure rate for WSD, constant and ORD failure rates

	Per WT Year			
Leuchars Model	Total Power Generated (MWh)	Total Power Lost (MWh)	Total Power Lost as a percentage of Total Power Generated (%)	Mean Failure Rate
WSD Failure Rates	5388.230	42.176	0.78	1.342
Constant failure rates	5393.976	36.430	0.67	1.329
ORD Failure Rates	5399.996	30.410	0.56	1.238

The merits of using a WSD failure rate model to calculate the yield of an onshore site with a low annual mean wind speed is not as convincing as for a site with the resource of FINO. The difference in using failure rates from the ORD and those calculated using WSD failure rates is 6.020 MWh when using constant annual failure rates in the simulation and 11.766 MWh when using WSD failure rates, as shown in Table 6-10. Per WT year this equates to £571.90 and £1117.77 respectively.

2.3.3. FINO 5 MW model

As discussed previously in Chapter 6.2.3, the 2.3 MW onshore WT model does not fully take advantage of the potential energy of the FINO site. The capacity factor of the FINO model from Chapter 6.2.3.1 is 54 %, which is exceptionally high. A larger WT would be used in reality for a site like this, such as a 5 MW WT generator.

In this section a 5 MW WT with the parameters shown in Table 6-11 is used to generate a simple 5 MW FINO model. With the exception of the power coefficient, these are based on the NREL offshore reference WT [6-12]. The difference in performance in using WSD failure rates in the analysis, compared to constant failure rates is assessed and compared to the original FINO model from Chapter 6.2.3.1 that used 2.3 MW WT parameters shown in Table 6-7.

Table 6-11: 5 MW WT parameters

Rating	5MW
Cut in speed	3 m/s
Rated Speed	11.5 m/s
Cut out speed	25 m/s
Power Coefficient (C_p)	0.375
Rotor radius	63 m
Air Density	1.2 kg/m_3
Hub Height	90 m

A power curve for this WT was estimated, using the WT parameters shown in Table 6-11 and the wind power formula from Equation 6-2. The power curve is illustrated in Figure 6-31.

The difference between the outputs of the 2.3 MW FINO model and the 5 MW FINO model are shown in Table 6-12. The 5 MW model generates 17% more electricity throughout the year, but loses 16% more power throughout the year. Additionally, the power lost as a percentage of the total power generated decreases to 1.203% in the 5 MW model from

1.247% in the 2.3 MW model (shown in Chapter 6.2.3.1). The capacity factor when using a 5 MW WT for the FINO wind resource is 24%, which is much more reasonable.

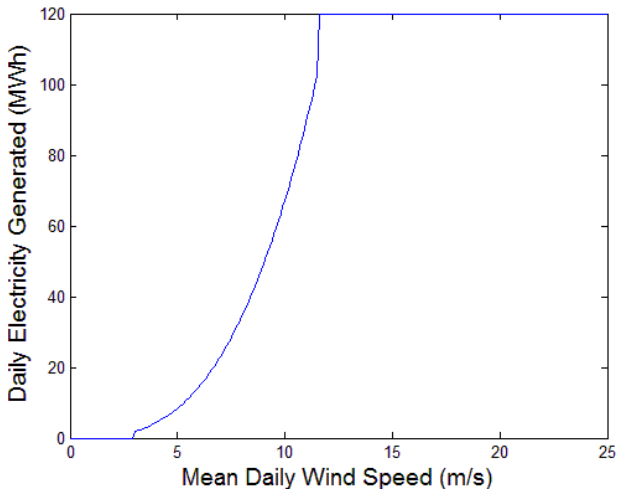

Figure 6-31: Power curve of the 5 MW WT

The reason for the improved performance of the 5 MW WT is because it is able to generate higher amounts of electricity and the differences between the 2.3 MW and 5 MW WT power curves.

Table 6-12: Mean monthly outputs of WSD failure rate 2.3 MW and 5 MW FINO models

Month	Power Generated (MWh)		Power Lost (MWh)		Power Lost as a % of Power Generated		Failure Rate (Failures per WT Year)	
	2.3MW	5MW	2.3MW	5MW	2.3MW	5MW	2.3MW	5MW
Jan	1132.701	1283.262	17.257	19.836	1.524	1.546	2.232	2.241
Feb	912.407	1067.989	13.145	15.379	1.441	1.440	1.869	1.886
Mar	1066.756	1215.389	15.374	17.314	1.441	1.425	2.135	2.142
Apr	748.443	912.885	9.114	10.595	1.218	1.161	1.686	1.671
May	830.915	974.756	9.697	10.940	1.167	1.122	1.835	1.820
Jun	575.476	736.151	5.375	6.612	0.934	0.898	1.498	1.489
Jul	695.402	870.789	6.444	7.758	0.927	0.891	1.678	1.662
Aug	732.170	894.878	6.579	7.985	0.899	0.892	1.675	1.710
Sep	910.828	1083.151	9.711	11.334	1.066	1.046	1.879	1.913
Oct	1009.582	1173.710	11.539	13.827	1.143	1.178	2.038	2.033
Nov	1164.985	1282.186	15.650	17.817	1.343	1.390	2.281	2.264
Dec	1061.460	1202.107	15.332	17.350	1.444	1.443	2.130	2.105

The difference between the WSD failure rate 5 MW FINO model ($\lambda_{Seasonal}$) and the constant failure rate 5 MW FINO model ($\lambda_{staionary}$) is shown in Table 6-13. It shows that the WSD model generates less power than the constant model by 14.9 MWh per WT year. If this 5 MW machine was used onshore this difference in estimated yield would equal £1415 per WT year, or £283,100 per year for a wind farm of 200 WTs.

Table 6-13: Mean monthly outputs of WSD failure rate 5 MW FINO model and the constant failure rate 5 MW FINO model

Month	Power Generated (MWh)		Power Lost (MWh)		Power Lost as a % of Power Generated		Failure Rate (Failures per WT Year)	
	λ_{WSD}	$\lambda_{Stationary}$	λ_{WSD}	$\lambda_{Stationary}$	λ_{WSD}	$\lambda_{Stationary}$	λ_{WSD}	$\lambda_{Stationary}$
Jan	1283.262	1287.662	19.836	15.436	1.546	1.199	2.241	1.943
Feb	1067.989	1070.646	15.379	12.722	1.440	1.188	1.886	1.785
Mar	1215.389	1218.275	17.314	14.428	1.425	1.184	2.142	1.948
Apr	912.885	913.268	10.595	10.212	1.161	1.118	1.671	1.883
May	974.756	974.850	10.940	10.846	1.122	1.113	1.820	1.956
Jun	736.151	735.303	6.612	7.460	0.898	1.015	1.489	1.870
Jul	870.789	869.608	7.758	8.939	0.891	1.028	1.662	1.946
Aug	894.878	894.151	7.985	8.712	0.892	0.974	1.710	1.942
Sep	1083.151	1083.572	11.334	10.912	1.046	1.007	1.913	1.867
Oct	1173.710	1174.806	13.827	12.730	1.178	1.084	2.033	1.953
Nov	1282.186	1285.004	17.817	14.999	1.390	1.167	2.264	1.894
Dec	1202.107	1205.011	17.350	14.446	1.443	1.199	2.105	1.947
Total/ **Average**	*12697.25*	*12712.15*	*156.746*	*141.841*	**1.203**	**1.106**	**1.911**	**1.911**

If the ORD failure rates are used in the analysis instead, shown in column 3 of Table 6-2, the average annual production is 12782.01 MWh and the power lost is 71.98 MWh. The difference in this calculated annual production and that calculated by the FINO 5 MW λ_{WSD} model is £13138.73 per WT year using offshore electricity rates.

Therefore according to the WSD FINO model, if a wind farm operator assumed that failure rates offshore at FINO would remain consistent with onshore failure rates recorded at Site A and Site B, they would earn roughly £2.6 million less per year for a 200 WT offshore wind farm. This difference would be due to reduced reliability offshore and failures occurring

more frequently in the winter when potential electricity generation is at its highest. The extended downtime due to offshore logistics and accessibility is not accounted for by the model. This will be considered in more detail in the following chapter when a simplified offshore constraint model will be constructed by adapting the model shown in Figure 6-22.

2.4. Discussion

The WSD failure rate models for Leuchars and FINO estimate a reduction in output compared to traditional constant failure rate models. This estimation only analyses the electricity generated and energy lost, it does not include the costs of O&M that result from preventative and corrective maintenance.

The benefit of using the WSD failure rate model developed in this thesis is that monthly estimates can be made of component failures and the impact these failures have on production can be analysed in better detail than simply assuming constant failure rates. Losses in production in the winter due to increased failure rates and the increases in the summer due to reduced failure rates are also accounted for in the WSD failure rate model that otherwise would not be accounted for in a constant failure rate model. The WSD model calculates that the losses suffered in the winter are not compensated in the summer, as opposed to the constant models that are not detailed enough to consider this issue.

The constant and WSD models calculate much lower electricity generation than the ORD failure rate models. This is to be expected as the failure rates calculated by the FINO and Leuchars models are higher than those calculated in the ORD. If operators were to assume that WT failure rates would remain the same if they were subjected to FINO wind speeds substantially more energy would be lost than expected due to increases in component failure rates.

3. Chapter 6 Summary

This chapter has demonstrated simple application of the WSD failure rates calculated in Chapter 5.2.5.1. Component failure rates were calculated using the WSD failure rate model and the FINO and Leuchars input wind speed time series. As shown in Table 6-2 the failure rate of the system according to the FINO model was 1.910 failures per WT year and the availability was 98.90%. The Leuchars model showed a slight increase in failure rate of 8.24% compared to the ORD, but as the mean wind speed did not differ significantly compared to the calibration wind speed data, the change was not as great as FINO. The components most significantly affected by the high wind speeds at FINO were the control system, the yaw system and the drive train as shown in Table 6-2. Their failure rates were calculated by the FINO model to increase by 82%, 89% and 40% respectively.

Using the WSD failure rates, the FINO and Leuchars models plotted monthly component failure rates from the simulated data. The monthly failure rates calculated by the Leuchars model vary less significantly than those calculated by the FINO model

Finally the model was adapted in Chapter 6.2 to calculate electricity generation. It was found that using the FINO and Leuchars models that the energy lost on average per WT year was greater than if using models with constant failure rates. This percentage was higher in the FINO model than in the Leuchars Model.

In Chapter 6.2.3.3 a 5 MW model WT was simulated for the FINO model, in this example the difference in revenue calculated by the FINO model compared to model that had used the onshore failure rates of Site A and Site B was £2.6 million per year for a 200 WT wind farm.

The following Chapter analysis will be undertaken to determine if there is an economic advantage to having a spares strategy that varies each month according to the calculated WSD component failure rate.

4. Chapter 6 References

[6-1] J. Nilsson and L. Bertling, "Maintenance Management of Wind Power Systems Using Condition Monitoring Systems — Life Cycle Cost Analysis for Two Case Studies," *IEEE Trans. Energy Convers.*, vol. 22, no. 1, pp. 223–229, 2007.

[6-2] C. J. Crabtree, "Operational and Reliability Analysis of Offshore Wind Farms," in *EWEA 2012*, 2012.

[6-3] Defra, "CEFAS," 2014. [Online]. Available: http://www.cefas.defra.gov.uk/our-science/observing-and-modelling/monitoring-programmes/wavenet.aspx?RedirectMessage=true. [Accessed: 18-Sep-2014].

[6-4] D. McMillan and G. W. Ault, "Quantification of Condition Monitoring Benefit for offshore wind turbines," *Wind Eng.*, vol. 31, no. 4, 2007.

[6-5] J. Dowell, A. Zitrou, L. Walls, and T. Bedford, "Analysis of Wind and Wave Data to Assess Maintenance Access to Offshore Wind Farms," in *ESREL*, 2013.

[6-6] Deutsches Windenergie Institut, "FINO." [Online] Available: http://www.dewi.de/dewi/index.php?id=152 [Accessed: 18-Sep-2014].

[6-7] P. J. Tavner, D. M. Greenwood, M. W. G. Whittle, R. Gindele, S. Faulstich, and B. Hahn, "Study of weather and location effects on wind turbine," no. May 2012, pp. 175–187, 2013.

[6-8] S. Gill, B. Stephen, and S. Galloway, "Wind Turbine Condition Assessment Through Power Curve Copula Modeling," *IEEE Trans. Sustain. Energy*, vol. 3, no. 1, pp. 94–101, Jan. 2012.

[6-9] Department of Energy and Climate Change, "Increasing the use of low-carbon technologies," *UK Government*, 2014. [Online]. Available: https://www.gov.uk/government/policies/increasing-the-use-of-low-carbon-technologies/supporting-pages/offshore-wind. [Accessed: 16-Sep-2014].

[6-10] Department of Energy and Climate Change, "Consultation on the Transition from the Renewables Obligation to Contracts for Difference," 2013. [Online] Available: https://www.gov.uk/government/uploads/system/uploads/attachment_data/file/223489/ROtransitionconsultation17July2013.pdf [Accessed: 16-Sep-2014].

[6-11] Department of Energy and Climate Change, "Investing in renewable technologies – CfD contract terms and strike prices," 2013. [Online] Available: https://www.gov.uk/government/publications/investing-in-renewable-technologies-cfd-contract-terms-and-strike-prices [Accessed: 16-Sep-2014].

[6-12] J. Jonkman, S. Butterfield, W. Musial, and G. Scott, "Definition of a 5-MW Reference Wind Turbine for Offshore System Development," NREL, 2009. [Online] Available: http://www.nrel.gov/docs/fy09osti/38060.pdf [Accessed: 10-Sep-2014].

Chapter 7. Spares Optimisation Using Wind Speed Dependent Failure Rates

1. Background

1.1. Offshore Maintenance

The previous chapter demonstrated that a model can be developed that can calculate seasonal and annual WT component failure rates for an offshore site using wind speed dependent failure rates. Although simulating offshore logistics and accessibility is beyond the scope of this thesis, one possible application of the wind speed dependent failure rate models is offshore wind farm spares optimisation. This chapter will demonstrate a model that will use the seasonal and annual failure rates calculated in Chapter 6.1.1.1 and Chapter 6.1.2.1to design an optimum strategy for spares optimisation in corrective maintenance.

The importance of a maintenance strategy and therefore spares optimisation to the actual availability of an offshore WT was highlighted by Van Bussel and Zaaijer and is described in detail in IEC 61400-26-1 [7-1], [7-2]. The offshore availability is affected by the accessibility of the site, the limits of theoretical availability and by the maintenance strategy as shown in Figure 7-1 [7-1]. From an operator's point of view the only factor they can directly control is the maintenance strategy.

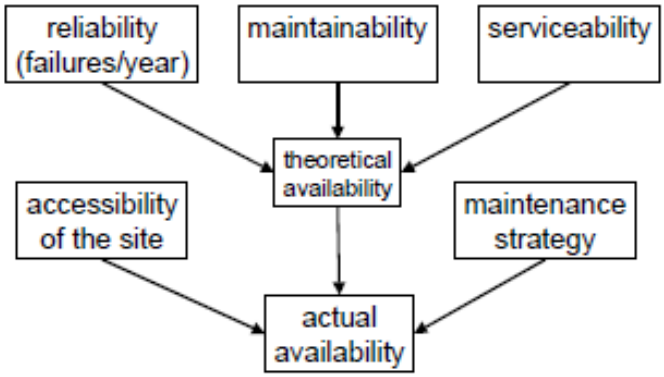

Figure 7-1: The impact of maintenance strategy on theoretical and actual availability [7-1]

Although a maintenance strategy includes preventative and corrective maintenance, this section will only focus on the latter. It is assumed that the two activities take place independent of one another and that both maintain separate inventories.

In Chapter 6.1.1.1 the FINO model calculated component failure rates for a WT subjected to offshore wind speeds. It produced annual component failure rates in Chapter 6.1.1.1 and more detailed seasonal component failure rates in Chapter 6.1.2.1 that showed how the reliability of each component was calculated to vary throughout the year due to the mean daily wind speed. The goal of Chapter 7 is to develop a model for finding the optimum spares strategy for an offshore wind farm subjected to the same offshore wind speeds and to use both the annual and seasonal failure rates to design the strategies.

Chapter 7.1 will briefly explain the theory behind spares optimisation before the FINO model used in the previous chapter is adapted in 0 to assess potential spares provision strategies for an offshore wind farm of 200 WTs. Offshore constraints are applied to the model in Chapter 7.2.4 before a range of scenarios are presented and assessed in Chapter 7.3.1 and Chapter 7.3.2. A sensitivity analysis of the model and the selected optimum strategies will be undertaken in Chapter 7.3.3, before finally in Chapter 7.3.4 the effectiveness of the model will be discussed.

1.2. Periodic Review Inventory System with Emergency Replenishments

Costs for maintaining a spares provision system include the purchasing of new components, the holding of these components, the cost of lost generation due to downtime and general costs associated with operation and maintenance [7-4].

There are two inventory renewal policies often used often in practice – the continuous and periodic review systems [7-5]. The continuous review inventory system is a common way of maintaining an inventory that involves tracking each component in the spares inventory and counting each time a component is removed to be used as a spare. This system requires a maximum level *S* for each component and a reorder level *s* (*S*, *s*) [7-4], [7-6]. Whenever the number of spares of a component falls below *s*, the component is reordered and the inventory returns to its maximum *S*. An example of the continuous review system is shown in Figure 7-2. In this example and in the following example Figure 7-3, for simplicity it is assumed that the lead time for components to be delivered is 0 hours.

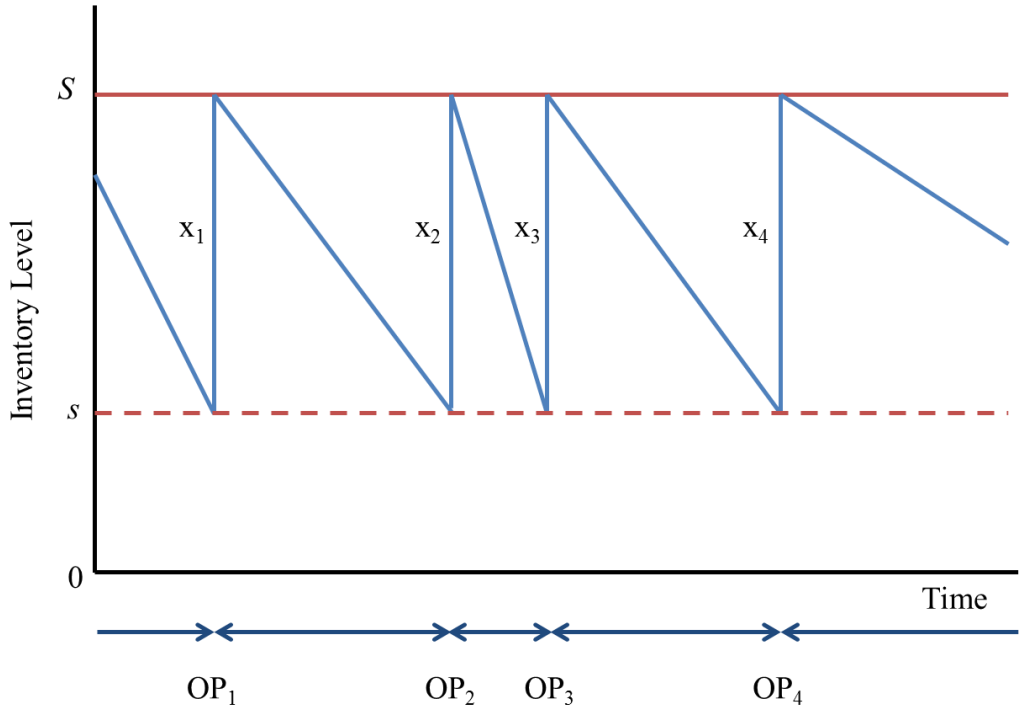

Figure 7-2: Example of continuous review system

The periodic system however differs in that rather than there being a level of stock that triggers a reordering of components, there is an ordering period (*OP*) at which the stock is reviewed and then topped up to the *S* level [7-7]. An example of this system is shown in Figure 7-3.

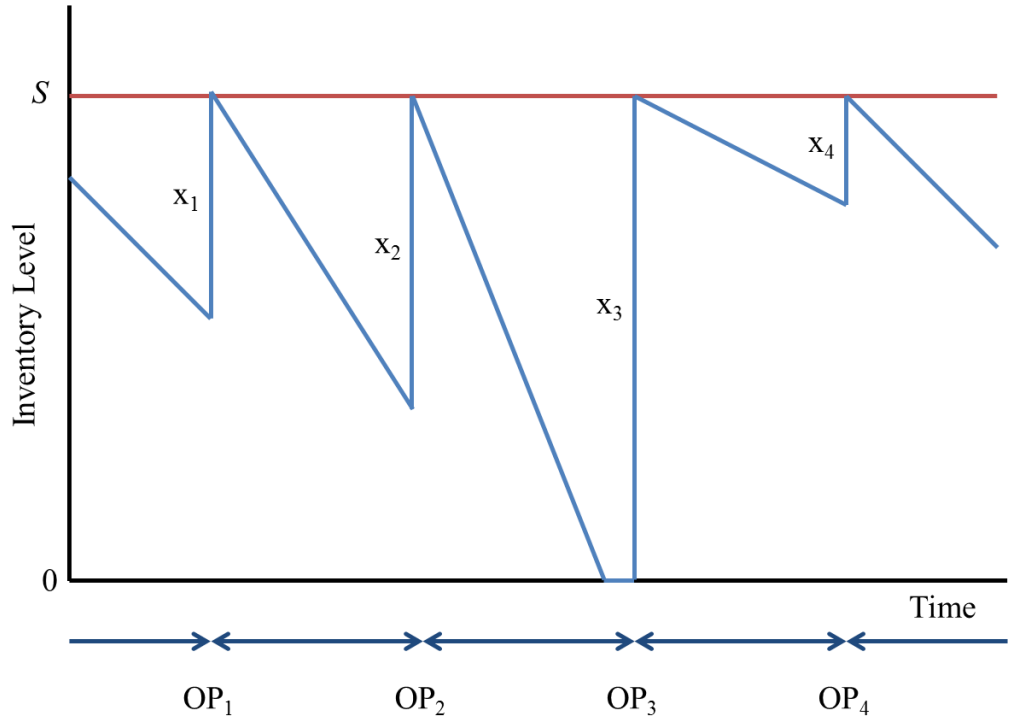

Figure 7-3: Example of periodic review system

The continuous review system ensures that stock levels do not reach 0 by reordering once the inventory level falls to *s*. In the example the lead time is 0 hours, however in reality it be could be any period greater than this. Therefore the reordering level can be optimised according to the failure rate and lead time to ensure that the risk of the inventory reaching 0 is minimised. Another benefit of the continuous system is that the stock levels ordered each time from the supplier *x*, are the same. However a downside to the system is that the ordering periods are not consistent, as shown in Figure 7-2. Although suppliers may benefit from filling consistent order volumes the timing is uncertain and this may lead to charges from the supplier if they have to fast-track an order [7-7].

The periodic system suffers from the opposite issues [7-7]. The ordering period is consistent each time, but the volume of each order is not. As shown in Figure 7-3 the ordered stock levels *x* are all different. From a supplier's point of view this system is also problematic. Additionally the periodic system does not protect against reaching empty stock levels, as shown at OP_3. If this were the inventory level for an offshore wind farm, any failures beyond the period of time when the inventory level reached 0 would result in a long period of downtime and significant lost generation.

For an offshore wind farm, neither system is suitable. The option used in this thesis is a hybrid of both systems, referred to as the Periodic Review Inventory System with Emergency Replenishments. This system has been used previously by Chiang and Gutierrez and by Tagaras and Vlachos to develop systems where orders are placed at regular intervals, like a periodic review inventory system, but also allow emergency orders to be placed at any time if the stock levels drop below a certain level [7-7], [7-8]. In Chiang and Gutierrez's model, emergency orders can be placed at any time and have shorter lead in times but are subject to significantly higher costs [7-8]. In the Tagaras and Vlachos model, the emergency orders follow the same time and cost conditions, but can only be made at specific review times [7-7].

For this analysis, the Chiang and Gutierrez approach will be used. But additionally there will be three ordering modes as opposed to Chiang and Gutierrez's two modes. These modes are:

- A scheduled order made at each scheduled ordering period
- An unscheduled order, made when the inventory level drops below the reorder level *s*
- An emergency order which is made when the inventory level reaches 0

An example of this inventory system is shown in Figure 7-4, where each unscheduled order requires a lead time of t = *LT*. The scheduled ordering periods (*OP*) are shown at regular

intervals, while an unscheduled order (*UO*) occurs after OP_1 and an emergency order (*EO*) after OP_2. Scheduled orders do not have a lead time as they are organised well in advance to replenish stocks while the emergency order has no lead time but costs a considerable amount more than an unscheduled order.

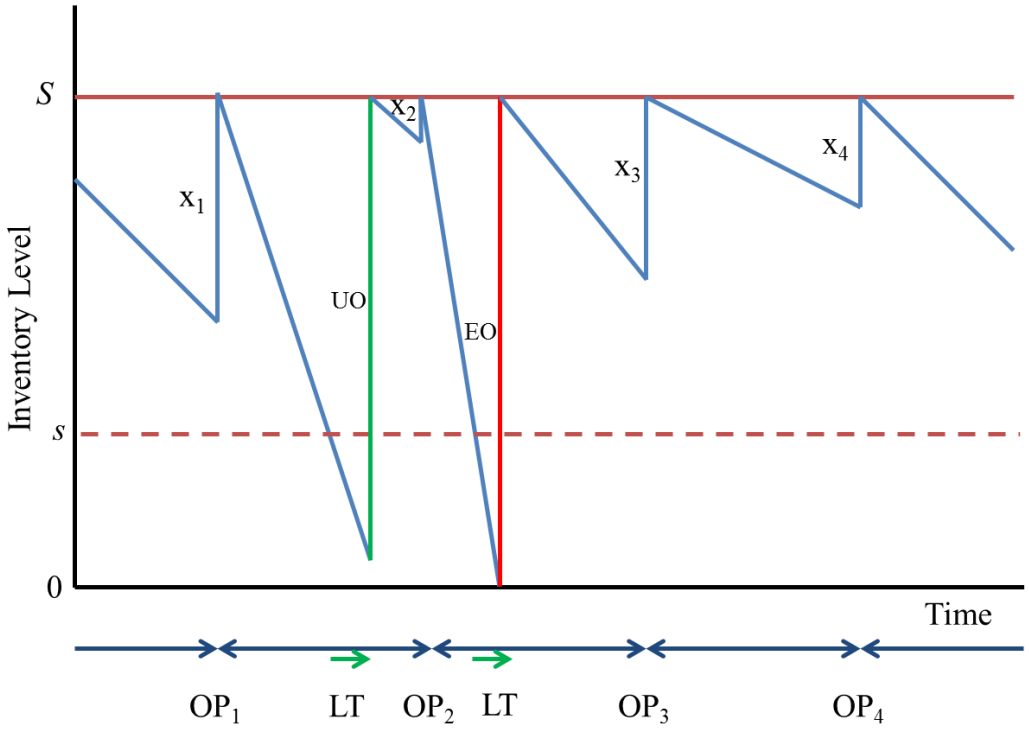

Figure 7-4: Periodic inventory review system with emergency replenishments

1.3. Offshore Wind Farm Inventory System

1.3.1. Maximum and Reorder Levels

The periodic inventory review system with emergency replenishments can be applied to the corrective maintenance strategy of an offshore wind farm of 200 WTs. If failure rates have been calculated for each component, the inventory levels *S* and *s* of each component can be easily calculated from the number of failures expected to occur over a set time period. In the case of the ORD from Site A and Site B, the annual failure rates for each component are shown in column 2 of Table 7-1. For a 200 WT wind farm, the annual number of expected failures can be calculated by multiplying the annual component failure rate by 200, as shown in column 3.

Table 7-1: Maximum and reorder levels (*S*, s) using ORD and β_S and β_s factors that equal 2 and 0.1 respectively

Component	λ (Failures per WT Year)	Expected annual failures for a 200 WT farm	Maximum stock level (*S*)	Reorder level (*s*)
Emergency system	0.026	5	10	1
Met Instruments	0.075	15	30	3
Rotor	0.047	9	19	2
Blade Pitch System	0.068	14	28	3
Drive Train	0.156	31	62	6
Yaw System	0.151	30	60	6
Hydraulics	0.078	16	32	3
Control System	0.520	104	208	21
Generator	0.031	6	12	1
Lifting System	0.010	2	4	0
Nacelle	0.016	3	6	1
Tower	0.060	12	24	2

In this case, the maximum and reorder levels *S* and *s*, shown in columns 4 and 5 respectively, are calculated by applying the maximum and reorder factors β_S and β_s respectively, to the expected number of annual failures in column 3 and rounding to the nearest component. The factors β_S and β_s in Table 7-1 are 2 and 0.2 respectively.

For this example the inventory would initially be stocked to level *S*, failures would then take place and the stocks of each component would deplete until level *s* was reached, at which time the stock level of that component would be returned to level *S* after an unscheduled order and a lead time of *LT*.

As the maximum level was calculated using the annual failure rate, the stocks would be unlikely to be depleted to *s* level for quite some time. Although it may seem sensible to over stock and reduce risk, holding such a large volume of spares is costly and would require a very large holding facility that would only be at capacity for a short period of the year as the stocks depleted. It is more effective to build a smaller facility and reduce the *OP*.

As found by Kabir and Olayan, failure distributions have a significant impact on the optimum spares strategy [7-9]. If the failure rate of a component were to remain constant throughout a year then maximum and reorder component levels based on annual failure rates may be a suitable spares strategy.

However as discussed in the previous sections, the failure rates of WT components change seasonally and the potential losses due to downtime also vary, increasing in the winter and decreasing in the summer. Therefore it may be the case that spares levels may be too low in the winter and too high in the summer. If this were the case the risk of being under stocked would be high in the winter due to high wind speeds and the cost of holding and purchasing components would be unnecessarily high in the summer when failures would be less likely to happen. The most economic strategy could be to order more stock in the winter and less stock in the summer – therefore reducing the risk of being under stocked in the winter and decreasing the holding cost in the summer.

1.3.2. Emergency and Unscheduled Orders

However, these economics depend entirely upon the risks of each individual site which varies according to accessibility, water depth, wind speed conditions and model of WT.

These risks are represented in the inventory system by charges that apply to unscheduled and emergency orders.

If an offshore wind farm allows the stock levels to deplete to the point that there are no spares left and an emergency order is placed the suppliers, in this case the OEM, may charge an additional fee as compensation so that the order can be fast tracked past those already in the order book and delivered straight away [7-10]. If the required component is large, like a gearbox or a blade, a heavy lift vessel may also have to be hired at short notice and high cost to deliver the component to site and fit it to the WT [7-1], [7-11]. To prevent emergency orders from occurring to a project and impacting the profitability of the asset, asset managers may also be penalised by the asset owner for bad performance if they allow spares levels to deplete to the point where generation is lost unnecessarily.

Even in the case of unscheduled orders there is a lead in time for new stock to be ordered, dispatched and delivered. While the order is still in process there is always the risk that the stock level could deplete further and reach the point where there are no spare components left, resulting in an emergency order needing to be placed or a fine from the owner.

Therefore considering the risks involved in keeping spare components under stocked and the expense of over stocking, it is important that an optimum inventory strategy is found with suitable S and s levels. The spares optimisation model will use the periodic review inventory system with emergency replenishments to design an optimum component spares holding strategy. The following section will describe the spares optimisation model and the parameters and constraints applied to the model to represent the inventory risks.

2. Spares Optimisation Model Description

The downtimes recorded in the ORD all correspond to failures that take place on sites that operate according to onshore conditions and onshore logistics. Therefore to model downtimes that are related to offshore logistics, the wind speed dependent downtime function is removed from the FINO model shown in Figure 6-22 and instead, a spares provision function is added, as illustrated in Figure 7-5.

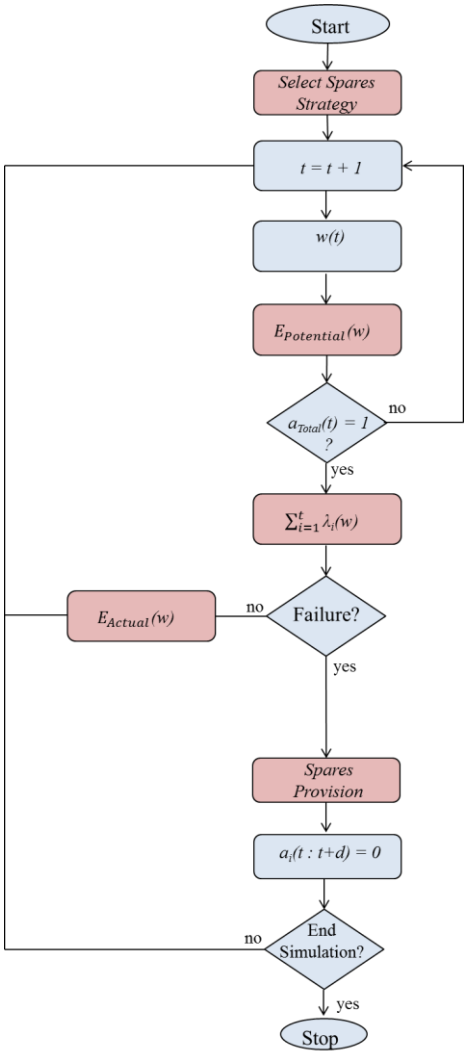

Figure 7-5: Flow chart of spares optimisation model

The spares optimisation model differs to the previous models in that downtime is no longer solely a function of wind speed. If the spares provision is under stocked when a failure

occurs, there will be a longer downtime than if the spares provision were correctly or over stocked. This is because the downtime comprises of the waiting time to either replace the failed component with a spare from the inventory, or to wait for a spare to be delivered so it can be fitted. The average downtime period for an individual failure is therefore now a function of spare component availability, while the availability of a WT is a function of wind speed and spare component availability.

The model still works in the same way as in the previous Chapter – failures are generated by MCMCS according to the wind speed dependent failure rates and FINO wind speed time series. The wind speed dependent failure rates are the same as those calculated Chapter 5.2.5.1. However the addition of the spares provision function allows the model to evaluate how effective different maintenance strategies are when they are applied to the wind farm. The more effective the strategy is, the lower the cost of corrective maintenance. Therefore high wind speeds will continue to cause more component failures, but the effectiveness of the spares strategy will determine how long the WT remains down.

The model relies on the assumption that every downtime that occurs is due to a failed component that requires complete replacement and that when the failure occurs this replacement is carried out if or when a spare is available. The ORD records each downtime that occurs to a WT and categorises whether the outage is due to corrective or preventative maintenance. However it is not always clear in the dataset whether a component has been replaced, refurbished or, in the case of electrical components, simply reset. The implications of this assumption will be discussed further in Chapter 7.3.4

2.1. Spares Provision Function

The purpose of the spares provision function is to introduce all of the aspects discussed in Chapter 7.1 into the model. It operates as a function within the main model, as shown in Figure 7-5 and performs calculations at each time step.

As described in Figure 7-6, the spares provision function first determines which component has failed – in this case the failed component is *i* – it then determines whether there is a spare component available with which to repair *i*. If there is a spare component it is removed from the inventory and used. The WT suffers downtime due to the repair being carried out d_{repair}, this downtime is then applied to the component availability a_i in the step after the spares provision function, as shown in Figure 7-5.

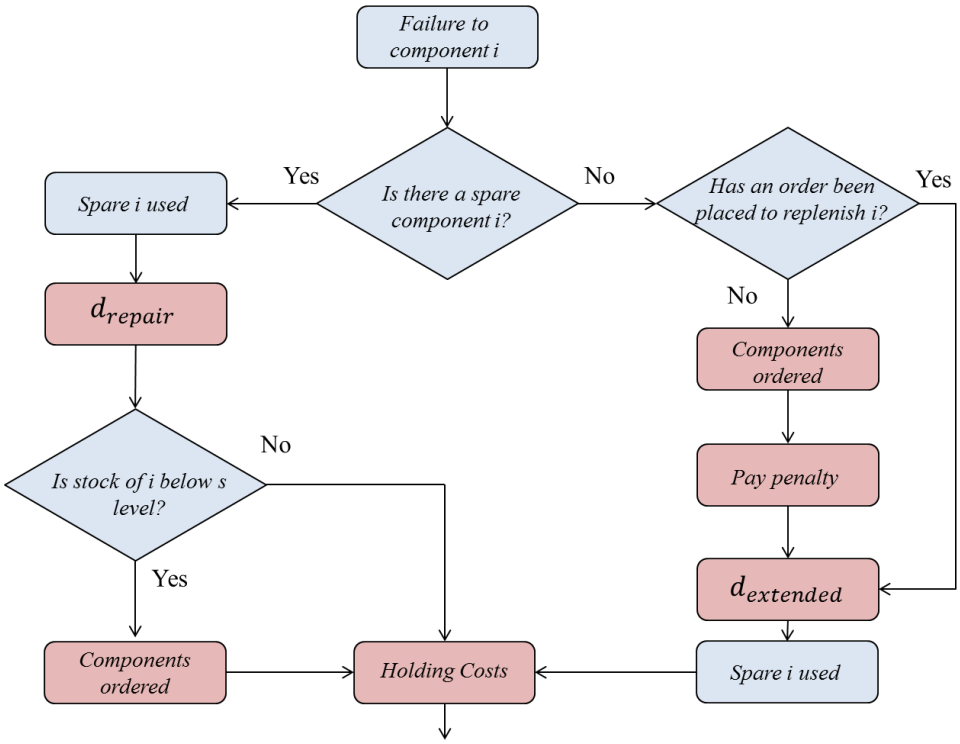

Figure 7-6: Flow chart of spares provision function

The function then checks the stock level of component *i*, if it is below level *s* new components are ordered to return the stock level to *S*. Costs are incurred in doing this, firstly

the cost of the components and secondly the cost of making an unscheduled order to the OEM.

If there is not a spare component, the function first checks if an order has been placed already in a previous time step to replenish the stocks. If an order has not been placed, new components are ordered, the WT is shut down for an extended downtime until they arrive ($d_{extended}$) and a penalty is paid. If an order for *i* has already been placed, the model shuts the WT down for $d_{extended}$. As spares have already been ordered, further component costs and penalties are not paid.

At the end of the process, whether a spare component *i* was available or not, the stock levels for that day are counted and the holding costs are calculated by multiplying the number components stored that day by the daily rate.

2.2. Inventory levels

The initial component stock levels are set prior to the when the model begins a simulation by varying the maximum and reorder level factors β_S and β_s and multiplying them by the number of WTs and the component failure rates as shown previously in Table 7-1.

However, as opposed to using the annual failure rate in Table 7-1, the spares optimisation model uses the monthly failure rates so that levels *S* and *s* are set to provide the wind farm with enough components to last a month.

By ordering components on a monthly basis rather than annually, like in Table 7-1, smaller holding facilities can be used and the inventory will be at low capacity for shorter periods of the year. Holding costs will therefore be reduced, while the total annual cost of ordering components remains the same.

At the end of each month the components are scheduled to be reordered automatically to level *S* without any additional charges such as penalties or ordering costs. The components arrive for use on the first day of the month.

If β_S and β_s were to equal 1 and 0.4 respectively, the maximum and reorder levels *S* and *s* of the control system would vary from month to month as shown in Figure 7-7. These monthly levels are dependent on the monthly failure rates calculated using the model. The monthly failure rates have been calculated using the FINO model from Chapter 6.1.2.1. Therefore the model must first calculate monthly failure rates from the prior simulations in Chapter 6.1.2.1 and then use these calculated monthly failure rates to set a spares strategy. Throughout this Chapter, the analysis undertaken first requires the results calculated from Chapter 6.

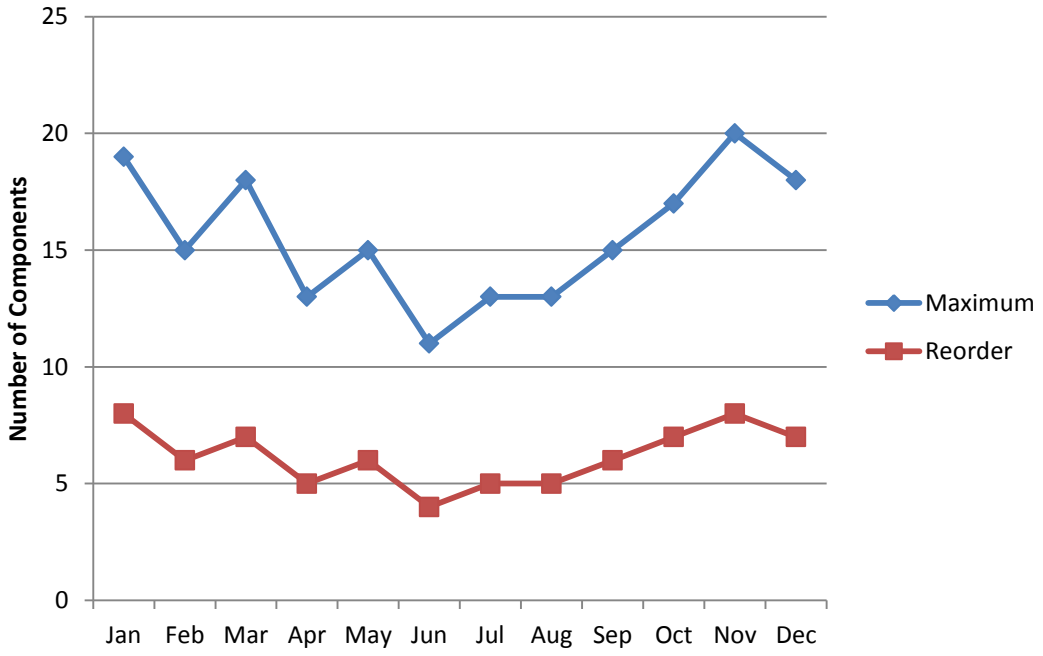

Figure 7-7: Monthly maximum and reorder levels for the control system using β_S and β_s factors of 1 and 0.4 respectively

Had a constant constant failure rate been used in this case, as opposed to monthly failure rates, the monthly maximum and reorder levels of the inventory would have been 16 and 6 control system components respectively each month throughout the year. The risk of keeping a constant stock level throughout the year is shown in the months January, March, October, November and December where the expected number of failures in those months exceeds 16. If not enough spares are available to repair the WT and the level drops to 0, a penalty will be issued by the model and energy will be lost. In the summer however fewer than 16 failures are expected to occur, therefore the inventory would be overstocked. Holding costs at this time of year would therefore be higher, although it would be unlikely that any penalties would be issued.

However, by varying the inventory levels throughout the year the risks posed by winter wind speeds can be mitigated by holding more spares of the components most likely to fail. Equally costs can be reduced in the summer by holding fewer spares.

2.3. Estimating Component Costs

Calculating the cost of each component is vital in planning effective maintenance strategies. Aalthough all the WT components consist of many subcomponents (i.e. the drive train is made up of the gearbox, bearings, the high speed shaft and many other subcomponents) this analysis assumes that each component is a single entity with a single wind speed dependent failure rate function. There is no distinction in the model between a gearbox failure and a high speed shaft failure; they are both categorised drive train failures. The component cost of a gearbox is roughly 13% of the overall WT cost [7-12]. However the cost of replacing gear box oil is considerably less. The cost of replacing a drive train component in this analysis must therefore reflect the costs of all its subcomponents and probabilities of each of them failing.

The ORD unfortunately does not include information on component costs. Therefore component costs will be estimated in this section using the ORD and estimated O&M costs from the literature. According to a report undertaken by Riso National Laboratory the average cost of O&M for a typical onshore wind farm is about 0.6 €/kWh - 0.7 €/kWh of generated energy in a year [7-13]. A value of 0.65 €/kWh is assumed.

From May 2013 to March 2014 Site A and Site B achieved capacity factors of 28% and 24% [7-14], [7-15]. The capacity factor of both sites combined was approximately 26.5%. If an assumption is made that these annual performances are typical of Site A and Site Band also typical of an onshore wind farm, then O&M costs can be estimated using the Riso National Laboratory figures.

The cost of O&M for both sites was calculated as shown in Equation 7-1 and Equation 7-2. Using an exchange rate of 0.8 UK pounds to 1 euro, this equals £ 27762.94. This was rounded up to bring the annual cost of O&M per WT to be £30000.

$$Annual\ Generation = Hours\ in\ a\ year \times WT\ Rating \times Capacity\ Factor \quad \textbf{Equation 7-1}$$

$$= 365 \times 24 \times 2.3 \times .265 = 5339.22\ MWh$$

$$Annual\ Cost\ of\ O\&M = Annual\ Generation\ (kWh) \times Costof\ O\&M/kWh \quad \textbf{Equation 7-2}$$

$$= 5339.22 \times 1000 \times 0.65 = \ €34704.93$$

Of this £30000, half of this cost was assumed to be due to corrective maintenance. The other £15000 would be taken up by insurance, labour, balance of plant, preventative maintenance and administration. This assumption was taken as research from Rademakers and colleagues quoted typical corrective maintenance and preventative maintenance costs as being roughly 0.005 – 0.010 €/kWh and 0.003 – 0.006 €/kWh respectively [7-16].

Component costs were calculated according to the downtime on average per failure to each component, as shown in Equation 7-3. These values were then normalised as shown in Table 7-2. The component failure rate λ was then multiplied by the normalised downtime values $\hat{d}$, shown in column 5 of Table 7-2. This value is the normalised downtime multiplied by the probability of a failure occurring in a year; it was then summed for all twelve components. The total cost of O&M attributed to corrective maintenance was then divided by this summed value as shown in Equation 7-3. Finally this scalar was multiplied by the normalised downtime for each component.

$$Component\ Cost_i = \left(\frac{15000}{\sum_{j=1}^{n} \lambda_j \widehat{d_j}}\right) \times \hat{d}_i \quad \textbf{Equation 7-3}$$

This method gave component costs that were weighted according to the downtime they caused to the system for each failure. They are shown in column 6 of Table 7-2.

Table 7-2: Estimated component cost

Component	Downtime per failure (hours)	Normalised Downtime ($\hat{d}$)	λ (Failures per WT year)	Failure Rate x Normalised Downtime	Component Cost (£)
Emergency system	0.7	0.001	0.026	3.8E-05	200.3
Meteorological Instruments	6	0.013	0.075	1.0E-03	1860.9
Rotor	158.2	0.352	0.047	1.6E-02	48746.6
Blade Pitch System	28.7	0.064	0.068	4.3E-03	8846.9
Drive Train	89.6	0.199	0.156	3.1E-02	27600.5
Yaw System	22.8	0.051	0.151	7.7E-03	7040.4
Hydraulics	71.3	0.159	0.078	1.2E-02	21979.1
Control System	28.0	0.062	0.520	3.2E-02	8638.7
Generator	31.0	0.069	0.031	2.2E-03	9561.2
Lifting System	8.1	0.018	0.010	1.9E-04	2505.2
Nacelle	2.1	0.005	0.016	7.4E-05	654.7
Tower	3.2	0.007	0.060	4.2E-04	970.9

If these component costs are applied to the Calibration model, which is the wind speed dependent failure rate model that uses the calibration wind speed data as an input, the model returns an annual mean cost of corrective maintenance of £14873. This is 0.85% lower than the expected value of £15000.

When the component costs shown in Table 7-2 are applied to the FINO model, the mean annual cost of corrective maintenance is calculated to be £22086. The seasonal costs calculated by the FINO model for the control system, drive train and rotor are shown in Figure 7-8. The values shown for each month are equivalent annual costs and are calculated by multiplying the mean monthly component costs by 12. The costs are displayed in this convention so that seasonal component costs can be easily compared to the annual mean cost.

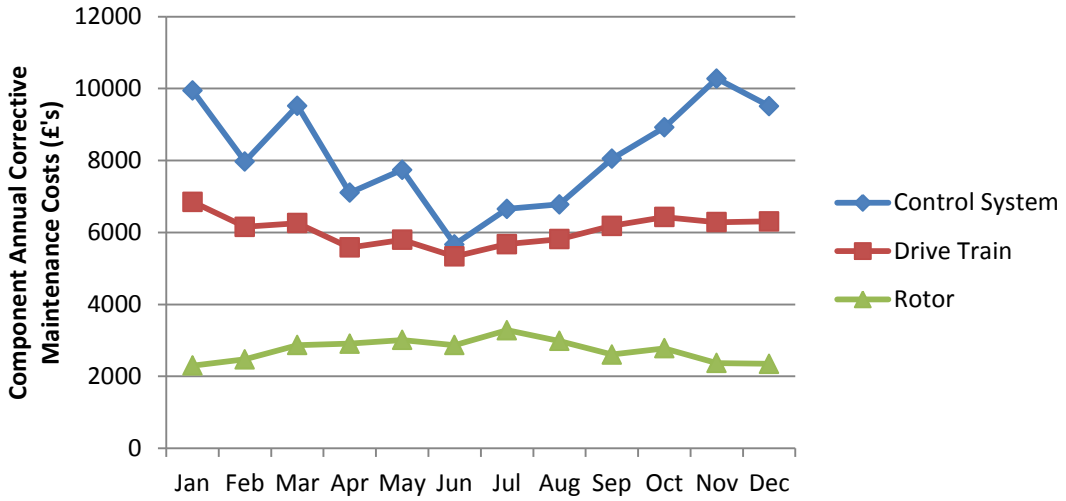

Figure 7-8: Corrective maintenance costs of the control system, drive train and rotor calculated from the FINO model

The rotor costs increase in the summer according to the FINO model. This is because the costs are directly influenced by the monthly failure rate, which in the rotor's case increases during the summer according to the FINO model.

The rotor failure rate increases in the summer for the same reasons that the blade pitch system also increases in the summer according to the FINO model – this was discussed Chapter 6.1.3. The wind speed dependent failure rate of the rotor is shown in Figure 7-9, the failure rate for days when the mean daily wind speed is above 13 m/s is 0. As a result of this the FINO model experiences many winter days when the rotor cannot fail.

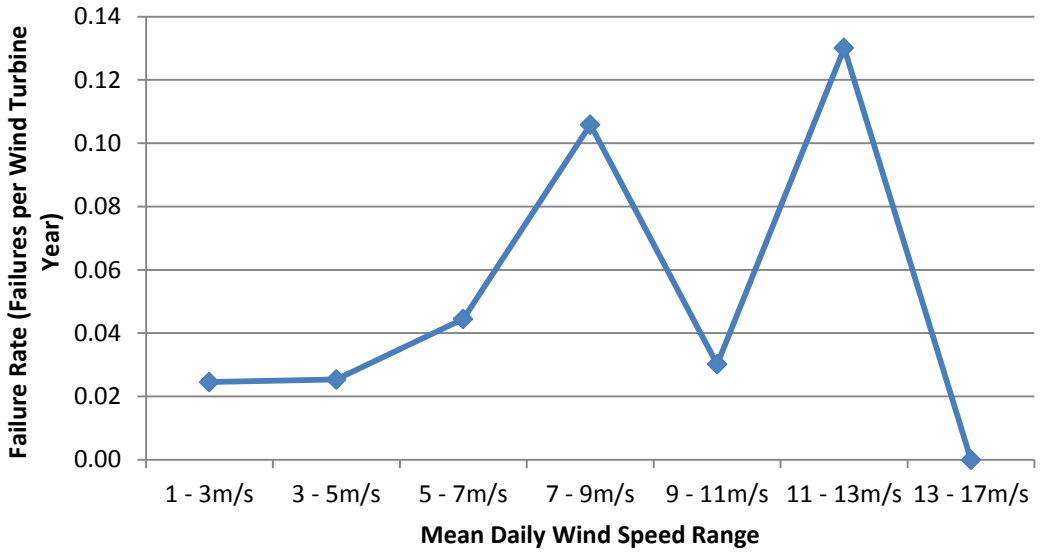

Figure 7-9: Wind speed dependent failure rates of the rotor

As discussed previously, the failure rate above 13 m/s is 0 with other components such as the blade pitch system. But because the component cost of the rotor was the third most expensive in terms of its cost per failure, this may have implications on the accuracy of the spares optimisation model.

This highlights a potential flaw in the FINO model. But as the failure rate of the rotor is so low this issue only becomes problematic when costs are applied to the FINO model. In the ORD the rotor has a high downtime per failure because of a single occurrence of a blade failure which caused 110 days of downtime. The remaining rotor failures only had an average downtime of 11 hours. The presence of this catastrophic blade failure in the dataset means that the average downtime of a rotor failure is approximately 160 hours. This high average downtime gives its corrective maintenance cost a high weighting.

If this failure is removed from the dataset the rotor becomes a component with far less influence on the output of the FINO spares optimisation model. Removing this failure from the model would increase the weighting of other components such as the drive train and the

control system. However it would mean that the FINO model becomes less representative of reality because the probability of the WT suffering a catastrophic blade failure is zero.

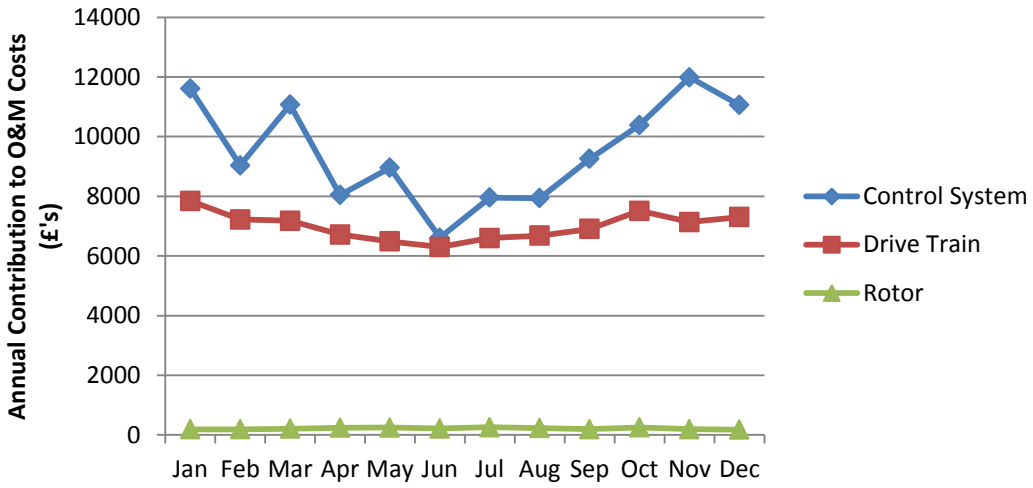

Figure 7-10: Monthly contributions to the annual O&M costs of the blade pitch system, hydraulic system and rotor from the FINO model once the catastrophic rotor failure was removed from the dataset

The effect of removing the catastrophic blade failure from the analysis is shown in Figure 7-10 where the cost of a rotor component is reduced from £48747 to £3893, a reduction of 79%. The impact this change has on the overall monthly cost of the whole system is shown in Figure 7-11. The difference between the two FINO models is not actually that significant: the average annual cost with the blade failure is £22,690, while removing the blade failure reduces the cost to £22,090 due to the reduction in lost generation caused by the long period of downtime. In the case of many components, data is scarce and removing other significant data points as well as the catastrophic blade failure only makes it less representative of the data. The failure rate of the rotor as discussed before is also very low. Consequently because of these reasons the blade failure remained in the model.

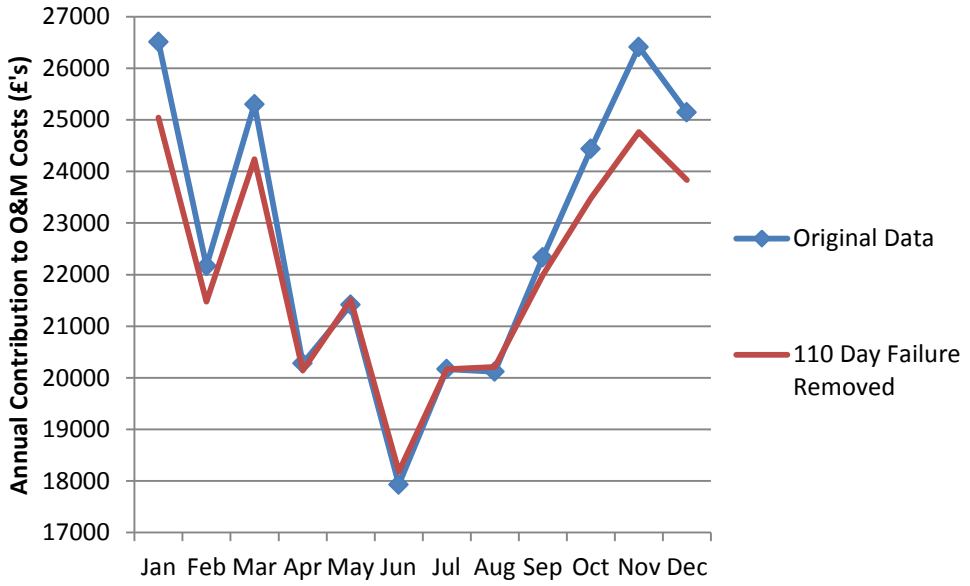

Figure 7-11: Monthly comparison of corrective maintenance costs for the whole WT system from the FINO model when the catastrophic rotor failure is included and removed from the dataset

2.4. Offshore Seasonal Constraints

As discussed previously, creating a complex offshore accessibility and vessel logistics computer program is beyond the scope of this thesis. Therefore more basic constraints have been put on the model by applying seasonal downtimes and costs. To reduce computational time the year is split into only two seasons that run from October – March and April – September. The latter will be referred to as summer, while the former is winter.

Repair time (d_{repair}) is the downtime applied to the model if a spare component is available to be fitted to a WT immediately. In the winter time this downtime is likely to be higher than summer due to:

- Poor WT accessibility due to high significant wave height [7-17]–[7-19]
- Health and safety restrictions on access to the nacelle and use of heavy lifting cranes due to high wind speeds [7-20]
- Increased competition in vessel hire from other offshore wind farms causing a lower availability [7-11]

For these same reasons, extended downtime ($d_{extended}$) due to waiting for components to be delivered and then fitted will also increase in the winter. But additionally in the winter there will be an increased demand from other wind farms for spare components and if the components are large enough that they need to be delivered by vessels there will be reduced sailing times due to the weather and sea conditions.

As the downtime per failure was calculated to increase in the winter using the onshore ORD, this is also reflected in this model. Two sets of downtimes are used in the model for both d_{repair} and $d_{extended}$, a winter value and a summer value.

Penalty charges also vary seasonally as the purpose of the charge is to represent the risk of a failure that occurs when the maintenance strategy is not adequate enough to ensure the

availability of spare components that can be fitted immediately. This risk accounts for the cost of hiring vessels to either sail to the WT to carry out the repair, or to deliver components to site from the manufacturer at short notice. This charge should also therefore be significantly higher during winter due to the accessibility and vessel availability issues already explained previously. Furthermore, from the point of view of the owner, they would want as little downtime in winter as possible because of the higher lost revenue due to higher potential energy generation. They could therefore penalise an operator more in the winter than in the summer for any unnecessary downtime. The model therefore changes the penalty charge depending on the month the WT is operating in – the winter charge is also significantly higher in each case to represent the more extensive risks at this time of year.

Unscheduled orders that are made when the order drops below the reorder level *s*, are also subject to an additional charge. Because of the higher risks and expense of ordering components in the winter, this value changes seasonally. The risk to generation when the WT falls below *s* is less than when the level falls to 0. Therefore the cost of making an unscheduled order is only 10% of the penalty cost.

Lastly a charge is made to every component held in the spares inventory per day. This charge represents the holding cost and consists of the personnel, plant and overheads related to the operation and maintenance of the wind farm. This cost is assumed to remain constant throughout the year and so does not have a winter value and a summer value. However in the case of many components the volume of components held in the winter increases due to the spares strategies – this therefore means the total expense of holding components increases in the winter. This cost varies according to the number of personnel working on site, the size of the holding facilities and various other overheads related to the operations base including the number of CTV's required per turbine and fuel costs – both of which increase with the distance from the operations base to the wind farm.

2.5. Optimised Spares Strategy Example

To elucidate how the model works, three spares strategies are assessed for a 200 WT wind farm subjected to FINO wind speeds. The cost and downtime parameters used in the model are the same for each strategy, as shown in Table 7-3. The spares optimisation model brings together the functionality of the previous demonstrated applications in Chapter 6.1 and Chapter 6.2 to calculate an optimum spares strategy using the wind speed time series of the site in question (in this case FINO) and the wind speed dependent failure rates calculated in Chapter 5.2.5.1.

As described in Chapter 7.2, the model generates failures according to the input wind speed time series. A spares strategy is set for the simulation and its effectiveness is economically assessed. Offshore constraints are applied to the model to represent the economic difficulties of operating an offshore wind farm as described in the previous section. The suitability of each tested strategy will depend on the offshore constraints applied to the model and the input wind speed used to generate the component failures.

The FINO spares optimisation model is used in this example. It is assumed that the monthly failure rates, calculated previously using the FINO model in Chapter 6.1.2.1, are known and therefore are used to plan the monthly maximum and reorder levels for each strategy, shown in columns two and three in Table 7-3 as the maximum and reorder factors β_S and β_s. The parameters in Table 7-3 that are seasonal are presented in the format winter / summer. Each parameter is explained in greater detail in Chapter 7.3.1

Table 7-3: Downtime and cost parameters used for each spare strategy

Spares Strategy	Maximum factor (β_S)	Reorder factor (β_s)	d_{repair} (hours)	$d_{extended}$ (hours)	Penalty (£)	Holding (£/comp-onent day)	Unsche-duled Order (£)
a)	1.2	0.4	48 / 12	240 / 72	125000 / 25000	200	12500 / 2500
b)	1	0					
c)	1.2	1					

Strategy a) sets a high maximum level to ensure that there are enough spare components available to avoid penalties, it also sets a β_s of 0.4 to ensure that when levels drop close to 0 an unscheduled order is made.

The second strategy b) however sets lower factors to reduce the cost of holding components, however because the reorder level is 0, the risk of falling to 0 components and a failure occurring is higher.

The final strategy c) has a β_S of 1.2 and a β_s of 1 – this means that the risk of the spares holding falling to 0 is very small, as after the levels drop by 17% (to the reorder level *s*), an unscheduled order is placed to increase the level back to *S*. This means that although the risk of a penalty is very low, the holding costs and ordering costs will be high.

All three strategies have their merits – the optimum strategy depends on the parameters selected. For a site with low holding costs and high penalty costs it would make sense to have a strategy that has a high maximum and reorder level to keep the spares levels high. However for a site with high holding costs, low penalty costs and short extended downtimes it would be preferable to keep a low stock because the risk of being without a component might make more financial sense than keeping high stock levels.

Figure 7-12 shows the results of a one year simulation of the FINO model for each of the three strategies, focusing on the control system spares levels. In each case the y axis indicates the level of the spare control system components on each day throughout the year.

The time series shows that at the beginning of every month the holdings increase or remain the same. This is because there is a scheduled order every month to return the levels to *S*, however because *S* varies from month to month due to the seasonal failure rates, the levels may already be greater than *S* at the start of the month. An example is shown in Figure 7-12 a) when at the start of June the holdings did not increase. This is because during May the

levels decreased to below the reorder level for that month; components were then reordered and returned to the *S* May level. Although failures to the control system did occur before the start of June, the levels remained higher than the *S* level of June when the time came to make the scheduled order at the start of the month – the spares level therefore remained the same.

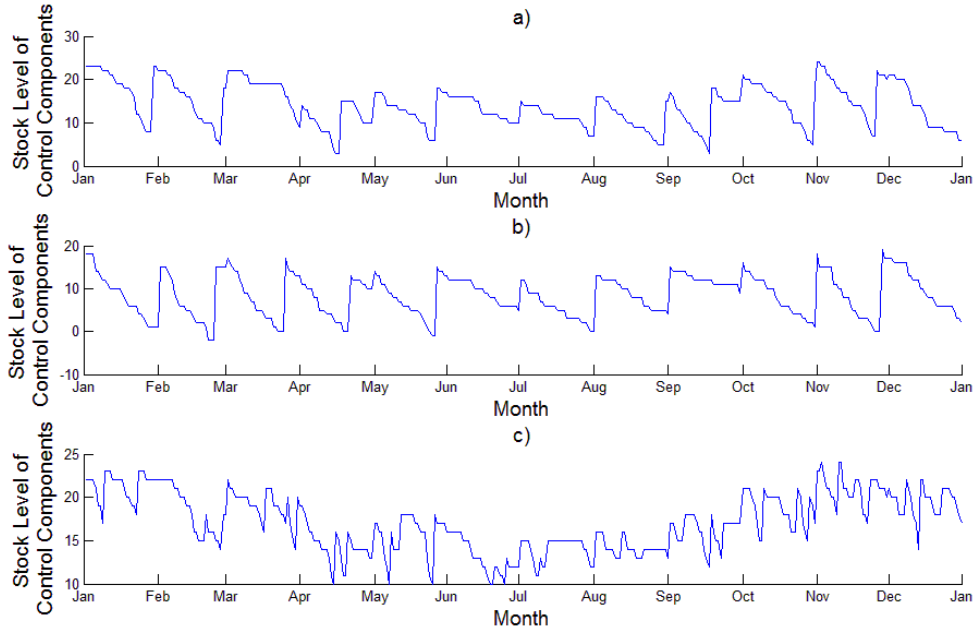

Figure 7-12: Control system spares levels throughout one year period using strategies a), b) and c)

Strategy a) makes more unscheduled orders of control system components throughout the year than b). This is because the difference between the maximum level and the reorder level in a) is less than b). Strategy c) however clearly makes the most unscheduled orders, most frequently in November because of the high wind speeds and higher probability of control system failure.

The three systems deal differently with the high wind speeds (and therefore high number of control system failures) in November. Strategies a) and b) each place unscheduled orders in November because levels drop below reorder level. Strategy c) however makes 4 unscheduled orders to ensure the levels remain above *s* level. In this case neither strategy was able to manage November effectively – a good strategy would have ensured enough

spares were ordered to last for the month, incurring no penalties and minimising holding and ordering costs.

The only instances of penalties being issued for bad management of the spares strategy is for February and May, by strategy b). The spares level also drops to 0 in March and April before stocks are reordered. The high reorder levels of strategies a) and c) prevent penalties occurring in the case of the control system – however holding costs are higher as a result.

The total cost of each strategy over the same year is shown in Table 7-4. These costs comprise of the holding costs, component costs, unscheduled order costs, lost generation due to downtime and penalty costs.

As shown in Table 7-4, the costs of the 200 WT wind farm are highest for each strategy in the winter months when the unscheduled ordering and penalty costs are higher and the downtimes are longer. Over the first year of the simulation, strategy b) is the most economical with a total cost of £8,568,499 or £42,842 per WT year. However November, which was the month with the highest wind speed and highest component failure rates, was least economically managed by strategy b) – in this case the best strategy was a).

Table 7-4: Total costs incurred by 200 WT wind farm in the first year of using strategies a), b) and c)

Month	Total Costs per Strategy (£)		
	a	b	c
Jan	1287191	1155905	1494692
Feb	864173	885766	1128330
Mar	1302983	998645	1065723
Apr	369957	366142	313087
May	487805	440108	597072
Jun	372162	309569	254346
Jul	342407	276003	312556
Aug	396376	346546	346187
Sep	348069	403687	433923
Oct	1198972	1189010	1274271
Nov	915588	1288913	1219726
Dec	1071672	908206	1168610
Total	**8957355**	**8568499**	**9608522**

Table 7-5 gives a better description of where these costs come from by breaking each month and strategy down into factors that are used to calculate the total cost. Strategy b) was the cheapest in terms of holding costs and unscheduled ordering costs, but the most expensive for component cost, lost generation and penalty costs. Strategy a) was the second most expensive in each area with the exception of penalty costs in which it was the cheapest, while strategy c) was least expensive in terms of component costs and lost generation, but the most expensive for unscheduled orders and holding costs.

As illustrated in Figure 7-13, the cost of lost generation is the highest contribution to maintenance costs of all five factors in the simulation. To reduce this cost a spares strategy should reduce as much as possible the extended downtimes, in this case strategy c) does that best, but does so at the expense of high holding costs.

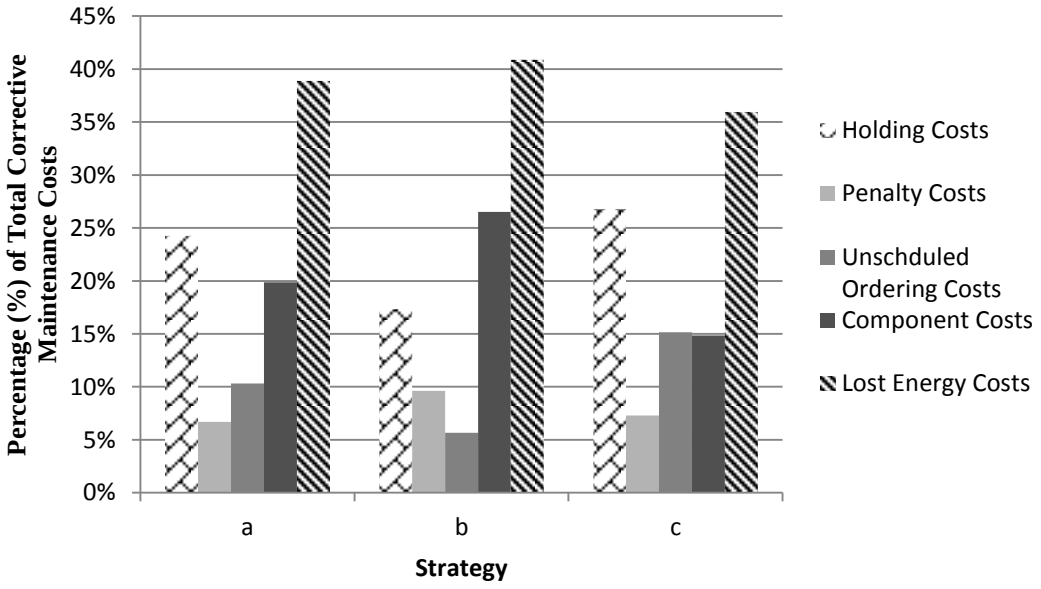

Figure 7-13: Contribution to total cost of each strategy by the costs of holding, penalties, unscheduled ordering, components and lost generation

In this example, strategy b) is the most economical. However these results are based only on a single year of simulation – were the model to be simulated over a longer period of time and were more monthly samples taken it may be that a) or c) would be the most economical. This

example also uses only one set of costs – if the holding costs were to fall for example, strategy c) may become the most economical. Lastly this example only examines a very limited range of spares strategies; it is likely that there is a more economical β_S and β_s than 1 and 0.

The following section will use a wider range of costs and examine more spares strategies. It will also use longer periods of simulated data from which to draw a more reliable conclusion.

Table 7-5: Break down of costs incurred for a 200 WT wind farm using maintenance strategies a), b) and c).

Month	Holding Costs per Strategy (£)			Penalty Costs per Strategy (£)			Unscheduled Ordering Costs per Strategy (£)			Component Costs per Strategy (£)			Lost Generation Costs per Strategy (£)		
	a	b	c	a	b	c	a	b	c	a	b	c	a	b	c
Jan	219000	133000	253800	0	125000	125000	162500	62500	187500	509814.95	425450.08	563401.52	395876.02	409955.01	364990.75
Feb	168800	119600	207600	125000	125000	375000	150000	50000	187500	35286.774	229840.71	18894.357	385086.42	361325.08	339335.51
Mar	224800	123000	238400	125000	125000	0	150000	75000	187500	198215.72	146024.08	87429.637	604967.14	529620.62	552393.02
Apr	149000	99400	191600	0	0	0	22500	22500	32500	65277.709	96670.204	11449.542	133178.92	147571.64	77537.163
May	168400	113600	201800	25000	25000	25000	35000	22500	47500	141123.11	156410.91	181300.35	118282.07	122597.3	141471.73
Jun	168200	115400	182200	50000	50000	0	20000	25000	22500	88495.626	69268.27	12968.195	45466.326	49900.943	36677.322
Jul	164200	108000	196600	0	0	0	20000	10000	35000	129764.37	104626.38	43604.777	28442.957	53376.361	37351.18
Aug	162400	127800	194200	25000	0	25000	27500	15000	40000	136061.06	177206.21	48321.302	45414.544	26539.461	38665.771
Sep	170600	140200	207200	0	0	25000	12500	15000	40000	73058.976	193879.94	78027.706	91909.598	54607.054	83695.521
Oct	194600	137600	229000	125000	250000	0	137500	37500	237500	175133.25	234745.88	256087.82	566739.22	529164.26	551683.11
Nov	209200	133600	235600	0	0	0	62500	87500	262500	106779.61	299536.33	83225.063	537108.84	768276.22	638400.45
Dec	172000	133000	236000	125000	125000	125000	125000	62500	175000	120929.94	138131.88	42153.975	528742.01	449573.68	590456.5
Total	**2171200**	**1484200**	**2574000**	**600000**	**825000**	**700000**	**925000**	**485000**	**1455000**	**1779941**	**2271791**	**1426864**	**3481214**	**3502508**	**3452658**

3. Results

Throughout Chapter 6 the impact of wind speed dependent failure rates on WT performance have been analysed. This section aims to use this knowledge and apply it to the area of spares optimisation to reduce the cost of maintaining an offshore WT.

The FINO wind speed time series, as discussed previously, originates from an offshore platform in the North Sea. As the previous chapters have shown that there is a clear difference in seasonal variation and strength of wind speed between Leuchars and FINO, this section will only examine the application of a spares optimisation model for the FINO model. Applying offshore constraints to the Leuchars model would be of no benefit because offshore sites experience greater wind speeds and generate much more electricity.

Therefore using the theory explored in Chapter 7.1 and the model described in Chapter 7.2, this section will analyse multiple spares strategies and determine the total cost of implementing each one when applied to the FINO model.

Secondly, the suitability of using a seasonal approach – such as in Chapter 7.2.5 – with *S* and *s* values that vary from month to month according to seasonal component failure rate, will be compared to a constant constant approach where *S* and *s* values remain constant through the year. In both cases the maximum and reorder levels have been calculated using the wind speed dependent failure rate FINO model. In the constant approach the calculated annual component failure rates in Table 6-2 in Chapter 6.1.1.1 are used in designing an appropriate strategy. However in the case of the seasonal approach, the knowledge which is gained in Chapter 6.1.2.1 by calculating component monthly failure rates is used to devise a strategy. The average cost per WT for the two different approaches, referred to as the seasonal and constant approaches, will be analysed for each the spare strategy.

A broad range of values for each parameter are used in this analysis because of the lack of operational knowledge currently available in the literature. The main point of this analysis therefore is to demonstrate the ability of the spares optimisation model to plan an economical strategy and to exhibit an application of wind speed dependent failure rates that have been used to calculate the *S* and *s* values in both the seasonal and constant approaches. When there is greater operational experience and better informed cost and downtime figures in the literature, the parameters of this model can be reset and more accurate analysis can be undertaken on a site by site basis.

3.1. Model Parameters

The wind speed dependent failure rates generated by the FINO model in Chapter 6.1.1.1 are used to calculate the maximum and reorder levels (*S*, s) of each component, each month, for the various spares strategies using the same procedure demonstrated in Chapter 7.2.5.

Two approaches to spares strategies are assessed that both use wind speed dependent failure rates, a seasonal option and a constant option. In the constant option, monthly failure rates are simply calculated by dividing the annual failure rate of each component by 12 – the levels therefore remain constant from month to month throughout the simulations. In the seasonal case, the component spares levels vary according to the component monthly failure rate calculate in Chapter 6.1.2.1. Figure 7-14 shows an example of these two differing approaches that use the strategy where factors β_S and $\beta_{s,}$ are1 and 0.4 respectively.

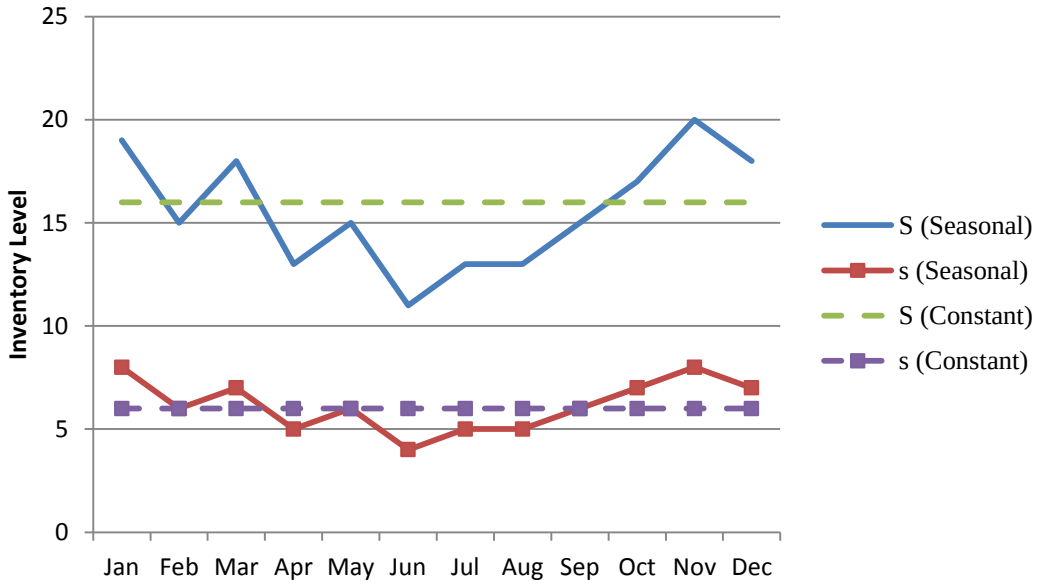

Figure 7-14: Seasonal spares strategy and constant spares strategy when β_S and β_s equal 1 and 0.4 respectively

Many factors influence the downtimes and costs of an offshore wind farm such as: the distance to shore, the sea states, the model size and model of WT, the position of the wind farm in relation to port facilities and to the OEM and the water depth. Each offshore wind

farm is affected in a differently way, positively or negatively, for each variable. Due to this uncertainty and the significant knowledge gaps exist in the literature, there is not a typical set of downtimes and costs frequently used in the literature that can be applied to this model. Therefore three scenarios are simulated, a high cost, medium cost and low cost input scenario labelled HC, MC and LC respectively.

The mechanism for simulating failures (through the use of wind speed dependent failure rates and MCMCS) remains the same for each scenario. The costs and downtimes used in each of these scenarios are shown in Table 7-6, Table 7-7 and Table 7-8. In the future, more reliable estimates of these values can be made and applied to this model when costs and downtimes are better understood.

The MC scenario uses values that have been estimated from various sources of information in the literature and are judged to be reasonable costs and downtimes of an offshore wind farm. The HC scenario represents possible downtimes and costs for an offshore WT located at a site like Dogger Bank which is located very far from shore and in hostile sea conditions. The LC scenario shows the cost and downtime characteristics of an offshore site located near shore, such as a UK round 1 site.

Table 7-6: Extended and repair downtimes for each input scenario

Downtime	Season	Downtime Scenario		
		HC	MC	LC
$d_{extended}$ (hours)	Winter	480	240	120
	Summer	144	72	36
d_{repair} (hours)	Winter	96	48	24
	Summer	24	12	6

Table 7-7: Penalty costs and unscheduled order costs for each input scenario

Penalty and Reordering Cost Scenario	Winter		Summer	
	Penalty Cost (£)	Unscheduled Order Cost (£)	Penalty Cost (£)	Unscheduled Order Cost (£)
HC	250000	25000	50000	5000
MC	125000	12500	25000	2500
LC	62500	6250	12500	1250

Table 7-8: Daily holding costs for each input scenario

Holding Cost Scenario	Cost per Component Day (£)
HC	400
MC	200
LC	100

3.1.1. Downtimes

The values of downtimes $d_{extended}$ and d_{repair} used in the model scenarios are shown in Table 7-6. The summer values in both cases are significantly less than the winter to reflect the difficulties caused by wind speed and sea state in the winter as previously discussed. The range of values used as downtimes have been estimated based on research carried out by Feuchtwang and Infield [7-21]. Feuchtwang and Infield specifically investigated how delays waiting for suitable weather windows affected WT downtime and how the wave height threshold of a vessel influences this. Using North Sea data, they found that for a failure that required a downtime of 1 day, the average delay in waiting for a suitable weather window in which to repair the WT would be 1 – 8 days [7-21]. This delay depended safety limit of the vessel; if it could operate in 2m significant wave heights it would be 1 day, but if it could only operate at 1m the delay would be 8 days.

Additionally research was undertaken by Dowell to assess the waiting time required for access to a WT to preform minor maintenance on a generator in the North Sea [7-22]. Minor maintenance in this case required less than one day to carry out repairs and access using a crew transfer vessel (CTV) that typically has operational limits of between 1m to 2.5m

significant wave height [7-22]. The waiting time consisted only of delays due to constraints on safe sea states and wind speeds. Dowell found that for this minor repair to be carried out with waiting time of less than 10 hours, the probability in summer and winter was approximately 85% and 35% [7-22].

As the waiting times in the spares optimisation model take into account delays caused by component and vessel availability, whereas Dowell and Feuchtwang and Infield do not, downtimes $d_{extended}$ and d_{repair} were estimated using the results from both papers as a guide. As a result, $d_{extended}$ in the MC scenario is roughly three times greater in the winter than in the summer to reflect the difference between summer and winter waiting time found by Dowell [7-22].

3.1.2. Penalty and Unscheduled Order Costs

The penalty costs for each scenario are shown in Table 7-7. The winter costs are 5 times higher than the summer costs to account for the increase in vessel cost, the reduced accessibility and therefore resultant increase in hire periods. The higher winter penalties are imposed for the purpose of ensuring that the spares strategy in the winter will reduce the potential risk of losing valuable generation while wind speed is high. The costs have been estimated from [7-1], [7-23], [7-24]. The reordering costs, described in Chapter 7.2.4, are 10% of the cost of the penalty costs and are also shown in Table 7-7.

The average cost of a jack up barge according to the website Rigzone, is £65,000 per day [7-23]. However not every failure requires a jack up barge. When a downtime filter of 48 hours was applied to the FINO model, the failure rate of the whole system was 0.44 failures per WT year. This means that 23% of the failures that occur in the FINO model have downtimes greater than 48 hours – if these failures are assumed to require a crane the rest require a CTV vessel with an estimated day rate of £3,500 which consists of fuel costs and captain [7-25]. The weighted cost a vessel is therefore calculated to be £17645. In the MC scenario, winter

$d_{extended}$ is 10 days – assuming that a vessel is required for half of that period the total hire cost would be £88,225. As this cost does not include the cost of securing the vessel or further penalties imposed by the operator, the penalty price is rounded up to £125,000 in the winter. The summer cost is estimated to be approximately a fifth of the winter cost as only 1 day of the $d_{extended}$ is assumed to require a vessel.

3.1.3. Holding Costs

Daily component holding costs were estimated assuming that the process of storing a component consisted of:

- The cost of floor space within a warehouse
- The cost of maintaining spare components
- Daily staff costs for holding component
- Cost of plant and holding of boats
- Overheads

The daily cost of floor space was calculated to be 45p/m^2 [7-26]. The size of each component varies; some components such as blades are very large, while others like the control system are small. The floor space of a nacelle was taken as the average floor space per component. Using the nacelle dimensions described in the NREL reference offshore WT, the floor space occupied by a nacelle is taken to be 4m x 10m [7-27]. Assuming that a 2m space is required around the nacelle for plant and personnel, the occupied floor space is calculated to be 112 m^2. Applying the daily cost of 45p/m^2, the daily cost equals £50.40.

Staff costs were estimated assuming that on average three personnel are present at the storage facility throughout each day. According to employment websites a crane operator is paid approximately £17/hour, it is assumed that the hourly expense to the operator per employee at the storage facility is £20/hour after insurance, pensions and other expenses. This equals £1440 per day. Using a β_S factor of 1, the mean *S* level of components stored at

the beginning of a typical month is 32, this number should theoretically drop to zero at the end of the month as failures occur and components are replaced. Therefore taking an average of 16 components stored at any given day, the price of a single component per day in personnel costs is therefore estimated to be £90.

The weight of a nacelle is 82 tonne, the plant required to move this component would need to be capable of lifting 100 tonnes. A warehouse would very likely use a gantry crane; however the price of a 100 tonne gantry crane was unavailable. The daily hire price of a mobile 100 tonne crane is on average £834 according to the crane hire company Ainscough [7-28]. It is likely that a fixed gantry crane would be less expensive than a mobile crane, therefore a cost of £500 a day is assumed. Additionally smaller plant will be required for moving smaller components; for this a daily rate of £100 is assumed. Per component this equals £37.50.

Although the daily hire rate of a CTV is included in the downtime costs (Chapter 7.3.1.1, page 276), the cost of holding the CTV's and reserving them for use each day is included in the holding cost. These costs also include the personnel required to maintain the CTVs and the facilities needed to dock them.

The total daily holding costs of floor space, personnel and plant per component day are therefore £177.90. These costs do not included warehouse overheads or the cost of maintaining the spare components or the holding cost of CTVs. The MC scenario therefore assumes the total cost of holding a component per day is £200.

3.1.4. Maintenance Strategies

For each scenario, the life cycle of a 200 WT wind farm will simulated repeatedly by the spares optimisation model using the same spares strategy. The output of the model will be the cost of operating the wind farm. Once the results converge for each scenario the model will then test another spares strategy that uses another set of β_S and β_s factors. This will

continue until all the possible spares strategies have been tested by the model. The β_S and β_s of the spares strategies tested by the model are shown in Table 7-9. For each spares strategy, a seasonal spares strategy will be used and also a constant spares strategy, as demonstrated in Figure 7-14. Theoretically there is no limit to the strategies the spares optimisation model can test, those used in Table 7-9 were selected to give a broad range of scenarios but not so comprehensive that the computation time of the simulations became impractical.

In total 27 spare strategies are tested. This is done twice for the constant and seasonal strategies. Each strategy is then tested using each downtime and cost scenario. Therefore in total 162 sets of simulations are undertaken for every combination of spares strategy and downtime and cost scenario.

Table 7-9: β_S and β_s factors for each spares strategy tested by the spares optimisation model

Maintenance Strategies	β_S	β_s
I	1	0
II	1.2	0
III	1.4	0
IV	1.6	0
V	1.8	0
VI	2	0
VII	1	0.4
VIII	1.2	0.4
IX	1.4	0.4
X	1.6	0.4
XI	1.8	0.4
XII	2	0.4
XIII	1	0.8
XIV	1.2	0.8
XV	1.4	0.8
XVI	1.6	0.8
XVII	1.8	0.8
XVIII	2	0.8
XIX	1.2	1.2
XX	1.4	1.2
XXI	1.6	1.2
XXII	1.8	1.2
XXIII	2	1.2
XXIV	1.6	1.6
XXV	1.8	1.6
XXVI	2	1.6
XXVII	2	2

3.2. FINO Model Cost Scenarios

The seasonal spares approach produced the lowest corrective maintenance costs for two of the three scenarios modelled as illustrated in Figure 7-15. Table 7-10 shows that, the HC and MC scenarios both performed more economically when a seasonal component stocking approach was taken, opposed to maintaining a constant level of each component in the spares holding. For the LC scenario however, the constant spares approach was the most economical option.

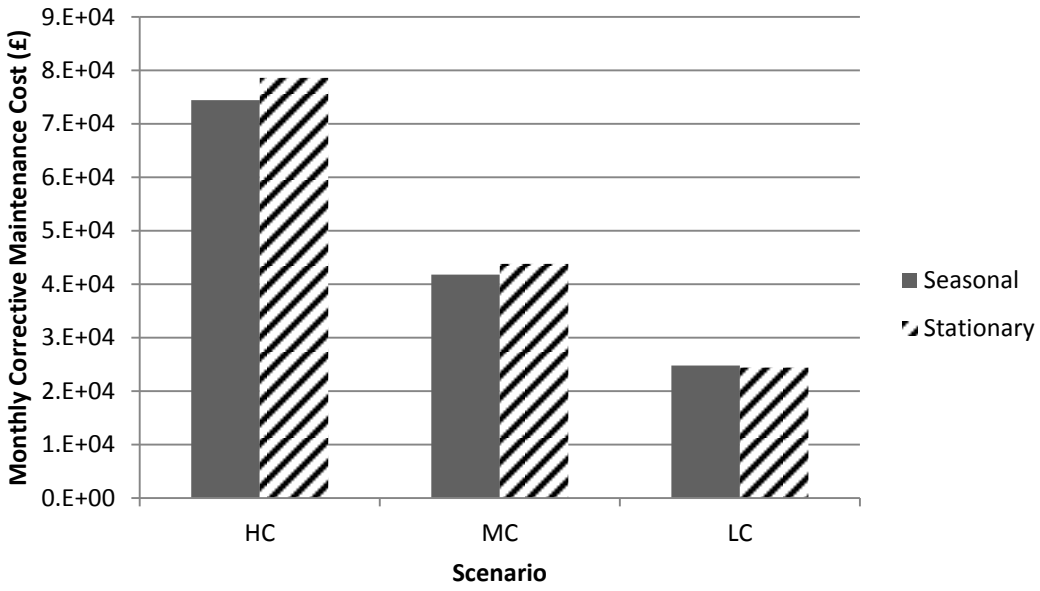

Figure 7-15: Monthly Corrective Maintenance Costs using constant and seasonal approach

As described in Table 7-10, in the case of both the HC and the MC scenarios the optimum seasonal spares strategy to use, according to the simulated data, were β_S and β_s factors that equal 1 and 0.4 respectively. These factors mean that at the start of each month the spares levels are equal to the expected number of failures that will occur that month, calculated by the seasonal failure rate FINO model from Chapter 6.1.2.1. Once the spares level of a component drops to 40% of that expected value, an unscheduled order is made to return the component spares level to the number of expected failures for that month. The risk of

incurring a penalty cost is therefore reduced as an order is placed in advance of spares levels dropping to 0.

Table 7-10: Summary of optimum strategies for each scenario

Scenario	Optimum Strategy (β_S, β_s)	Corrective Maintenance Cost (£'s per WT year)		(Constant–Seasonal)/ Seasonal (%)	Difference in Wind Farm Life Corrective Maintenance Cost (£'s)
		Seasonal	Constant		
HC	(1, 0.4)	7.44E+04	7.86E+04	5.34	16.8E+06
MC	(1, 0.4)	4.18E+04	4.38E+04	4.52	8E+06
LC	(1.2, 0.8)	2.48E+04	2.44E+04	-1.20	-1.6E+06

For the HC scenario, the difference in corrective maintenance costs using the same β_S and β_s factors, but taking a constant approach to spares levels, is 5.34%. For a 200 WT wind farm over 20 years, this results in a difference of roughly £16.8 million of expenditure just on corrective maintenance, as shown in Figure 7-16.

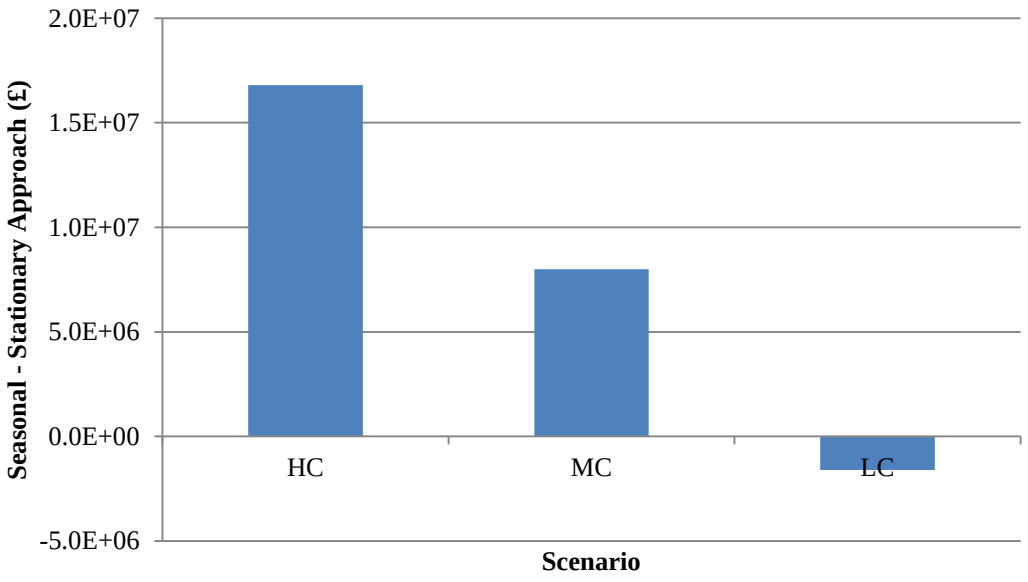

Figure 7-16: Difference in wind farm life corrective maintenance cost between using the optimum strategy with a seasonal or constant approach

The mean monthly cost of corrective maintenance for HC scenario wind farm is shown in Figure 7-17. The highest cost throughout the year is due to lost generation. The lost generation is so high because the repair and extended downtimes for the HC scenario are such long periods of time, resulting in a lot of lost generation when a WT fails. As the model uses offshore wind CfD electricity costs, the impact of the lost generation is magnified. In the summer however, because of the reduction in extended and repair downtime and the lower wind speeds, the holding costs become the highest cost as the downtimes reduce because of the lower risk. The summer is the time of year the holding costs are at their lowest because of the reduced quantity of spare components held. But because those costs are not influenced in the model by the season they are the biggest contributor to the monthly corrective maintenance costs at that time of year.

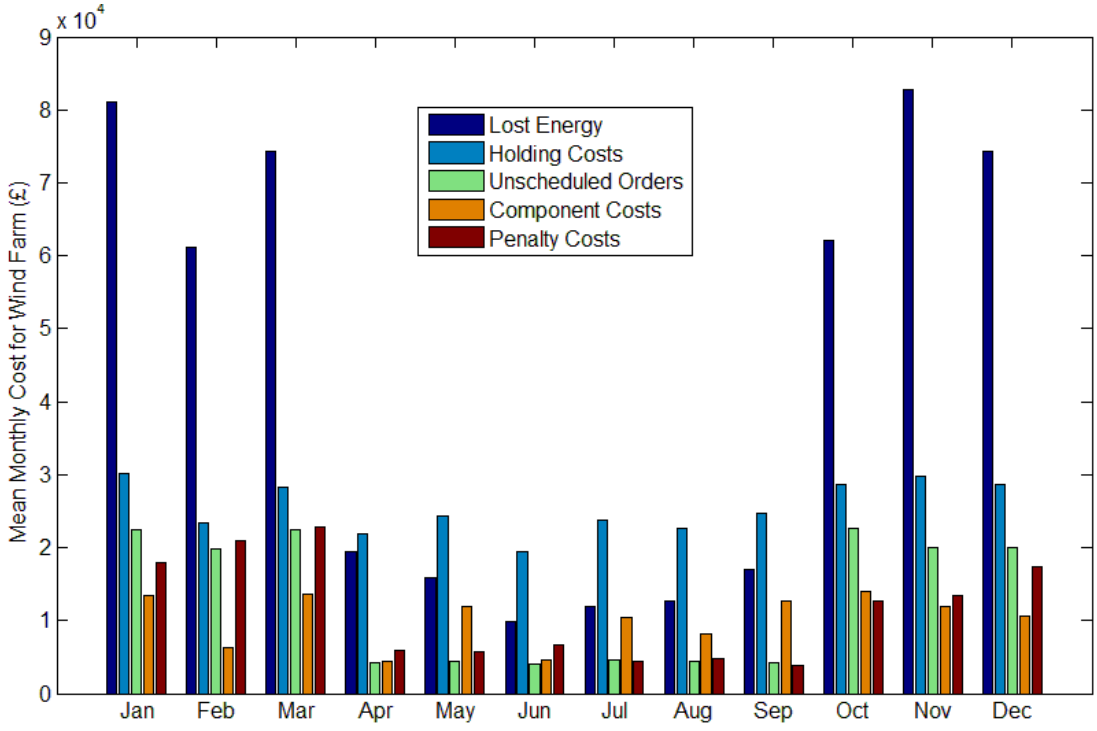

Figure 7-17: Breakdown of mean monthly wind farm corrective maintenance costs for HC scenario using optimum maintenance strategy and a seasonal component stocking approach

In the MC scenario all the costs and downtimes reduce, but the component costs remain the same – they therefore become a more influential factor in the corrective maintenance costs as

shown in Figure 7-18. The other model variables remain the same proportionally as in Figure 7-17 because the optimum strategy is the same, as shown in Table 7-10. The component costs are proportionally quite high in May, July, August and September due to the different *S* and *s* levels each month. In April and June component costs are lower, this is either because unscheduled orders are commonly made the previous months, or because the spares ordered at the start of the previous month did not deplete to the reorder level before the monthly scheduled order was made.

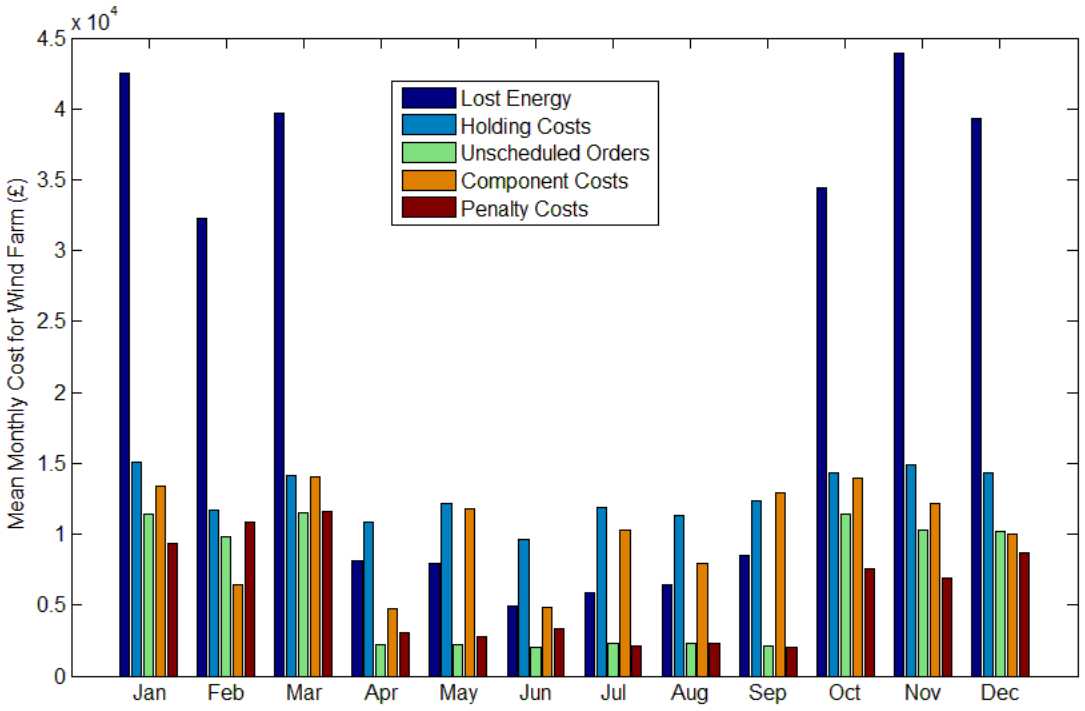

Figure 7-18: Breakdown of mean monthly wind farm corrective maintenance costs for MC scenario using optimum maintenance strategy and a seasonal component stocking approach

For the LC scenario the optimum strategy is to maintain a constant spares level and use β_S and β_s factors of 1.2 and 0.8 respectively. The change in strategy is illustrated in Figure 7-19, where the component costs are less variable each month as the *S* and *s* levels remain the same.

Because a constant strategy is used, it should be expected that penalty costs would increase as a proportion of the total corrective maintenance costs, however as shown in Figure 7-20

this is not the case. The reason for this is due to the optimum strategy selected, as $\beta_S = 1.2$, meaning that the maximum level *S*, is higher. This should mean that holding costs become an issue, but because the cost of holding a component in this scenario is so low, as a percentage of overall corrective maintenance cost for this strategy, it is approximately the same as the proportional costs of holding in the HC scenario.

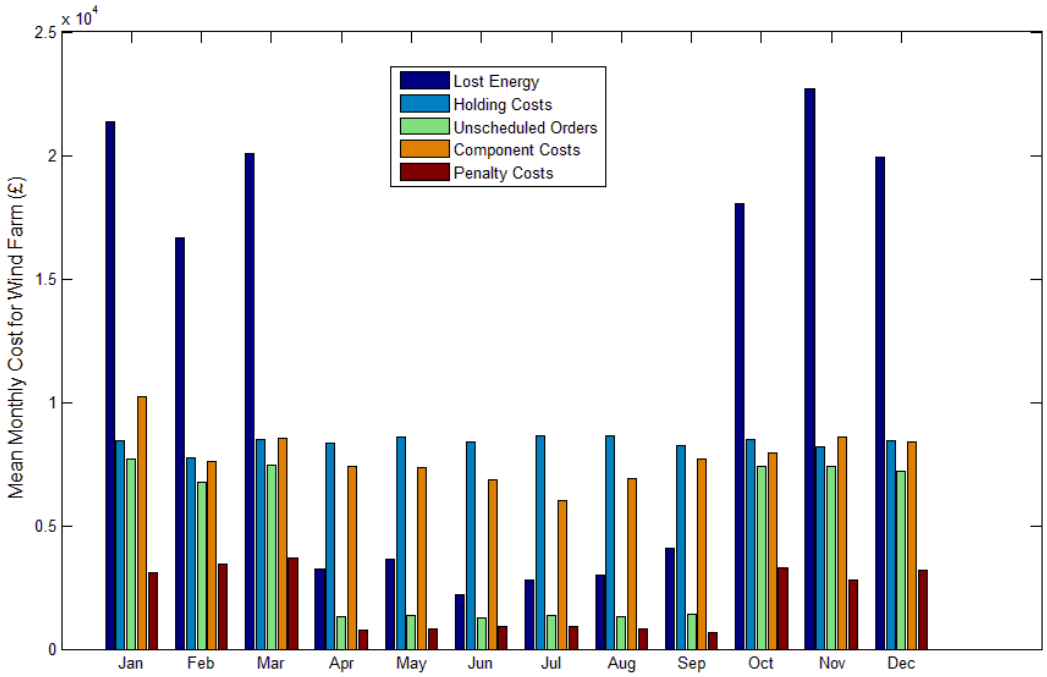

Figure 7-19: Breakdown of mean monthly wind farm corrective maintenance costs for LC scenario using optimum maintenance strategy and constant component stocking approach

The impact of the penalty costs on the overall corrective maintenance cost decreases as the applied costs and downtimes are reduced from HC to LC. In the LC case the contribution is significantly lower than in the HC or MC scenario, this is because the strategy is to hold a higher amount of spares at the start of every month reducing the likelihood that a penalty will need to be issued because of stock levels reaching 0. The reason that penalties still occur despite reordering factors being 0.8 is because the level of spares required in the winter is underestimated because of the use of a constant strategy.

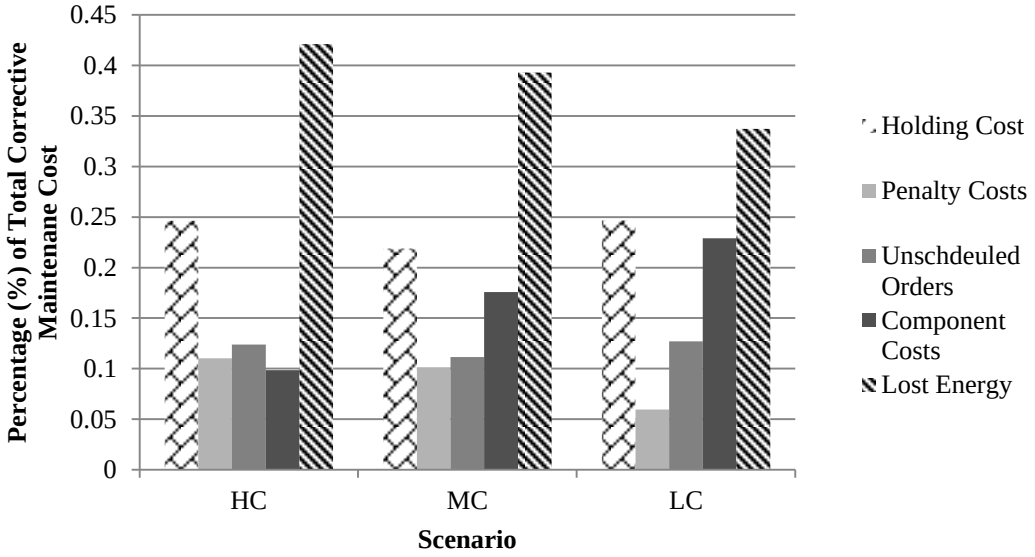

Figure 7-20: The percentage breakdown of total corrective maintenance costs for each scenario using their optimum spares strategy and component stocking approach

The unscheduled costs cost more than the penalty costs in each scenario. In the HC and MC scenarios the optimum strategies are the same and so there is not a great deal of difference between the two. However the more cautious strategy for the LC scenario means that unscheduled orders are made more frequently because the spares levels fall below the reordering levels more often.

As illustrated in Figure 7-19 the significance of the component cost increases as the other costs begin to fall. The effect of this increase reduces the impact of lost generation in the LC scenario compared to HC and MC. The reduction in downtime brings the contribution of lost generation to the overall corrective maintenance cost from 42% to 33%, as shown in Figure 7-20.

The results show that in the case of the HC scenario and MC scenario the selection of a seasonal spares approach is advantageous. However in the LC scenario, because the penalties and risk of lost generation is so much lower, it is more economical to maintain a constant strategy. These results were expected as the LC scenario represents onshore

operating conditions most closely and is therefore not affected in the same way by the environment.

In the case of the HC scenario, which is the most extreme and may represent the costs faced at a location like Dogger Bank most accurately of the three, savings of 5.34% are calculated to be made by adopting a strategy based on a seasonal spares stocking approach. The difference between these two approaches, using the optimum strategy of β_S and β_s equalling 1 and 0.4 respectively, is described in Figure 7-21. The cost that has the biggest impact on the seasonal approach being the most economical is the holding costs, that are higher in the constant approach because they store too many components during the summer that do not get used. The holding costs are also higher in the constant approach because the number of CTVs held in the summer is the same as that in the winter, despite fewer failures taking place. A more cost effective solution would be to reduce the CTVs in the summer and increase in the winter as the seasonal approach does.

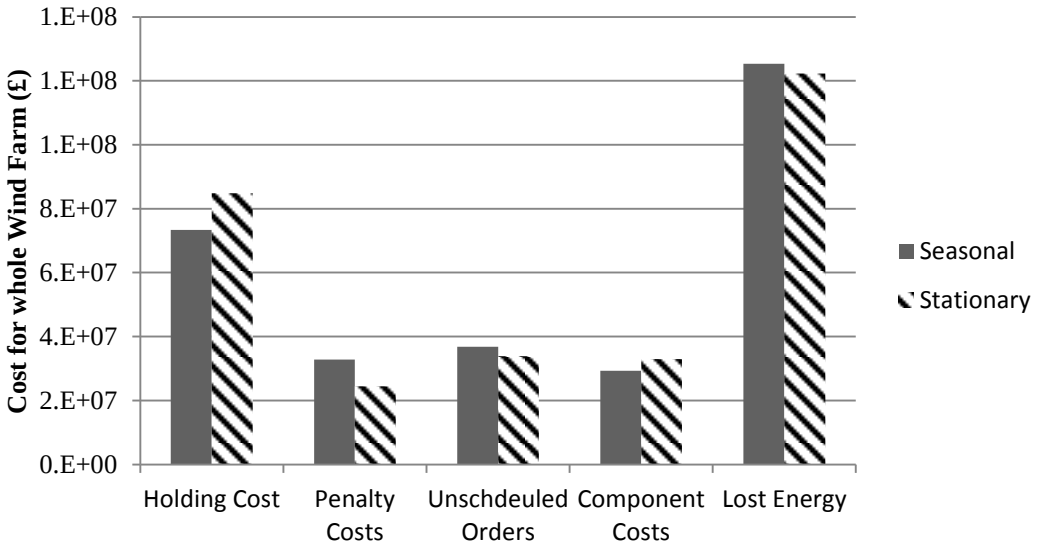

Figure 7-21: Comparison of wind farm costs for HC scenario using a seasonal and constant component stocking strategy where β_S and β_s equal 1 and 0.4 respectively

As previously discussed, experience in operating offshore wind farms is scarce and so these costs used to estimate downtime, holding cost, penalty cost, unscheduled cost and component costs are not typical of a single specific offshore wind farm. In fact, each offshore wind farm will face different costs depending on the location of their wind farm, the distance from their port that houses their spare components, the depth of their water and the sea state. The following chapter will explore how these differing costs affect the model by performing a sensitivity analysis. Then the effectiveness of the model and the suitability of this application for wins speed dependent failure rates will be discussed.

3.3. FINO Model Sensitivity Analysis

In the previous section, the spares optimisation model found optimal spares strategies for three arbitrary cost scenarios. The scenarios used costs and parameters that were estimated from limited available data. Therefore the results shown in the previous section describe those specific scenarios which may not be reflective of any real offshore wind farm. The model results depend entirely on the parameters used. In the case of the LC scenario the constant approach was the most economical. It is likely that for offshore wind farms with different parameters to those used in this analysis, that a constant approach would also be the most sensible option.

In this section the sensitivity of the FINO spares optimisation model to each of these estimated parameters will be assessed. The difference between using a seasonal and constant approach will be calculated while running the two optimum strategies calculated in the previous section. The following costs and parameters will be analysed:

- Component costs
- Penalty and unscheduled order costs
- Holding costs
- Extended and repair downtimes (d_{repair} and $d_{extended}$)

The base case from which the sensitivity analysis will be performed is the MC scenario described in 0. Each parameter will then be separately increased by 100% or reduced by 50% to evaluate how sensitive the model is to each of them. The advantage of this approach over the one taken in the previous section is that a more detailed analysis can be undertaken to investigate why the model calculates that one approach is better than another. It will also show the parameters which are most important to the model and each strategy.

In total there are 3 different values available to each parameter (-50%, MC and +100%). There are therefore 64 possible combinations of the four parameters with different values

that can be evaluated for each of the twenty seven strategies shown in Table 7-9. This would take an extremely long time to analyse computationally and would be of limited value.

Therefore only two strategies will be assessed in the sensitivity analysis – they are the optimum strategy of the HC and MC scenario in the previous section where β_S and β_s were equal to 1 and 0.4 respectively and the optimum strategy for LC where they equal 1.2 and 0.8 respectively. By varying each parameter only once at a time, 9 sets of simulations are carried out for each strategy. These consist of the MC case and 2 sets of simulations for each of the 5 parameters.

The results of the sensitivity analysis are shown in Figure 7-22 and Table 7-11. The benefit of using the seasonal stocking approach when using the MC parameters and optimum strategy is 4.52%, as shown in Table 7-10. The holding costs, penalty and unscheduled costs, extended and repair downtimes and component costs are individually increased and decrease by 100% and 50% respectively. These are the same costs and downtimes modelled in the HC and LC scenarios previously, shown in Table 7-6, Table 7-7 and Table 7-8.

The parameter this strategy is most sensitive to is the cost of penalties and unscheduled orders. When this increases by 100% the difference between using a seasonal stocking approach and a constant approach increases to 7.12%, as illustrated in Table 7-11. Therefore, if a wind farm with the characteristics of the MC scenario were to find that the costs of penalties and unscheduled orders increased, possibly due to an increase in jack-up vessel cost, there would still be a benefit in using spares factors of 1 and 0.4. However if the costs decrease the benefit of using the strategy and approach also decreases. In this case the spares optimisation model could be used to find the optimum strategy for these new parameters.

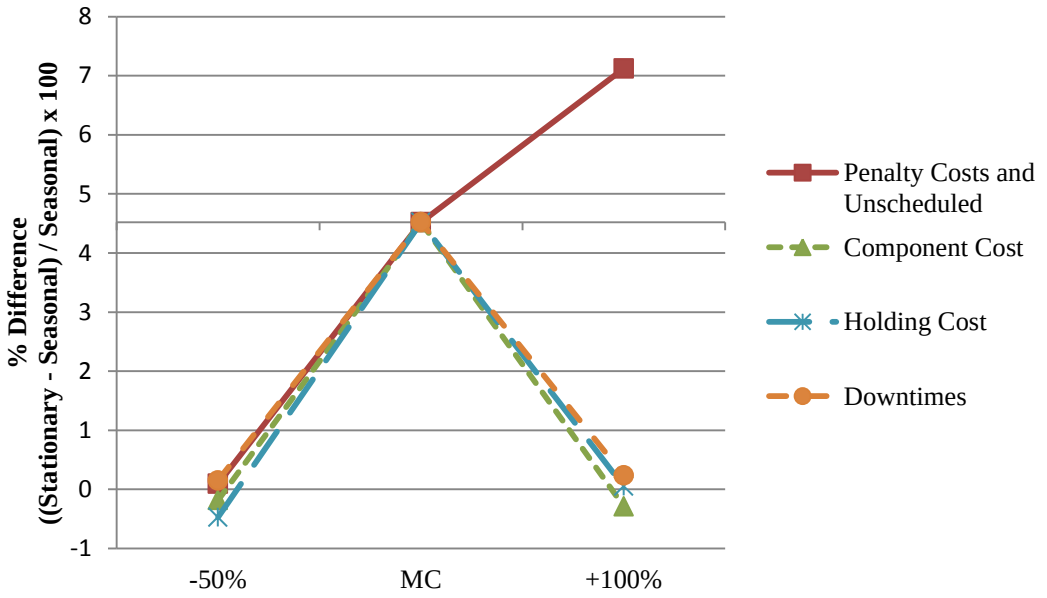

Figure 7-22: Sensitivity analysis showing the benefit of taking a seasonal component stocking approach when using optimum HC and MC strategy (β_S and β_s equal 1 and 0.4)

When the downtimes, holding costs and component costs increased and decreased by 100% and 50% respectively, the benefit of using the seasonal stocking approach decreases from the base case MC scenario. As shown in Table 7-11, of these parameters when the downtime is increased by 100% that it still remains beneficial to maintain the seasonal spares approach with the optimum MC and HC strategy. In this case the benefit is only 0.24%, which equates to approximately £100/WT year.

Table 7-11: Sensitivity analysis of spares optimisation model using the optimum MC and HC strategy

	% Difference ((Constant - Seasonal) / Seasonal) x 100		
Parameter	- 50%	MC	+ 100%
Penalty Costs and Unscheduled	0.10	4.52	7.12
Component Cost	-0.18	4.52	-0.29
Holding Cost	-0.47	4.52	0.05
Downtimes	0.15	4.52	0.24

The same sensitivity analysis is undertaken using the LC optimum strategy, which was to use factors of 1.2 and 0.8. When this strategy is applied to a wind farm with MC parameters, the

calculated difference in corrective maintenance costs between using a seasonal approach and a constant approach is -0.39%. The best approach is therefore to maintain constant spares levels throughout the year. However when the sensitivity analysis is undertaken, the benefit of using the constant approach decreases in each case, as shown in Figure 7-23.

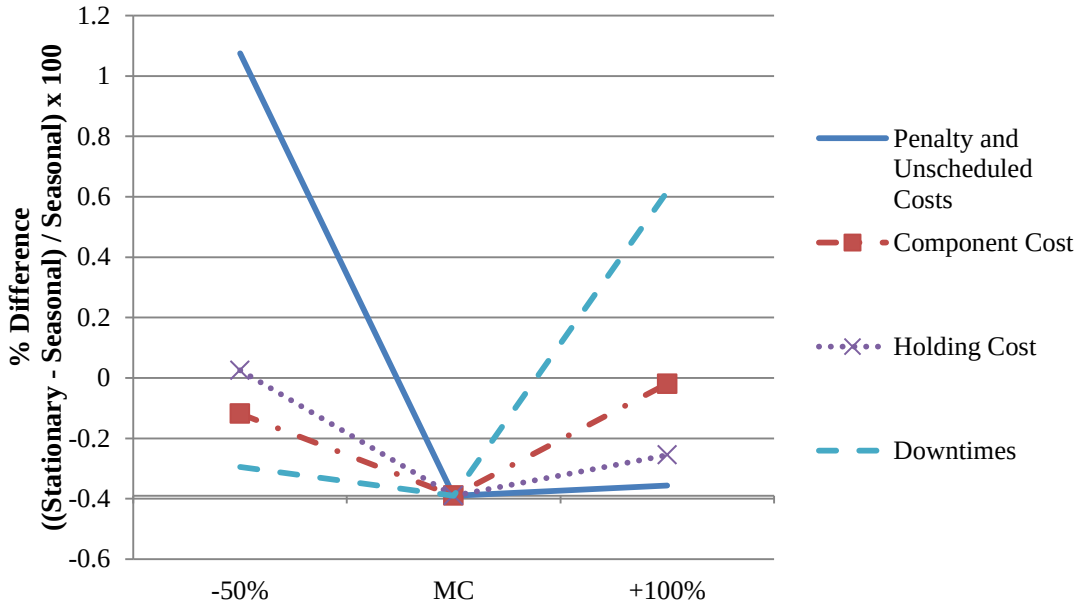

Figure 7-23: Sensitivity analysis showing the benefit of taking a seasonal component stocking approach when using a strategy where β_S and β_s are equal 1.2 and 0.8

As shown in Table 7-12, the switch to a seasonal stocking approach using this strategy becomes beneficial when the holding costs or the penalty and unscheduled order costs decrease and finally if the extended and repair downtimes increase by 100%.

Table 7-12: Sensitivity analysis of spares optimisation model using a strategy where β_S and β_s are equal 1.2 and 0.8

	% Difference ((Constant - Seasonal) / Seasonal)x100		
Parameter	- 50%	MC	+ 100%
Penalty Costs and Unscheduled	-0.36	-0.39	1.07
Components	-0.02	-0.39	-0.12
Holding	-0.26	-0.39	0.02
Downtime	0.62	-0.39	-0.29

In the event that the parameters do increase or decrease by 100% or 50% respectively from the MC scenario values (shown in Table 7-6, Table 7-7 and Table 7-8), the spares optimisation model calculates that the following spares strategies and approaches shown in Table 7-13 would be the most economical options to be taken. In six of the eight cases a seasonal approach is the best option.

Table 7-13: Optimum spares strategies and approaches for sensitivity analysis parameters

Percentage Increase				Approach (Seasonal or Stationary)	Optimum Spares Strategy (β_S, β_s)	Corrective Maintenance Cost (£'s per WT Year)
Penalty and Unscheduled Order Cost	Comp Costs	Holding Cost	d_{repair} and $d_{extended}$			
100%	0	0	0	Stationary	1.2, 0.4	49,478
-50%	0	0	0	Seasonal	1.2, 0.8	38,166
0	100%	0	0	Seasonal	1.2, 0.8	48,038
0	-50%	0	0	Seasonal	1.2, 0.4	38,089
0	0	100%	0	Stationary	1.0, 0.4	52,620
0	0	-50%	0	Seasonal	1.4, 0.8	36,319
0	0	0	100%	Seasonal	1.2, 0.4	56,543
0	0	0	-50%	Seasonal	1.2, 0.4	34,640

When the penalty and unscheduled order cost is increased and when the downtimes are increased, a constant approach using β_S and β_s factors of 1.2 and 0.4 is the best strategy. However as shown in Chapter 7.3.2, the most economical option when every parameter is increased by 100% is a seasonal spares stocking approach and a strategy of 1 and 0.4. The results shown in Table 7-13 therefore demonstrate that neither a seasonal or constant approach is the most economical when the costs or downtime parameters are increased.

3.4. Discussion

The FINO model's primary application, as shown in Chapter 6, was to calculate the component failure rates of a WT subjected to FINO wind speeds and calculate the impact of these failures on performance. The aim of the analysis undertaken in this chapter was to use the results of the FINO model in Chapter 6 and design an offshore wind farm spares optimisation model that could calculate corrective maintenance costs for a variety of offshore scenarios. Many different strategies were assessed, using a seasonaland constant spares approach. The optimum strategy, whether constant or seasonal, was determined using the MCMCS wind speed dependent failure rate model, described in 0.

The results in Table 7-10 show that in the HC and MC scenario there is a benefit in designing a spares strategy that takes into account the seasonality of component failure rates due to wind speed. For the LC scenario however the optimum strategy uses a constant approach. The results suggest that in some cases, substantial savings could be made to the corrective maintenance cost by taking a seasonal approach when designing the strategy as opposed to a constant approach. For the modelled wind farm of 200 WTs, the benefit of adopting a seasonal strategy is roughly £16.8 million in the HC scenario and £8 million in the MC scenario.

However there are many issues with the spares optimisation model, many of which relate to the problems previously discussed in Chapter 6.1.3 relating to the MCMCS and wind speed dependent failure rate aspects of the model. The model also assumes that every failure that occurs requires a replacement, which in reality is not likely to be the case. The component failure rates calculated in Chapter 7.2.3 are based on this assumption that all corrective maintenance results in component replacement this assumption as it is unclear within the ORD whether components have been rehabilitations or replacements are made in the event of corrective maintenance. If component rehabilitations were considered, these costs would need to be calculated from the £15,000 corrective maintenance estimation made in Chapter

7.2.3 and the logistical costs of performing a repair off shore would also have to be estimated. Further issues would also need to be considered. Firstly, what would be the impact of rehabilitation on the failure rate of the component and how perfect or imperfect the repair would be? Secondly, if reliability was reduced after component rehabilitation, what would be the most cost effective corrective maintenance option for an offshore wind farm? The assumption that all failures result in replacement was therefore made to reduce the complexity of the model and the scope of this thesis.

As discussed previously, the costs, downtimes and other parameters used in this analysis are estimates and approximations due to the lack of data available from operating offshore WTs. Unlike onshore WTs, for which maintenance is not generally problematic or risky, offshore maintenance is affected greatly by the location of the wind farm. As discussed previously, operational risks are also greater offshore due to the higher value of offshore wind energy, which is 63% greater offshore according to CfD, and the mean daily wind speed which provides a far more profitable resource. Any downtime experienced offshore has greater consequences due to the costs and logistics of maintenance and the greater potential loss for every hour the WT remains down.

Because of this unpredictability, three scenarios were modelled. The HC and LC were extreme examples and it is likely that the majority of offshore wind farms would have costs somewhere in between their calculated range of £78,600 - £24,400 per WT year for corrective maintenance alone. However the extreme scenarios demonstrate that the model gives reasonable corrective maintenance cost estimations in either case.

These estimates for each scenario are conservative however. The model uses the same wind speed dependent failure rates calculated using the ORD. An assumption is made that component failure rates remain constant for wind speeds greater than 13 m/s. This assumption is a reasonable one to make onshore as the mean wind speed is much lower,

however as shown in Chapter 4.2.3 the daily mean wind speed frequently rises above 13 m/s offshore. For some of the less reliable components, such as the control system and the yaw system, the failure rates increase until reaching the 13 m/s to 17 m/s range. There is nothing to suggest that they would not continue to rise beyond this point. However to calculate these failure rates, reliability data must become available for sites that are subjected to mean daily wind speeds above 17 m/s.

Because of this lack of data, the model cannot be validated properly by comparing calculated corrective maintenance costs to those actually found on an operating offshore site. However, it was estimated by Rademakers and colleagues in 2009 that corrective maintenance offshore would be roughly 0.005 – 0.010 €/kWh [7-16].

Using these costs for the FINO model, where as shown in Chapter 6.2.3.1 the total generated by the 2.3MW FINO WT was 10841.125 MWh/WT year, the corrective maintenance costs per WT year would equal €54,205 – €108,410 or roughly £43,500 – £87,000. Using the total generated by the 5MW FINO model, shown in Chapter 6.2.3.3, this cost increases to £51,000 - £102,000 per WT year. The lower range of these estimates are reasonably close to the calculated corrective maintenance cost of the MC and HC scenarios of £41,800 and £74,400, shown in Table 7-10.

In Chapter 7.3.3 a sensitivity analysis is undertaken for two of the strategies – the optimum HC and MC strategy and the optimum LC strategy (β_S and β_s equal 1, 0.4 and 1.2 and 0.8 respectively). As each parameter value increases and decreases, as shown in Table 7-13, other strategies become the optimum options. This demonstrates that the model parameters are vital in calculating the optimum strategy and that two offshore wind farms will very likely have two different optimum strategies.

The analysis only evaluates two approaches, constant and seasonal. It is possible that a hybrid of the two could be an optimum approach in some cases. Alternatively, rather than

ordering components on a monthly basis, it would be more economical if they were ordered more or less frequently. A more advanced model could explore these options in more detail.

4. Chapter 7 Summary

The maintenance strategy of an offshore wind farm is extremely important to asset performance due to issues with access, component reliability, logistics and vessel costs. Chapter 7 uses the wind speed dependent failure rate MCMCS FINO model from Chapter 6 to find the optimum corrective maintenance strategy for a 200 WT offshore wind farm subjected to FINO mean daily wind speeds.

A periodic review inventory system with emergency replenishments is used to manage the spare component levels of the offshore wind farm. This system consists of a maximum spares level *S* and a reorder level *s*. WT failures are simulated using the FINO model and various spares strategies are tested using maximum and reorder factors β_S and β_s. These factors are multiplied by the expected number of failures to occur at the wind farm over the period of a month. These monthly failure rates are either calculated using the annual FINO model component failure rates calculated in Chapter 6.1.1.1 or the monthly FINO failure rates calculated in Chapter 6.1.2.1. In the formers' case the *S* and *s* levels remain constant throughout the year, whereas in the latter's case they vary from month to month and relate to the component failure rate calculated according to the mean daily wind speed.

Basic offshore constraints are added to the spares optimisation model to simulate the logistic and access issues experienced offshore, these are described in Chapter 7.2.4. These constraints vary in the summer and the winter. Costs and downtimes are applied to the offshore constraints, detailed in Chapter 7.3.1.

Three scenarios are modelled using a range of cost and downtime values. The MC scenario and HC scenario are both calculated to have an optimum strategy that uses a seasonal approach and β_S and β_s factors of 1 and 0.4 respectively. The benefit of using a seasonal approach over a constant approach in these cases equates to £16.8 million and £8 million over the lifetime of the wind farm. The LC scenario's optimum strategy however uses higher

β_S and β_s factors of 1.2 and 0.8 respectively and a constant stock level approach which over the lifetime of the wind farm saves £1.6 million.

From the sensitivity analysis in Chapter 7.3.3, it is clear that the model and the suitability of each spares strategy is very sensitive to the parameter costs and downtimes, as shown in Figure 7-22 and Figure 7-23. As risks at each offshore wind farm will be very different, optimum spares strategies will differ in each case. In some cases however there is an economic advantage in considering the seasonality of component failure rates when designing a spares strategy.

5. Chapter 7 References

[7-1] G. J. W. van Bussel and M. B. Zaaijer, "Reliability, Availability and Maintenance aspects of large-scale offshore wind farms , a concepts study .," in *Proceedings of MAREC*, 2001.

[7-2] IEC61400-26-1, *Part 26-1: Time Based Availabiltiy for Wind Turbines*. 2011.

[7-3] K. Shyjith, M. Ilangkumaran, and S. Kumanan, "Multi-criteria decision-making approach to evaluate optimum maintenance strategy in textile industry," *J. Qual. Maint. Eng.*, vol. 14, no. 4, pp. 375–386, 2008.

[7-4] R. Sarker and A. Haque, "Optimization of maintenance and spare provisioning policy using simulation," *Appl. Math. Model.*, vol. 24, no. 10, pp. 751–760, Aug. 2000.

[7-5] S. Setyaningsih and M. H. Basri, "Comparison Continuous and Periodic Review Policy Inventory Management System Formula and Enteral Food Supply in Public Hospital Bandung," *Int. J. Innov. Manag. Technol.*, vol. 4, no. 2, 2013.

[7-6] J. B. Dilworth, *Production and Operations Management*. New York: McGraw-Hill, 1993.

[7-7] G. Tagaras and D. Vlachos, "A Periodic Review Inventory System with Emergency Replenishments," *Manage. Sci.*, vol. 47, no. 3, pp. 415–429, 2001.

[7-8] C. Chiang and G. J. Gutierrez, "Optimal Control Policies for a Periodic Review Inventory System with Emergency Orders," *Navel Res. Logisitcs*, vol. 45, no. 2, pp. 187–204, 1997.

[7-9] A. B. M. Zohrul Kabir and A. S. Al-Olayan, "A stocking policy for spare part provisioning under age based preventive replacement," *Eur. J. Oper. Res.*, vol. 90, no. 1, pp. 171–181, Apr. 1996.

[7-10] J. Moller, "Author Conversation." 2013.

[7-11] G. Marsh, "What Price O & M ?," *Focus (Madison).*, vol. 8, no. June, pp. 22–27, 2007.

[7-12] Y. Feng, Y. Qiu, C. J. Crabtree, H. Long, and P. J. Tavner, "Monitoring wind turbine gearboxes,"*Wind Energy* vol 16, no 2, pp. 728–740, 2013.

[7-13] P. E. Morthorst, "Wind Energy - The Facts. Costs and Prices volume 2," 2009.

[7-14] Variable Pitch, "Site A," 2014. [Online]. Available: http://www.variablepitch.co.uk/stations/718/. [Accessed: 01-Jul-2014].

[7-15] Variable Pitch, "Site B," 2014. [Online]. Available: http://www.variablepitch.co.uk/stations/65/. [Accessed: 04-Jul-2014].

[7-16] L. W. M. M. Rademakers, H. Braam, M. B. Zaaijer, and G. J. W. van Bussel, "Assessment and Optimisation of Operation and Maintenance of Offshore Wind Turbines," in *EWEC*, 2009.

[7-17] P. W. Cheng, G. J. W. van Bussel, G. M. van Kuik, and J. H. Vugts, "Reliability-based Design Methods to Determine the Extreme Response Distribution of Offshore Wind Turbines," *Wind Energy*, vol. 6, no. 1, pp. 1–22, Jan. 2003.

[7-18] J. J. Nielsen and J. D. Sørensen, "On risk-based operation and maintenance of offshore wind turbine components," *Reliab. Eng. Syst. Saf.*, vol. 96, no. 1, pp. 218–229, Jan. 2011.

[7-19] J. Phillips, P. Reynolds, L. Gosden, G. Hemmingsen, I. Mcdonald, G. Mackay, W. Hines, P. O. Repower, J. Brown, and J. Beresford, "A Guide to UK Offshore Wind Operations and Maintenance." 2014. [Online] Available: http://www.4-power.eu/media/3109/offshore-wind-guide-june-2013.pdf [Accessed 4-Jul-2014]

[7-20] D. McMillan and G. Ault, "Towards Quantification of Condition Monitoring Benefit for Wind Turbine Generators," in *EWEA*, 2007.

[7-21] J. B. Feuchtwang and D. G. Infield, "The offshore access problem and turbine availability - probabilistic modelling of expected delays to repairs," in *European Offshore Wind Conference*, 2009.

[7-22] J. Dowell, A. Zitrou, L. Walls, and T. Bedford, "Analysis of Wind and Wave Data to Assess Maintenance Access to Offshore Wind Farms," in *ESREL*, 2013.

[7-23] Rigzone, "Offshore Rig Day Rates," *2014*. [Online]. Available: http://www.rigzone.com/data/dayrates/. [Accessed: 16-Jul-2014].

[7-24] D. McMillan and I. Dinwoodie, "Forecasting Long Term Jack up Vessel Demand for Offshore Wind," in *ESREL*, 2013.

[7-25] Marcon International, "Crew Boat Market Report," 2012. [Online]. Available: http://www.marcon.com/library/market_reports/2012/cb02-12.pdf. [Accessed: 13-Aug-2014].

[7-26] East Midland Self Storage, "Storage Prices," 2014. [Online]. Available: http://www.em-storage.co.uk/uk-self-storage-prices.html. [Accessed: 13-Aug-2014].

[7-27] J. Jonkman, S. Butterfield, W. Musial, and G. Scott, "Definition of a 5-MW Reference Wind Turbine for Offshore System Development," NREL, 2009. [Online] Available: http://www.nrel.gov/docs/fy09osti/38060.pdf [Accessed: 10-Sep-2014].

[7-28] Ainscough Crane Hire, "Project Management at the Highest Level," 2011. [Online]. Available: http://www.vertikal.net/uploads/tx_filelinks/ca_2011_9_p16-27.pdf. [Accessed: 13-Aug-2014].

Chapter 8. Discussion and Conclusions

1. Defining the Relationship between Wind Speed and Component Reliability

As described in detail in Chapter 5, WSD (Wind speed dependent) failure rates were calculated using reliability data from the two onshore wind farms and wind speed data from onsite met masts. The mean wind speed that occurred each day when a component failed was therefore determined.

This combined dataset allowed the calculation of the following:

- The probability of a component failing on a given day
- The probability of a mean daily wind speed occurring when a component fails
- The probability of a mean daily wind speed occurring

Bayes Theorem was then used to calculate the probability of a failure to a component on a given day, given a mean daily wind speed. The component failure rate in this case is dependent on the mean daily wind speed.

Using this approach meant that the relationship between mean wind speed and component failure rate could be plotted for the two onshore wind farm sites. This relationship was then extrapolated to other sites using MCMCS.

Figure 8-1 shows the wind speed dependent failure rate of the whole system and the standard annual failure rate which is not WSD and was calculated using the ORD. At the higher wind speed ranges the WSD failure rate is significantly greater than the constant annual failure rate, while at the low wind speeds the WSD failure rate is less.

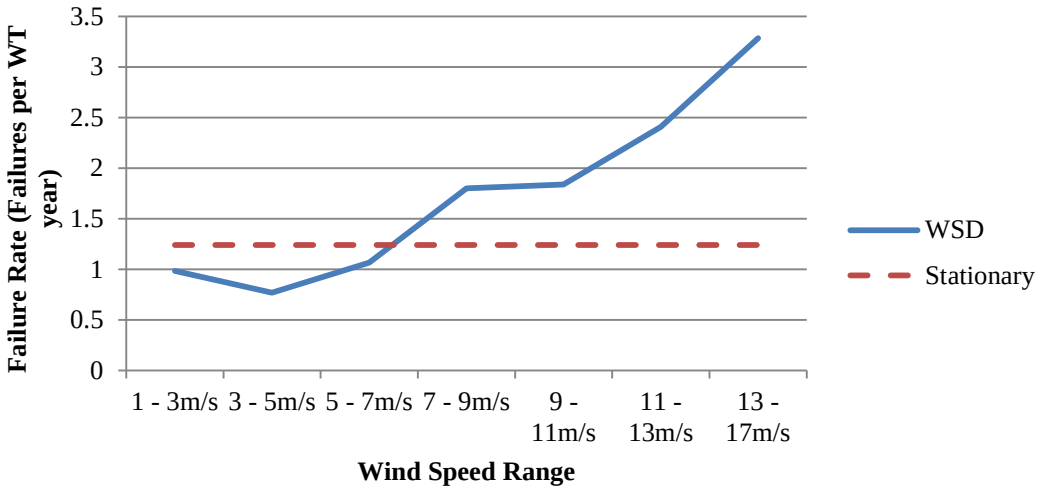

Figure 8-1: WSD failure rates and constant annual failure rate from the ORD

For the two of the least reliable components, the control system and the yaw system, this relationship holds, as shown in Figure 5-16 and Figure 5-18. In the met mast data that was used to calibrate the model, the variability the wind speed in a typical day increased at higher mean daily wind speeds (as shown in Figure 8-2) – therefore the control system worked harder on days with higher mean wind speed which could have led to an increase in failures.

The failure rate of the drive train increases up until the 9 m/s – 11 m/s wind speed range, as shown in Figure 5-18. The rated wind speed of the WT is 11.5 m/s – beyond this wind speed the failure rate decreases. This, as explained in Chapter 6.2.3.1, was expected as beyond rated the drive train maintains a constant torque.

Despite the successes in modelling the WSD failure rates of the three least reliable components, very few of the more reliable components failed often enough during the recorded period for reliable WSD failure rates to be plotted. For example, there were only 12 generator failures in the dataset. This is a major component, however because it failed so few times during the recorded period its WSD failure rate, as shown in Figure 8-3, appeared to show a peak failure rate at the low wind speed range 1 m/s – 3 m/s.

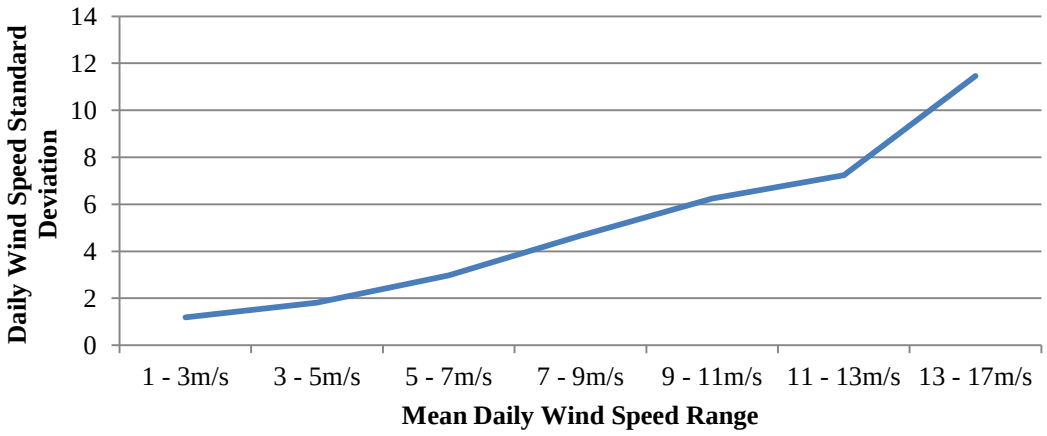

Figure 8-2: Relationship between mean daily wind speed and daily wind speed standard deviation

The generator also was calculated to have a failure rate of 0 for wind speeds in the 13 m/s – 17 m/s range, as was the rotor. Because the model assumes that the failure rate beyond 17 m/s is the same as that calculated for the highest wind speed range this means that when the MCMCS model was run, the probability of a failure occurring on a day with a wind speed 13 m/s or greater was 0.

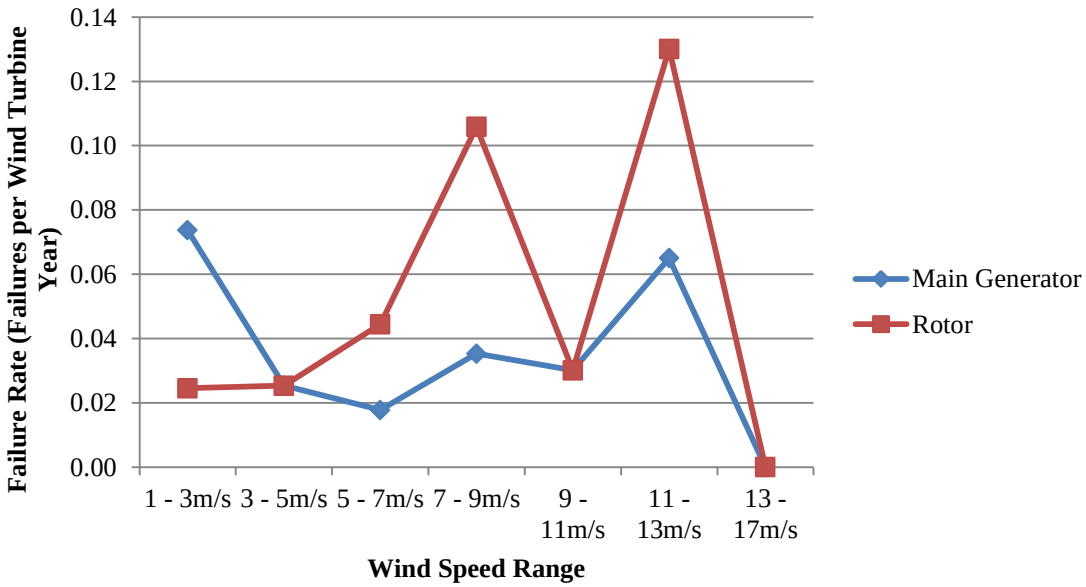

Figure 8-3: WSD failure rates of the main generator and rotor

This result was also the case for other components and meant that when the FINO model was run in Chapter 6.1.1.1, the failure rate of some components decreased. This was discussed in more depth in Chapter 6.1.2.1. To confirm whether these components do fail less frequently in high wind speeds, more reliability data is required, preferably from wind farms that operate at sites with high mean wind speeds.

The model assumes that the wind speed measured on site by the met mast is also the wind speed experienced by the failed WT. Both sites cover very large areas and it is therefore not possible to guarantee that the mean daily site wind speed is also the mean daily wind speed of the failed WT. However the wind speed of the site is a reasonable metric to measure the site conditions. Had detailed SCADA been available for each WT over the recorded period, more detailed wind speeds could have been used in the analysis.

However, even if more detailed wind speeds are gathered the model still relies on another assumption which is that any failure that occurs is directly linked to the mean daily wind speed on the day of failure. Failures in mechanical components are often the result of wear over a long period of time; therefore the origin of the failure is likely to have appeared some time before the component became unusable and failed.

The operator monitors their SCADA data and uses advanced algorithms to detect abnormal readings and diagnose the location of the failure. The point where the readings go from normal to abnormal is assumed to be the point where the component has failed – however it is possible that in many cases the wear begins before that point and in this case a prior wind speed event may be responsible for the failure.

2. Industrial Applications

2.1. Seasonal Component Failure Rates

The importance of understanding how failure rates change seasonally was highlighted in Chapter 6.1.2, where Figure 6-7 shows how the offshore wave conditions change from winter to summer. For offshore WTs, the sea conditions in winter make the asset difficult to access safely and so any failure that occurs will cause logistical and economic problems.

The component failure rates during each month, calculated by the FINO model, are shown in Table 8-1. According to the model the least reliable components fail more often in the winter than in the summer. However the issues with the lack of data for some components, considered in the previous section, are evident as some components have higher summer failure rates. The FINO model highlights this problem because it has such a high mean wind speed and therefore has days that reach above 13 m/s more regularly, where the calculated failure rate is 0. For components such as the generator and rotor, the failure rate in the winter decreased compared to the summer.

Although these results are counter-intuitive, the components they concern have such low failure rates that their contribution to the overall model is quite small. However in terms of risk the rotor does make a difference to the model. If risk is calculated simply using Equation 8-1, where the component cost is multiplied by the failure rate, the rotor is calculated to be the component that causes the fourth highest risk, as shown in Figure 8-4.

$$Risk = Cost\ of\ Failure \times Probability\ of\ Failure \quad \textbf{Equation 8-1}$$

If the rotor risk is reduced as was proposed in Chapter 7.2.3, the risk would reduce from the £2291 shown in Figure 8-4 to £183.

Table 8-1: FINO model monthly component failure rates

Month	Failure Rate (Failures per WT year)											
	Blade Pitch System	Control System	Drive Train	Emergency System	Hydraulic System	Lifting System	Main Generator	Met Instrume-nts	Nacelle	Rotor	Tower	Yaw System
Jan	0.078	1.154	0.235	0.006	0.097	0.008	0.028	0.054	0.048	0.049	0.112	0.360
Feb	0.063	0.917	0.224	0.007	0.083	0.009	0.024	0.065	0.040	0.054	0.097	0.285
Mar	0.070	1.081	0.230	0.011	0.105	0.009	0.029	0.057	0.047	0.056	0.106	0.330
Apr	0.059	0.793	0.202	0.012	0.085	0.011	0.030	0.076	0.025	0.056	0.091	0.238
May	0.069	0.876	0.214	0.010	0.086	0.009	0.030	0.072	0.033	0.062	0.094	0.260
Jun	0.066	0.657	0.195	0.018	0.076	0.013	0.031	0.087	0.019	0.053	0.080	0.200
Jul	0.065	0.779	0.207	0.014	0.081	0.014	0.031	0.090	0.021	0.069	0.088	0.229
Aug	0.067	0.781	0.210	0.013	0.077	0.014	0.030	0.080	0.023	0.064	0.089	0.227
Sep	0.066	0.946	0.226	0.011	0.090	0.010	0.027	0.069	0.033	0.055	0.097	0.291
Oct	0.073	1.037	0.235	0.008	0.094	0.010	0.030	0.066	0.037	0.059	0.107	0.315
Nov	0.070	1.204	0.225	0.005	0.103	0.006	0.025	0.043	0.051	0.052	0.107	0.353
Dec	0.067	1.109	0.235	0.008	0.099	0.006	0.029	0.043	0.046	0.050	0.102	0.342

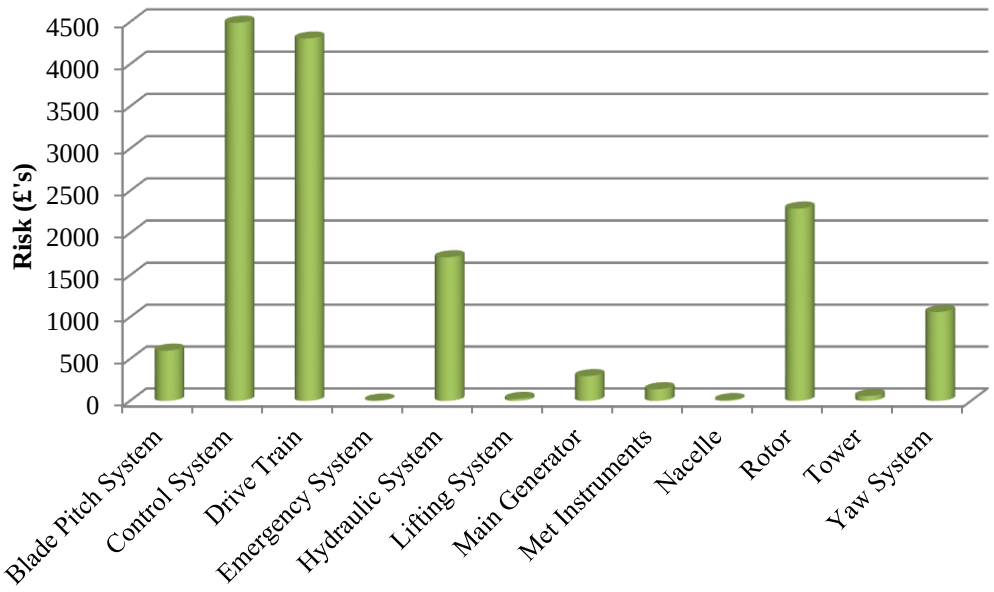

Figure 8-4: Component risk

The blade failure that occurred during the recorded period skews the component cost – this was discussed in more detail in Chapter 7.2.3. A larger dataset, which contained more rotor failures, would give a better reflection of the actual risk the rotor imposes. A better estimate of component cost would also be of benefit to the model as it is calculated according to downtime.

When downtime filters were applied to the monthly failure rates it was found in Chapter 6.1.2.2 that for the more severe failures (when the downtime filter was increased to 48 hours) the monthly calculated failure rates for the FINO model became more seasonal. This is shown in Figure 8-5, where the most seasonal component, when a downtime filter of 48 hours was applied, was the yaw system. As discussed in Chapter 6.1.2.2, the failure rate of the yaw increases by 283% from June to November.

Despite the WSD failure rate of the rotor equalling 0 for mean daily wind speeds greater than 13 m/s (as shown in Figure 8-3), the probability of a failure occurring that causes a

downtime greater than 48 hours increases by 88%. However winter failure rates of the main generator, hydraulic system and meteorological instruments fall compared to the summer.

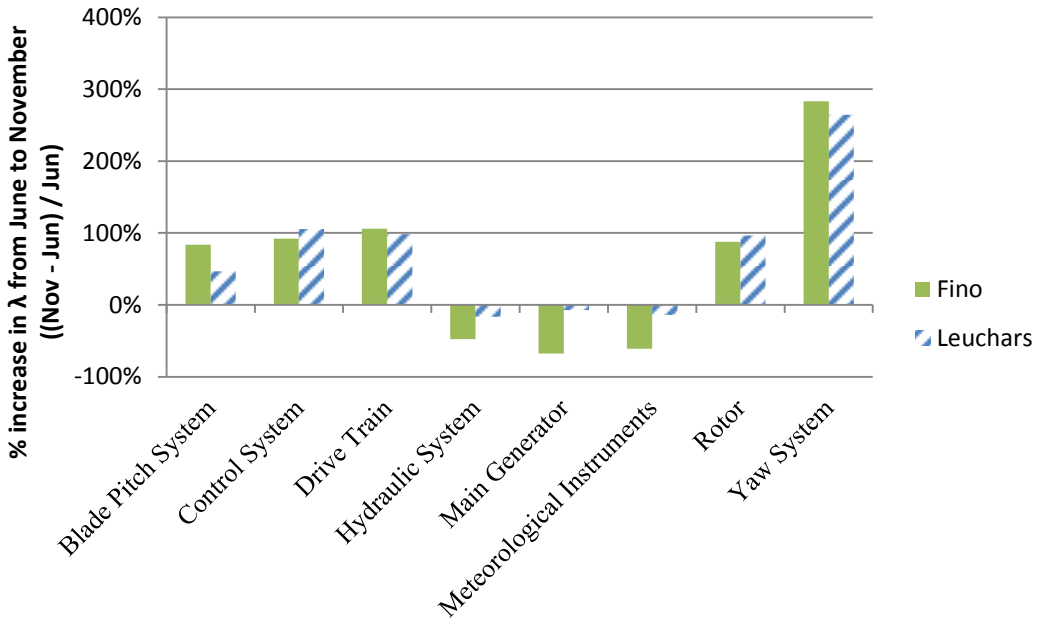

Figure 8-5: Increase in component failure rate of 48 hour downtime filtered FINO model from June to November

As discussed in Chapter 6.1.2.4, the component failure rates of the Leuchars model are not as great as the FINO model; however they do show similar seasonal variation as shown in Figure 8-5, when a downtime of 48 hours is also applied to the data. This also demonstrates that there is a possible application for the model to be used for onshore wind farm sites.

2.2. Energy Yield Assessment

Chapter 5 and Chapter 6.1 established that in the case of the recorded reliability from the operator, failures occurred more often in the winter due to high wind speeds. Failures at this time of year were more likely to have caused significantly longer periods of downtime, as discussed in Chapter 6.1.2.

Therefore when a failure occurs in the winter the energy lost is greater than in the summer as the downtime is longer and the potential energy lost is higher. Equally in the summer the downtimes are lower and so are the losses.

Using traditional constant annual failure rates it is not possible to analyse the impact of more frequent winter failures on the energy yield produced by the WT. However by using the WSD failure rate model the impact of seasonal failure rates was assessed in Chapter 6.2.

Figure 8-6 shows the energy lost from each of the models analysed in Chapter 6.2.3.1 – Chapter 6.2.3.3. A clear seasonal trend is show where more energy is lost in the winter than in the summer months. This is most significant in the FINO models.

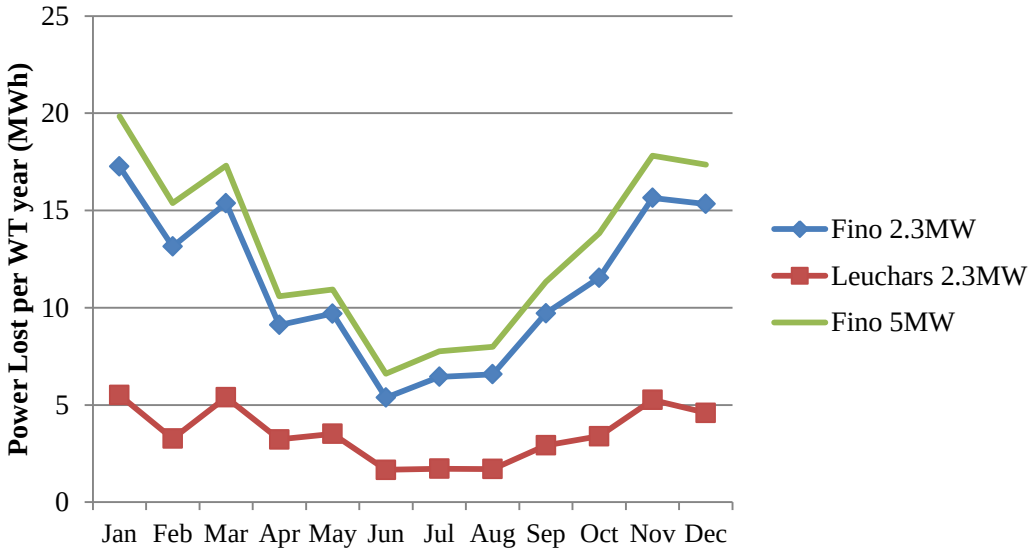

Figure 8-6: Power lost per WT year due to corrective maintenance for the FINO and Leuchars models using 2.3 MW and 5 MW WTs

However Figure 8-6 does not present the entire influence of the higher failure rates in the winter periods. Figure 8-7 shows how the monthly lost power as a percentage of total power generated also follows a seasonal trend. Had the failure rates not been WSD and were instead constant, lost power would still be highest in the winter as that is the period of time when the potential energy is the highest. Therefore losses would also be greatest at this time of year.

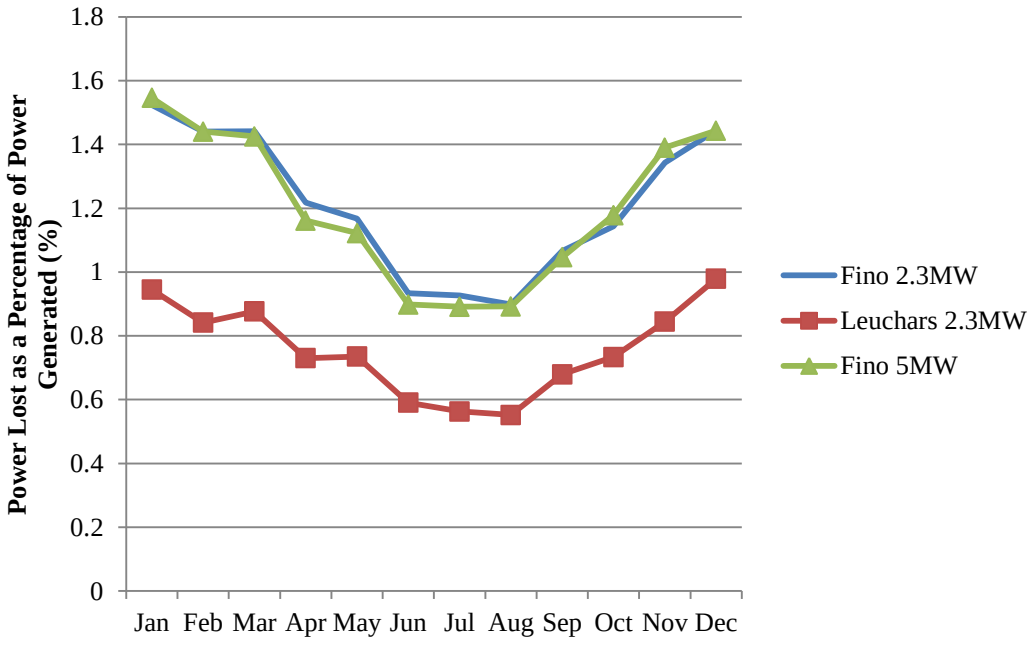

Figure 8-7: Monthly power lost as a percentage of power generated due to corrective maintenance for the FINO and Leuchars models using 2.3 MW and 5 MW WTs

In Figure 8-7 it is shown that a larger proportion of failures are occurring in the winter and thus causing an increase in the winter periods. Had failure rates been constant, these plots would have shown relatively straight lines.

The effect of the increase in lost power in the winter was described in Chapter 6.2 and is summarised in Table 8-2. Because of the high availability and low failure rate of onshore WTs, the difference in income calculated using a constant failure rate (calculated using the WSD failure rates in Chapter 6.1.1) and a WSD failure rate model is shown in column 6 of

Table 8-2. In each case the constant failure rate approach overestimates the generated power by neglecting to account for the increased number of failures in winter. For a 200 WT wind farm, the difference between the two approaches would equal £5.4 million over its 20 year lifetime.

Table 8-2: Summary of income difference between WSD and constant failure rate models used in energy yield assessment

	Per WT Year				
	WSD Failure Rates		Constant failure Rates		Income Difference Between Constant and WSD (£)
Model	Power Generated (MWh)	Total Power Lost (MWh)	Power Generated (MWh)	Total Power Lost (MWh)	
Leuchars 2.3 MW	5388	42	5394	36	517
FINO 2.3 MW	10841	135	10850	126	829
FINO 5 MW	12697	157	12712	142	1341

Had the WSD failure rates not been used at all and instead the failure rates from Site A and Site B (shown in Chapter 4.1.4) were used to estimate the energy yield, the difference between that and the WSD models are shown in Table 8-3. In the FINO 5 MW offshore case the difference is £12714 per WT year. This figure is conservative as it does not account for offshore access, logistical issues or preventative maintenance that would further reduce the availability of the WT.

Table 8-3: Summary of income difference between WSD failure rate models and ORD failure rate model

	Per WT Year			
	ORD Failure Rates		Income Difference between ORD Failure Rate Models and WSD Failure Rate Models (£)	
Model	Power Generated (MWh)	Total Power Lost (MWh)	Onshore Rate (£90/MWh)	Offshore Rate (£150/MWh)
Leuchars 2.3 MW	5400	30	1059	1765
FINO 2.3 MW	10915	61	6638	11063
FINO 5 MW	12782	72	7628	12714

Over a 20 year lifetime the failure rates from the ORD would overestimate the yield by £254k. For the FINO 2.3 MW model the same difference, but using onshore electricity rates, would be £133k.

The electricity rate in the case of all the analysis undertaken was assumed to remain constant throughout the year, when in reality the price increases in the winter (when demand is highest) and decreases in the summer. Were these fluctuations accounted for in the model, the differences between the WSD and constant models would be even greater.

The model therefore demonstrated that – were the relationship between wind speed and component failure rates calculated in Chapter 4 to be representative of typical WT behaviour – energy yield is overestimated due to a higher probability of failures occurring in winter. This overestimation is greatest for sites that experience high mean annual wind speeds. In the case of an offshore site, failures will occur at periods when the wind speed is highest and the access is therefore lowest.

2.3. Spares Optimisation

The impact of the offshore environment on corrective maintenance cost was assessed in Chapter 7. The model calculated that the cost of corrective maintenance for a 2.3 MW WT, subjected to FINO wind speeds, would be substantially higher than that calculated for a 2.3 MW WT subjected to typical onshore wind speeds, (see Chapter 7.3.2). This is shown in Figure 8-8.

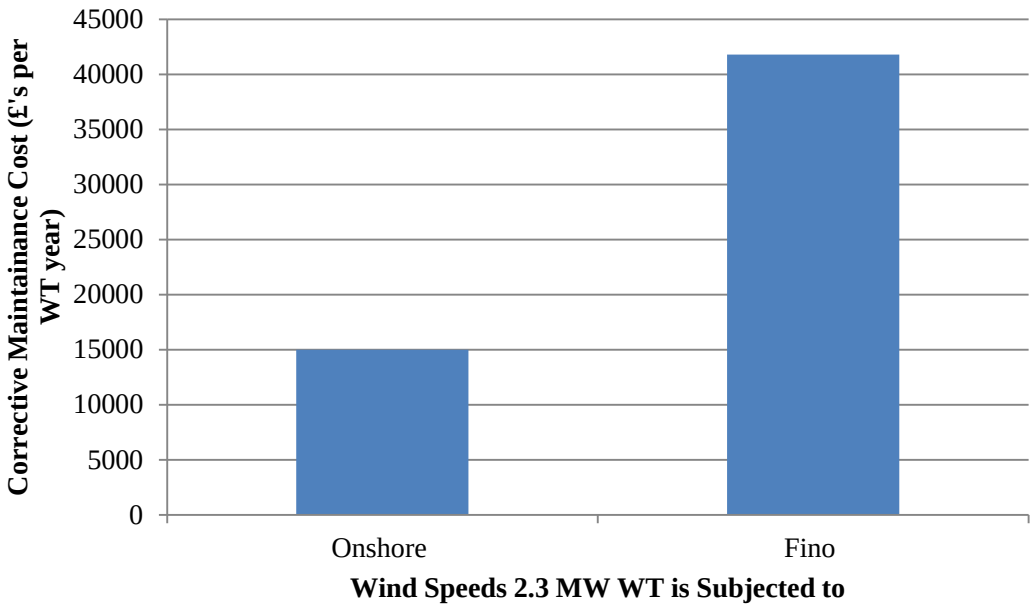

Figure 8-8: Cost of corrective maintenance for a 2.3 MW WT when subjected to typical onshore and offshore wind speeds

The reason for this increase was due to a combination of the seasonal failure rates calculated by the FINO model and the cost of offshore logistics that result from failures that occur more frequently in the winter due to high wind speeds.

The difference in calculated corrective maintenance cost between a FINO model where failures are generated using the wind speed and therefore WSD failure rates and a second model that uses traditional annual failure rates generated randomly is shown in Figure 8-9. The seasonal offshore constraints described for the three cost scenarios remain the same in

each model (shown in Chapter 7.2.4), but the probability of failure in the constant models case does not change according to the wind speed. Figure 8-9 therefore shows that even if the correct annual component failure rates can be calculated for an offshore site, as in the case of the constant failure rate model, the O&M costs are underestimated compared to the WSD FINO model. The difference between the WSD and constant failure rate models is roughly 9% for each of the cost scenarios. In the HC case this equals £23 million over the lifetime of a 200 WT wind farm.

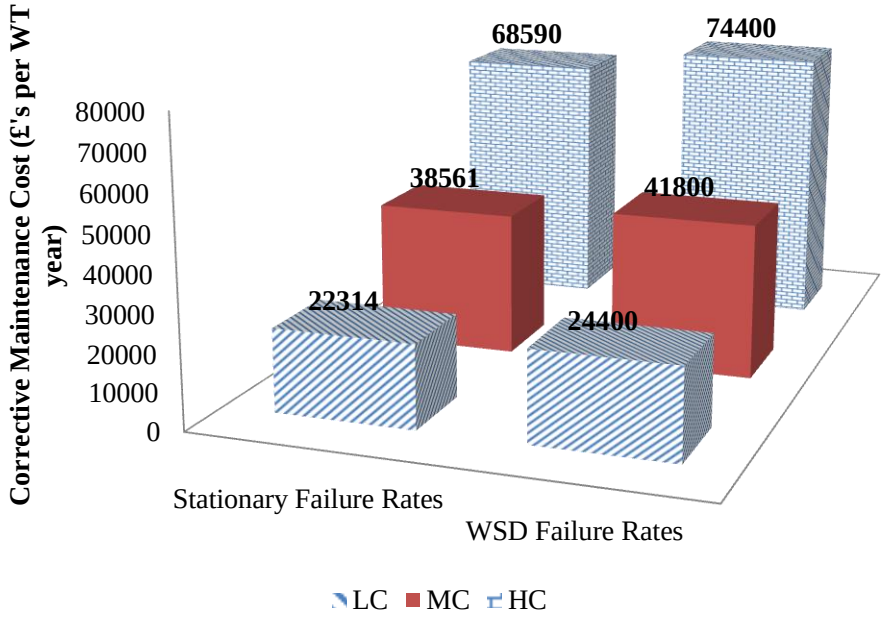

Figure 8-9: Corrective maintenance cost for FINO model when constant failure rates and WSD failure rates are used in model

The influence of the wind speed on preventative maintenance optimisation is not explored in this thesis. However the wind speed would very likely influence the scheduling of preventative maintenance because of WT access. If corrective maintenance does increase in the winter due to high wind speeds, it is likely that preventative maintenance will have to be performed in the summer when conditions are would present better access to service the WTs. Therefore the spares holding for preventative maintenance would be ordered in

advance for the summer and vessels would also very likely be hired if they are believed to be required. Because preventative maintenance can be planned in advance, the costs of components and vessels are unlikely to be as high as that of the corrective maintenance. The lost energy as a result of the downtime will also be far less due to the low wind speeds. Therefore the estimation made by Rademakers that preventative maintenance will be roughly 60% of the cost of corrective maintenance discussed in Chapter 7.2.3 may give a good reflection of the costs.

3. Appraisal of Results

The main aim of this thesis was to model the impact of wind speed on WT component failure rates and gain a better understanding of possible applications of this knowledge and therefore its value. As data was limited, the relationship between some components and wind speed is still unknown. However in the case of the least reliable components (the control system, yaw system and drive train) it is clear that at periods of high wind speed the probability of failure is greater.

The reliability dataset that was used in all the analysis (the ORD) comes from two Scottish onshore wind farms and contains roughly 400 WT years of reliability data. The sites are located within 30 miles of each other and are therefore subjected to very similar climates. The model of WT used at each site is the same and they are roughly the same age. As a result it could be argued that the results in this thesis are only really applicable to wind farms that operate using 2.3 MW WTs in the central belt of Scotland and are in the useful life period of their lives. However as different WT models, sited in different countries, have similar reliability attributes as the WTs used in this analysis, it could also be argued that these results may give a good reflection of how typical WTs perform.

Bayes Theorem was used to plot how wind speed impacted component failure rates. This was a very simple process which required the mean daily wind speed to be known when a failure occurred. It relied on the assumption that the wind speed recorded by the onsite met masts were the same as those experienced by the failed WT. Both sites are relatively large and at some periods were only served by one available met mast. The wind speeds experienced by the met masts were unlikely to be the same as those experienced instantaneously by the failed WTs, however because the wind speeds were averaged over a day this value is likely to be more indicative of conditions experienced across the whole site at that time. This approach also assumes that the wind speed experienced on the day of

failure was the cause of the failure, when it may be that conditions at some day in the past may have caused deterioration to start only for the failure to occur days later. In many cases failures are likely to have begun before being spotted by the operator or by any algorithm using the SCADA data. In the future there may be better algorithms for detecting the very beginning of deterioration and this model could then be modified to use this more accurate data.

The failure rates calculated by using Bayes Theorem were then used in MCMCS to produce more data with which to analyse. This data however was produced using limited input wind speed data. In the case of the FINO input wind speed data, 6 years of data was available which was repeated to create 20 year wind speed datasets. Despite these issues the model produced outputs that compared well to real data and allowed conclusions to be drawn that were very similar to those made by other authors in this area.

The model used in this analysis uses limited data in a simple way that involves established methods used by other authors who have also carried out research in this area. The model can easily be adapted to accommodate additional data from other wind farms that use different models of WTs. The costs used in the analysis are conservative and in Chapter 7 covered a wide range of scenarios which are applicable to different offshore wind farm sites that will operate under different conditions. The failure rate of components beyond 17 m/s are also conservatively assumed to be the same as those at 13 m/s, rather than extrapolating the failure rates. The results from the FINO model therefore suggest a reliability best case scenario.

The analysis performed for offshore wind farms uses onshore data and offshore constraints estimated from the data. Each offshore wind farm will experience different operations problems depending on their location from shore, their depth of water and distance to nearest port facility. This thesis outlines a model that can be adapted by those with better offshore

operational data and experience to determine the impact of wind speeds on offshore WT operation.

It can also be used by onshore operators who want to perform more accurate onshore yield assessments that account for the impact of frequent winter failures. Were this model to be adopted by a developer it could be used to examine how different WT models would perform on a selected site and the time of year certain components would be most likely to fail.

4. Further Work

Work should be carried out to gain a better understanding of exactly why certain components fail at high wind speeds from a physical point of view. Although hypothesis are raised for the control system, yaw system and drive train more work should be undertaken to prevent these failures from occurring. In the case of the control system it may be economical to build in system redundancies, particularly for offshore WTs.

During this research it became apparent that some components were removed from WTs once they failed and were then refurbished and used as spare components in the event that a failure occurred once again. The impact of this strategy is not properly modelled in this thesis as it was assumed that when a WT was repaired, the component failure rates were the same regardless of whether the repaired component was refurbished or a replacement. The failure rates were calculated from the whole dataset, which included a mixture of replacements and refurbishments. However it is not clear what strategy would be used by operators of offshore wind farms. If it could be discovered what components in the ORD were replacements or refurbishments, WSD failure rates could be calculated and analysis could be undertaken to determine what the best spare component strategy could be.

This model could be used to examine the implications of using direct drive WTs over geared WTs. From the results, it does appear that geared drive trains may suffer more failures when subjected to offshore wind speed conditions (see Chapter 6.1.1.1). How direct drive WTs perform however is unknown. The recent shift from manufacturers such as Siemens and Alstom to direct drive may be as a result of the increased gearbox failures due to high wind speeds and frequent variation between above and below rated operational strategies.

The impact of turbulence and wind shear is likely to directly affect WT reliability. Unfortunately this could not be measured accurately for each WT due to there only being two met masts located on each site. The value calculated by the met masts was not used in

the analysis (similarly to using the mean daily wind speed) because the impact of the site topography at each WT would not be accounted for and it was decided this was extremely important. If more wind speed data was available for each WT analysis should be performed to determine the impact of wind shear and turbulence on reliability. This may be particularly important offshore where the rotors are substantially larger and where there may be a considerable difference in wind speed from the lowest point of the swept area to the top.

Lastly, this model uses data from WTs that operated in the useful life period of their operational life. The model therefore does not consider the effects of aging or burn in. The reliability data used in this analysis should be updated to include the most recent year's data – Site B may be starting to suffer from wear out as it will soon be entering its tenth year of operation. With the effects of aging accounted for, better economic lifetime performance assessments can be made, using this model, for potential wind farm sites.

Appendix I – Convergence Criterion

The simulations carried out in this thesis were done so using Monte Carlo simulation (MCS). When using MCS it is important to set a stopping rule for the simulation and this is done so by setting a convergence criterion.

The simulations in this thesis were carried out in sets of 4000 WT years. This consisted of the lifetime (20 years) of a 200 WT wind farm. After each set of simulations, the results were calculated before the next set began. This process was programmed to continue until the simulation met the convergence criteria after which the simulation stopped.

Convergence was reached if the mean WT availability after 5 sets of simulations remained the same, or was within 0.001% of each other. An example of a simulation meeting this criterion is show in Figure I-1. In this example the MCS stopped after 64 sets of simulations which equated to 256000 WT years of simulated data.

Appendix II – Component Wind Speed Dependent Failure Rates

The following shows WSD failure rate plots of each WT component with no downtime filter applied.

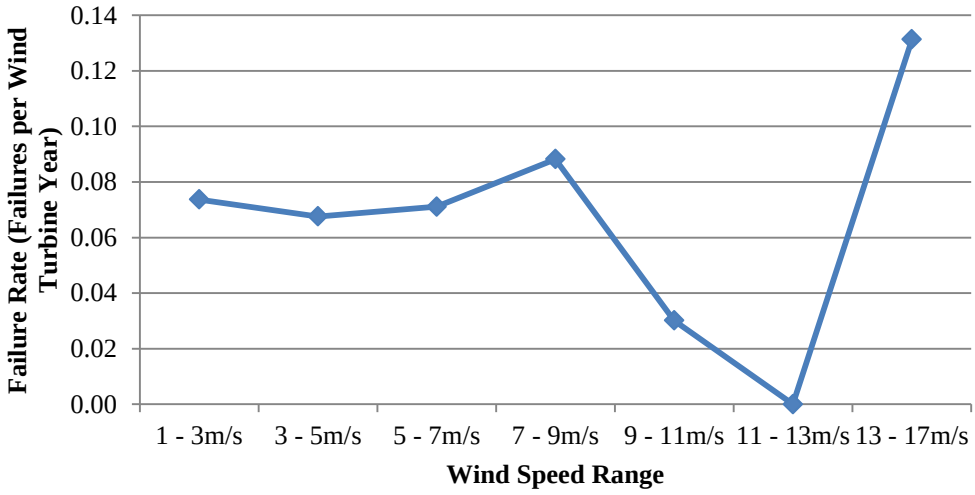

Figure II-1: Blade Pitch System WSD failure rate plot

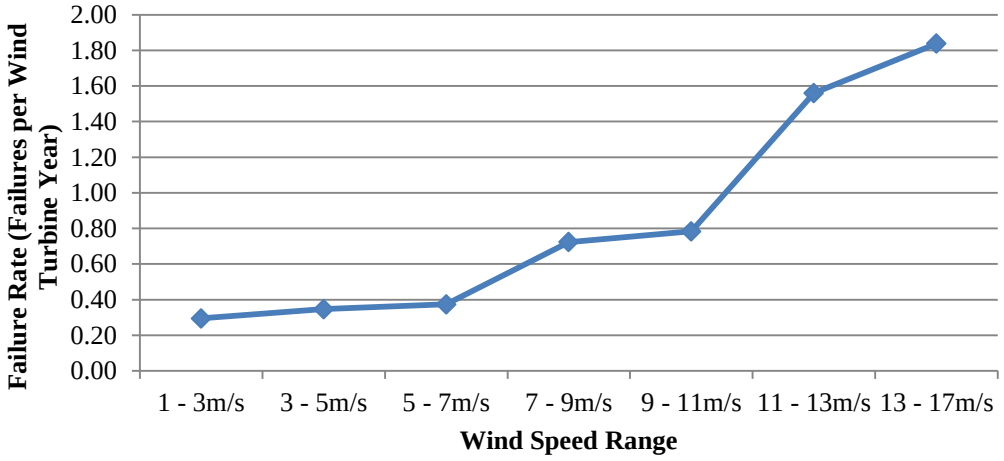

Figure II-2: Control System WSD failure rate plot

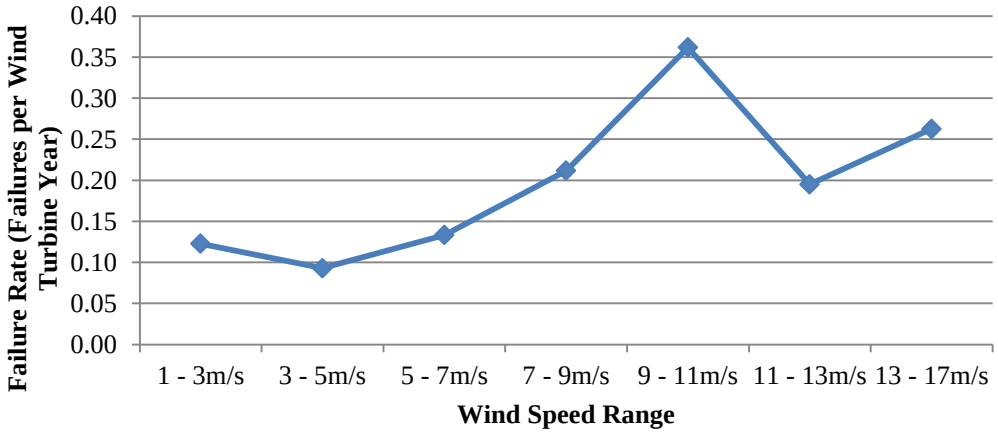

Figure II-3: Drive Train WSD failure rate plot

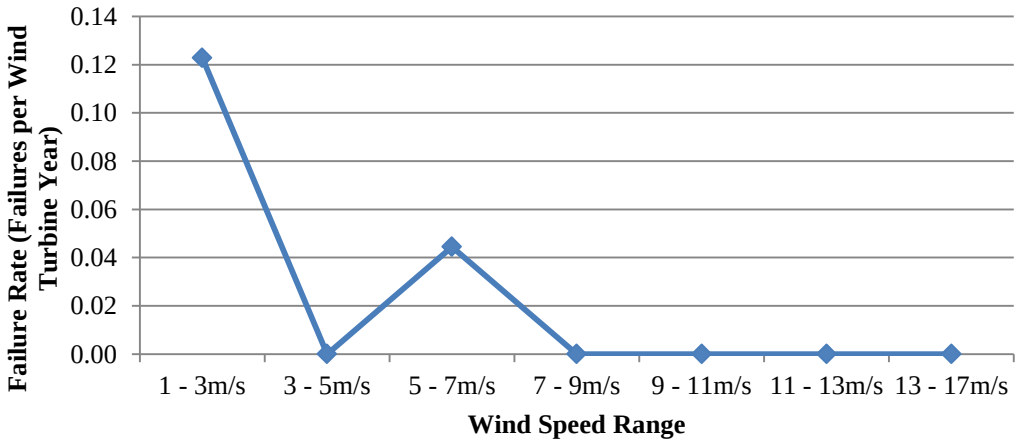

Figure II-4: Emergency System WSD failure rate plot

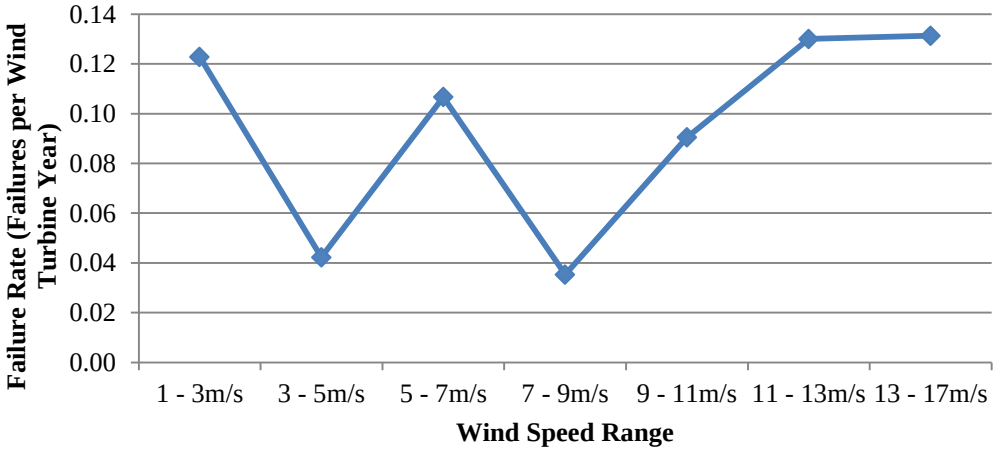

Figure II-5: Hydraulic System WSD failure rate plot

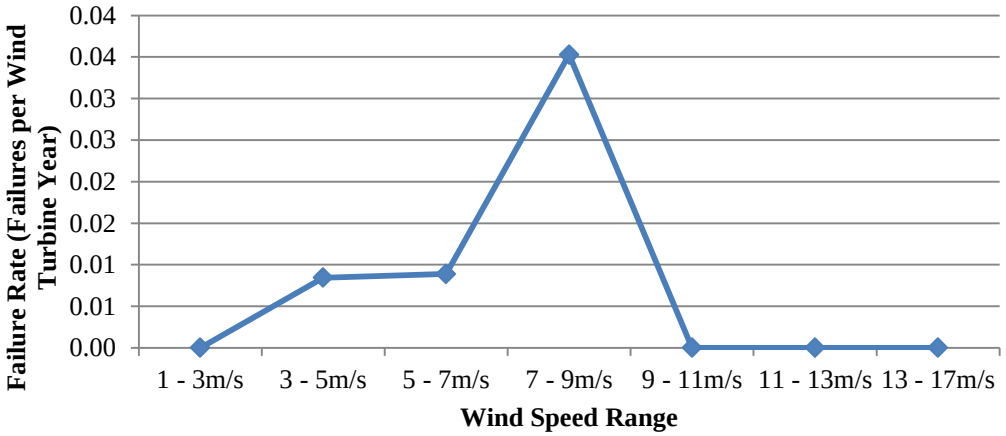

Figure II-6: Lifting System WSD failure rate plot

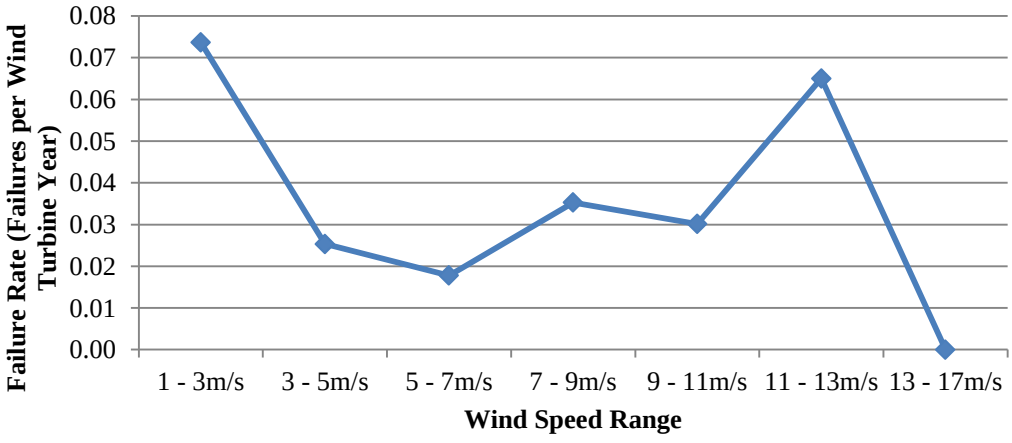

Figure II-7: Generator WSD failure rate plot

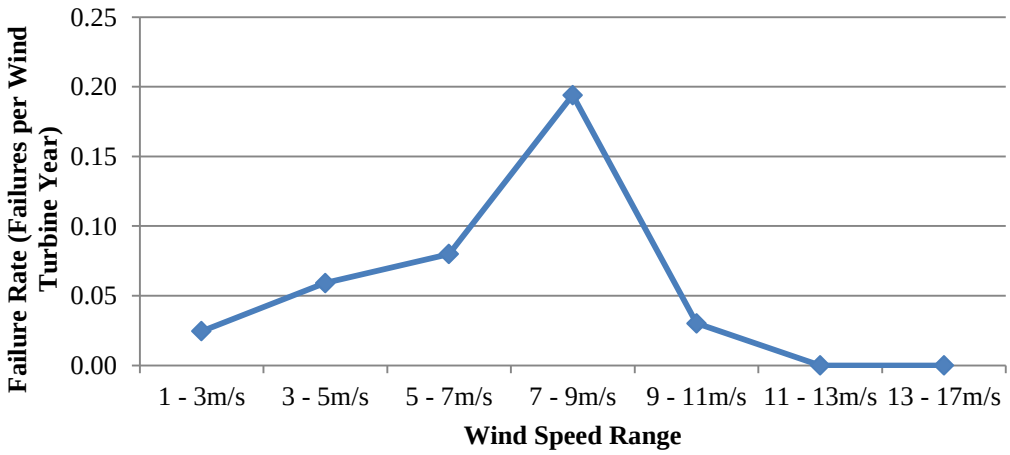

Figure II-8: Meteorological Instruments WSD failure rate plot

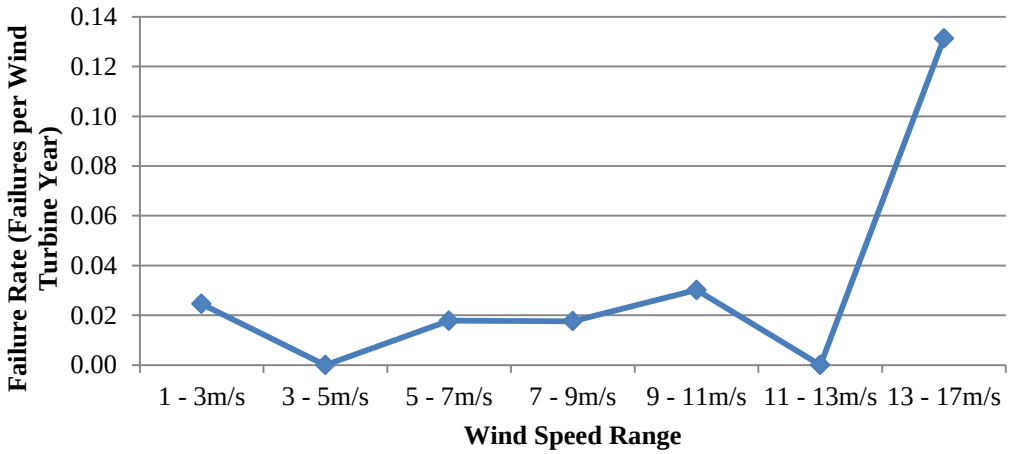

Figure II-9: Nacelle WSD failure rate plot

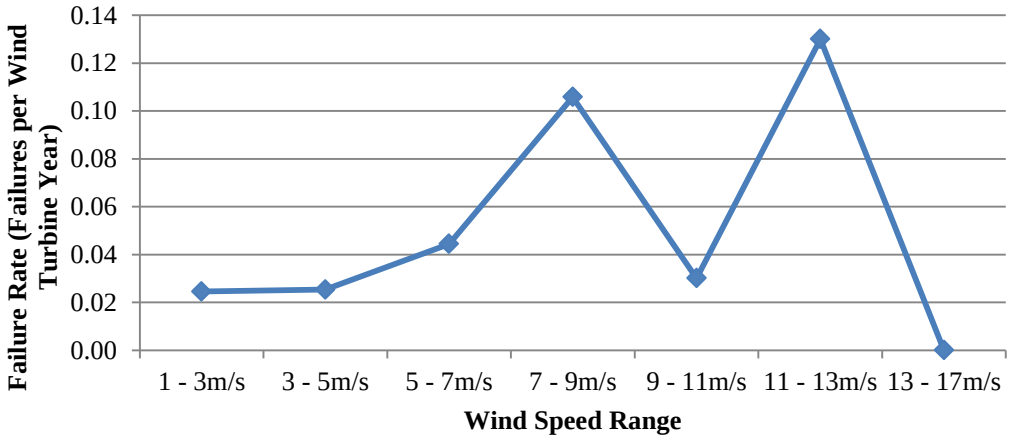

Figure II-10: Rotor WSD failure rate plot

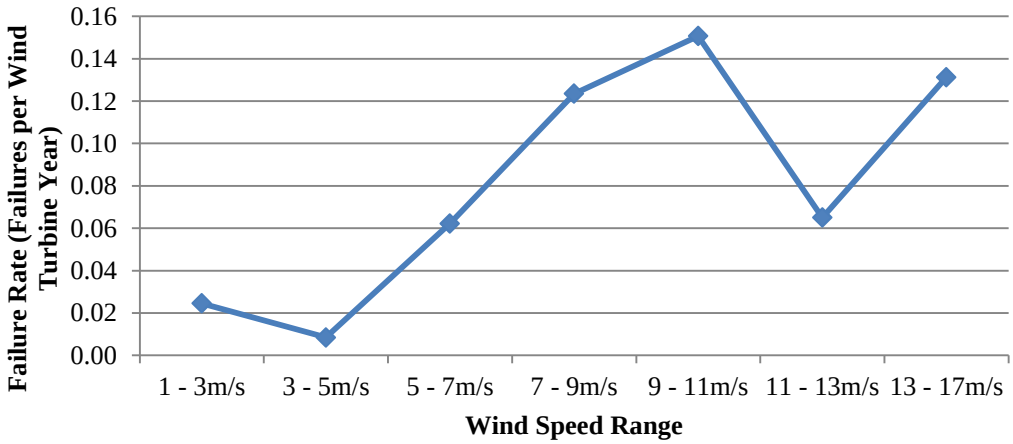

Figure II-11: Tower WSD failure rate plot

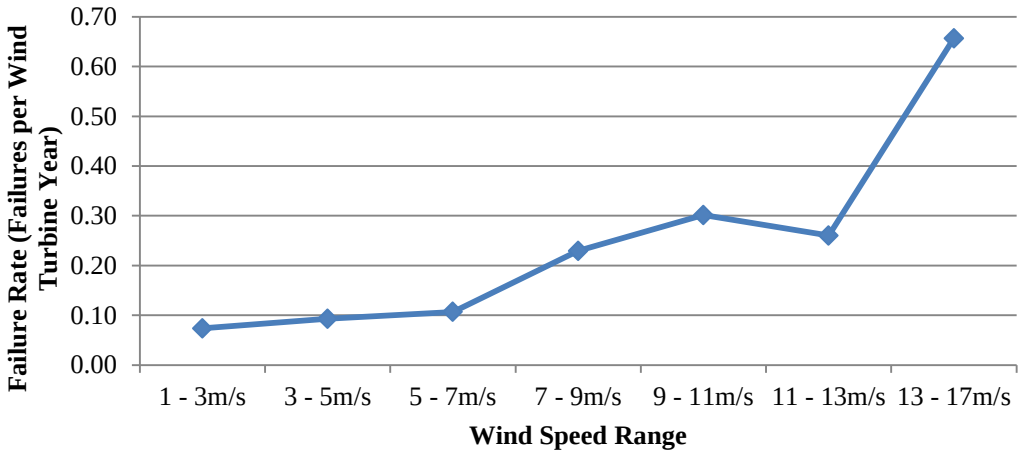

Figure II-12: Yaw System WSD failure rate plot